

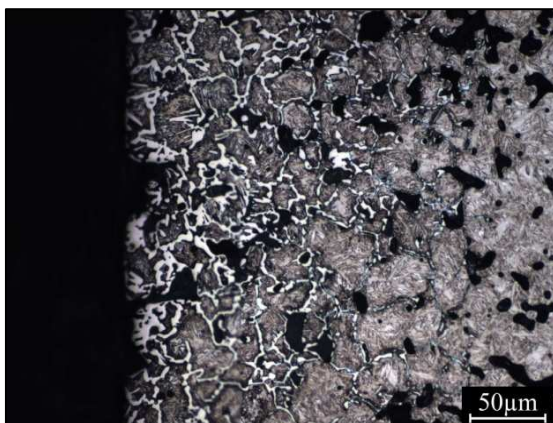
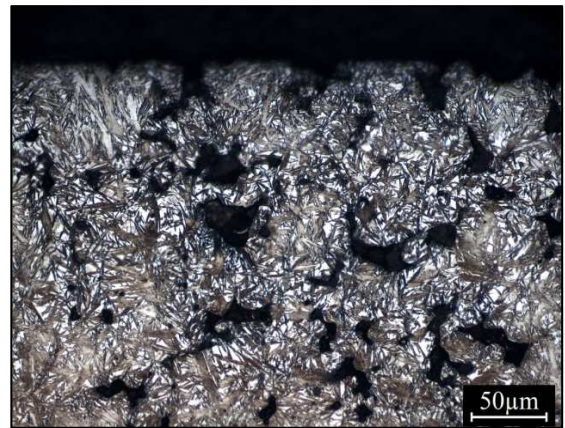


UNIVERSITY  
OF TRENTO - Italy

Department of Materials Engineering  
and Industrial Technologies

Doctoral School in Materials Engineering – XXIII cycle

**Effect of surface  
treatments on  
mechanical  
properties of low  
alloy sintered steels**





UNIVERSITY  
OF TRENTO - Italy

Department of Materials Engineering  
and Industrial Technologies

Doctoral School in Materials Engineering – XXIII cycle

---

---

# **Effect of surface treatments on mechanical properties of low alloy sintered steels**

Elena Santuliana

April 2011

Doctoral Committee:

Prof. Gian Domenico Sorarù - Università degli studi di Trento

Prof. Herbert Danninger - Technische Universität Wien

Prof. Michel Vert - Université de Montpellier I

Prof.ssa Laura Montanaro - Politecnico di Torino

*To my mother*

## Index

<b>Introduction</b> .....	1
<b>1. Low Pressure Carburizing</b> .....	4
<b>1.1. Carburizing: microstructure and properties</b> .....	4
<b>1.2. Low pressure carburizing</b> .....	9
1.2.1. <i>Introduction</i> .....	9
1.2.2. <i>The process</i> .....	12
1.2.3. <i>Low pressure carburizing of PM steels</i> .....	13
<b>2. Plasma Nitriding</b> .....	17
<b>2.1. Nitriding: microstructure and properties</b> .....	17
<b>2.2. Plasma nitriding</b> .....	19
2.2.1. <i>Introduction</i> .....	19
2.2.2. <i>The process</i> .....	21
2.2.3. <i>Plasma nitriding of PM steels</i> .....	22
<b>3. Shot Peening</b> .....	25
<b>3.1. Shot peening parameters</b> .....	26
<b>3.2. Shot peening and thermochemical treatments</b> .....	27
<b>3.3. Shot peening of PM steels</b> .....	28
<b>4. Materials and Experimental Procedures</b> .....	30
<b>4.1. Materials</b> .....	30
4.1.1. <i>Compaction</i> .....	31
4.1.2. <i>Sintering</i> .....	31
4.1.3. <i>Secondary treatment</i> .....	31
<b>4.2. Experimental procedures</b> .....	31

*Index*

---

4.2.1. Chemical analysis.....	32
4.2.2. Density and porosity.....	32
4.2.3. Dilatometry.....	32
4.2.4. Metallography.....	33
4.2.5. Hardness and microhardness.....	33
4.2.6. Impact test.....	33
4.2.7. Transverse rupture strength (TRS) test.....	34
4.2.8. Bending fatigue test.....	35
4.2.9. Fractography.....	35
<b>5. Chromium Steels: as sintered microstructure and mechanical properties.....</b>	<b>36</b>
<b>5.1. Effect of carbon content, density and sintering temperature on microstructure and microhardness.....</b>	<b>36</b>
<b>5.2. Impact toughness.....</b>	<b>47</b>
5.2.1. A simplified model for impact strength of sintered steels.....	50
5.2.1.1. Yield load.....	55
5.2.1.2. Maximum load.....	56
5.2.1.3. Deflection.....	58
5.2.1.4. Impact energy.....	59
<b>5.3. Surface densification by shot peening.....</b>	<b>60</b>
5.3.1. Effect on microstructure and microhardness.....	61
5.3.2. Surface morphology.....	63
<b>5.4. Concluding remarks.....</b>	<b>65</b>
<b>6. Low Pressure Carburizing of Chromium Steels.....</b>	<b>67</b>
<b>6.1. Three steps LPC– LPC 1.....</b>	<b>68</b>
6.1.1. Effect of porosity.....	68
6.1.2. Effect of chemical composition of the steel.....	71

---

6.1.3. Comparison between closed porosity and surface densification.....	73
<b>6.2. Five steps LPC– LPC 2.....</b>	<b>76</b>
6.2.1. Microstructures and microhardness profiles.....	77
6.2.2. Impact toughness.....	81
<b>6.3. Microstructural improvement of overcarburized materials..</b>	<b>83</b>
6.3.1. Solution annealing treatment.....	83
<b>6.4. Fatigue resistance.....</b>	<b>87</b>
6.4.1. Microstructure and microhardness profile.....	88
6.4.2. Fatigue resistance.....	90
6.4.3. Fracture surface analysis.....	92
6.4.4. Evaluation of low pressure carburizing effect on the fatigue resistance.....	95
<b>6.5. Concluding remarks.....</b>	<b>96</b>
<b>7. Plasma Nitriding of Chromium Steels.....</b>	<b>98</b>
<b>7.1. Microstructures and microhardness profiles.....</b>	<b>98</b>
7.1.1. 20 hours nitriding and 8 hours diffusion at 480°C.....	98
7.1.2. 48 hours nitriding and 24 hours diffusion at 480°C.....	101
7.1.3. Effect of surface densification.....	104
<b>7.2. Impact toughness.....</b>	<b>106</b>
<b>7.3. Fatigue resistance.....</b>	<b>110</b>
<b>7.4. Post nitriding shot peening.....</b>	<b>112</b>
7.4.1. Microstructure.....	112
7.4.2. Microhardness profile.....	113
7.4.3. Fatigue resistance.....	115
<b>7.5. Fracture surface analysis.....</b>	<b>117</b>
<b>7.6. Evaluation of the plasma nitriding effect on the fatigue resistance.....</b>	<b>120</b>
<b>7.7. Concluding remarks.....</b>	<b>121</b>

---

<b>8. Shot Peening of Chromium Steels</b> .....	123
<b>8.1. Surface densification</b> .....	124
<b>8.2. Strain hardening</b> .....	126
<b>8.3. Residual stresses</b> .....	127
<b>8.4. Fatigue resistance</b> .....	129
<b>8.5. Concluding remarks</b> .....	130
<b>9. Chromium Free Steels: as sintered microstructure and mechanical properties</b> .....	132
<b>9.1. Effect of carbon content, density and sintering temperature on microstructure and microhardness</b> .....	132
<b>9.2. Impact toughness</b> .....	138
<b>9.3. Surface densification by shot peening</b> .....	140
<i>9.3.1. Effect on microstructure and microhardness</i> .....	140
<i>9.3.2. Surface morphology</i> .....	142
<b>9.4. Concluding remarks</b> .....	143
<b>10. Low Pressure Carburizing of Chromium Free Steels</b> .....	145
<b>10.1. Three steps LPC– LPC 1</b> .....	146
<i>10.1.1. Effect of porosity</i> .....	146
<i>10.1.2. Comparison between closed porosity and surface densification</i> .....	149
<b>10.2. Five steps LPC- LPC 2</b> .....	151
<i>10.2.1. Microstructures and microhardness profiles</i> .....	152
<i>10.2.2. Impact toughness</i> .....	154
<b>10.3. Microstructural improvement of overcarburized materials</b> .....	156
<i>10.3.1. Tempering treatment</i> .....	156
<b>10.4. Fatigue resistance</b> .....	158
<i>10.4.1. Microstructure and microhardness profile</i> .....	158
<i>10.4.2. Fatigue resistance</i> .....	159
<i>10.4.3. Fracture surface analysis</i> .....	161

---

<b>10.4. Concluding remarks.....</b>	163
<b>11. Conclusions.....</b>	164
<b>12. Appendix.....</b>	168
<b>12.1. Impact properties of as sintered steels.....</b>	168
<b>12.2. Microstructures of as sintered steels.....</b>	171
<b>12.3. A simplified model for impact strength of sintered steels..</b>	177
12.3.1. <i>Ferritic- Perlitic steels.....</i>	177
12.3.2. <i>Bainitic (- Perlitic) steels.....</i>	179
12.3.3. <i>Perlitic steels.....</i>	181
<b>12.4. Microstructures and microhardness profiles of LPC</b>	
<b>steels.....</b>	183
12.4.1. <i>Three steps LPC- LPC 1.....</i>	183
12.4.2. <i>Five steps LPC- LPC 2.....</i>	185
<b>12.5. Microstructures and microhardness profiles of PN steels....</b>	189
<b>13. References.....</b>	193



## **Introduction**

Powder Metallurgy (PM) is a net- shape and cost effective technology used for the production of steel parts having good mechanical properties and geometrical precision. In the conventional press and sinter process, the voids among the powder particles cannot be completely eliminated, and the as sintered microstructure contains a certain amount of residual porosity. Mechanical properties are consequently lower than those of the corresponding wrought steels [1]. In particular, the fatigue resistance is significantly affected by porosity; crack tends to nucleate in correspondence of clusters of pores, and to propagate along the network of interconnected pores [2, 3].

Fatigue resistance can be improved on increasing the density, reducing pore size and pore clustering and enlarging the sintered ligaments between pore, or, similarly to wrought steels, by thermochemical (carburizing and nitriding) or mechanical treatments (shot peening).

Carburizing consists in a surface carbon enrichment, which gradually decreases towards the core. After quenching high carbon martensite is formed at the surface, characterized by high hardness and a compressive residual stresses suitable for wear and fatigue resistance. Low pressure carburizing is a variant of the conventional gas carburizing performed under sub-atmospheric pressure with pressurized gas quenching. It is quite attractive for carburized PM sintered steels, for two main reasons.

1. Porosity increases the surface exchange area, enhancing the risk of oxidation mainly in Cr and Cr-Mn steels. Low pressure carburizing uses propane or acetylene, as carburizing gas, which does not contain oxidizing agents.

2. Quenching oil remains entrapped in the open porosity, and has to be eliminated. The possibility to combine low pressure carburizing with gas quenching results in clean parts as well as lower distortion.

However, the combination between the very high carburizing potential of LPC and the large surface area of porous steels results in overcarburizing, with the precipitation of grain boundary carbides in Cr steels, and the formation of retained austenite in the case in Cr free ones [4, 5]. This problem can be solved by either increasing density, to close the residual porosity, or rolling and shot peening, to eliminate the surface porosity.

Nitriding is based on the nitrogen enrichment of the surface layers of steel. On the base of nitrogen content the surface microstructure can be divided in two zones: the compound and the diffusion layer. The former is in principle a ceramic layer, whilst the latter consists in the base matrix hardened by solid solution and by the precipitation of nitrides. The nitride precipitation induces a compressive residual stress field which offers a resistance to the nucleation and propagation of the fatigue crack, improving the fatigue resistance. In order to obtain a hardened and deep diffusion layer the steel has to contain alloying elements with a high affinity for nitrogen, as chromium and molybdenum. Nickel and manganese have a negligible interaction with nitrogen. Among the different nitriding processes, plasma nitriding is recommended for sintered steel. Plasma nitriding is less sensitive to porosity than gas nitriding due to the particular mechanism of nitrogen diffusion (volume diffusion) which allows a uniform diffusion front on the steel surface and a homogeneous nitrogen distribution [6, 7]. Therefore, a preliminary surface densification is not necessary.

Shot peening is a flexible and cost effective solution to improve the fatigue performances of mechanical parts, as gears and springs, thanks to the compressive residual stress generated below the surface and the surface work hardening. The improvement in fatigue resistance is more effective if shot peening is applied on case hardened steels, because of the more stability of the

## *Introduction*

---

compressive residual stresses. Since the fatigue strength of sintered steels strongly depends on the material density, shot peening is a useful technique to improve such property, owing to the densification of the surface layer [8, 9]. The fatigue cracks nucleates beneath this layer and since it cannot propagate in a compression field, it moves towards the core.

This PhD thesis is part of the an international research project, "Höganäs Chair project- fourth round", financed by Höganäs AB, world leader in the production of ferrous powders, involving four research institutions: Trento University, Technique University of Wien, Carlos III University of Madrid and Slovak Academy of Science, Institute for Materials Research, Kosice. The aim of the project is to carry out a cooperative study to design highly performing structural steels by the conventional Powder Metallurgy process.

This thesis has the aim to investigate different hardening treatments (plasma nitriding, low pressure carburizing and shot peening) carried out on four powders containing chromium (Cr-Mo, Mn) or not (Ni- Mo(-Cu)). The base approach consists in the microstructural study correlated with the results of the mechanical tests. Impact properties and fatigue resistance are carried out to evaluate the embrittlement, caused by surface treatments and the behavior of the materials under cycling loading, respectively.

The surface treatments were carried out with industrial treatments in order to transfer easily the results to the industrial applications.

## 1. Low Pressure Carburizing

### 1.1. Carburizing: microstructure and properties

Carburizing is a thermochemical diffusion process in which the steel will pick up carbon to a quantity determined by atmosphere, temperature, time at temperature and different carbon activity between atmosphere and material. This process allows a surface carbon enrichment in the pieces heated at the temperature where austenite is stable. Carbon atoms diffuse as interstitial in the austenite matrix and after quenching are responsible for the formation of a martensite surface layer with high hardness and characterized by a compressive residual stresses, suitable for wear and fatigue resistance. Since martensite start temperature ( $M_s$ ) is lowest at the surface where carbon content is the highest, the core transforms into ferrite-perlite or bainite on cooling, whereas the surface become martensitic. Martensite has a higher specific volume than ferrite, perlite and bainite, therefore, a compressive residual stress is established in the surface layer which is in equilibrium with tensile stress at core. After carburizing process the materials are tempered to convert the very brittle tetragonal martensite into the less crack susceptible cubic martensite [10, 11].

Many factors affect this process, including alloying elements and carbon, which set  $M_s$ , see equation 1.1, and hardenability, as shown in figure 1.1.

$$M_s(^{\circ}\text{C})=561-474(\%C)-33(\%Mn)-17(\%Ni)-17(\%Cr)-21(\%Mo) \quad (\text{eq. 1.1})$$

## Chapter 1: Low Pressure Carburizing

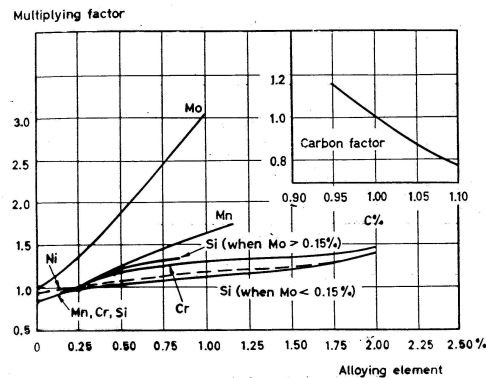


Figure 1.1: alloying elements effect on hardenability [10]

Alloying elements traditionally used for improving hardenability in carburized steels are manganese, chromium, molybdenum, and nickel. Chromium and molybdenum are strong carbide formers. Manganese is not a potent carbide former as chromium, however promotes cementite networks. In the standard range of carburizing steel, nickel and silicon reduce the lattice parameter of iron, making the solubility of the interstitial more difficult and retarding carburizing [11, 12, 13]. They have the tendency to inhibit the formation of grain boundary carbides, enhancing the formation of austenite.

The different microstructure between surface and core is accomplished by changes of mechanical properties. The fracture occurs at case-core interfaces when heavy contact loads create stresses that exceed the strength of the microstructure at this distance below the surface. Subsurface crack initiation is moved towards the interior by producing deeper cases, by using alloy steels with higher base hardenability and by increasing core carbon content.

Hardness is a property commonly measured in carburized steels and is used as a quality control parameter to document carburizing success and to establish case depths. One of the most commonly accepted techniques is to measure the microhardness profile of the carburized steel. The distance from the surface to the

## Chapter 1: Low Pressure Carburizing

point where the microhardness drops to a given hardness, (550HV), is defined as the case depth.

The successful of carburizing depends on the control of four principal variables [14, 15]:

**Carbon Potential.** Carbon potential, at a specific temperature, is defined as the carbon content in thermodynamic equilibrium with the surrounded atmosphere. The carbon potential of the furnace atmosphere must be greater than that on the surface of the work pieces and this difference is the driving force for carburizing.

**Carbon activity.** The carbon activity of a solute is defined as the vapor pressure of the substance, i.e. carbon, divided by the vapor pressure of the pure substance in its standard condition, which is graphite. Carbon activity in austenite is an indicator of the reactivity of carbon as a solute. However, the ratio cannot be measured directly, but only indirectly using for example equation 1.2, in which carbon activity is related to the carbon content of austenite (fig. 1.2):

$$a_C = f_i \cdot \%C \quad (\text{eq. 1.2})$$

where  $f_i$  is the activity coefficient and is chosen so that  $a_C = 1$ . Carbon activity in austenite decreases with temperature.

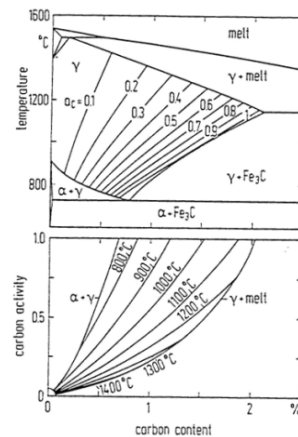


Figure 1.2: carbon activity in austenite [15]

## Chapter 1: Low Pressure Carburizing

The carbon activity influences the carbon flux ( $dm/dt$ ), from the carburizing atmosphere to the steel parts, by the equation 1.3.

$$dm/dt = F\beta(a_g - a_s) \quad (\text{eq. 1.3})$$

where  $F$  is the exchange surface area,  $\beta$  is the coefficient of carbon transfer (fig. 1.3),  $a_g$  and  $a_s$  are the carbon activity in the gas and the steel, respectively. Equation 1.3 show clearly the direct proportionality between the carbon flux and the exchange surface area.

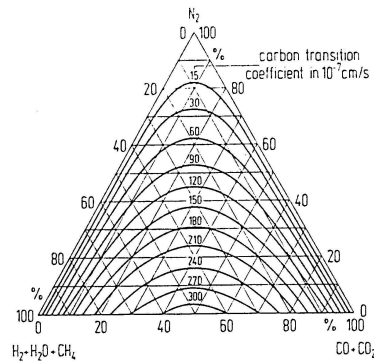


Figure 1.3: the carbon transition coefficient [15]

The alloying elements in carburizing steels have a pronounced effect on carbon activity and shift the boundary between the phase field of austenite and austenite plus cementite. The definition of carbon activity in an alloyed austenite ( $a_{CA}$ ) is expressed by equation 1.4.

$$a_{CA} = f a_C \quad (\text{eq. 1.4})$$

where  $a_C$  is the carbon activity for unalloyed steel and  $f$  is the parameters that considers the effect of various alloying elements [15] (fig. 1.4). The alloying elements traditionally used for improving hardenability in carburized steels are manganese, chromium, molybdenum and nickel:

## Chapter 1: Low Pressure Carburizing

$$f = (0.13-0.0055\%Cr); (0.025-0.01\%Mo); (0.0365+0\%Mn); (0.03+0.00365\%Ni);$$

$$(0.15+0.033\%Si)$$

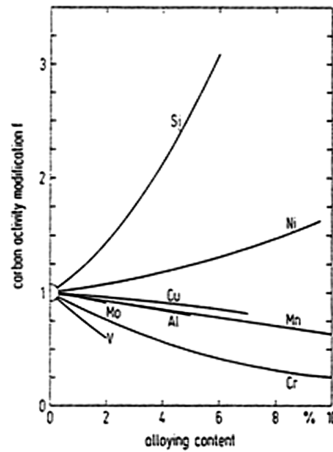


Figure 1.4: effect on carbon activity of different alloying elements [15]

Chromium and molybdenum tend to decrease the activity coefficient, while nickel tends to raise it. As a consequence, a chromium-molybdenum steel will take on more carbon, whilst nickel ones will take on less carbon.

**Carbon diffusion.** The effect of time, temperature and local carbon content on carbon diffusion in austenite can be expressed by Fick's laws. The first Fick law (eq. 1.5) states that the flux ( $J$ ) of the diffusing substance is proportional to the local carbon gradient ( $\Delta C$ ).

$$J = -D\nabla C \quad (\text{eq. 1.5})$$

The constant of proportionality is the diffusion coefficient  $D$ ; it is a function of carbon content and temperature by an Arrhenius equation. Fick's second law is reported in equation 1.6:

$$\frac{C - C_0}{C_s - C_0} = 1 - \operatorname{erf}\left(\frac{X}{2\sqrt{Dt}}\right) \quad (\text{eq. 1.6})$$



## Chapter 1: Low Pressure Carburizing

where  $C$  is local carbon content at distance  $X$ ,  $C_0$  is the initial carbon content in the steel prior to carburizing and  $C_s$  the surface carbon content that correspond to the carbon level of atmosphere. Combining the two laws and with true values of the diffusion coefficient, it is possible to predict the carbon gradient and depth of penetration occurring for any combination of time, temperature, and surface carbon concentration.

**Temperature and time.** Since carburizing is controlled by diffusion, temperature is the most powerful parameter in controlling the depth and the amount of carbon diffusion into the parts. The diffusion rate of carbon in austenite increases greatly on increasing temperature, thus shortening the total process time (fig. 1.5). At a constant carburizing temperature case depth is proportional to the square root of time.

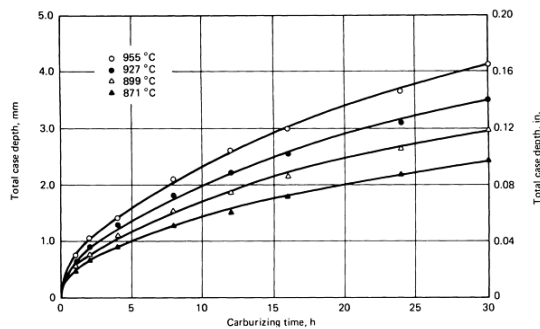


Figure 1.5: effect of the carburizing time and temperature on case depth [11]

## 1.2. Low pressure carburizing

### 1.2.1. Introduction

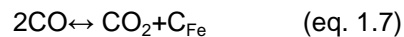
For case hardening of wrought steel, low pressure carburizing (LPC) is increasingly used in the last years [16]. This technique is a variation of the conventional gas carburizing performed under sub-atmospheric pressure. LPC runs under non

## *Chapter 1: Low Pressure Carburizing*

---

equilibrium conditions in two steps: austenite carbon enrichment up to saturation point, defined pure carburizing or boost, and diffusion of carbon, called pure diffusion. The carbon content at the surface of the steel reaches very rapidly the saturation level and the carbon penetration is deeper than after gas carburizing, thanks to the higher temperature (950°C) respect to the traditional endothermic process. The result is a homogeneous and hardened case and a very clean environment.

The standard carburizing, carried out in endogas or in CO containing atmosphere, uses CO as carburizing agent and the metallic surface catalyses a reversible chemical reaction, relies on Boudouard's equation (eq. 1.7), at temperatures of about 850- 900°C [4, 11]:



A clearly defined equilibrium carbon activity (eq. 1.8) can be given as:

$$a_c = K \frac{P(\text{CO})^2}{P(\text{CO}_2)} \quad (\text{eq. 1.8})$$

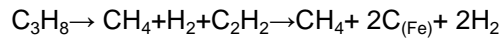
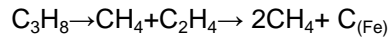
The introduction of oxygen containing compound may result in oxidation. In steels containing alloying elements with high oxygen affinity, like chromium, manganese or silicon, some internal oxidation of these elements can occur along the grain boundaries. Oxides layers are diffusion barriers for carbon penetration and affects negatively the fatigue performances. If sufficient depletion of the alloying elements occurs, hardenability may decrease to the point at which non-martensitic products are formed. The surface has now low hardness and therefore fatigue resistance is reduced. Therefore oxides have to be first reduced.

Low pressure carburizing uses hydrocarbons, as methane (eq. 1.9), propane (eq. 1.10) and acetylene (eq. 1.11), as carburizing agent. These avoid the introduction of oxygen compounds, and therefore the oxidation, and generate a large amount of carbon at the workpiece surface. By using hydrocarbons the carburizing reaction is a virtually irreversible decomposition with different carbon available [4, 5, 8]. The

## *Chapter 1: Low Pressure Carburizing*

---

dissociations take usually place in the temperature range between 900°C- 1000°C at pressures below 20mbar and are given below:



Propane and acetylene generate an higher average carbon flux, 140 and 160g/m<sup>2</sup>h respectively, than methane (5g/m<sup>2</sup>h). Methane molecule breaks down at pressure below 10mbar and at temperature of up to 1050°C, so at normal carburizing temperature and at low pressure (below 20mbar) it has basically no carburizing power and behaves like an inert gas. Pyrolysis of acetylene does not forms methane and as a result, more carbon is transferred to the work pieces. Moreover, acetylene tends to dissociate only in contact with metallic surface which allows an uniform carburizing of steels; the higher carbon available allows to carburizing eventually complex geometries. All these considerations put acetylene significantly ahead of propane. Despite the high carbon availability and the high carburizing capability no soot is formed in low pressure carburizing at pressure of 10mbar.

## Chapter 1: Low Pressure Carburizing

### 1.2.2. The process

Low pressure carburizing is a four-steps process, as reported in figure 1.6 [11, 14, 16- 18]:

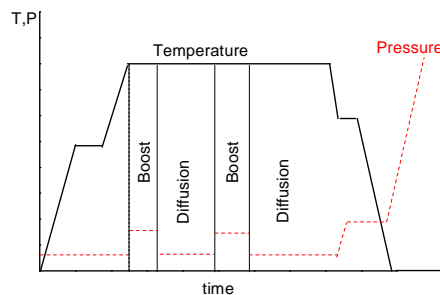


Figure 1.6: low pressure carburizing cycle

**Heat:** the first step is to heat steel up to the carburizing temperature, typically 950°C, and to maintain at the carburizing temperature only long enough to ensure that the steel is uniformly at temperature. During the first step, surface oxidation must be prevented, and any surface oxides present must be reduced. Steels with high oxygen affinity alloying elements usually require a higher vacuum level prior to carburizing.

**Boost step:** this step results in carbon absorption by austenite up to the limit of carbon solubility at the process temperature. The boost step consists into injecting pure hydrocarbon or a mixture of hydrocarbon and nitrogen by pulsation, on increasing the partial pressure up to 30mbar.

Carbon transfer occurs by dissociation of the hydrocarbon gas on the surface of the steel and by direct absorption of the carbon by the austenite. The carbon transfer is so effective that the limit of carbon solubility in austenite is reached after only a few minutes.

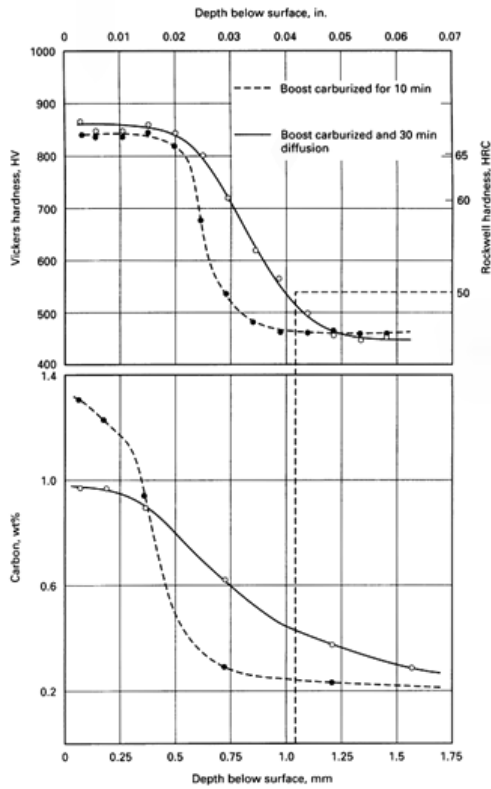


Figure 1.7: microhardness profile and carbon content after boost and boost-diffusion steps [10]

**Diffusion step:** carbon transferred penetrates into the material resulting in a lower surface carbon content and a more gradual case- core transition. The diffusion step is usually performed at low vacuum of about 2mbar and at the same temperature used for carburizing.

Depending on the desired case depth, repeated boost and diffusion steps can be used (fig. 1.7).

**Quenching step:** The cooling of the steel from the diffusion temperature to room temperature, is performed by a partial pressure of gas (6-20bar nitrogen). After quenching the material is tempered to convert the tetragonal martensite into cubic martensite.

### 1.2.3. Low pressure carburizing of PM steels

Sintered steels react faster with the surrounded atmosphere than wrought ones due to their large surface area and therefore require a strict control of the carburizing. The interconnected porosity constitute a preferential way for the carburized gas penetration in the bulk. Consequently, the hardened layer is not uniform and an unusual carbon enrichment can be found in the inner zones.

## Chapter 1: Low Pressure Carburizing

Low pressure carburizing is a suitable candidate to carburized sintered parts because of the more homogeneous and well- defined case layers and the shorter times especially if combined with high pressure gas quenching. Oil quenching requires complicate and expensive washing operations in order to remove oil from the pores.

At low density ( $\leq 6.8\text{g/cm}^3$ ) the penetration of the carburizing agent is so quickly that overcarburizing can occurs. Surface carbon contents raise up to 1.80%- 3.0% and carburized steels with large amounts of carbide forming elements, such as chromium and molybdenum, respond most effectively forming large volumes of massive carbides (fig. 1.8).

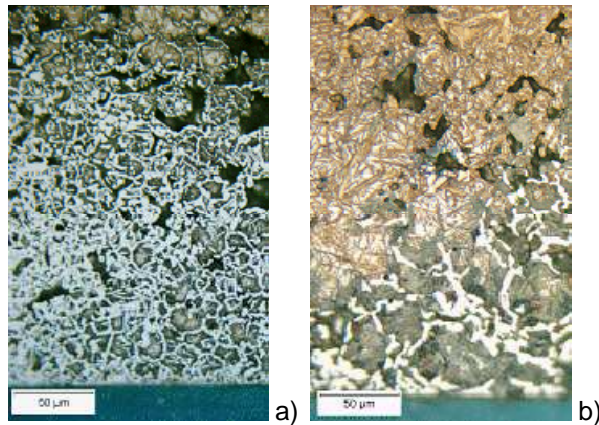


Figure 1.8: low density steels carburized at 920°C: a) ACrM and b) Astaloy Mo [5]

Below this carbides thick layer a second layer is formed that contained carbides at the grain boundaries, whilst grains contained martensite and a large amount of retained austenite, which causes the hardness to drop significantly. These carbides are difficult to dissolve during later stage of carburizing and it is necessary a post solution annealing treatment [4]. By figure 1.8 it is clear that the chromium is a stronger carbides former than molybdenum. In presence of nickel, which is not a carbides former, overcarburizing causes the formation of retained austenite in the

## Chapter 1: Low Pressure Carburizing

---

case. On increasing the treatment temperature the networks of carbide become smaller, whilst the amount of retained austenite tends to increase (fig. 1.9). This effect is due to a decrease in carbon activity and an increase in the solubility of carbon in austenite. A third consequence is the decrease of diffusion step time, shortening the total treatment time [5].

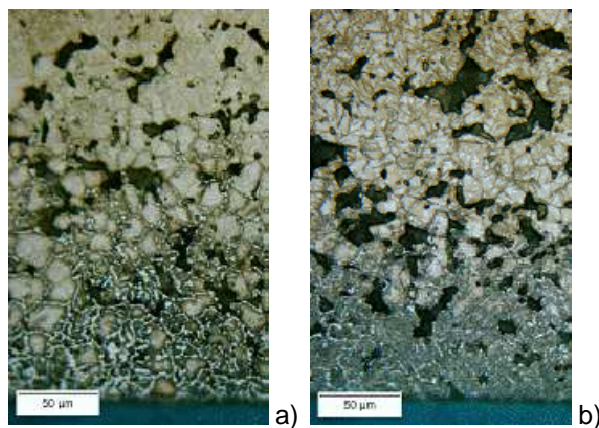


Figure 1.9: low density ACrM carburized at: a) 950°C and b) 1050°C [5]

By using acetylene as carburizing gas instead of propane, the carburizing temperature is higher and a better penetration of cavities is allowed. However, the high carburizing ability of acetylene gives too much carbon at the surface of the component, which is detrimental especially with large surface area. The ability to form and to absorb carbon is very high using the acetylene gas and it is the reason for the large degree of carbide formation. Therefore, in presence of low density it may be better to use propane.

However, in a recent work Danninger et al. have observed the absence of overcarburizing in low pressure carburized Astaloy 85Mo blanks with graded porosity. The core hardness was not affected by the process and a deep microhardness profile is achieved [19].

On exceeding density of  $7.4\text{g/cm}^3$ , where closed porosity can be found, a uniform case depth is achieved (fig. 1.10).



Figure 1.10: surface densified ACrM carburized at 1050°C [5]

At this density the material starts to behave very much as a solid steel. The gas penetrates into the parts homogeneously, due to the slow diffusion rate of carbon through the interface, forming a surface martensitic microstructure with eventually a low amount of austenite. This sintered density can be reached by means of warm compaction with second pressing or high velocity compaction. Post sintering operations, such as rolling or shot peening, can be used to close the surface porosity. This method is particularly efficient for parts subjected to fatigue bending loads or high surface pressures, since the stress decreases rapidly from the surface into the part. The improvement in fatigue resistance is significant and due to the cracks behavior which nucleate below the densified layer and eventually grow towards the surface [5, 20].

The mechanical properties of low pressure carburized sintered steels have not been adequately investigated in literature, however the known data allow to predict an excellent fatigue resistance, in absence of surface overcarburizing [13, 20]. Kanno et al. [20] have shown that low pressure carburizing increases fatigue resistance of around 30% respect to the as sintered condition, however it is lower compared to that of gas carburized steels. Possible reason for this lower fatigue performance is the presence of carbides and retained austenite.





- **Diffusion layer** is characterized by low nitrogen concentration. It can be described as the base microstructure hardened by solid solution and by the precipitation of nitrides; the type and size of these precipitates depend on the chemical composition of the steel. The dissolved nitrogen and the volume expansion of nitrides precipitation causes a compressive residual stress field in the diffusion layer, whilst the compound layer results in a tensile residual stress.

In order to obtain an appreciable hardening and depth of the diffusion layer, materials containing alloying elements with a high affinity for nitrogen, like chromium, aluminum and, molybdenum, have to be selected (fig. 2.2). Copper, nickel and manganese have a negligible interaction with nitrogen.

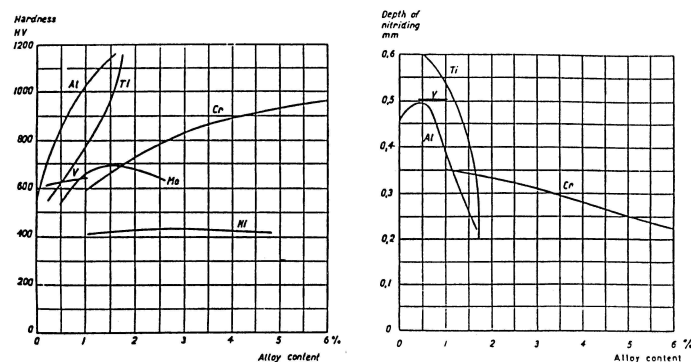


Figure 2.2: alloying elements effect on hardness and case depth [21]

Aluminum is the strongest nitride former, however, more than 1% causes the formation of surface cracks in working condition because the ductile core cannot support the hard case layer. Chromium is a very desirable element because it increases the mechanical properties of steels on increasing both hardenability and nitrability [21, 22]. Chromium forms stable nitrides, but, with high concentration, makes difficult the nitriding treatment because of the high affinity for oxygen that induces surface oxidation. Molybdenum forms stable nitrides at nitriding temperature and reduces the risk of embrittlement. The presence of nickel in the

steel is ineffective to the hardness of the nitride layers due to the low affinity for nitrogen [23].

Looking at the mechanical properties of nitrided steels, the increase in the fatigue resistance is due to the hardened surface and mainly to the compressive residual stresses in the diffusion layer. The fatigue crack nucleate below the surface, where the maximum tensile stress results from the superimposition of residual stress and applied stress, and stop growing inside the diffusion layer [24, 25].

Nitriding can be considered like a finishing operation because it permits minimum distortions and high dimensional control due to the absence of phase transformation.

## **2.2. Plasma nitriding**

### *2.2.1. Introduction*

Plasma nitriding (or ion nitriding) is an extension of conventional nitriding processes using plasma- discharge physics. An electric current is applied in vacuum, in order to reach a differential potential of about 500-1000V, and consequently nitrogen particles are dissociated, ionized and accelerated on the surface components.  $N^+$  ions impact on the steel surface, acquiring an electron and emitting a photon. This emission, which represents the return of nitrogen ions to their atomic state, creates the visible glow discharge that is typical of plasma techniques. The impact between ions and components takes place at high kinetic energy and maintains the component at the nitriding temperature . This results in a very fast saturation of  $\alpha$ -iron so only a few minutes later a coherent layers of iron nitrides exist in equilibrium with the saturated iron.

The two essential factors of the fast diffusion of nitrogen in plasma nitriding are: the high surface concentration of nitrogen, which is of particular relevance at the

beginning of the process, and the increased rate of nitrogen penetration due to the different diffusion mechanism.

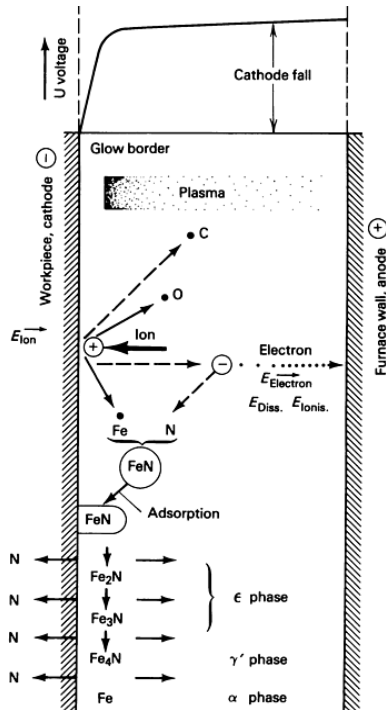


Figure 2.3: interaction between nitrogen ions and surfacepiece [11]

In the early stage of the plasma nitriding process a nitrogen rich phase (FeN) is condense on the nitrated surface as the result of sputtered Fe atoms combining with the incoming nitrogen atoms. Because FeN is not a thermally stable compound it immediately dissociates into lower nitrides. At each dissociation stage, one atom of nitrogen is released, which becomes ready to diffuse into the iron matrix. The nitrogen atoms undergo a volume diffusion, allowing a plane diffusion front (fig. 2.3).

Ion nitriding, like other nitriding processes, produces several distinct structural zones on the base of nitrogen content which include a layer of iron-nitride compounds at the surface ( $\epsilon$  and  $\gamma'$ ) and the diffusion layer made of a saturated solid solution with a fine dispersion of sub micrometric nitride particles. During

the process, different alloy and iron atoms combine with the nitrogen as it diffuses into the material, forming a hardened surface and case [6, 7].

The facility in control of the plasma nitriding variables (temperature, pressure, gas mixture, gas flux, current and voltage) allows a better control of the surface layer with thickness, microstructure and properties well defined. The limitation of plasma nitriding is the equipment cost in comparison with the traditional nitriding process and therefore it is not suitable for the treatment of small components.

2.2.2. The process

A plasma nitriding system is shown in figure 2.4. The component to be nitrided are cleaned and charged in a vacuum furnace. The process of plasma nitriding can be resumed in four steps [11, 14]:

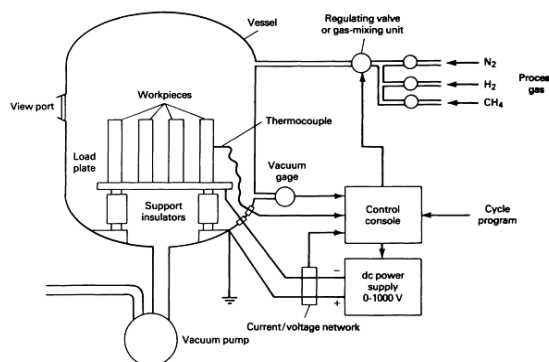


Figure 2.4: typical ion-nitriding system [11]

**Vacuum.** Vacuum is carried out by mechanical pump until about 7-13Pa. This operation is necessary to remove the air and some contaminants presented in the furnace atmosphere.

**Heat.** Heating is assured by resistors, connected to the cathode (work surface piece). During the heating the pressure is increased to lead over the electrical discharge concentration.

**Plasma.** After load is heated to desired temperature, process gas is admitted at a flow rate determined by the load surface area, on increasing pressure up to  $10^2$ - $10^3$ Pa. An electric current is applied and consequently nitrogen particles are dissociated, ionized and accelerated to the surface. The thickness of the glow discharge can be modified by pressure, temperature, composition, potential, electrical current and gas mixture. Usually the thickness is about 6mm.

**Cooling.** The load is cooled by inert-gas circulation.

2.2.3. Plasma nitriding of PM steels

The importance of plasma nitriding as thermochemical treatment for sintered steels has grown together with the idea to produce components for mechanical application with suitable mechanical properties. The main problems in nitriding PM steels is the effect of porosity on nitrogen diffusion and consequently on the diffusion layer thickness. The presence of interconnected pores increases the surface area and enhances the nitrogen absorption and penetration into the bulk of materials. Due to the particular mechanism of nitrogen enrichment the ion nitriding process is less sensitive to the porosity than the other gaseous surface treatments. The diffusion front is uniform on the steel surface which allows an homogeneous nitrogen distribution [6, 7, 26, 27]. Therefore, a preliminary closure of interconnected porosity, performed by expensive operations, is not necessary.

As shows in figure 2.5, in plasma nitrided sintered the compound layer has a good compactness and a uniform thickness in the range 4–10 $\mu\text{m}$ . The compound layer is formed essentially of  $\gamma'$  and  $\epsilon$ , the amount of  $\gamma'$  increases on increasing the treatment temperature and decreasing the density ( $<7.0\text{g}/\text{cm}^3$ ), whilst introducing small amounts of carbon ( $\text{CH}_4$ ) and on increasing density ( $>7.3\text{g}/\text{cm}^3$ ),  $\epsilon$  phase tends to increase [27- 31].

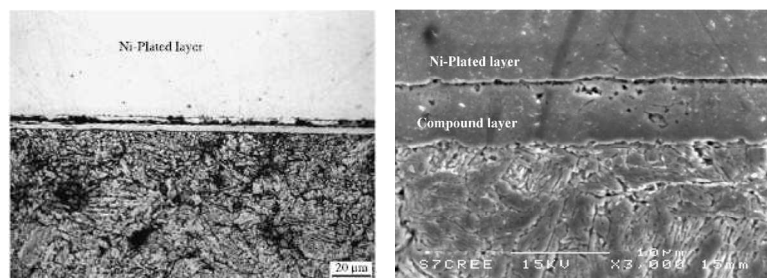


Figure 2.5: compound layer of plasma nitrided sample [31]

Regarding the mechanical properties of plasma nitrided sintered steels, the increased in fatigue resistance is noticeable and due to the surface hardness and

## Chapter 2: Plasma Nitriding

mainly to the compressive residual stresses built up in the diffusion layer. The fatigue crack nucleates in depth, for stresses upper than the difference between residual stress and applied stress, and stops growing inside the diffusion layer [32-34]. The treatment increases wear resistance significantly, and its effect on surface plastic deformation and microcracking is superior than that of through hardening and plasma carburizing. [22, 30].

However, nitriding causes a greater embrittlement in the base material than carburizing: both processes cause a reduction of ductility but this is accomplished by an increase in strength in carburizing only. In nitriding there is not such a compensation between brittleness and strength, then the loss of toughness is much more significant [35].

To improve the toughness of the nitrided steels the hardness of the diffusion layer should be decreases. In principle the microhardness can be reduced by reducing: the nitrogen content in the atmosphere and/or increasing the nitriding temperature. Reducing the nitrogen content in the atmosphere the microhardness of the specimens decreases, as reported in figure 2.6. The microhardness profile of 6.9g/cm<sup>3</sup> ACrM sintered at 1120°C shows a reduction from 990HV0.025 to 920HV0.025 by changing the atmosphere composition from 90N<sub>2</sub>-10H<sub>2</sub> to 60N<sub>2</sub>-40H<sub>2</sub> [31].

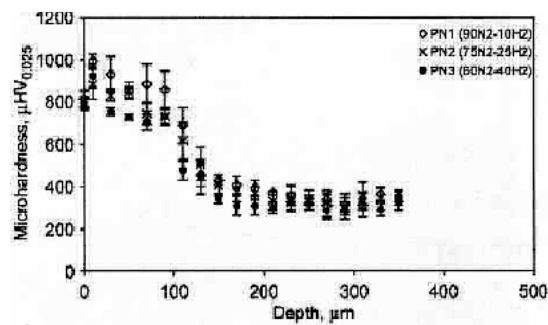


Figure 2.6: microhardness profile changing the atmosphere composition [31]

## *Chapter 2: Plasma Nitriding*

---

Higher nitriding temperatures can improve case hardness but there is a maximum temperature which limit further progress. This maximum temperature depends on the alloying elements and it is fixed by decarburization. It is well know that decarburization is enhanced by high temperature and influences hardness negatively. In order to reduce these negative effect, nitriding treatments should be carried out at lower temperature. Therefore, a compromise is necessary [36].



### **3. Shot Peening**

Shot peening is a mechanical surface working process in which the steel surface is bombarded with a flow of spherical shot at room temperature. Each shot strikes the material creating a small indentation or dimple. The kinetic energy is sufficient to cause the plastic deformation of the subsurface layer and consequently to produce a compressive residual stress field, useful to prevent crack nucleation or to stop crack propagation. Since the fatigue crack does not nucleate or propagate into a compressed material, the compressive residual stress improves the fatigue properties of the treated component up to approximately 70% in comparison to the untreated condition. Therefore shot peening is the most economical and practical method of ensuring surface residual compressive stresses [37- 41]. The compressive residual stress is induced by two phenomena, as reported in figure 3.1: the core constrain on the surface layers (fig. 3.1a), and the Hertzian pressure induced by the impact of each shot (fig. 3.1b) [38, 42].

Therefore, the compressive stress profile has a maximum under the surface which is, at least, as great as half the tensile strength [43].

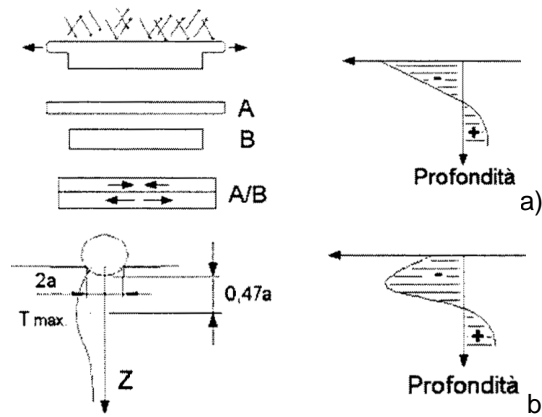


Figure 3.1: compressive residual stress profile: a) surface layers and b) Hertzian pressure

The compressive stress distribution through the thickness of the material can be investigated with the X-ray diffraction method, using  $\sin^2 \psi$  technique. It is not practical to take measure beyond a depth of  $100\mu\text{m}$  and moreover, since fatigue tests are performed in axial direction, only residual stress in this direction are usually measured.

### 3.1. Shot peening parameters

The improve in fatigue performance depends on the shot penning parameters such as the coverage, Almen intensity, relative hardness between shots and material and shots diameter and type [44].

**Shots.** The shots can be made from cast iron, stainless steel, glass and ceramic. For steel parts is typical to use hard steel shots in the range of 55-65HRC or ceramic shots, with hardness comparable to 57-63HRC. To archived high residual stress at great depth under the surface, parts must be peened with shots as hard as the steel surface. Shots can have different diameters depending on the treated surface, and on increasing the diameter the maximum compressive residual stress value increases.

### Chapter 3: Shot Peening

**Coverage.** Coverage is defined as the percentage ratio between peened surface and the original surface (minimum 85%) of the treated steel.

**Peening (Almen) intensity.** The shot peening intensity is defined as the amount of impact energy delivered to the part by the shots. Shot peening intensity is controlled by Almen plats. They are standardized thin plates placed in parallel to the treated material, which receive the same treatment. The deflected shape, due to the deformation induced by residual stress, is called Almen intensity [45]. The intensity is established by plotting the saturation curve, as shown in figure 3.2, and assuming that the required intensity (determined by the arc height) falls on the right side of the knee of the curve. By doubling the time of exposure, the arc height of a test should not increase by more than 10% (the coverage is 100%).

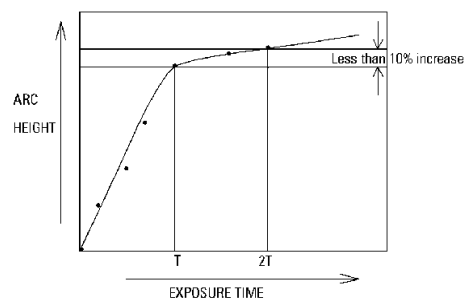


Figure 3.2: intensity determination curve [44]

**Impact Angle.** The impact angle represents the angle between the shots beam and the steel surface.

#### 3.2. Shot peening and thermochemical treatments

In literature many papers attest that shot peening is more effective in fatigue improvement if it is combined to high strength steels, owing to the greater stability of the residual stress. Therefore the combination between shot peening and thermochemical treatments, as carburizing or nitriding, should increase further the

mechanical properties of the steels. In particular, it is possible to find many studies and researches about shot peening application to carburized materials. If shot peening is applied on carburized surface, surface fatigue resistance is increased up to approximately 8- 15% [20, 41]. The case of nitriding plus shot peening is less investigated and applied; this is usually attributed to the fact that nitriding is able by itself to give adequate hardness and fatigue strength and also to the fact that, in high-cycle fatigue applications, cracks in nitrided elements start from an internal inclusion, thus preventing to make effective the residual stresses induced by shot peening. Croccolo et al. [46] have shown that the effectiveness of shot peening on nitrided components is related to the inclusion rate and to the typical inclusion dimension of the steel. The fatigue resistance is increased by shot peening from 3% to 20% with respect to nitriding condition. Pariente et al [47] have demonstrated that shot peening has a positive effect on the fatigue behavior of nitrided elements. The microhardness of steels is increased, just under the surface where residual compressive stresses are higher, and the fatigue resistance is enhanced. In both the cases no appreciable modifications in surface microstructure are archived because the nitriding temperature is not sufficient to modify the grain aspect.

### **3.3. Shot peening of PM steels**

The most decisive parameter in powder metallurgy is density since an increase in density usually improves mechanical properties of the steels. In the manufacturing of sintered steels different ways are used to increase density: after single press and sintering density is around  $7.1\text{g/cm}^3$ . By double pressing and double sintering technique, densities of about  $7.5\text{g/cm}^3$  can be reached. By techniques like powder forging and hot isostaic pressing, full density ( $7.8\text{g/cm}^3$ ) can be exceeded. However, these techniques are very expensive and in many case a local surface densification is sufficient to increase the fatigue properties of PM parts. Sonsino et

### *Chapter 3: Shot Peening*

---

al. [8] have demonstrated that surface rolling improves the endurance resistance by roughly 100%. This is due to the interaction of different mechanisms: the surface densification, the increase of hardness and the build-up of compressive residual stresses which contribute to stop crack propagation.

A very effective and economic post sintering alternative to increase the fatigue properties is shot peening. The improvement in fatigue strengths, reported by Saritas et al. [9], ranges from 30% (pure iron) to 48% (Fe-0.5%C) with respect to the as sintered condition. This increase in fatigue performance is due to both compressive residual stresses and surface densification, which closes most of the pores in surface layers, up to 400 $\mu$ m depth.

The effective stress distribution in the subsurface layers can be obtained by superimposing the applied stress and the residual stresses. Therefore, the fatigue crack nucleates beneath this layer in correspondence to a cluster of pores or a large pore and propagate along the network of interconnected pores. Shot peening moves the site for crack initiation towards the interior, improving the fatigue resistance.

However, too heavy shot peening is not beneficial to the mechanical properties of the treated material because the hardened layer produced could be eroded by excessive shot peening [9]. Moreover, it could impair dimensional and geometrical precision of steel parts, which is one of the main attracting characteristics of PM components.

## 4. Materials and Experimental Procedures

### 4.1. Materials

Two main groups of low alloyed steels were investigated: Cr containing steels and Cr free ones. The chemical composition of the powders produced by Höganäs, AB [48], used for the preparation of the specimens, is reported in table 4.1.

Table 4.1: nominal composition (wt.%) of the powders investigated

Code	Powders	%Cr	%Mo	%Mn	%Ni	%Cu	%Fe
Cr steels	ACrL	1.5	0.2				bal.
	AD4	0.8		0.4			bal.
	ACrM	3	1.5				bal.
Cr free steels	ALH		0.9		0.9		bal.
	DLH		0.9		0.9	2	bal.

Astaloy CrL was widely studied and applied in manufacturing of PM parts while the other steels are based on new powders. The powders are water atomized prealloyed with Cr, Mo and Ni. Cu was added by diffusion bonding.

Graphite C-UF4 was added to the powder mixes to obtain a final carbon content of 0.05%, 0.2% and 0.4%. Conventional lubricant, typically 0.6% of Kenolube, was added to the powder mixes.

## *Chapter 4: Materials and Experimental Procedures*

---

### *4.1.1. Compaction*

Different compaction methods were used depending on the required density. In order to obtain a green density of  $6.8\text{g/cm}^3$  and  $7.0\text{g/cm}^3$ , cold compaction with 600MPa applied pressure was used. Green density of  $7.4\text{g/cm}^3$  was obtained by using warm compaction.

### *4.1.2. Sintering*

Sintering was carried out at two different temperatures: 1250°C and 1120°C with 60 and 30 minutes of isothermal holding respectively. The lower temperature was carried out in a continuous belt furnace in a 90%N<sub>2</sub>/10%H<sub>2</sub> atmosphere, the cooling rate obtained in this furnace is close to 0.8°C/s. The higher temperature sintering was carried out in a batch furnace in a 90%N<sub>2</sub>/10%H<sub>2</sub> atmosphere, the cooling rate obtained in this furnace is close to 1°C/s.

### *4.1.3. Secondary heat treatment*

Secondary heat treatments were carried out in industrial plants. The parameters of heat treatment cycles (low pressure carburizing, plasma nitriding and shot peening) are reported in the relevant section in the following chapters.

## **4.2. Experimental procedures**

A general overview on the experimental and testing procedures is presented below.

## *Chapter 4: Materials and Experimental Procedures*

---

### *4.2.1. Chemical analysis*

The combustion techniques (LECO) are used for the determination of carbon, nitrogen, oxygen in steels. The techniques are useful for the analysis of these elements over a wide concentration range.

Tests have been done in accordance with ASTM E1019 (Standard Test Methods for Determination of Carbon, Sulfur, Nitrogen, and Oxygen in Steel and in Iron, Nickel, and Cobalt Alloys) on specimens of about 0.5-1g.

### *4.2.2. Density and porosity*

Density was measured in according to ASTM B 328-96. Specimens impregnation was made in oil with a density of  $0.823\text{g/cm}^3$ . Measurements were performed on a precision balance (Gibertini E42) with sensibility of 0.001g.

### *4.2.3. Dilatometry*

The study of the variation of the relative change in length as a function of temperature was carried out by means of a dilatometer (DIL 805A/D quenching and deformationdil by Bähr-Thermoanalyse). Dilatometric tests were performed on 4x4x10mm samples which were positioned in the chamber in contact with the alumina bars. The control of temperature was made by means of a thermocouple welded on the specimen. Experiments were carried out in an inert atmosphere to avoid the oxidation of samples.



## Chapter 4: Materials and Experimental Procedures

---

### 4.2.4. Metallography

Metallographic characterization was carried out by a LOM microscopy (LEICA DC300) on polished and etched samples. The etching agents are listed in table 4.2.

Table 4.2: Etching solutions

Materials	Etching agents	Composition
AD4	Nital 2%	2% Nitric acid solution in ethanol
ACrL, ALH and DLH	Nital- Picral	50% Nital- 50% Picral
	Picral 2%	2% Picric acid solution in ethanol

### 4.2.5. Hardness and microhardness

Hardness and microhardness of materials were measured by the Vickers method (ASTM c 730-98). The applied load was 10 Kg for hardness test and from 0.05 - 0.1Kg in case of microhardness test. The reported values represent the average of 7 indentations.

### 4.2.6. Impact test

Impact tests were carried at room temperature on unnotched test bars (ASTM E 23), using a Charpy instrumented pendulum (Wolpert). During the test the impact direction was perpendicular to the compaction surface, according to the standard. Available energy was 150J with a impact velocity of 3.9m/s. In figure 4.1 the typical impact load-deflection curve is reported.

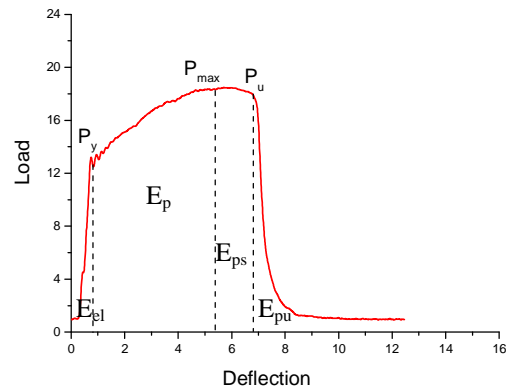


Figure 4.1: theoretical load-deflection curve

The absorbed impact energy can be divided in energy required for elastic deformation ( $E_{el}$ ), for plastic deformation until crack nucleation ( $E_p$ ) and for propagating fracture: stable crack propagation ( $E_{ps}$ ) and unstable crack propagation ( $E_{pu}$ ).

Moreover, the yielding load ( $P_y$ ), the maximum load ( $P_{max}$ ), the load at the onset of unstable crack propagation ( $P_u$ ) and the correspond deflection can all be determined from the record.

Given the density of the investigated materials, the energy required for the propagation is quite low and negligible with respect to that necessary for crack initiation.

#### 4.2.7. Transverse Rupture Strength (TRS) test

The transverse rupture test defines the stress, calculated from the three-point formula, required to break a specimen supported near the ends when a compressive force is applied parallel to the pressing direction of specimen (ASTM B 528-05). This test is only applied to relatively brittle materials. According to the standard ASTM B 925-03, the rectangular test specimen dimensions are 12,7x 31,8x 6,35mm.

## Chapter 4: Materials and Experimental Procedures

### 4.2.8 Bending fatigue test

Modified ISO 3928 specimens were used to perform bending fatigue tests. In figure 4.2 the unnotched specimen is shown with an attention on the particular edge geometry which eliminates the influence of the shape edge on crack nucleation [49].

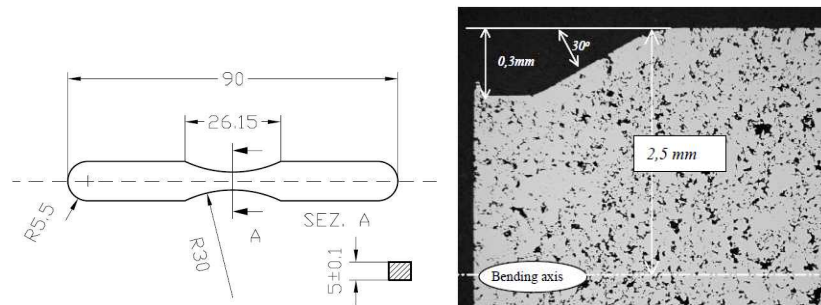


Figure 4.2: Modified ISO 3928 test specimen with chamfered edges [49]

Fatigue tests were carried out in 4 points bending mode on a Schenck machine, at 30Hz of frequency and with load ratio  $R = \sigma_{\min} / \sigma_{\max} = -1$ . The fatigue resistance, defined as 50% survival value, was calculated by the stair case method with a run out of  $2 \times 10^6$  cycles (standard MPIF 56- 2001). The stair case step was fixed at 15 MPa.

### 4.2.9. Fractography

The surface and the fracture surface of the materials were observed at the ESEM.

## 5. Chromium Steels: as sintered microstructure and mechanical properties

### 5.1. Effect of carbon content, density and sintering temperature on microstructure and microhardness

The materials investigated in this part are ACrL and AD4. Graphite was added to the base powder in order to obtain 0.05% ( $\pm 0.04$ ), 0.2% ( $\pm 0.04$ ) and 0.4% ( $\pm 0.02$ ) carbon. Impact bars were compacted to green density of 6.8g/cm<sup>3</sup>, 7.0g/cm<sup>3</sup> and 7.4g/cm<sup>3</sup>. Sintering was carried out at 1120°C (L) and 1250°C (H). The carbon content in the as sintered materials is reported in table 5.1, with reference to the nominal one. The analysis was carried out only on 6.8g/cm<sup>3</sup> steels.

Table 5.1: results of carbon analysis

	Green/nominal %C	As sintered %C
ACrL 6.8g/cm <sup>3</sup> 1120°C	0.05	0.06
ACrL 6.8g/cm <sup>3</sup> 1250°C	0.05	0.02
ACrL 6.8g/cm <sup>3</sup> 1120°C	0.2	0.19
ACrL 6.8g/cm <sup>3</sup> 1250°C	0.2	0.16
ACrL 6.8g/cm <sup>3</sup> 1120°C	0.4	0.44
ACrL 6.8g/cm <sup>3</sup> 1250°C	0.4	0.31
AD4 6.8g/cm <sup>3</sup> 1120°C	0.05	0.09
AD4 6.8g/cm <sup>3</sup> 1250°C	0.05	0.03
AD4 6.8g/cm <sup>3</sup> 1120°C	0.2	0.22
AD4 6.8g/cm <sup>3</sup> 1250°C	0.2	0.17
AD4 6.8g/cm <sup>3</sup> 1120°C	0.4	0.47
AD4 6.8g/cm <sup>3</sup> 1250°C	0.4	0.30

## Chapter 5: Chromium Steels

Because of the high oxygen affinity of chromium, the oxide which covers the powder particles is very stable. The main reducing agent is graphitic carbon associated with high temperature, which is beneficial both for complete reduction and for optimum mechanical properties [50, 51]. However, decarburization takes place in the samples sintered at 1250°C and it increases on increasing the green carbon content (fig. 5.1).

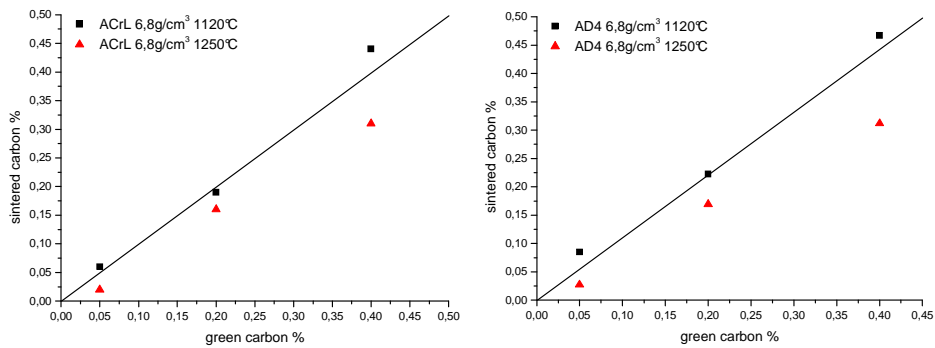


Figure 5.1: sintered carbon vs green carbon for ACrL and AD4

The as sintered density of ACrL and AD4 is presented in figure 5.2 as a function of carbon content.

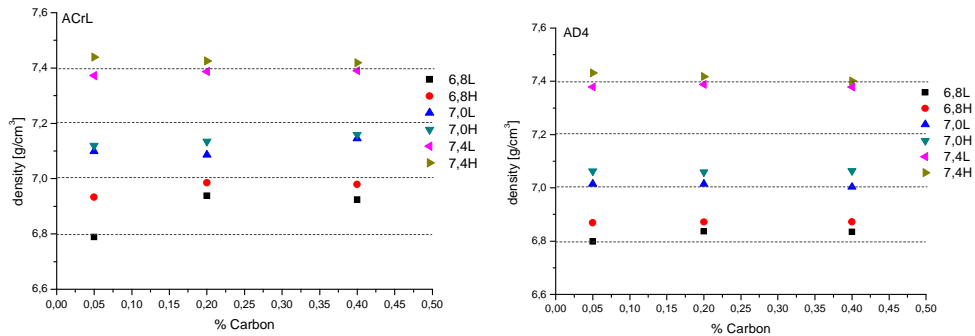


Figure 5.2: as sintered density of ACrL and AD4

As sintered density slightly increases with high sintering temperature [48]. The increase in density induced by high sintering temperature is tendentially higher in cold compacted specimens than in warm compacted ones and decreases on increasing carbon content. The maximum increase is  $0,15\text{g/cm}^3$ . Total porosity, presented in figure 5.3 as sum of closed and open porosity, decreases on increasing green density, carbon content and sintering temperature. The residual porosity is almost fully closed in  $7.4\text{g/cm}^3$  materials.

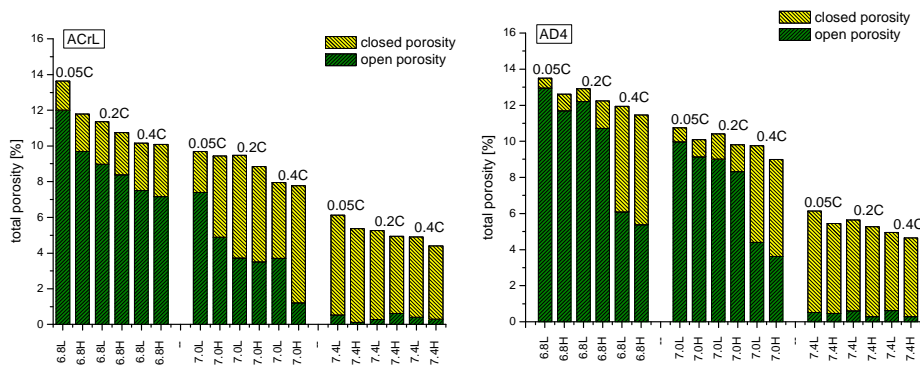


Figure 5.3: porosity of ACrL and AD4

It is well known that porosity is not uniformly distributed in the sintered steels. Pore aspect can be described by using two factors,  $F_{\text{circle}}$  and  $F_{\text{shape}}$ , determined by image analysis on metallographic samples.  $F_{\text{circle}}$  represents the profile irregularity of pores ( $F_{\text{circle}} = \pi A/P^2$ ), whilst  $F_{\text{shape}}$  is representative of the pore elongation ( $F_{\text{shape}} = D_{\text{min}}/D_{\text{max}}$ ). Both parameters range from 0 (elliptic pore) to 1 (circular pore). The reference to the ellipse morphology diagram (fig. 5.4) may help in recognizing the effect of process variables on pore characteristics. Figure 5.5 shows that the parameters, which are expected to improve pore morphology, i. e. higher density and sintering temperature, move the experimental points of 0.05% C ACrL towards the upper right corner of the diagram. In particular, the effect of sintering temperature is more evident.

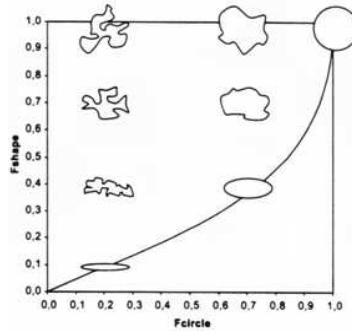


Figure 5.4: ellipse morphology diagram

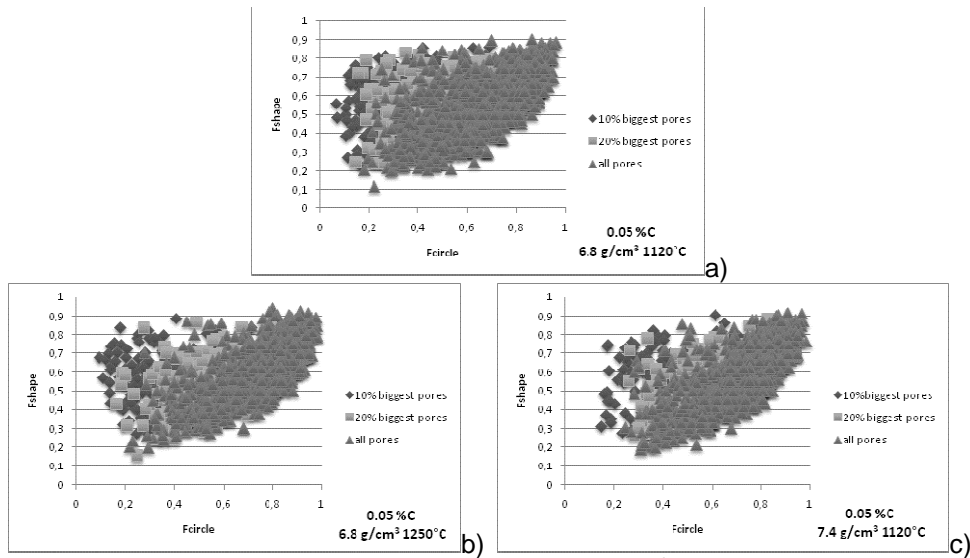


Figure 5.5:  $F_{circle} - F_{shape}$  of 0.05%C ACrL: a)  $6.8\text{g/cm}^3$  sintered at  $1120^\circ\text{C}$ , b)  $6.8\text{g/cm}^3$  sintered at  $1250^\circ\text{C}$  and c)  $7.4\text{g/cm}^3$  sintered at  $1120^\circ\text{C}$

Figures 5.6 and 5.7 present the typical microstructures of the  $6.8\text{g/cm}^3$  steels for different carbon contents. Microstructure is mainly: ferritic in 0.05%C steels, ferritic-perlitic in 0.2%C steels, with a large amount of perlite (around 40%) in ACrL, bainitic in 0.4%C ACrL and ferritic perlitic (around 50- 50) in 0.4%C AD4. An increase in sintering temperature results in the refining of the perlite and bainite, whilst the increase in density does not influence the microstructure.

*Chapter 5: Chromium Steels*

The effect of the sintering temperature can be interpreted considering that the CCT curves move towards the right on increasing the temperature from which austenite is cooled down. All the other microstructures are reported in appendix.

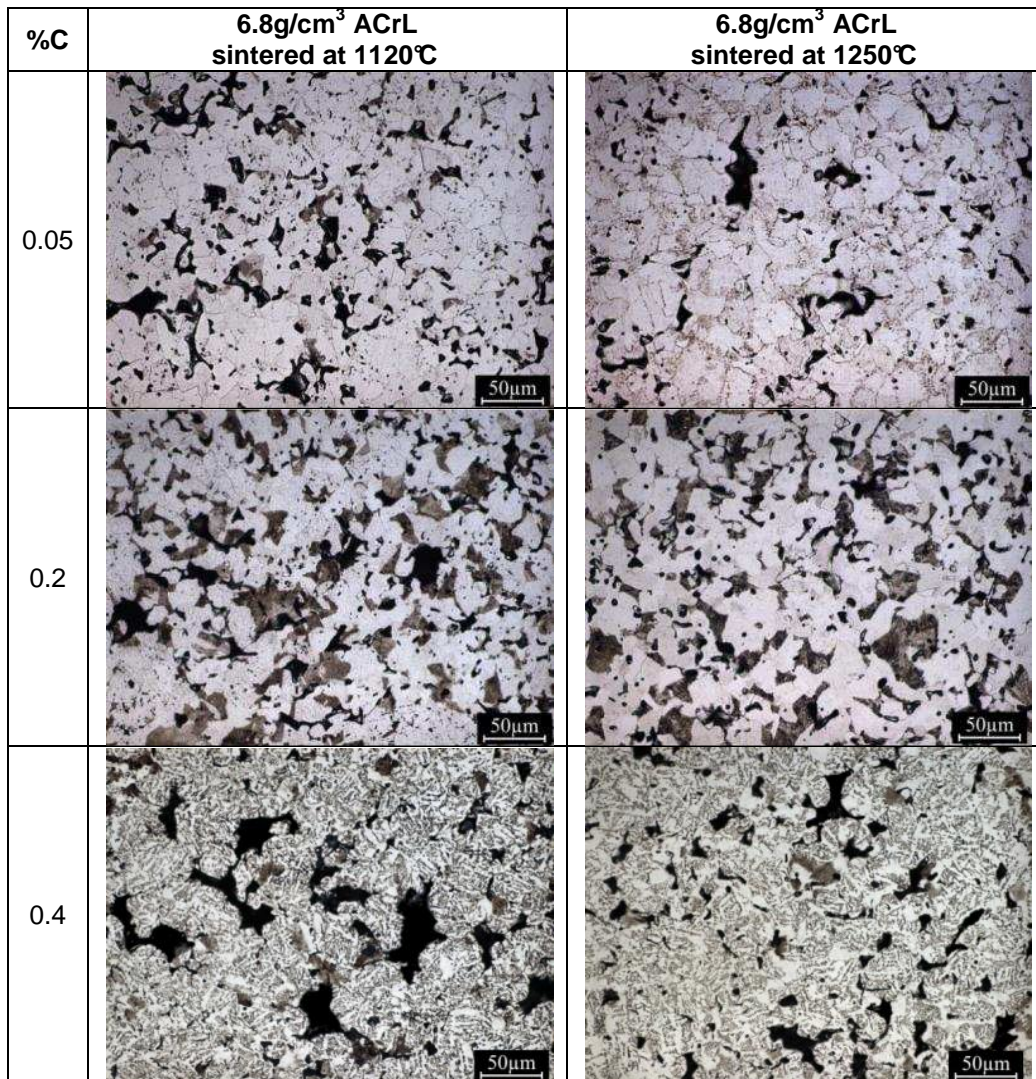


Figure 5.6: microstructures of 6.8g/cm<sup>3</sup> 0.05%, 0.2% and 0.4%C ACrL sintered at 1120°C and 1250°C



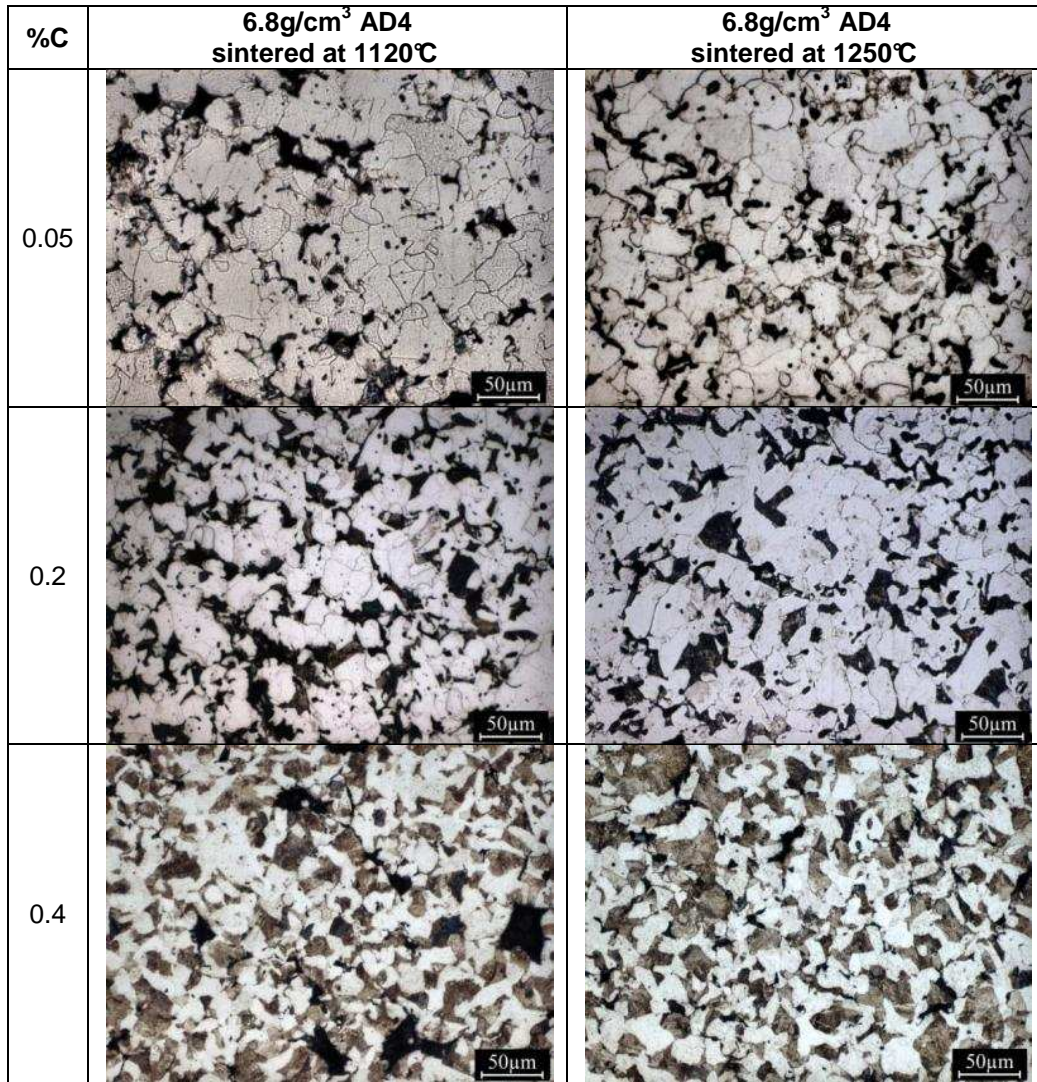


Figure 5.7: microstructures of 6.8g/cm<sup>3</sup> 0.05%, 0.2% and 0.4%C AD4 sintered at 1120°C and 1250°C

*Chapter 5: Chromium Steels*

Hardness and microhardness of the materials are listed in table 5.2-5.3.

Table 5.2: hardness and microhardness of as sintered ACrL

Material	%C	Density [g/cm <sup>3</sup> ]	T sintering	HV10	HV0.05
ACrL	0.05%C	6.8	1120°C	56 ± 1	87 ± 5
			1250°C	60 ± 1	90 ± 5
		7.0	1120°C	65 ± 1	88 ± 9
			1250°C	68 ± 1	123 ± 3
		7.4	1120°C	84 ± 1	115 ± 14
			1250°C	92 ± 4	122 ± 7
	0.2%C	6.8	1120°C	79 ± 6	118 ± 15
			1250°C	80 ± 2	131 ± 21
		7.0	1120°C	89 ± 2	124 ± 19
			1250°C	91 ± 1	142 ± 18
		7.4	1120°C	113 ± 2	145 ± 17
			1250°C	114 ± 3	149 ± 14
	0.4%C	6.8	1120°C	126 ± 4	248 ± 33
			1250°C	158 ± 3	271 ± 16
		7.0	1120°C	150 ± 8	253 ± 17
			1250°C	168 ± 6	273 ± 20
		7.4	1120°C	207 ± 1	246 ± 15
			1250°C	211 ± 3	247 ± 40

Table 5.3: hardness and microhardness of as sintered AD4

Material	%C	Density [g/cm <sup>3</sup> ]	T sintering	HV10	HV0.05
AD4	0.05%C	6.8	1120°C	54 ± 2	87 ± 3
			1250°C	54 ± 2	86 ± 11
		7.0	1120°C	62 ± 1	98 ± 9
			1250°C	62 ± 3	93 ± 16
		7.4	1120°C	84 ± 1	102 ± 6
			1250°C	92 ± 9	117 ± 5
	0.2%C	6.8	1120°C	71 ± 1	101 ± 11
			1250°C	73 ± 1	132 ± 12
		7.0	1120°C	78 ± 2	103 ± 14
			1250°C	81 ± 1	143 ± 22
		7.4	1120°C	101 ± 1	131 ± 16
			1250°C	103 ± 4	150 ± 31
	0.4%C	6.8	1120°C	96 ± 1	172 ± 16
			1250°C	95 ± 2	180 ± 27
		7.0	1120°C	104 ± 2	169 ± 23
			1250°C	114 ± 5	176 ± 26
		7.4	1120°C	136 ± 3	166 ± 15
			1250°C	143 ± 4	215 ± 15

0.05% and 0.2%C ACrL has a microhardness similar to AD4 with the same carbon content, since the materials have the same microstructure and the solution hardening effect of the alloying elements is very similar (fig. 5.8).

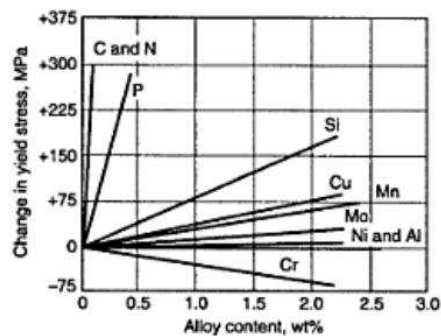


Figure 5.8: effect of alloying elements on solution hardening

## Chapter 5: Chromium Steels

The microhardness of 0.4%C ACrL is greater than that of 0.4%C AD4, because of the different microstructure. According to the multiplying hardenability factors, the two materials have the same hardenability but chromium and molybdenum have a greater effect on retarding the perlite formation than manganese, favouring the formation of bainite.

To confirm the different microstructures of the two materials, a dilatometry investigation of the austenite transformations on cooling was carried out. The variation of the relative change in length as a function of temperature achieved by 7.0 g/cm<sup>3</sup> ACrL sintered at 1120°C is reported in figure 5.9 f or 0.05%C and 0.4%C.

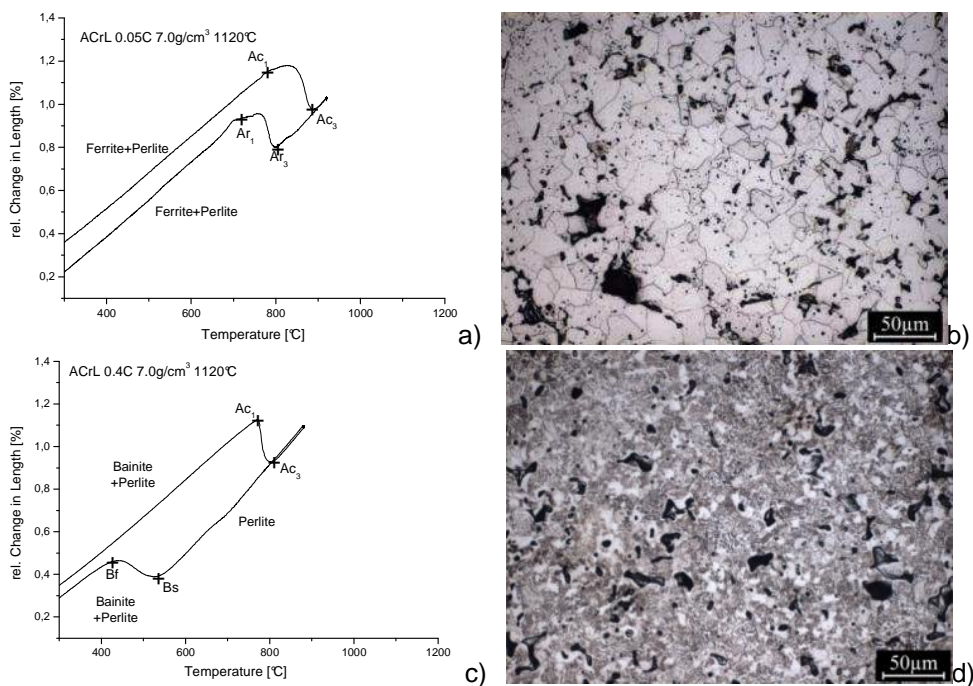


Figure 5.9: dilatometric curve (a) and microstructure (b) of 7.0g/cm<sup>3</sup> 0.05%C ACrL, dilatometric curve (c) and microstructure (d) of 7.0g/cm<sup>3</sup> 0.4%C ACrL

The formation of austenite takes place between  $A_{c1}$  and  $A_{c3}$  temperatures that represent the temperature at which the ferrite (with trace of perlite, - perlite), in

## Chapter 5: Chromium Steels

0.05%C steels, and bainite (- perlite), in 0.4%C materials, to austenite transformation starts and ends, respectively [52, 53].  $A_{c1}$  is defined as the temperature at which the linear thermal expansion deviates from the linearity. This behaviour is caused by the volume contraction associated with the austenite formation. Likewise the transformation finish temperature  $A_{c3}$  is determined by extrapolating the linear portion of the curve after transformation.

The  $A_{r3}$  and  $A_{r1}$  temperatures correspond to start and end temperature of austenite decomposition into ferrite (- perlite), respectively (fig. 5.9a). The final microstructure, composed of ferrite (- perlite), is confirmed by the metallographic analysis reported in figure 5.9b.

On increasing the carbon content (fig. 5.9c) a different transformation takes place during cooling. Figure 5.9d shows that the final microstructure is composed of bainite and trace of perlite. Since perlite is formed at higher temperature than bainite, there is no doubt that the first slight volume expansion corresponds to the transformation of austenite into perlite, whereas the expansion shown at the lower temperature corresponds to the austenite to bainite transformation.  $B_s$  is the temperature at which the dilatometric curve deviates from the linearity due to the volume expansion associated to the bainite formation;  $B_f$  is the temperature at which the austenite to bainite transformation ends. The transformation temperatures thus determined are shown in table 5.4.

Table 5.4: transformation temperatures determined by dilatometry

T [°C]	ACrL		AD4	
	0.05%C	0.4%C	0.05%C	0.4%C
$A_{c1}$	770	770	740	740
$A_{c3}$	890	808	880	808
$A_{r3}$	790		788	686
$A_{r1}$	747		750	637
$B_s$		529		
$B_f$		441		

## Chapter 5: Chromium Steels

---

The ferrite, perlite and bainite percentages, measured by image analysis, are reported in table 5.5.

Table 5.5: phase fractions

Microstructure	ACrL		AD4	
	0.05%C	0.4%C	0.05%C	0.4%C
Ferrite	95%		95%	50%
Perlite	5%	12	5%	50%
Bainite		88%		

The variation of the relative change in length as a function of temperature carried out on  $7.0\text{g/cm}^3$  AD4 sintered at  $1120^\circ\text{C}$  is reported in figure 5.10 f for 0.05%C and 0.4%C. The dilatometric and metallographic analysis show the formation of the same microstructure of ferrite plus perlite but the amount of perlite increases on increasing the carbon content (tab. 5.5). The transformation temperatures are shown in table 5.4.

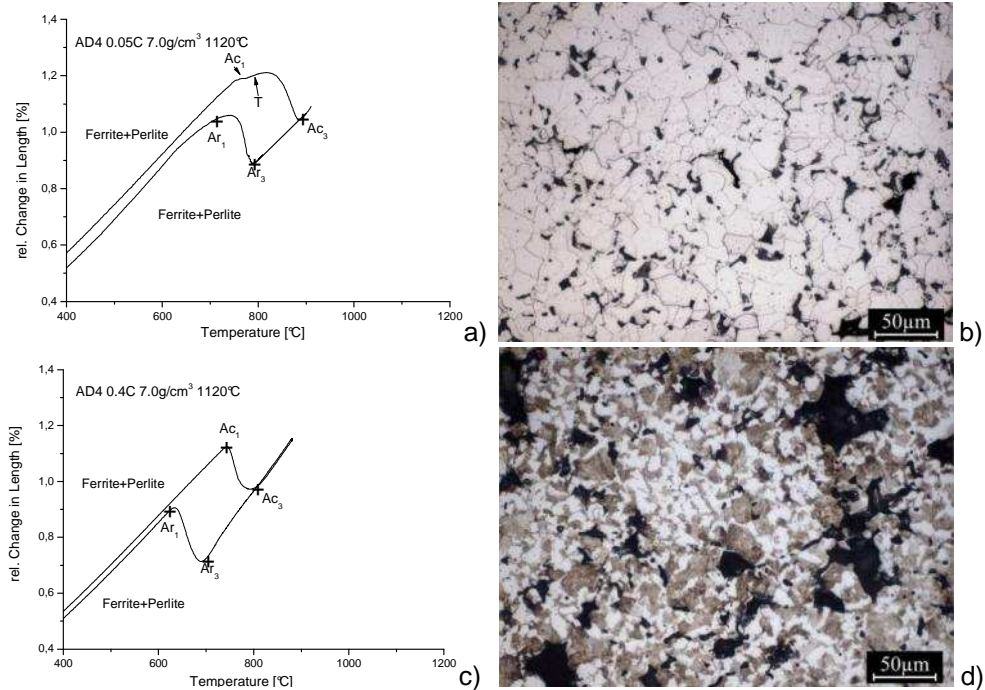


Figure 5.10: dilatometric curve (a) and microstructure (b) of  $7.0\text{g/cm}^3$  0.05% C AD4, dilatometric curve (c) and microstructure (d) of  $7.0\text{g/cm}^3$  0.4% C AD4

The dilatometry results of the austenite transformation on cooling confirm the microstructures shown in figures 5.6 and 5.7. At the highest carbon content (0.4%) Cr and Mo have a greater effect on forming bainite than Mn, which favours the perlite formation.

## 5.2. Impact toughness

Figure 5.11 shows impact energy of the materials as a function of density, when sintering temperature is  $1120^\circ\text{C}$ . Figure 5.12 shows the effect of the sintering temperature on impact energy.

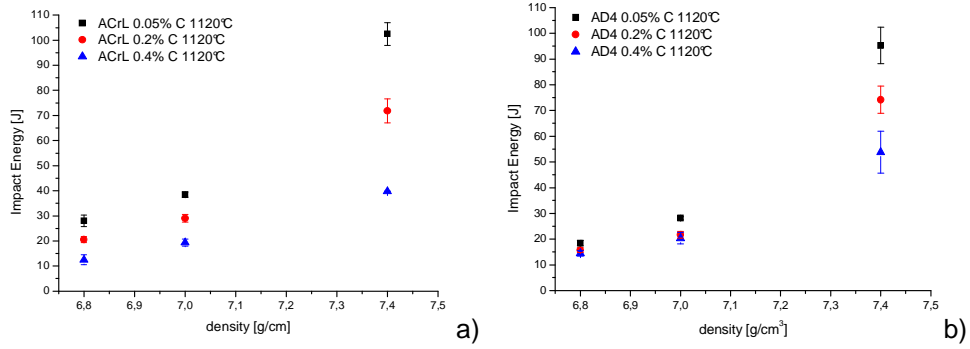


Figure 5.11: effect of density and carbon percentage on impact energy: a) ACrL and b) AD4

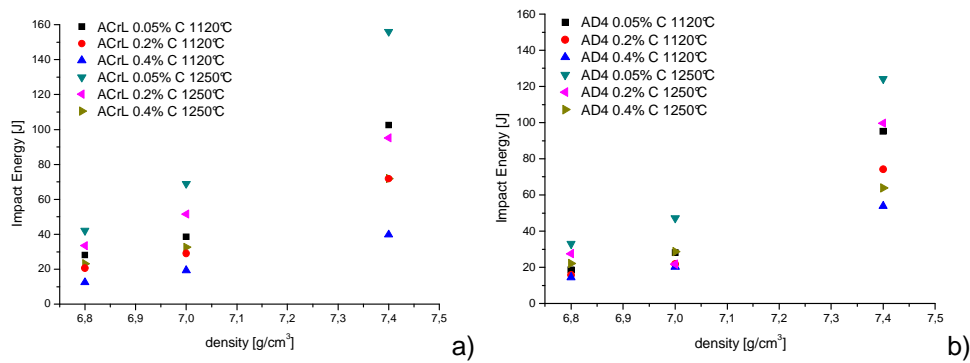


Figure 5.12: effect of sintering temperature on impact energy: a) ACrL and b) AD4

Impact energy increases with density, decreases with the carbon content and increases with the sintering temperature, as expected. All the materials have an elasto-plastic behaviour with a distinct yield point followed by strain hardening, as shown by the impact curves in figure 5.13.



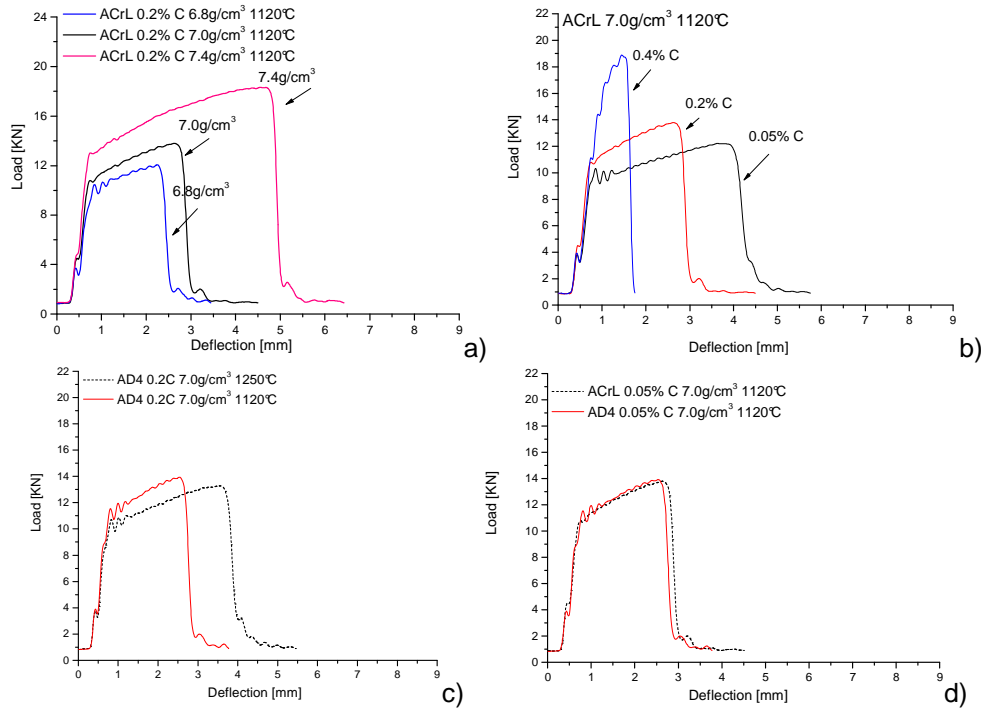


Figure 5.13: load- deflection curves as a function of: a) density, b) carbon percentage, c) sintering temperature and d) chemical composition

Concerning the effect of density, the comparison of impact curves of 0.2%C ACrL sintered at 1120°C, reported in figure 5.13a, indicates that yield load ( $P_y$ ), maximum load ( $P_{max}$ ) and deflection increase from 6.8g/cm<sup>3</sup> to 7.0g/cm<sup>3</sup> and even more to 7.4g/cm<sup>3</sup>, because of the increase in the load bearing section.

On increasing the carbon content, the load-deflection curves of 7.0g/cm<sup>3</sup> ACrL sintered at 1120°C, shown in figure 5.13b, indicate that deflection decreases whilst  $P_y$  and  $P_{max}$  increase. However, the overall effect is the decrease of the impact energy.

Figure 5.13c shows the load-deflection curves of 7.0g/cm<sup>3</sup> 0.2%C AD4 sintered at two temperatures. The effect of temperature is that of increasing ductility (represented by deflection), with a slight decrease of yield and maximum loads

## Chapter 5: Chromium Steels

(due to decarburization, tab. 5.6). The increase in ductility is due to the effect of the load bearing section by the high sintering temperature.

Table 5.6: carbon content of as sintered AD4

	%C
AD4 0.2%C 7.0 g/cm <sup>3</sup> 1120°C	0.209
AD4 0.2%C 7.0 g/cm <sup>3</sup> 1250°C	0.158

In the end, figure 5.13d shows the curves of the materials, with the same carbon content (0.05%), density (7.0g/cm<sup>3</sup>) and sintering temperature (1120°C). The load-deflection curves are very similar because the microstructures are the same. The results of the impact test (impact energy, P<sub>y</sub> and P<sub>max</sub>) are reported in appendix.

### 5.2.1. A simplified model for impact strength of sintered steels

Impact energy increases with density, but different correlations are observed at different sintering temperatures. Sintering temperature, in fact, increases the load bearing section even without increasing density, due to the growth of the neck size. Therefore, the possibility to correlate impact strength to the load bearing section of the sintered steels was investigated.

The load bearing section ( $\Phi$ ) can be calculated by the equations 5.1 and 5.2, which were determined in a previous work on low alloyed steels in a density range 6.6-7.1 g/cm<sup>3</sup> [54].

$$\Phi = (1 - K_p \cdot \varepsilon)^2 \quad (\text{eq. 5.1})$$

$$K_p = 5.58 - 5.7 \cdot F_{\text{circle}} \quad (\text{eq. 5.2})$$

where  $\varepsilon$  is the fractional porosity and  $F_{\text{circle}}$  represents the profile irregularity of pores.

Several ACrL based steels have been studied with different green density, carbon content and sintering temperature. They are listed in table 5.7 and their microhardness in table 5.8.

*Chapter 5: Chromium Steels*

Table 5.7: microstructures of the Cr steels investigated

ACrL	6.8g/cm <sup>3</sup>		7.0g/cm <sup>3</sup>		7.4g/cm <sup>3</sup>	
	1120°C	1250°C	1120°C	1250°C	1120°C	1250°C
0.05%C	Ferrite	Ferrite	Ferrite	Ferrite	Ferrite	Ferrite
0.2%C	50 Ferrite 50 Perlite	50 Ferrite 50 Perlite	50 Ferrite 50 Perlite	50 Ferrite 50 Perlite	50 Ferrite 50 Perlite	50 Ferrite 50 Perlite
0.3%C	20 Ferrite 80 Perlite	Bainite	20 Ferrite 80 Perlite	Bainite	-	-
0.4%C	20 Perlite 80 Bainite	20 Perlite 80 Bainite	20 Perlite 80 Bainite	20 Perlite 80 Bainite	20 Perlite 80 Bainite	20 Perlite 80 Bainite
0.5%C	20 Perlite 80 Bainite	20 Perlite 80 Bainite	20 Perlite 80 Bainite	20 Perlite 80 Bainite	-	-
0.8%C	Perlite	Perlite	Perlite	Perlite	-	-

Table 5.8: microhardness of the Cr steels investigated

ACrL HV0.05	6.8g/cm <sup>3</sup>		7.0g/cm <sup>3</sup>		7.4g/cm <sup>3</sup>	
	1120°C	1250°C	1120°C	1250°C	1120°C	1250°C
0.05%C	86.9±4.6	89.7±5.1	88.2±8.9	123.1±31.0	115.2±14.2	122.1±7.2
0.2%C	118.2±15.4	131.3±21.2	124.3±19.4	141.5±17.7	144.5±17.0	149.2±14.9
0.3%C	217.3±22.0	-	219.8±28.6	-	-	-
0.4%C	247.7±33.2	271.0±16.3	253.1±17.8	272.5±26.9	246.0±15.8	246.8±41.6
0.5%C	323.4±28.4	355.5±43.1	320.2±31.9	337.4±35.2	-	-
0.8%C	409.2±31.2	412.4±30.6	404.8±16.8	397.4±27.1	-	-

In this section only the investigation on ferritic steels (0.05%C) is analyzed and discussed, whilst the model results for the ferritic- perlitic, bainitic (- perlitic) and perlitic steels are reported in appendix.

*Chapter 5: Chromium Steels*

Table 5.9 reports the values of load bearing section, calculated by equations 5.1 and 5.2, for 0.05%C ACrL. The load bearing section depends significantly on sintering temperature, and the dependence increases with porosity (fig. 5.14).

Table 5.9: load bearing section of 0.05%C ACrL

0.05%C ACrL	6.8g/cm <sup>3</sup>		7.0g/cm <sup>3</sup>		7.4g/cm <sup>3</sup>	
	1120°C	1250°C	1120°C	1250°C	1120°C	1250°C
$F_{circle}$	0.65	0.77	0.66	0.76	0.71	0.76
$\epsilon$	0.136	0.128	0.097	0.094	0.061	0.054
$K_p$	1.88	1.19	1.82	1.25	1.56	1.25
$\Phi$	0.56	0.72	0.68	0.78	0.82	0.87

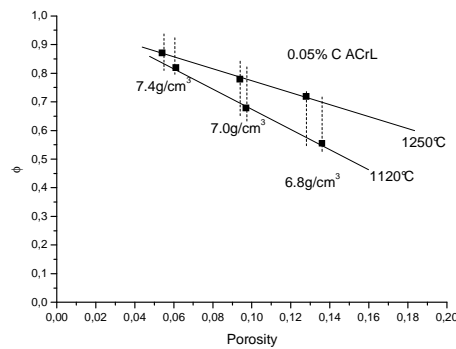


Figure 5.14: load bearing fraction as a function of porosity and sintering temperature

Impact toughness depends on strength, represented by yield load ( $P_y$ ) and maximum load ( $P_{max}$ ), and on ductility, represented by deflection ( $\delta$ ). However  $P_y$  and  $P_{max}$  do not show a direct correlation with the impact energy (fig. 5.15), whilst it is clearly evident the linear correlation between impact energy and deflection: the higher the ductility, the higher the impact strength of the steel (fig. 5.16).

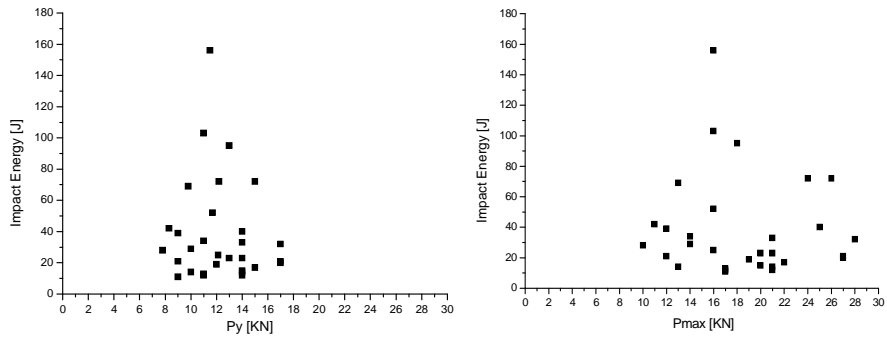


Figure 5.15: impact energy vs.  $P_y$  and  $P_{max}$

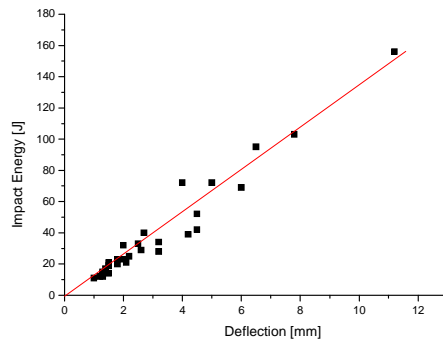
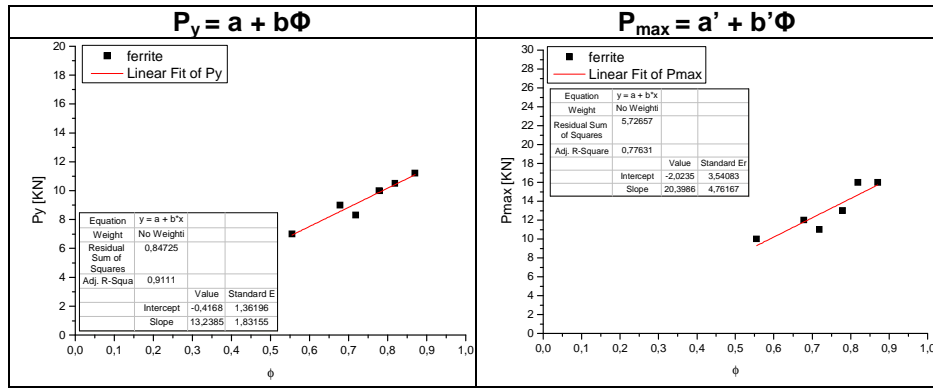


Figure 5.16: impact energy vs. deflection

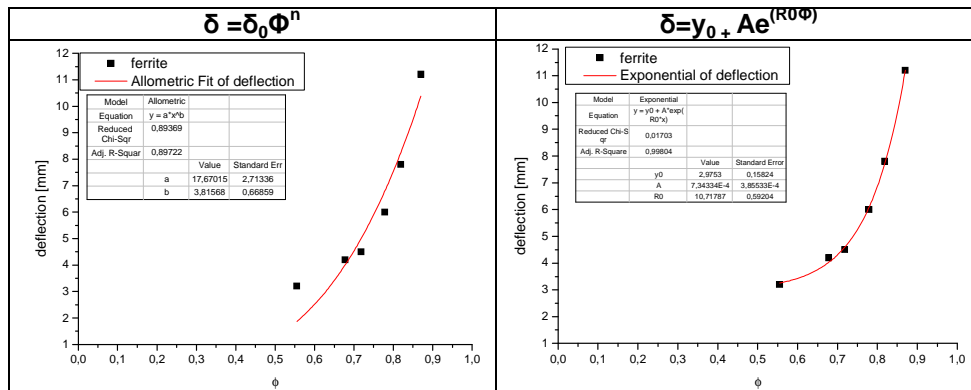
The suggested simplified model correlates  $P_y$  and  $P_{max}$ , to the load bearing fraction considering the equation between the corresponding parameters in tensile tests ( $\sigma_y$  and UTS, respectively) and the load bearing section, which is linear.

## Chapter 5: Chromium Steels

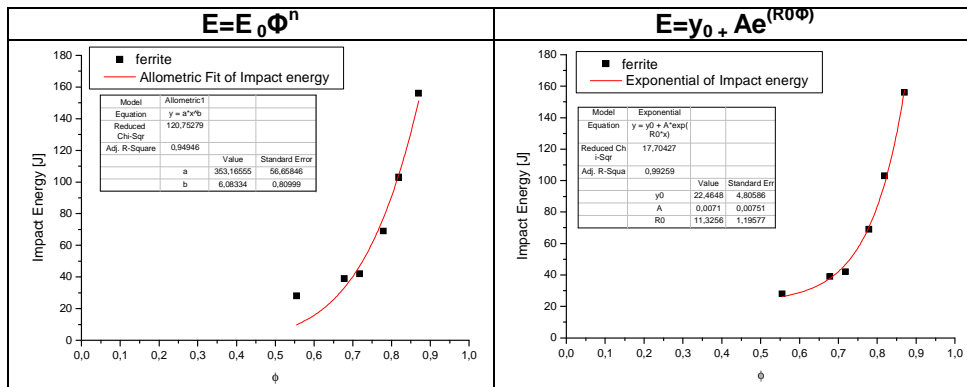


Where  $a$  ( $P_y$  when load bearing section is zero) does not have any real meaning and it is much lower than  $b$ . The linear correlation is verified quite well for  $P_y$  and less for  $P_{max}$ . The interpolating lines do not cross the origin of the diagram, confirming that the correlation is meaningless when the load bearing fraction is so low. It may be assumed that all the correlations are valid only when  $\Phi > 0.5$ .

In the case of deflection, two different equations (polynomial and exponential) are used considering that it increases even more on increasing the load bearing section.



The exponential correlation works better than the polynomial one. The same trend is archived by impact energy, as expected considering the correlation between impact energy and deflection shown in figure 5.16.



5.2.1.1. Yield load

Representing the yield load values, determined on all the investigated materials, on a single diagram (fig. 5.17), four different trends can be observed, grouped according to the microhardness of the steels and characterized by the following equations:

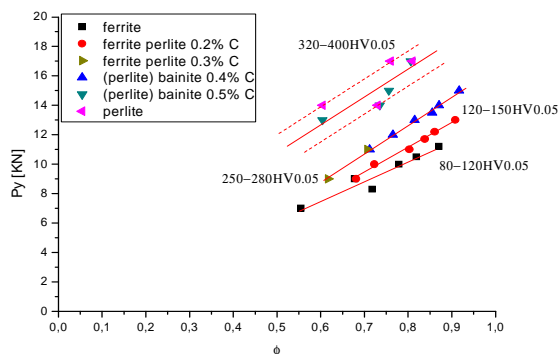


Figure 5.17: yield load vs load bearing section

- 1) 80-120 HV0.05:  $P_y = -0,4 + 13,2\Phi$
- 2) 20-150 HV0.05:  $P_y = -2,5 + 17,4\Phi$
- 3) 250-280 HV0.05:  $P_y = -2,6 + 19,1\Phi$
- 4) 320-400 HV0.05:  $P_y = 1,4 + 19,1\Phi$

The correlation between the yield load and the microhardness can be investigated (eq. 5.3), when load bearing section is equal to 1, and therefore the yield load is the yield load of the matrix ( $P_{y0}$ ):

$$P_{y(\Phi=1)} = P_{y0} = a + b \quad (\text{eq. 5.3})$$

A linear correlation is obtained (fig. 5.18), characterized by equation 5.4:

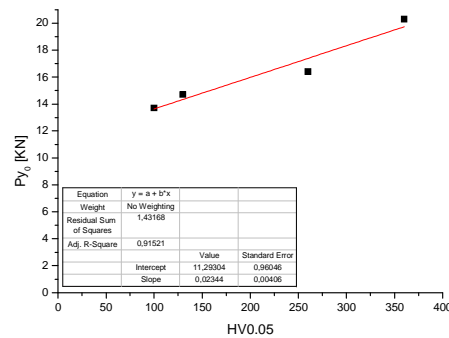


Figure 5.18:  $P_{y0}$  vs matrix microhardness

$$P_{y0} = 11.3 + 0.023HV0.05 \quad (\text{eq. 5.4})$$

### 5.2.1.2. Maximum load

In principle the same elaboration as for yield load could be made, to obtain a correlation between the maximum load of the matrix and microhardness. Three different trends can be observed in figure 5.19, grouped according to the microhardness of the steels and characterized by the following equations:



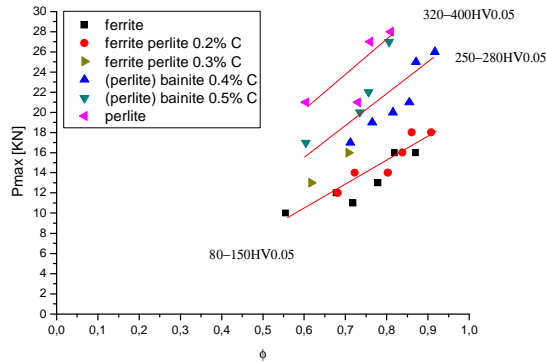


Figure 5.19: maximum load vs load bearing section

- 1) 80-120 HV0.05:  $P_{\max} = -4,3 + 24,06\Phi$
- 2) 250-280 HV0.05:  $P_{\max} = -2,07 + 29,95\Phi$
- 3) 320-400 HV0.05:  $P_{\max} = -0,63 + 34,27\Phi$

The correlation between the yield load and the microhardness is obtained (fig 5.20), when load bearing section is equal to 1 and the maximum load is the maximum load of the matrix ( $P_{\max 0}$ ).

The linear correlation is characterized by equation 5.5:

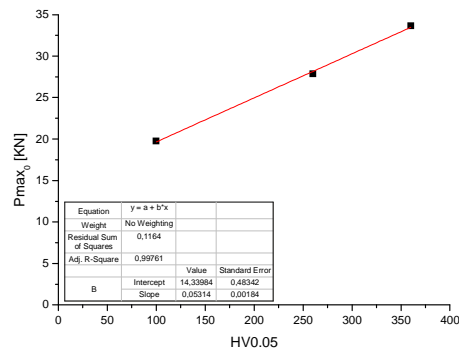


Figure 5.20:  $P_{\max 0}$  vs matrix microhardness

$$P_{\max 0} = 14,34 + 0,05HV0.05 \quad (\text{eq. 5.5})$$

5.2.1.3. Deflection

Representing all the deflection data on a single diagram (fig. 5.21), three different tendencies are recognized, grouped according to the matrix microstructure rather than to microhardness, and in particular to the ferrite content.

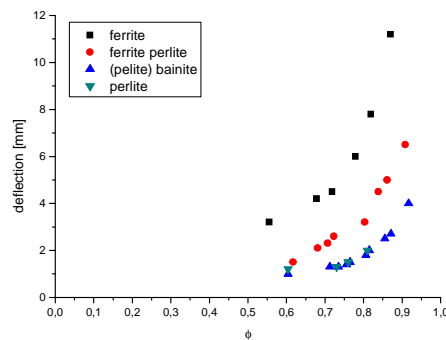


Figure 5.21: deflection vs load bearing section

- 1) ferritic matrix:  $\delta=17,67 \Phi^{3,81}$  (polynomial),  $\delta=2,98 + 7,34E-4 e^{(10,72\Phi)}$  (exponential)
- 2) ferritic- pearlitic matrix:  $\delta=9,28 \Phi^{4,08}$  (polynomial),  $\delta=0,88 + 0,096 e^{(7,02\Phi)}$  (exponential)
- 3) bainitic- perlitic matrix:  $\delta=3,60 \Phi^{4,82}$  (polynomial),  $\delta=0,89 + 1,54E-4 e^{(10,80\Phi)}$  (exponential)

$\delta_0$  is the deflection when the load bearing section is equal to one, i.e. the deflection of the matrix. It is calculated for both the models and the values are reported in figure 5.22 versus the ferrite content. The number of experimental points is too low to define a model, however it seems that when ferrite content decreases below 70-80% the deflection of the matrix tends to stabilize.

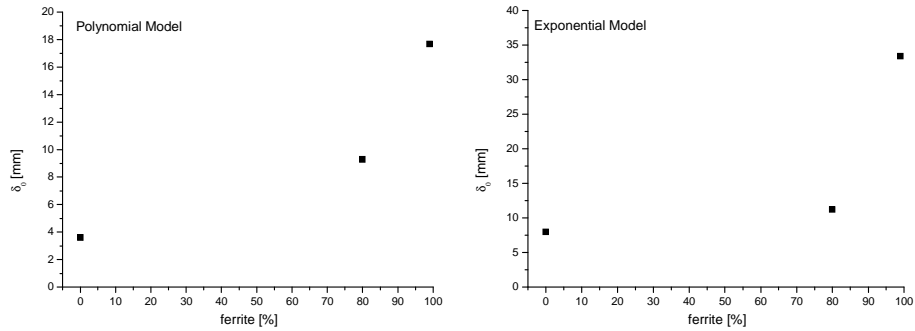


Figure 5.22: deflection vs ferrite content

#### 5.2.1.4. Impact energy

Impact energies can be grouped according to the matrix microstructure and in particular to the ferrite content, confirming three different trends with equations reported below (fig. 5.23).

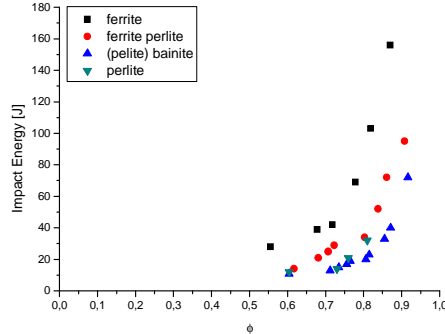


Figure 5.23: impact energy vs load bearing section

- 1) ferritic matrix:  $E=353,13 \Phi^{6,08}$  (polynomial),  $E=22,46 + 0,07 e^{(11,32\Phi)}$  (exponential)
- 2) ferritic- pearlitic matrix:  $E=160,23 \Phi^{5,76}$  (polynomial),  $E=11,43 + 0,01 e^{(9,88\Phi)}$  (exponential)
- 3) bainitic- perlitic matrix:  $E=113,07 \Phi^{7,98}$  (polynomial),  $E=11,71+1,75E-5e^{(16,41\Phi)}$  (exponential)

$E_0$  is the impact energy when load bearing section is equal to one, i.e. the impact energy of the matrix, calculated with both the models. The correlation between  $E_0$  and ferrite content cannot be defined since the number of experimental points is too low. However it seems that when ferrite content decreases below 70-80% the impact energy of the matrix tends to stabilize (fig. 5.24).

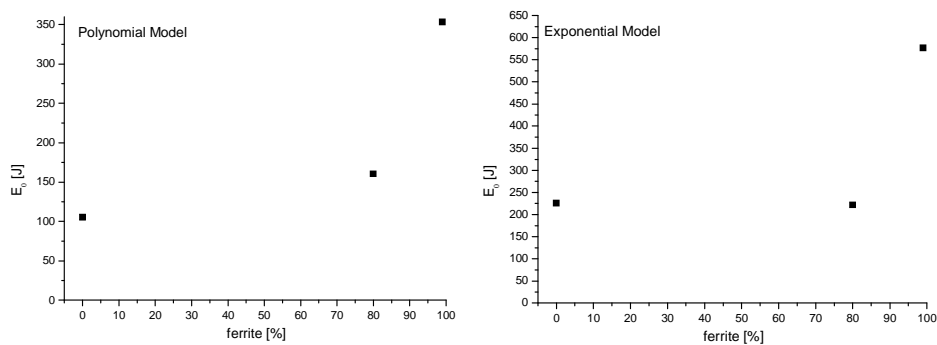


Figure 5.24: impact energy vs ferrite content

Even if the exponential model fits more precisely the impact energy/deflection vs load bearing section curves,  $E_0$  calculated with the polynomial model is more consistent with data reported in literature for wrought steels. Therefore the polynomial model may be preferred.

### 5.3. Surface densification by shot peening

Shot peening is used to improve the fatigue resistance of steels because of the compressive residual stresses and strain hardening. In porous steels, shot peening causes surface densification, as well. In this work, shot peening was used to densify the surface layers as a preliminary treatment for carburizing and nitriding. Shot peening was carried out on  $6.8\text{g/cm}^3$  materials sintered at  $1120^\circ\text{C}$ , with the following parameters: intensity 12A, shot ASH230, coverage 150%.

## Chapter 5: Chromium Steels

### 5.3.1. Effect on microstructure and microhardness

The microstructural analysis shows (fig. 5.25) that part of the shot peening energy is effectively spent for densification of the surface layers, due to extensive plastic deformation.

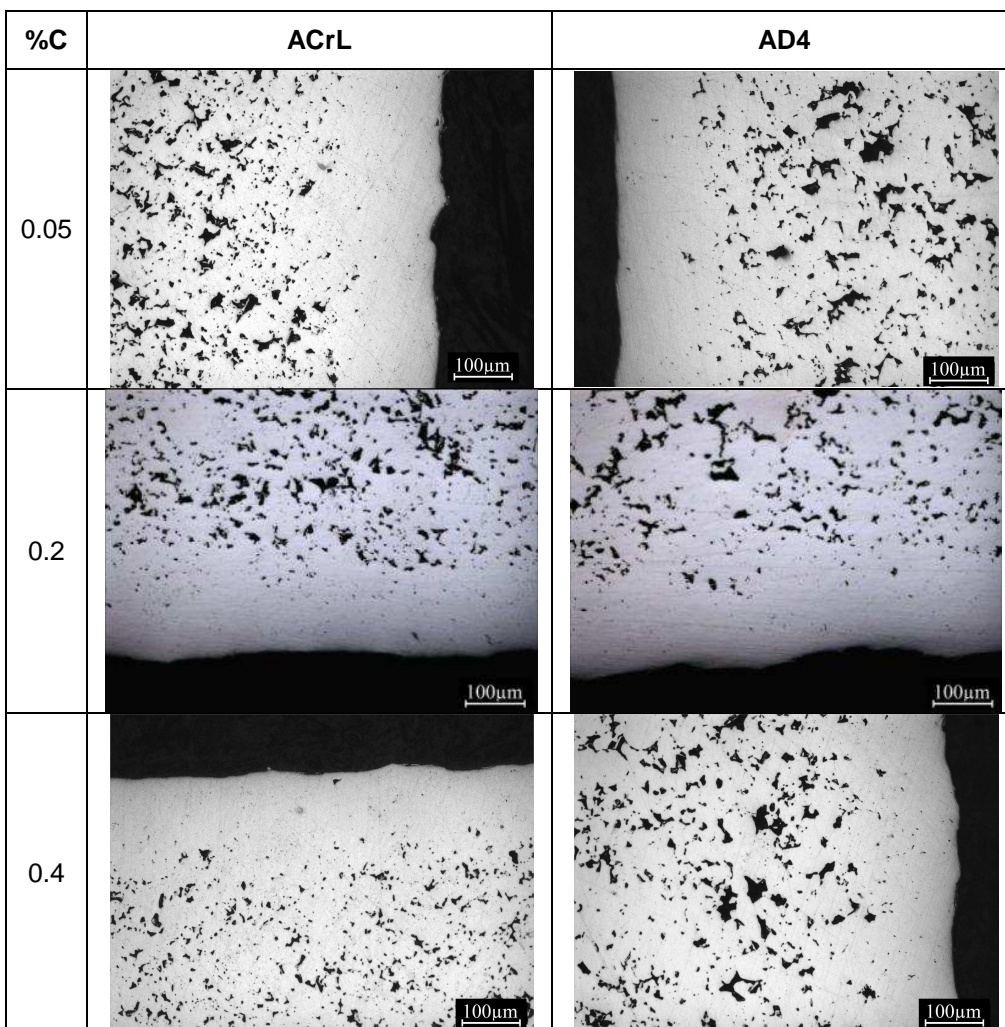


Figure 5.25: microstructures of  $6.8\text{g/cm}^3$  surface densified ACrL and AD4 sintered at  $1120^\circ\text{C}$

## Chapter 5: Chromium Steels

---

The thickness of the densified layers is reported in table 5.10 and the microhardness profiles are shown in figure 5.26. The thickness is around 100-130 $\mu\text{m}$ . The thickness of the strain hardening layer, which is the distance from the surface to the point where the microhardness drops to the core hardness, is higher than the densified one, confirming that the plastic strain penetrates in depth beneath the densified layer.

Table 5.10: densification depth of 6.8g/cm<sup>3</sup> surface densified 0.05%, 0.2% and 0.4%C ACrL and AD4 sintered at 1120°C

Materials	Thickness of densified layer [ $\mu\text{m}$ ]
ACrL 0.05%	113.4
ACrL 0.2%C	103.4
ACrL 0.4%C	102

Materials	Thickness of densified layer [ $\mu\text{m}$ ]
AD4 0.05%C	115.8
AD4 0.2%C	128.5
AD4 0.4%C	100.4

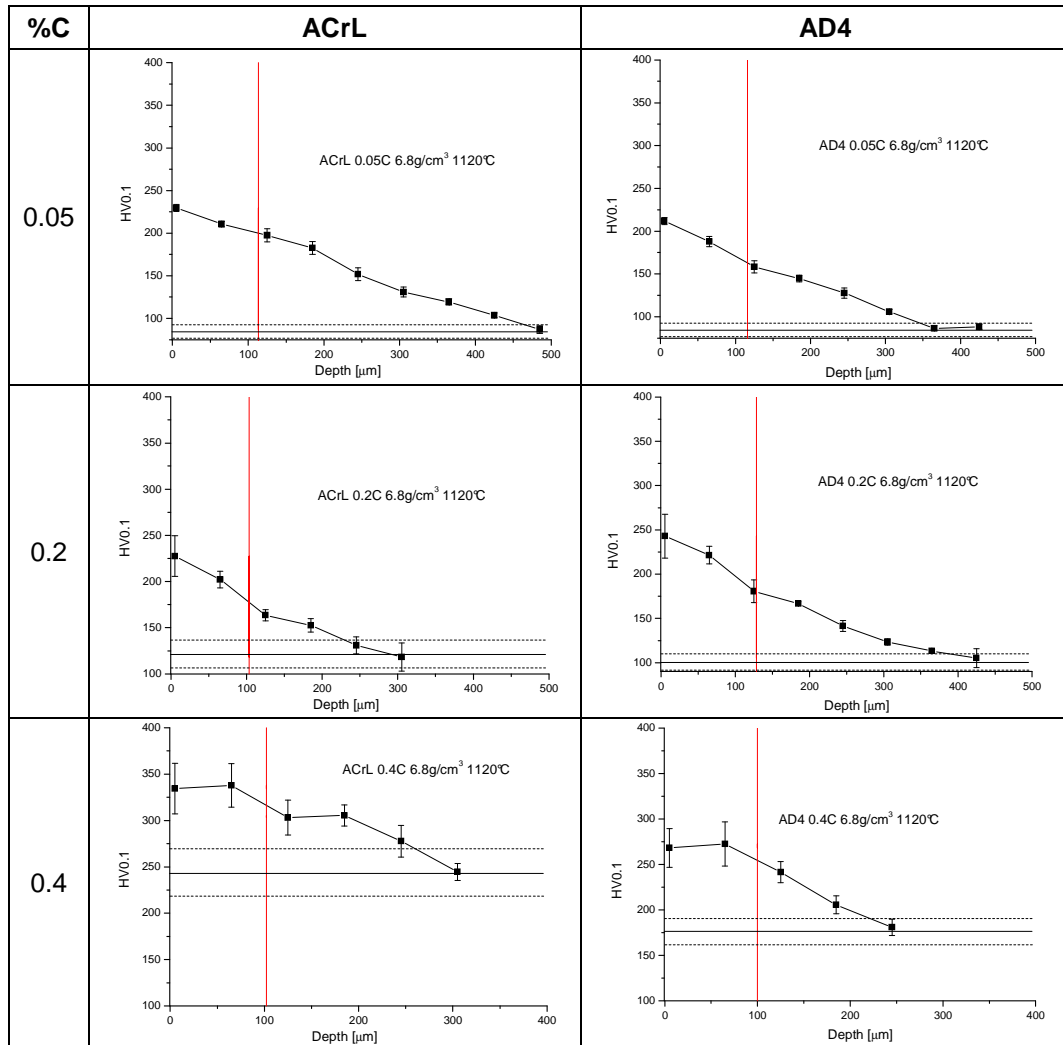


Figure 5.26: microhardness profiles and densified depths of 6.8g/cm<sup>3</sup> surface densified ACrL and AD4 sintered at 1120°C

### 5.3.2. Surface morphology

The surface morphology is shown in figures 5.27 and 5.28, comparing the as sintered condition to the surface densified one. The surface densification is clearly

evident, but several residual defects are left on the surface, which is quite irregular, significant of a poor surface quality.

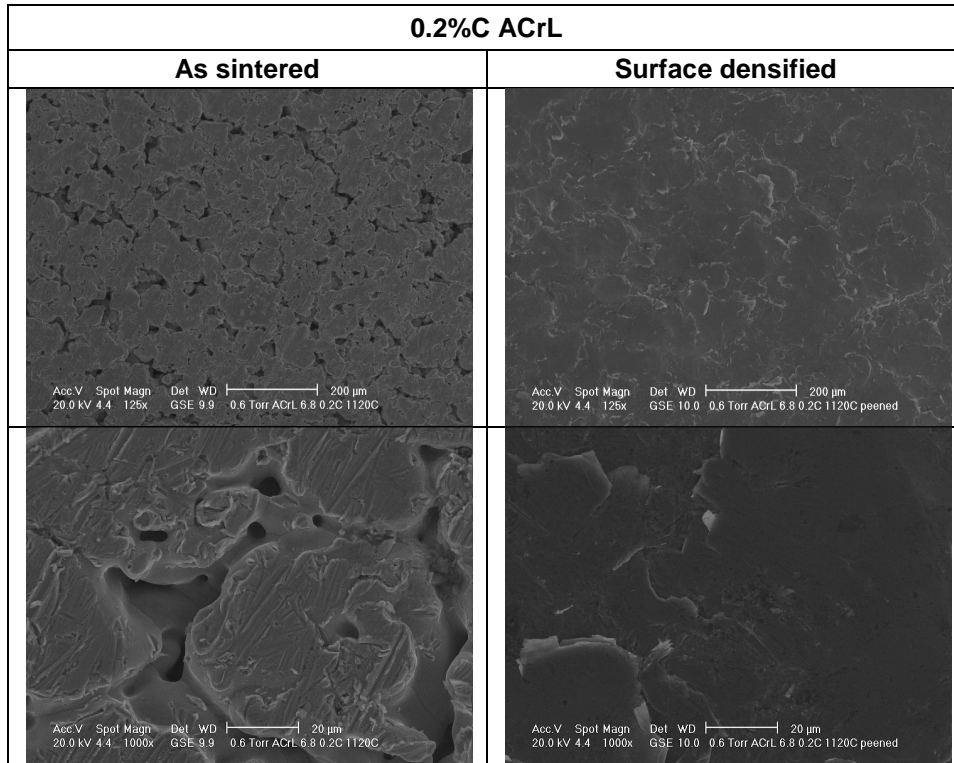


Figure 5.27:  $6.8\text{g/cm}^3$  0.2%C ACrL sintered at  $1120^\circ\text{C}$



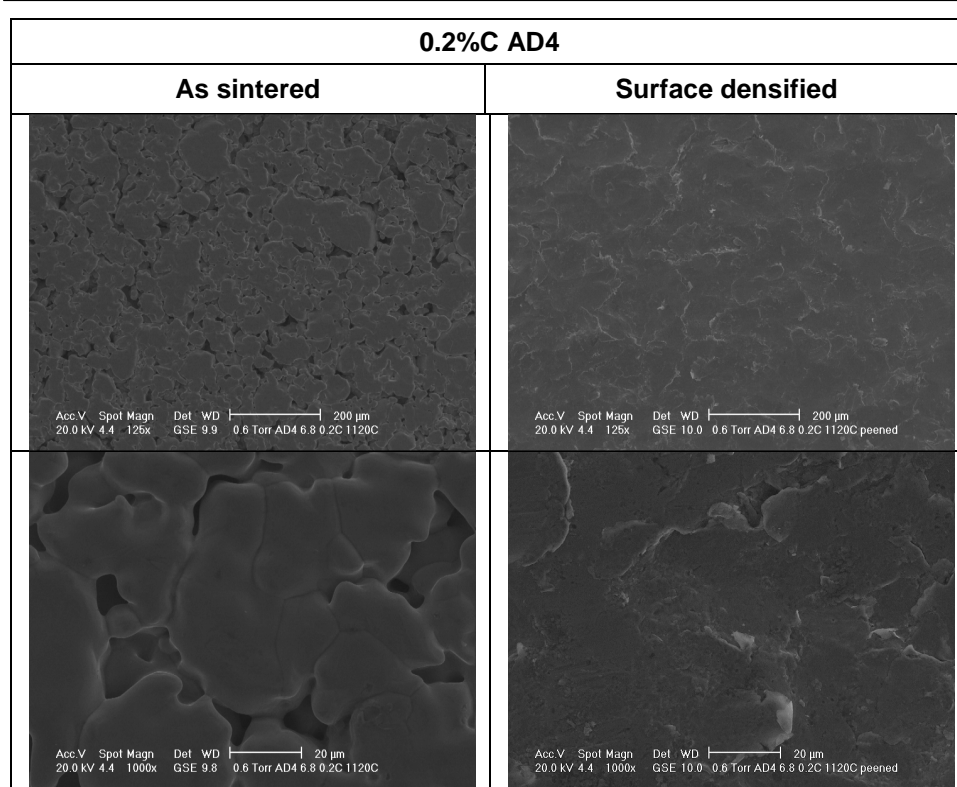


Figure 5.28:  $6.8\text{g/cm}^3$  0.2%C AD4 sintered at  $1120^\circ\text{C}$

#### 5.4. Concluding remarks

The results of the study on the influence of carbon content, density and sintering temperature on the microstructure and impact properties can be summarized as follows.

- Microstructures are: ferrite in 0.05%C steels, ferrite- perlite in 0.2%C steels, bainite in 0.4%C ACrL and ferrite plus perlite in 0.4%C AD4, without any significant effect of sintering temperature and density, confirmed also by the dilatometric study.
- On the base of impact results, the effect of density is an increase in yield load, maximum load and deflection because of the increase in load bearing

section. For the same reason, on increasing sintering temperature deflection increases, whilst yield and maximum load decrease because of a slightly decarburization. On increasing carbon content, impact toughness decreases because of perlite and bainite formation.

- A simplified model was proposed to correlate the impact toughness to the load bearing section, calculated through the image analysis of microstructures.  $P_y$  and  $P_{max}$  have a linear relationships with load bearing section, whilst  $\delta$  and  $E$  have a polynomial correlation. Concerning the microstructure effect,  $P_y$  and  $P_{max}$  are influenced by microhardness, whilst  $\delta$  and  $E$  by the ferrite content.
- Shot peening was used as a preliminary treatment to densify the surface. The densified layer thickness is around 130 $\mu$ m. However some residual defects are left on the surface and the surface profile is rather irregular. Shot peening parameters should be optimized to avoid such a residual defectiveness

## 6. Low Pressure Carburizing of Chromium Steels

In this study ACrL and AD4 with density  $6.8\text{g/cm}^3$ ,  $7.0\text{g/cm}^3$  and  $7.4\text{g/cm}^3$ , sintered at  $1120^\circ\text{C}$  and  $1250^\circ\text{C}$  and with two carbon contents ( 0.05% and 0.2%C) were considered. Some samples have been previously shot peened to densify the surface. After shot peening the specimens have been polished and grinded with SiC paper up to 1200 to remove the surface defects. The low pressure carburizing (LPC) was carried out in an ALD plant in DANA Company (Arco di Trento, Italy) with the target of a surface microhardness around 800-900HV0.1 and a case depth of 500-600 $\mu\text{m}$ . The treatment parameters are listed in table 6.1. The carburizing temperature was  $945^\circ\text{C}$  and gas was acetylene. Quenching was carried out with a nitrogen flux at 6 bar. Tempering at  $180^\circ\text{C}$  for 2 hours was carried out after LPC.

Table 6.1: LPC treatments

Treatment code	Boost + diffusion time (minutes)				
	I	II	III	IV	V
LPC 1	2 + 15	1 + 1	1 + 4		
LPC 2	2 + 10	1 + 15	1 + 19	1 + 27	1 + 4
LPC 3	2 + 10	1 + 15	1 + 21	1 + 4	

## Chapter 6: Low Pressure Carburizing of Chromium Steels

### 6.1. Three steps LPC- LPC 1

#### 6.1.1. Effect of porosity

Microstructures and microhardness profiles of ACrL sintered at 1250°C are shown in figures 6.1- 6.6.

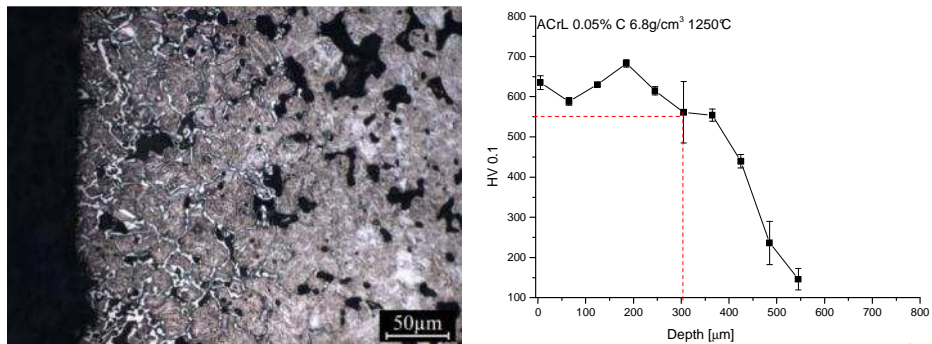


Figure 6.1: microstructure and microhardness profile of carburized 6.8g/cm<sup>3</sup> 0.05%C ACrL sintered at 1250°C

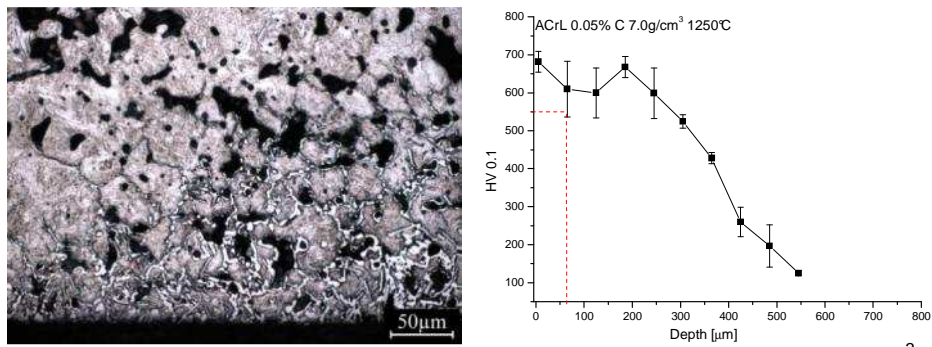


Figure 6.2: microstructure and microhardness profile of carburized 7.0g/cm<sup>3</sup> 0.05%C ACrL sintered at 1250°C

*Chapter 6: Low Pressure Carburizing of Chromium Steels*

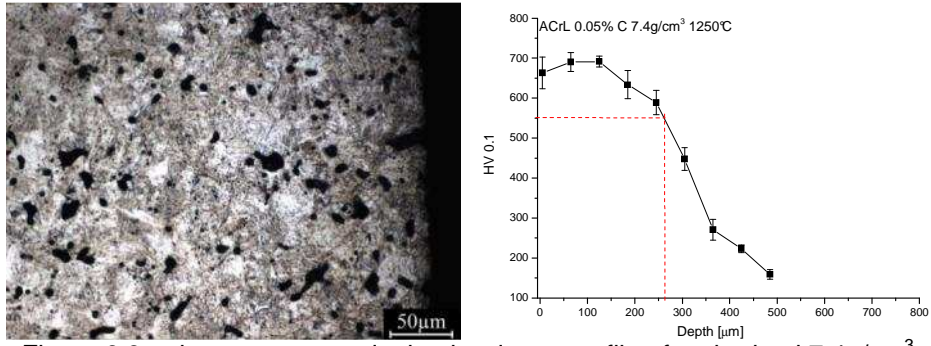


Figure 6.3: microstructure and microhardness profile of carburized  $7.4\text{g/cm}^3$   $0.05\%C$  ACrL sintered at  $1250^\circ\text{C}$

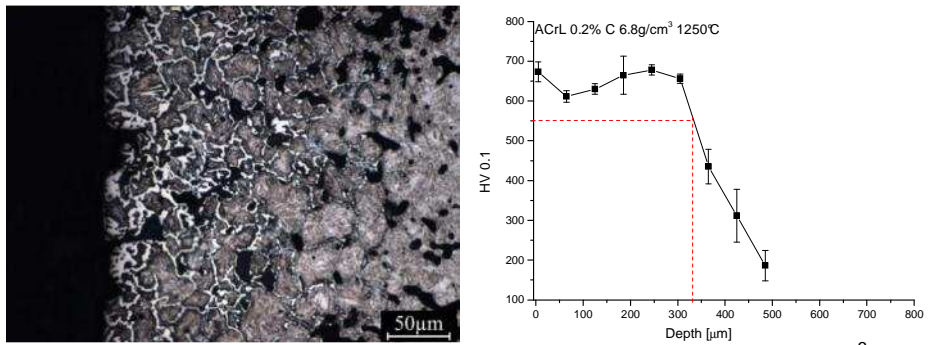


Figure 6.4: microstructure and microhardness profile of carburized  $6.8\text{g/cm}^3$   $0.2\%C$  ACrL sintered at  $1250^\circ\text{C}$

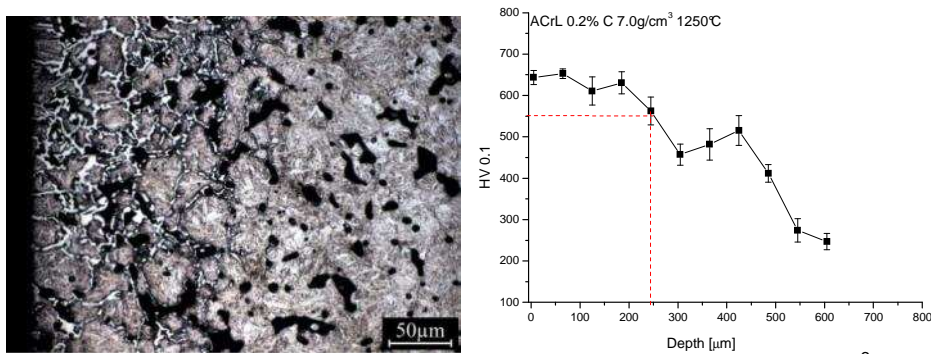


Figure 6.5: microstructure and microhardness profile of carburized  $7.0\text{g/cm}^3$   $0.2\%C$  ACrL sintered at  $1250^\circ\text{C}$

## Chapter 6: Low Pressure Carburizing of Chromium Steels

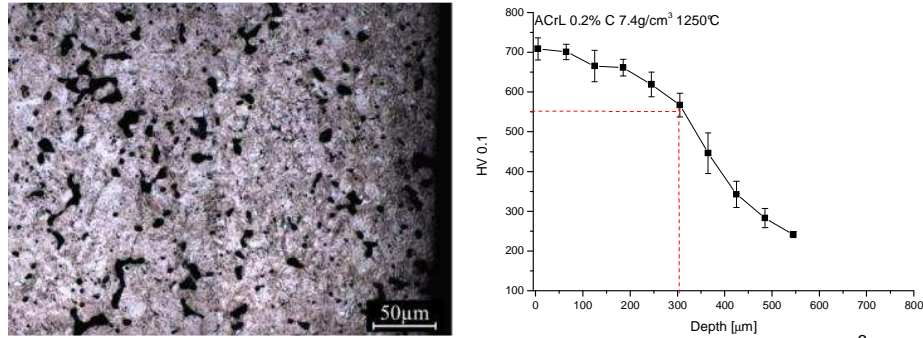


Figure 6.6: microstructure and microhardness profile of carburized  $7.4\text{g/cm}^3$  0.2%C ACrL sintered at  $1250^\circ\text{C}$

In the  $6.8\text{g/cm}^3$  and  $7.0\text{g/cm}^3$  specimens an extensive precipitation of proeutectoid carbides at the prior austenitic grain boundary occurs, since the “huge” exchange area, due to interconnected porosity, in combination with the high carbon potential of carburizing atmosphere enhances C pick-up. Precipitation involves a surface thickness of around  $100\mu\text{m}$ , where microhardness is lower than beneath, since grain boundary carbides do not contribute to hardening. The amount of carbides increases on increasing the base carbon content and no effect of the sintering temperatures was seen. Sintering at  $1250^\circ\text{C}$  does not improve porosity to such an extent that overcarburizing is avoided.

Figure 6.7 shows the XRD spectrum, elaborated to obtain the quantitative analysis of the microstructural constituents of the outer layer of the carburized surface (approximately  $5\mu\text{m}$  thin): martensite (46 %), cementite ( $\text{Fe}_3\text{C}$ , 49%), retained austenite (3%) and chromium carbide  $\text{M}_{23}\text{C}_6$  (2%). In a previous work on  $6.7\text{g/cm}^3$  0.35%C ACrM sintered at  $1250^\circ\text{C}$  and low pressure carburized with one step cycle, Danninger et al. [4] have reported that carbides are chromium cementite ( $\text{Fe, Cr}_3\text{C}$ ).

## Chapter 6: Low Pressure Carburizing of Chromium Steels

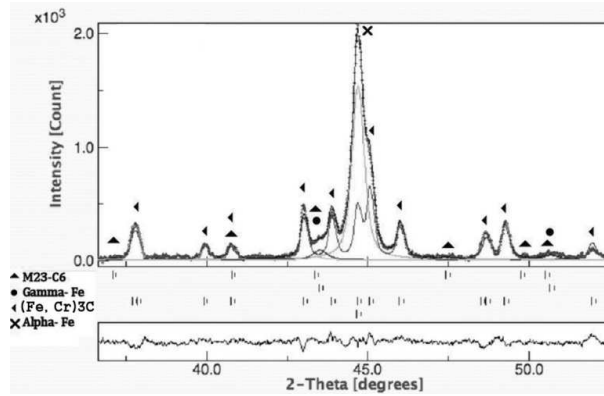


Figure 6.7: XRD pattern of LPC1 ACrL

Figures 6.3 and 6.6 show that overcarburizing is prevented in  $7.4\text{g/cm}^3$  steels and the microstructures result to be homogeneous. However the thickness of the case is too small and the surface microhardness is too low with reference to the target, as shown in table 6.2. Even in the best case, i.e.  $7.4\text{g/cm}^3$  steels, the target is not matched.

Table 6.2: surface microhardness and case depths of LPC 1 steels

ACrL	$6.8\text{g/cm}^3$		$7.0\text{g/cm}^3$		$7.4\text{g/cm}^3$		Target
	0.05%C	0.2%C	0.05%C	0.2%C	0.05%C	0.2%C	
HV0.1	640	670	670	650	650	700	800-900
$d_{550}$ [ $\mu\text{m}$ ]	300	330	60	250	250	300	500-600

### 6.1.2. Effect of chemical composition of the steel

Microstructures and microhardness profiles of  $6.8\text{ g/cm}^3$  and  $7.4\text{ g/cm}^3$  0.2%C materials sintered at  $1120^\circ\text{C}$  are reported in figures 6.8 -6.11.

*Chapter 6: Low Pressure Carburizing of Chromium Steels*

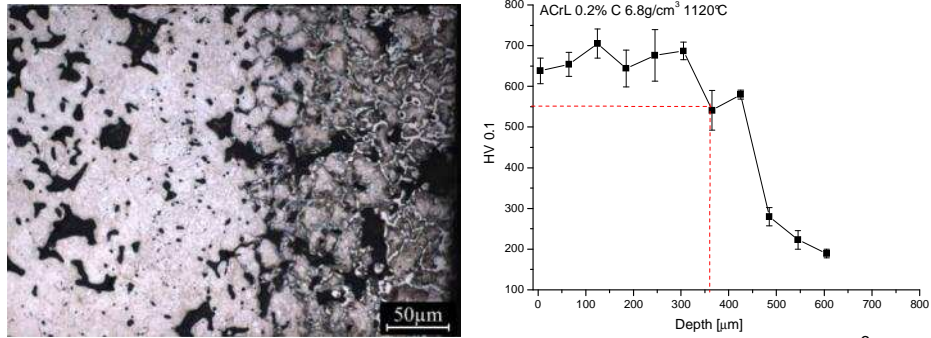


Figure 6.8: microstructure and microhardness profile of carburized  $6.8\text{g}/\text{cm}^3$  0.2%C ACrL sintered at  $1120^\circ\text{C}$

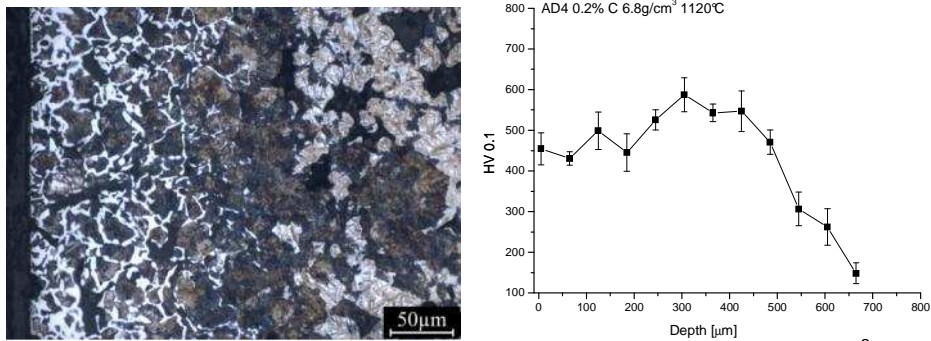


Figure 6.9: microstructure and microhardness profile of carburized  $6.8\text{g}/\text{cm}^3$  0.2%C AD4 sintered at  $1120^\circ\text{C}$

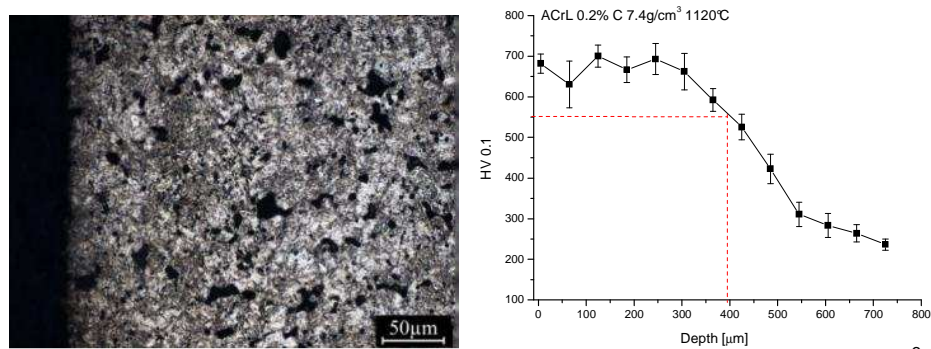


Figure 6.10: microstructure and microhardness profile of carburized  $7.4\text{g}/\text{cm}^3$  0.2%C ACrL sintered at  $1120^\circ\text{C}$



## Chapter 6: Low Pressure Carburizing of Chromium Steels

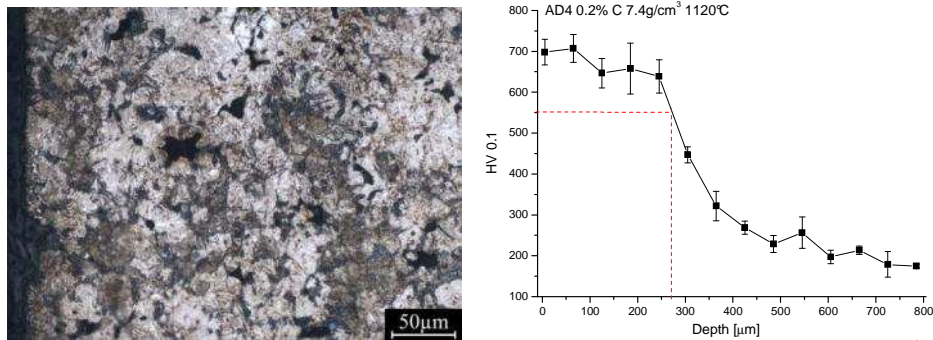


Figure 6.11: microstructure and microhardness profile of carburized 7.4g/cm<sup>3</sup> 0.2%C AD4 sintered at 1120°C

The grain boundary carbides precipitation occurs in 6.8g/cm<sup>3</sup> AD4, too. On increasing density up to 7.4g/cm<sup>3</sup> overcarburizing is fully avoided in ACrL and the microhardness profile is quite good. In 7.4g/cm<sup>3</sup> AD4 only a few carbides are present in the outer layers, however they do not affect the microhardness profile. The comparison between the microhardness profiles of 7.4g/cm<sup>3</sup> specimens shows that the case depth is greater in ACrL respect to AD4, because of the higher hardenability.

### 6.1.3. Comparison between closed porosity and surface densification

Microstructures and microhardness profiles of 7.4g/cm<sup>3</sup> and 6.8g/cm<sup>3</sup> surface densified 0.05%C steels are reported in figures 6.12- 6.15; sintering was carried out at 1120°C. The microstructures and microhardness profiles of the 0.2%C steels are shown in appendix.

*Chapter 6: Low Pressure Carburizing of Chromium Steels*

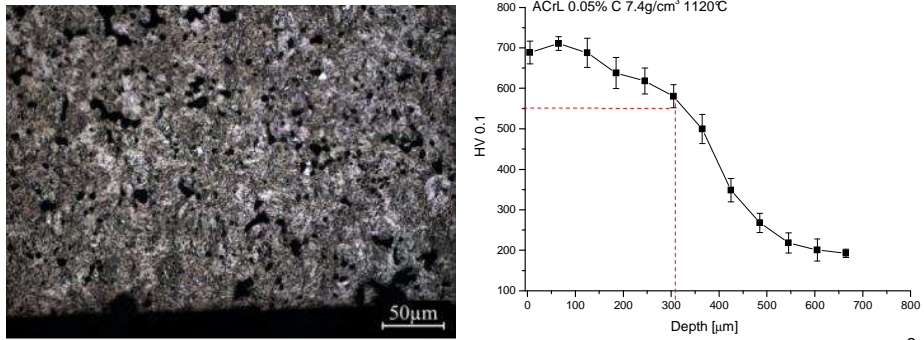


Figure 6.12: microstructure and microhardness profile of carburized 7.4g/cm<sup>3</sup> 0.05%C ACrL sintered at 1120°C

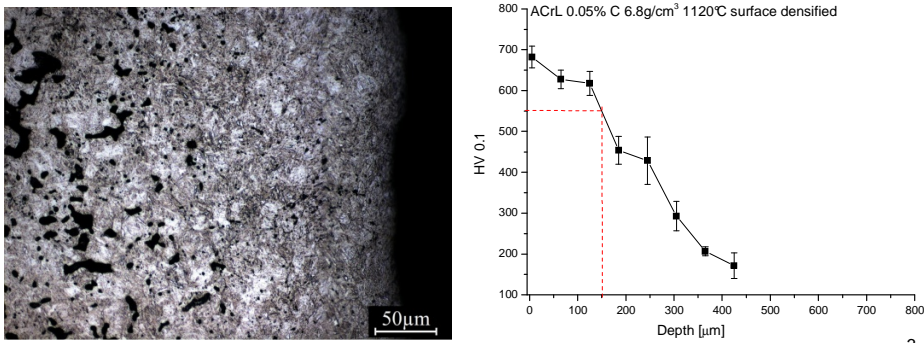


Figure 6.13: microstructure and microhardness profile of carburized 6.8g/cm<sup>3</sup> surface densified 0.05%C ACrL sintered at 1120°C

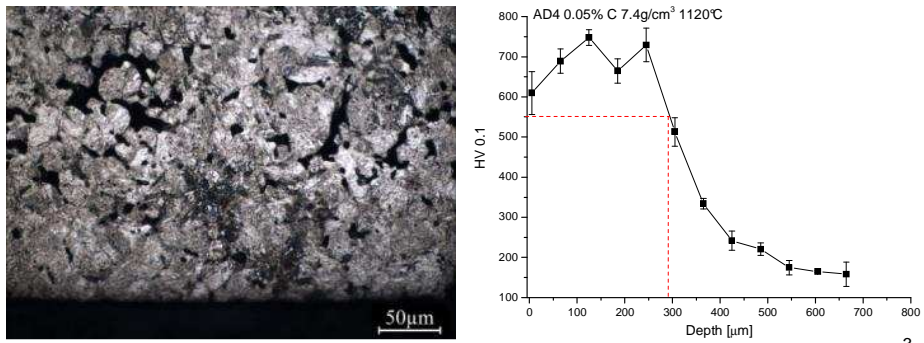


Figure 6.14 microstructure and microhardness profile of carburized 7.4g/cm<sup>3</sup> 0.05%C AD4 sintered at 1120°C

## Chapter 6: Low Pressure Carburizing of Chromium Steels

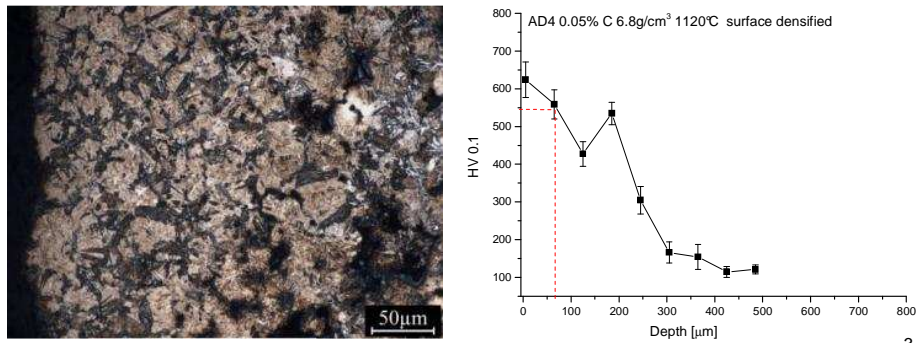


Figure 6.15: microstructure and microhardness profile of carburized 6.8g/cm<sup>3</sup> surface densified 0.05%C AD4 sintered at 1120°C

In all the surface densified materials, the microstructure of the case does not show the effect of overcarburizing and the microstructures are homogeneous, quite similar to those of the 7.4g/cm<sup>3</sup> ones. A difference can be appreciated between the microhardness profiles, which are deeper in the 7.4g/cm<sup>3</sup> specimens than in the surface densified ones independently on the base carbon content. The reason could lie in the effect of the surface porosity which, even if it is not communicating with the internal one, enhances the exchange surface area increasing the carbon pick-up. This results in a deeper effect of carburizing. To confirm the different C pick-up between 7.4g/cm<sup>3</sup> and surface densified materials surface carbon content of 0.05%C steels was analyzed and reported in table 6.3.

Table 6.3: carbon analyses

<b>0.05%C ACrL</b>	<b>6.8g/cm<sup>3</sup> surface densified</b>	<b>7.4g/cm<sup>3</sup></b>
1120°C	0.42	0.51
1250°C	0.47	0.49

<b>0.05%C AD4</b>	<b>6.8g/cm<sup>3</sup> surface densified</b>	<b>7.4g/cm<sup>3</sup></b>
1120°C	0.49	0.50
1250°C	0.46	0.61

## *Chapter 6: Low Pressure Carburizing of Chromium Steels*

The carbon pick-up on 7.4g/cm<sup>3</sup> materials is effectively slightly higher than that in surface densified ones. The greater amount of perlite in surface densified AD4 compared to the 7.4g/cm<sup>3</sup> one, is a further confirmation of the lower C pick-up in surface densified materials.

Table 6.4 reports the significant parameters of the microhardness profile: the surface microhardness (HV0.1) and the case depth (d<sub>550</sub>). Sintered temperature does not affected the results significantly.

Table 6.4: surface microhardness and case depths of LPC 1 steels

ACrL	7.4g/cm <sup>3</sup>		6.8g/cm <sup>3</sup> surface densified		Target
	0.05%C	0.2%C	0.05%C	0.2%C	
HV0.1	700	680	680	700	800-900
d <sub>550</sub> [μm]	300	400	150	230	500-600

AD4	7.4g/cm <sup>3</sup>		6.8g/cm <sup>3</sup> surface densified		Target
	0.05%C	0.2%C	0.05%C	0.2%C	
HV0.1	600	700	630	650	800-900
d <sub>550</sub> [μm]	290	280	80	80	500-600

### 6.2. Five steps LPC- LPC 2

On the basis of the results obtained with LPC 1, a five steps low pressure carburizing treatment (LPC 2) was carried out in order to increase the surface microhardness up to 800-900HV0.1 and case depth (d<sub>550</sub>) up to 600μm. LPC 2 was carried out only on 7.4g/cm<sup>3</sup> and surface densified steels, since low pressure carburizing causes an extensive grain boundaries carbides precipitation in 6.8g/cm<sup>3</sup> and 7.0g/cm<sup>3</sup> specimens

## Chapter 6: Low Pressure Carburizing of Chromium Steels

### 6.2.1. Microstructures and microhardness profiles

Microstructures and microhardness profiles of 0.05%C ACrL and AD4 are shown in figures 6.16- 6.23, whilst those of 0.2%C steels are reported in appendix.

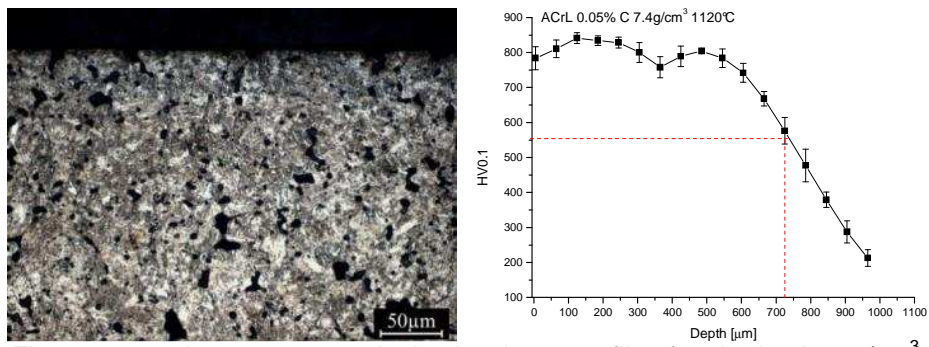


Figure 6.16: microstructure and microhardness profile of carburized 7.4g/cm<sup>3</sup> 0.05%C ACrL sintered at 1120°C

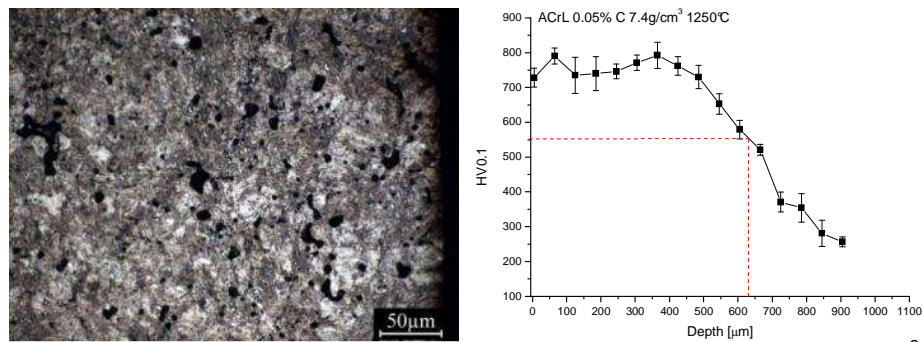


Figure 6.17: microstructure and microhardness profile of carburized 7.4g/cm<sup>3</sup> 0.05%C ACrL sintered at 1250°C

*Chapter 6: Low Pressure Carburizing of Chromium Steels*

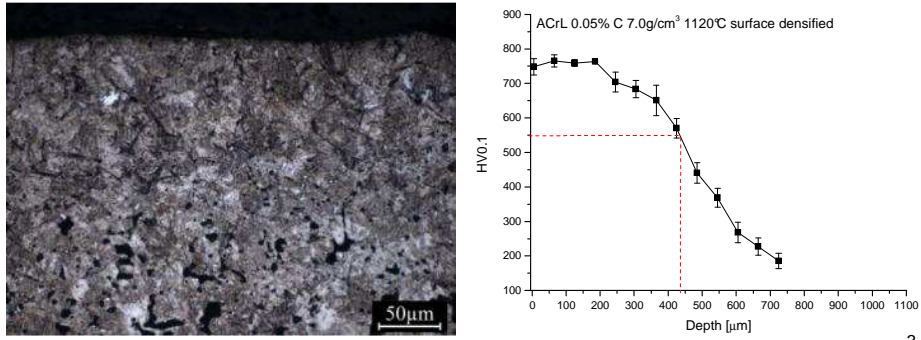


Figure 6.18: microstructure and microhardness profile of carburized 7.0g/cm<sup>3</sup> surface densified 0.05%C ACrL sintered at 1120°C

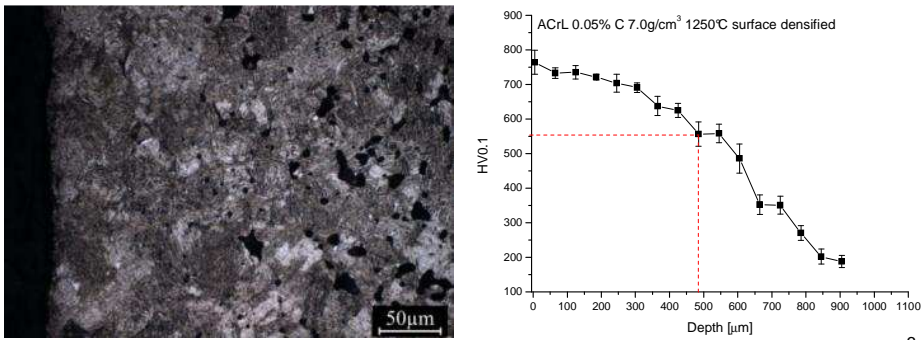


Figure 6.19: microstructure and microhardness profile of carburized 7.0g/cm<sup>3</sup> surface densified 0.05%C ACrL sintered at 1250°C

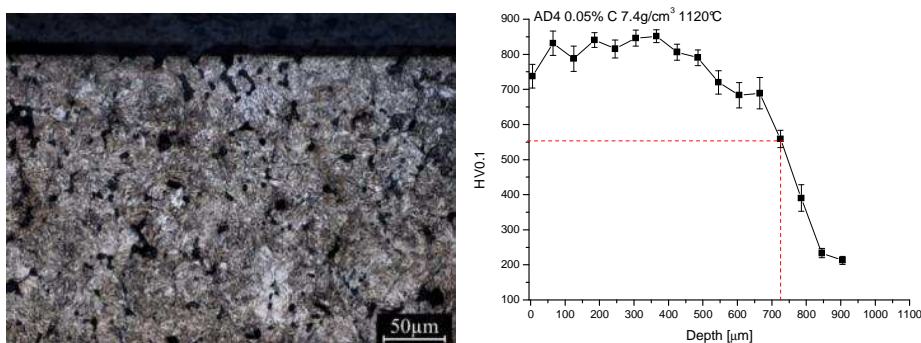


Figure 6.20: microstructure and microhardness profile of carburized 7.4g/cm<sup>3</sup> 0.05%C AD4 sintered at 1120°C

*Chapter 6: Low Pressure Carburizing of Chromium Steels*

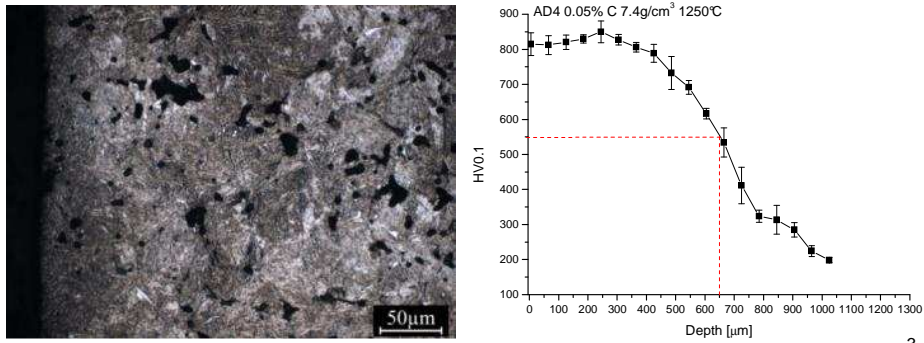


Figure 6.21: microstructure and microhardness profile of carburized 7.4g/cm<sup>3</sup> 0.05%C AD4 sintered at 1250°C

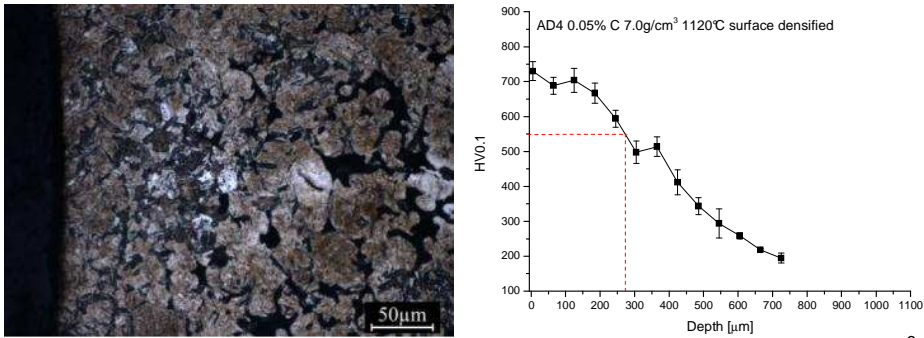


Figure 6.22: microstructure and microhardness profile of carburized 7.0g/cm<sup>3</sup> surface densified 0.05%C AD4 sintered at 1120°C

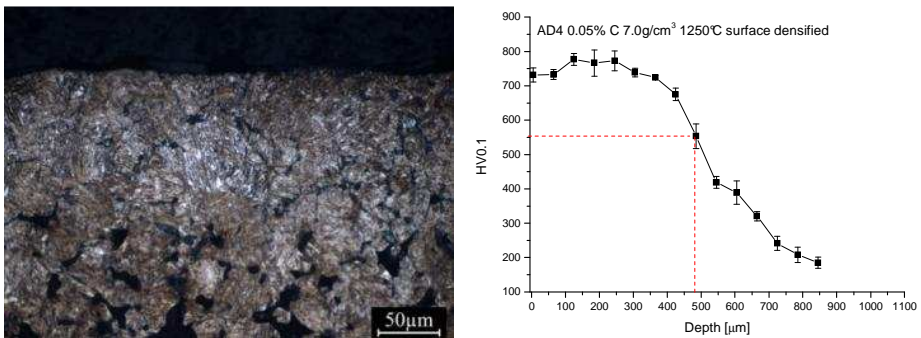


Figure 6.23: microstructure and microhardness profile of carburized 7.0g/cm<sup>3</sup> surface densified 0.05%C AD4 sintered at 1250°C

**Chapter 6: Low Pressure Carburizing of Chromium Steels**

---

In both the 7.4g/cm<sup>3</sup> and surface densified materials the microstructures of the case does not show the effect of overcarburizing. The microhardness profiles are deeper in the 7.4g/cm<sup>3</sup> specimens than in the surface densified ones because of the surface porosity role in warm compacted steels. Table 6.5 summarizes the representative data of the microhardness profiles. Carbon content does not have an appreciable effect on both surface microhardness and case depth.

Table 6.5: surface microhardness and case depths deep of LPC 2 steels

<b>ACrL</b>		<b>7.4g/cm<sup>3</sup></b>	<b>7.0g/cm<sup>3</sup> surface densified</b>	<b>Target</b>
1120°C	HV0.1	770	750	800-900
	d <sub>550</sub> [μm]	750	450	500-600
1250°C	HV0.1	750	760	800-900
	d <sub>550</sub> [μm]	650	500	500-600

<b>AD4</b>		<b>7.4g/cm<sup>3</sup></b>	<b>7.0g/cm<sup>3</sup> surface densified</b>	<b>Target</b>
1120°C	HV0.1	740	740	800-900
	d <sub>550</sub> [μm]	750	300	500-600
1250°C	HV0.1	800	740	800-900
	d <sub>550</sub> [μm]	650	500	500-600

The LPC 2 treatment effectively results in a deeper and harder case in comparison to LPC 1 and in agreement with the target.



## Chapter 6: Low Pressure Carburizing of Chromium Steels

### 6.2.2. Impact toughness

The results of impact tests, carried out on surface densified  $6.8\text{g/cm}^3$  and  $7.0\text{g/cm}^3$  specimens and  $7.4\text{g/cm}^3$  samples, are compared to the as sintered ones and summarized in table 6.6.

Table 6.6: impact test results of LPC 2 steels

SURFACE DENSIFIED SPECIMENS			Impact Energy [J]		$P_y$ [KN]		$P_{max}$ [KN]	
			As sint	Surface densified and carburized	As sint	Surface densified and carburized	As sint	Surface densified and carburized
ACrL								
%C	Density [ $\text{g/cm}^3$ ]	T sint [ $^{\circ}\text{C}$ ]						
0.05	6.8	1120	28	10	8	-	10	15
0.05	6.8	1250	42	10	8	-	11	17
0.05	7.0	1120	38	12	9	-	12	17
0.05	7.0	1250	69	11	10	-	13	18
0.2	6.8	1120	21	13	9	-	12	20
0.2	6.8	1250	34	11	9	-	14	19
0.2	7.0	1120	29	14	11	-	14	23
0.2	7.0	1250	52	13	10	-	16	21
AD4								
0.05	6.8	1120	18	12	9	-	10	13
0.05	6.8	1250	33	9	8	-	11	14
0.05	7.0	1120	28	10	9	-	11	15
0.05	7.0	1250	47	9	9	-	12	15
0.2	6.8	1120	16	10	8	-	13	14
0.2	6.8	1250	27	8	8	-	11	14
0.2	7.0	1120	22	12	9	-	14	17
0.2	7.0	1250	40	10	11	-	14	15

## Chapter 6: Low Pressure Carburizing of Chromium Steels

7.4g/cm <sup>3</sup> SPECIMENS			Impact Energy [J]		P <sub>y</sub> [KN]		P <sub>max</sub> [KN]	
			As sint	Carburized	As sint	Carburized	As sint	Carburized
ACrL								
%C	Density [g/cm <sup>3</sup> ]	T sint [°C]						
0.05	7.4	1120	103	9	11	-	16	22
0.05	7.4	1250	156	9	11	-	16	20
0.2	7.4	1120	72	13	13	-	24	25
0.2	7.4	1250	95	11	12	-	18	26
AD4								
0.05	7.4	1120	95	9	11	-	14	19
0.05	7.4	1250	124	15	11	-	14	19
0.2	7.4	1120	74	12	12	-	17	21
0.2	7.4	1250	100	10	12	-	17	21

The load-deflection curves of some materials are reported in figure 6.24.

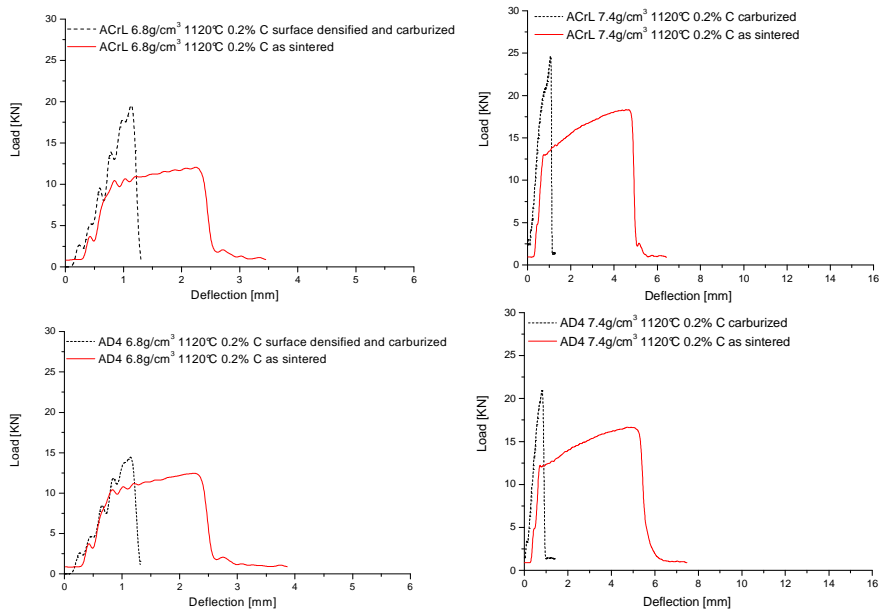


Figure 6.24: examples of load-deflection curves

## Chapter 6: Low Pressure Carburizing of Chromium Steels

All the carburized materials have an elastic behavior without any significant plastic deformation. The impact energy strongly decreases irrespective to carbon content, bulk density and sintering temperature and it ranges between 9 and 15J.

### 6.3. Microstructural improvement of overcarburized materials

#### 6.3.1. Solution annealing treatment

In order to improve the overcarburized microstructures, the grain boundary carbides have to be dissolved in the matrix to obtain a homogeneous carbide free microstructure.

The preliminary study was carried out on  $7.0\text{g/cm}^3$  0.2%C ACrL sintered at  $1120^\circ\text{C}$  and carburized with LPC1 cycle. The microstructure and microhardness profile of the as carburized material are reported in figure 6.25.

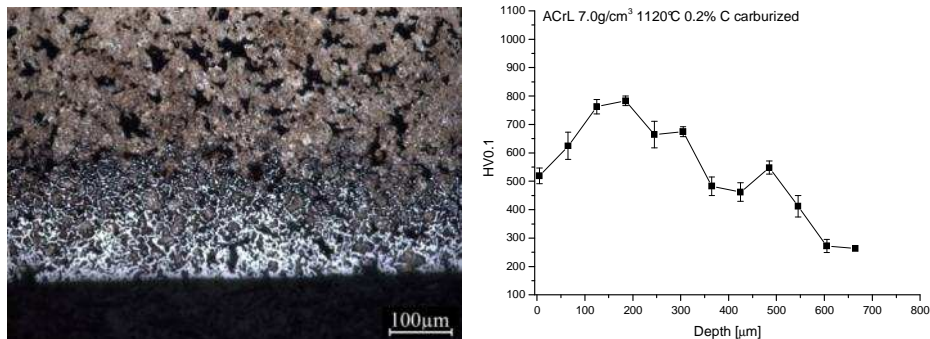


Figure 6.25: microstructure and microhardness profile of carburized  $7.0\text{g/cm}^3$  0.2%C ACrL sintered at  $1120^\circ\text{C}$

The case has an extensive grain boundary precipitation of carbides in an external  $200\mu\text{m}$ . The maximum microhardness corresponds to the boundary between this layer and the inner part of the case. The carbon content of the case calculated in a  $500\mu\text{m}$  thick surface layer, is 1.1%.

## Chapter 6: Low Pressure Carburizing of Chromium Steels

According to the Thermo-Calc diagram (fig. 6.26) cementite can be dissolved at temperature over 900°C. However carbides are chromium enriched, which results in an higher solution temperature than that of iron cementite. Consequently heat treatments have been carried out at 1050°C and 1100 °C.

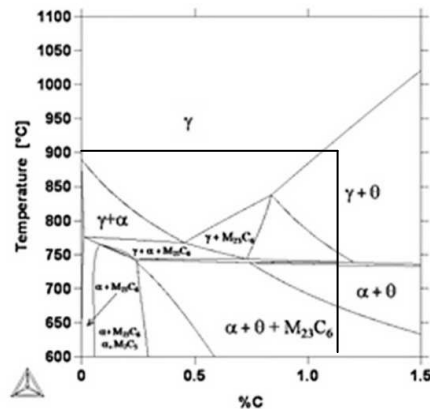


Figure 6.26: Thermo-Calc equilibrium diagram of ACrL

The preliminary solution annealing treatment was carried out with the following cycle:

- Heating up to 1050°C and 1100°C with a heating rate of 0.8K/s;
- Isothermal holding for 20 minutes;
- Cooling down by high pressure nitrogen flux at 2K/s and 5K/s.

The microstructure and the microhardness profile of the material treated at 1050°C are reported in figure 6.27.

## Chapter 6: Low Pressure Carburizing of Chromium Steels

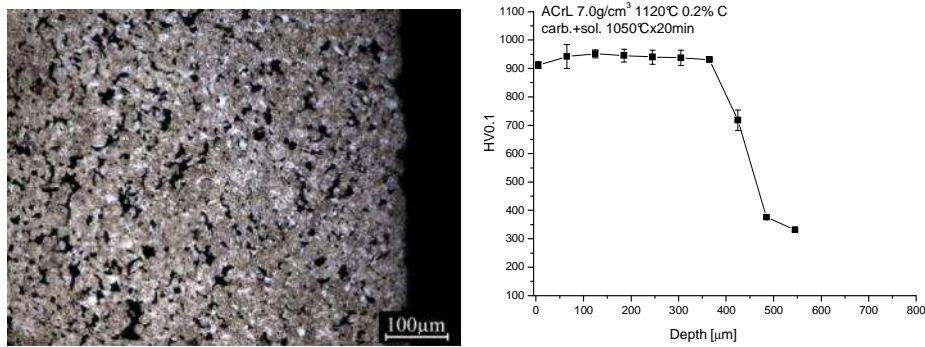


Figure 6.27: microstructure and microhardness profile of carburized of carburized  $7.0\text{g}/\text{cm}^3$  0.2%C ACrL sintered at  $1120^\circ\text{C}$  and solution annealed at  $1050^\circ\text{C}$

The SEM image (fig. 6.28) shows some residual carbides at the grain boundaries, which are not observed at the optical microscope. However, the microhardness profile has the typical trend of carburized steel, even though the microhardness decrease at around  $400\mu\text{m}$  is quite sharp.

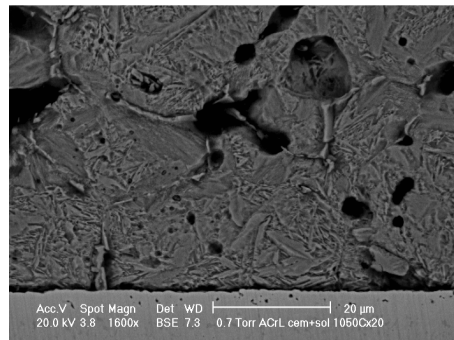


Figure 6.28: SEM micrograph of carburized  $7.0\text{g}/\text{cm}^3$  0.2%C ACrL sintered at  $1120^\circ\text{C}$  and solution annealed at  $1050^\circ\text{C}$

Since the dissolution of carbides is not complete at  $1050^\circ\text{C}$  the solution annealing temperature was increased up to  $1100^\circ\text{C}$  maintaining the same isothermal holding time. The effect of different cooling rates was investigated ( $2\text{K}/\text{s}$  and  $5\text{K}/\text{s}$ ). The microstructure resulting from a treatment with a cooling rate of  $2\text{K}/\text{s}$  is shown in figure 6.29.

*Chapter 6: Low Pressure Carburizing of Chromium Steels*

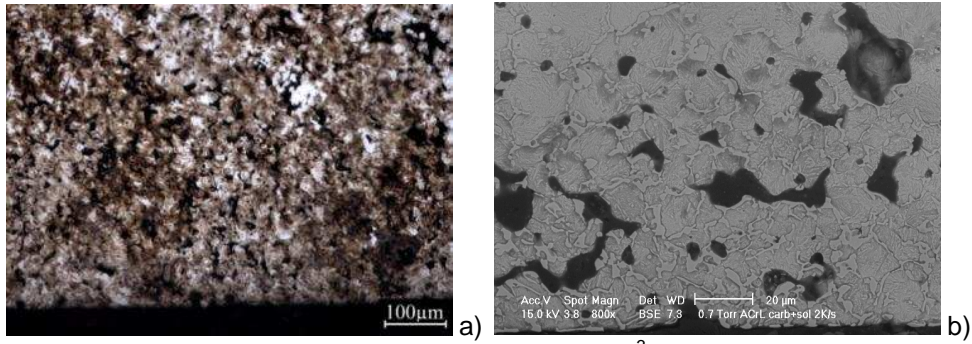


Figure 6.29: microstructures of carburized  $7.0\text{g/cm}^3$  0.2%C ACrL sintered at  $1120^\circ\text{C}$ , solution annealed at  $1100^\circ\text{C}$  and cooled down at 2K/s: a) LOM micrograph and b) SEM micrograph

The SEM image (fig. 6.29b) indicates some grain boundary precipitation in the case, which is completely eliminated by cooling down at 5K/s, as shown by the microstructural analysis in figure 6.30. The microhardness profile after cooling at 5K/s is reported in figure 6.31.

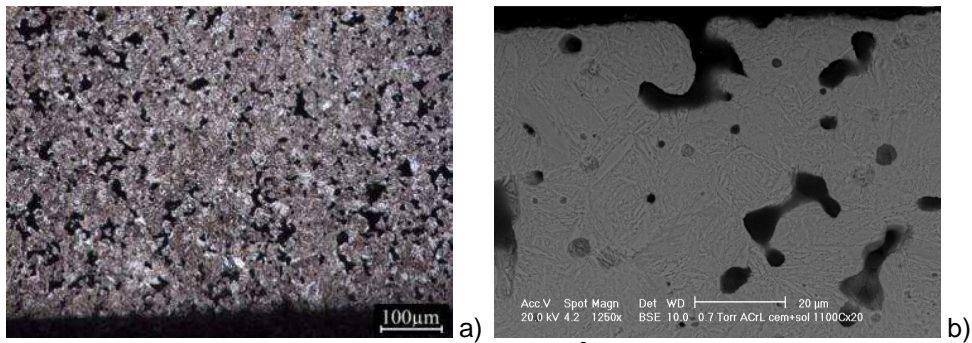


Figure 6.30: microstructure of carburized  $7.0\text{g/cm}^3$  0.2%C ACrL sintered at  $1120^\circ\text{C}$ , solution annealed at  $1100^\circ\text{C}$  and cooled down at 5K/s: a) LOM micrograph and b) SEM micrograph

## Chapter 6: Low Pressure Carburizing of Chromium Steels

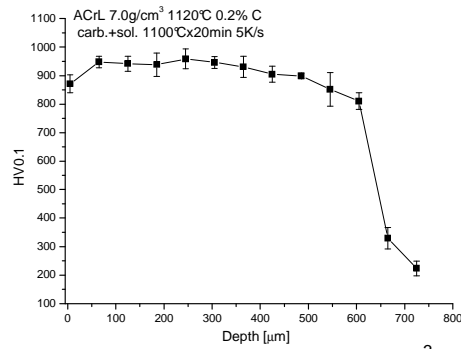


Figure 6.31: microhardness profile of carburized 7.0g/cm<sup>3</sup> 0.2%C ACrL sintered at 1120°C, solution annealed at 1100°C and cooled down at 5K/s

The microhardness profile is deeper thanks to the enhanced dissolution of carbides.

The impact resistance of solution annealed and 200°C tempered ACrL is reported in table 6.7 and compared to that of 7.4g/cm<sup>3</sup> and surface densified carburized material. In this case the solution annealing was carried out at 1150°C.

Table 6.7: impact energy of carburized 0.2%C ACrL with different porosity

Tempering [°C]	Impact Energy [J]		
	7.0g/cm <sup>3</sup> solution annealed	7.4g/cm <sup>3</sup>	7.0g/cm <sup>3</sup> surface densified
200	7	10-11	9-11

The impact toughness of the three materials after 200°C tempering is quite similar. The impact energy is slightly lower in the solution annealed specimen than those of the carburized 7.4 g/cm<sup>3</sup> density or surface densified materials.

### 6.4. Fatigue resistance

A four steps low pressure carburizing (LPC 3) was carried out to study the fatigue resistance of the steels. Since low pressure carburizing causes an extensive grain

## Chapter 6: Low Pressure Carburizing of Chromium Steels

boundaries carbides precipitation in  $6.8\text{g/cm}^3$  and  $7.0\text{g/cm}^3$  specimens, fatigue resistance was evaluated only for  $7.4\text{g/cm}^3$  and surface densified materials. Solution annealing can effectively eliminate overcarburizing, therefore fatigue tests were carried out also on solution annealed and tempered steels.

### 6.4.1. Microstructure and microhardness profile

The target for low pressure carburizing is a surface microhardness of around 800-900HV and a case depth of around 500-600 $\mu\text{m}$ . Microstructures and microhardness profiles of LPC 3 steels are shown in figures 6.32- 6.35.

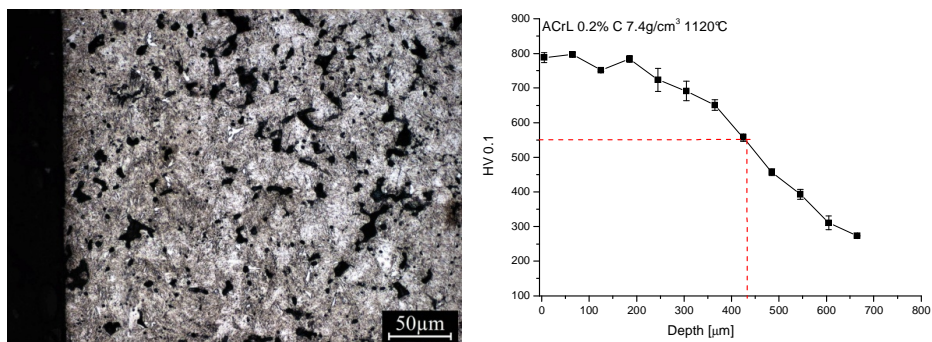


Figure 6.32: microstructure and microhardness profile of carburized  $7.4\text{g/cm}^3$  0.2%C ACrL sintered at  $1120^\circ\text{C}$

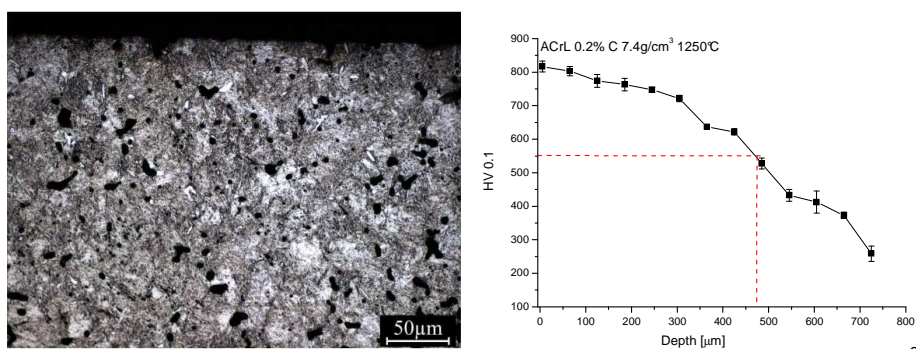


Figure 6.33: microstructure and microhardness profile of carburized  $7.4\text{g/cm}^3$  0.2%C ACrL sintered at  $1250^\circ\text{C}$



## Chapter 6: Low Pressure Carburizing of Chromium Steels

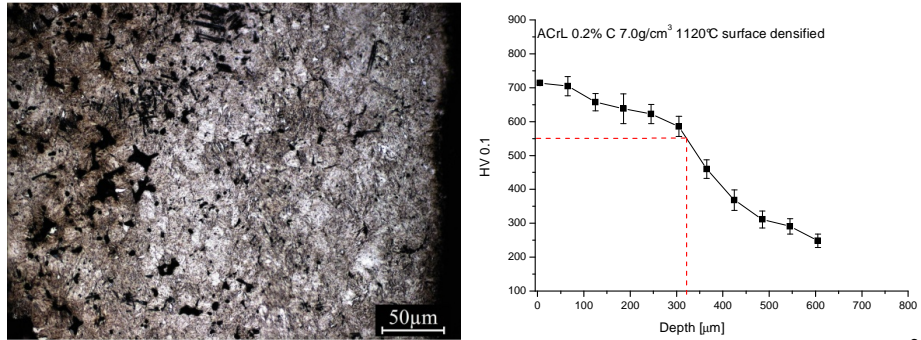


Figure 6.34: microstructure and microhardness profile of carburized 7.0g/cm<sup>3</sup> surface densified 0.2%C ACrL sintered at 1120°C

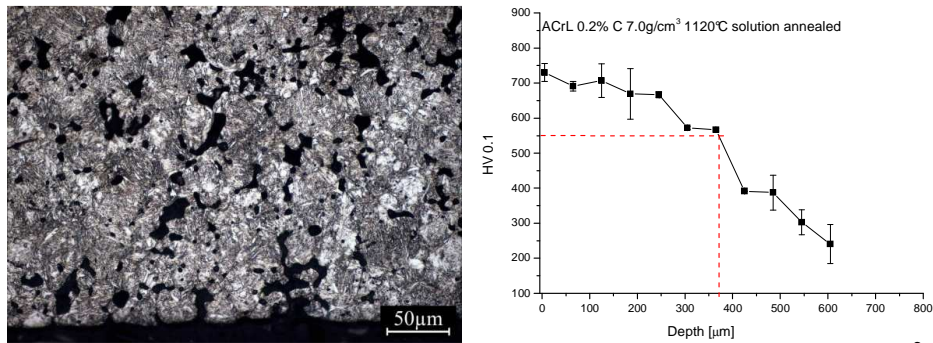


Figure 6.35: microstructure and microhardness profile of carburized 7.0g/cm<sup>3</sup> solution annealed 0.2%C ACrL sintered at 1120°C

In 7.4g/cm<sup>3</sup> materials the microstructure of the case is homogeneous for both the sintering temperatures; quite similar to those of the surface densified and solution annealed ones. Table 6.8 summarizes the representative data of the microhardness profiles (surface microhardness and  $d_{550}$ ) of the materials. The microhardness profiles are deeper in 7.4g/cm<sup>3</sup> specimens respect to the surface densified ones because of the absence of surface porosity. The solution annealed and 200°C tempered ACrL archives a deep microhardness profile similar to that of surface densified materials.

### *Chapter 6: Low Pressure Carburizing of Chromium Steels*

Sintered temperature does not affected the case microstructure and the microhardness profile, significantly. Therefore, the results of surface densified and solution annealed steels are reported only for the low temperature.

Table 6.8: microhardness and case depth of carburized steels

		<b>7.4g/cm<sup>3</sup> 0.2%C ACrL</b>	<b>Target</b>
1120°C	HV0.1	790	800-900
	d <sub>550</sub> [μm]	430	500-600
1250°C	HV0.1	820	800-900
	d <sub>550</sub> [μm]	480	500-600

<b>7.0g/cm<sup>3</sup> 0.2%C ACrL</b>			<b>Target</b>
	<b>Surface densified</b>	<b>Solution annealed</b>	
HV0.1	710	730	800-900
d <sub>550</sub> [μm]	360	360	500-600

#### *6.4.2. Fatigue resistance*

The results of the stair case method are reported in figure 6.36 and the fatigue resistance at  $2 \times 10^6$  cycles are listed in table 6.9.

## Chapter 6: Low Pressure Carburizing of Chromium Steels

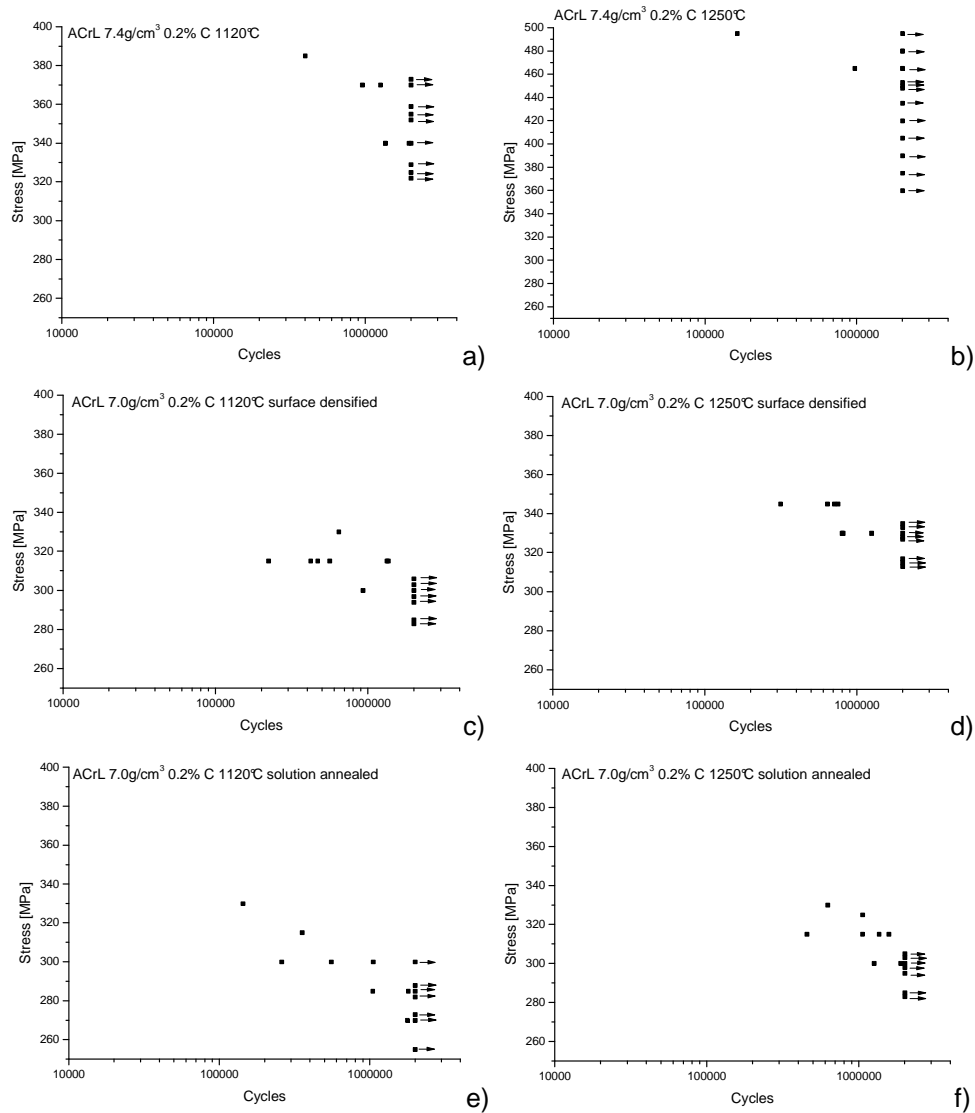


Figure 6.36: fatigue results of carburized 0.2%C ACrL: a) 7.4g/cm<sup>3</sup> sintered at 1120°C, b) 7.4g/cm<sup>3</sup> sintered at 1250°C, c) 7.0g/cm<sup>3</sup> sintered at 1120°C and surface densified, d) 7.0g/cm<sup>3</sup> sintered at 1250°C and surface densified, e) 7.0g/cm<sup>3</sup> sintered at 1120°C and solution annealed and f) 7.0g/cm<sup>3</sup> sintered at 1250°C and solution annealed

## Chapter 6: Low Pressure Carburizing of Chromium Steels

Table 6.9: fatigue resistance at  $2 \times 10^6$  cycles of low pressure carburized steels

	Fatigue resistance at $2 \times 10^6$ cycles [MPa]		
	7.4g/cm <sup>3</sup> 0.2%C ACrL	7.0g/cm <sup>3</sup> 0.2%C ACrL surface densified	7.0g/cm <sup>3</sup> 0.2%C ACrL solution annealed
1120°C	350±36	303±6	286±21
1250°C	473±25	331±7	303±6

The fatigue resistance of the solution annealed material is similar to that of the surface densified one, confirming that solution annealing is a real alternative to surface densification for low pressure carburizing of sintered steels. The 7.4g/cm<sup>3</sup> materials have the highest resistance, as expected.

### 6.4.3. Fracture surface analysis

The fracture surfaces of carburized materials are reported in figures 6.37-6.39.

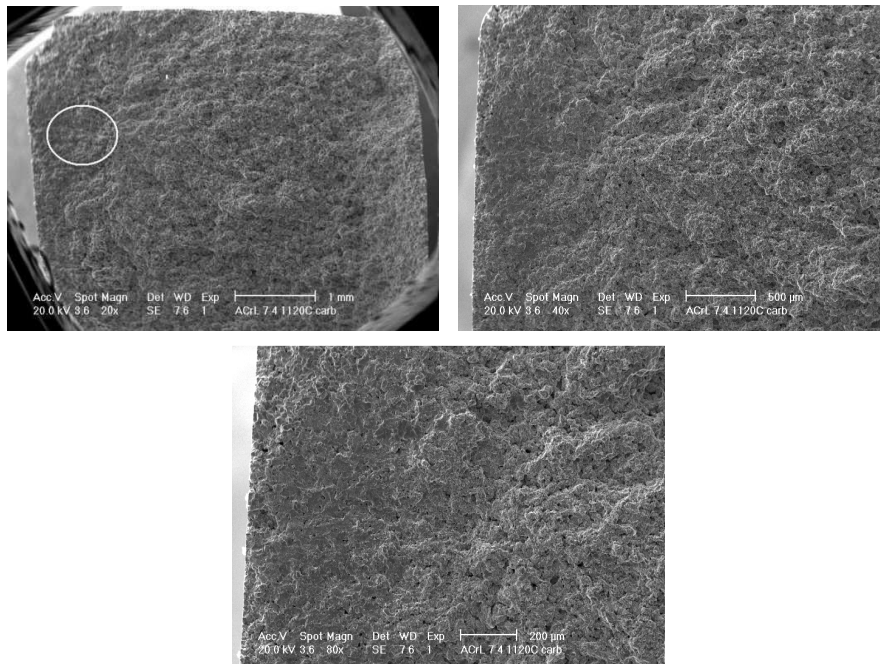


Figure 6.37: fracture surface of carburized 7.4g/cm<sup>3</sup> 0.2%C ACrL sintered at 1120°C

*Chapter 6: Low Pressure Carburizing of Chromium Steels*

---

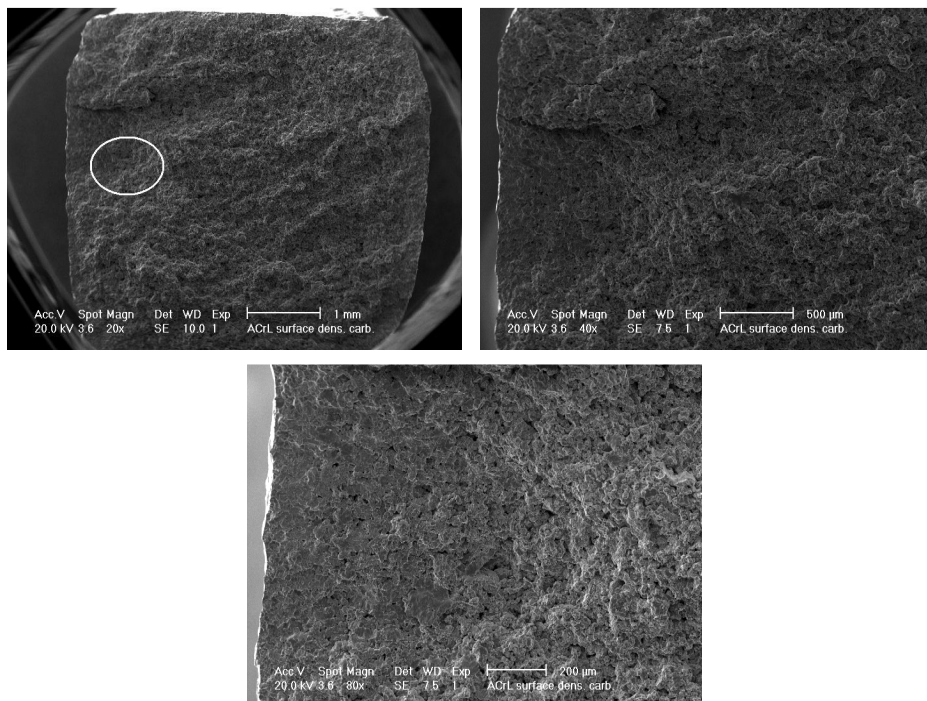


Figure 6.38: fracture surface of carburized  $7.0\text{g}/\text{cm}^3$  surface densified 0.2%C ACrL sintered at  $1120^\circ\text{C}$

## Chapter 6: Low Pressure Carburizing of Chromium Steels

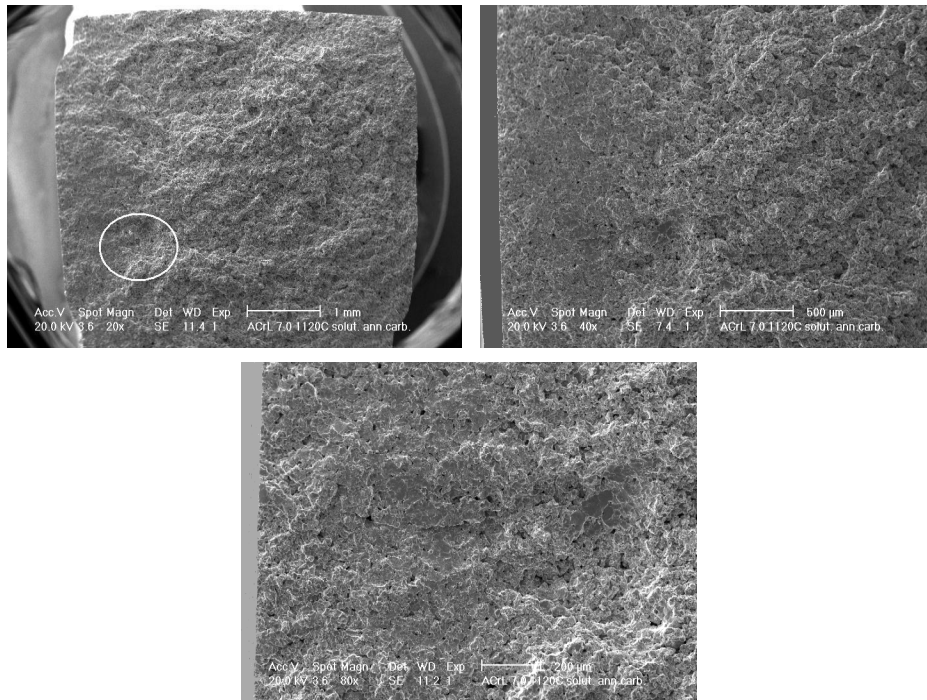


Figure 6.39: fracture surface of carburized  $7.0\text{g/cm}^3$  solution annealed 0.2%C ACrL sintered at  $1120^\circ\text{C}$

The analysis of the fracture surface shows a subsurface crack nucleation ( $300\text{-}400\mu\text{m}$ ), in correspondence of either a cluster of pores or a large pore, as usual in porous sintered steels. The movement of the fatigue crack initiation in the subsurface layers is due to both surface hardening and compressive residual stresses generated by carburizing; the crack nucleates in correspondence of the maximum tensile stress and where the hardness is not affected by the treatment.

The similar fatigue resistance of the surface densified and of the solution annealed steels is due to the very similar case hardness and depth. At the same time, the better fatigue resistance of the  $7.4\text{g/cm}^3$  steels is due to the deeper case, as well as to the higher bulk density, which improves the pore distribution (clusters) and size (large pores).

## *Chapter 6: Low Pressure Carburizing of Chromium Steels*

### *6.4.4. Evaluation of the low pressure carburizing effect on the fatigue resistance*

To evaluate the effect of low pressure carburizing on fatigue resistance of ACrL, the comparison with others thermochemical treatments is necessary. With reference to the data reported in table 6.10 the fatigue resistance of low pressure carburized  $7.4\text{g/cm}^3$  0.2%C ACrL sintered at  $1120^\circ\text{C}$  is similar to that reported by Kanno et al.[20], concerning to the same LPC steel with higher sintering temperature ( $1280^\circ\text{C}$ ). Kanno shows that shot peening increases the fatigue limit of low pressure carburized material, exceeding 470MPa. The same fatigue resistance is archived by low pressure carburized  $7.4\text{g/cm}^3$  0.2%C ACrL sintered at  $1250^\circ\text{C}$ .

Table 6.10: fatigue resistance of low pressure carburized ACrL steels

%C	Density [g/cm <sup>3</sup> ]	T Sintering	LPC	Shot peened	Fatigue resistance at $2 \times 10^6$ cycles [MPa]	
					Kanno et al. [20]	
0.2	7.3	$1280^\circ\text{C}$	LPC	NO	360-390	-
				YES	>470	-
0.2	7.4	$1120^\circ\text{C}$		NO	-	$350 \pm 36$
				0.2	7.4	$1250^\circ\text{C}$

The comparison with plasma carburized steels shows that the fatigue strength of the low pressure carburized  $7.4\text{g/cm}^3$  ACrL sintered at  $1120^\circ\text{C}$  is higher than that obtained by plasma carburizing, in particular on increasing sintering temperature (tab. 6.11). Moreover, the fatigue strengths of LPC surface densified steels and solution annealed ones are quite similar to those of plasma carburized  $7.1\text{g/cm}^3$  ACrL, confirming that solution annealing treatment represents an effective technique for low pressure carburizing of sintered steels with open porosity.

**Chapter 6: Low Pressure Carburizing of Chromium Steels**

Table 6.11: fatigue resistance of plasma carburized and low pressure carburized ACrL steels

%C	Density [g/cm <sup>3</sup> ]	T Sintering		Fatigue resistance at 2x10 <sup>6</sup> cycles [MPa]	
				Plasma carburized [35]	Low pressure carburized
0.2	7.1	1120°C		305±8	-
0.2	7.0	1120°C	<b>Surface densified</b>	-	303±6
0.2	7.0	1120°C	<b>Solution annealed</b>	-	286±21
0.2	7.1	1250°C		329±23	-
0.2	7.3-7.4	1120°C		337±6	350±36
0.2	7.3-7.4	1250°C		366±20	473±25

**6.5. Concluding remarks**

The results of the work on low pressure carburizing can be summarized as follows.

- In presence of open porosity Cr steels are overcarburized.
- Overcarburizing is avoided by a closed porosity, performed by both surface densification and on increasing density up to 7.4g/cm<sup>3</sup>.
- Case depth is deeper in 7.4g/cm<sup>3</sup> specimens, even in presence of a fully closed porosity, than in surface densified steels.
- Case depth is deeper in ACrL than in AD4 because of the greater hardenability.
- Target of surface microhardness and case depth is matched by a five steps treatment having a total boosting time of 6 minutes and diffusion time of 115 minutes.
- Carburizing causes the embrittlement of the materials, independently on bulk density. Impact behavior of all the carburized steels is purely elastic,



### *Chapter 6: Low Pressure Carburizing of Chromium Steels*

---

plastic deformation is completely suppressed by the thermochemical treatment.

- Overcarburizing can be eliminated by a solution annealing treatment followed by a tempering at 200°C.
- The plane bending fatigue resistance increases up to 470MPa after low pressure carburizing. The analysis of the fracture surface of the carburized steels shows subsurface crack nucleation in all the materials.

## 7. Plasma Nitriding of Chromium Steels

Plasma nitriding was carried out with two selected industrial treatments on the steels with density  $6.8\text{g/cm}^3$ ,  $7.0\text{g/cm}^3$  and  $7.4\text{g/cm}^3$ , sintered at  $1120^\circ\text{C}$  and  $1250^\circ\text{C}$  and with three carbon contents (0.05%, 0.2% and 0.4%). Some sample have been surface densified previously.

The treatments were carried out in an industrial plant (Vacuum Company, Milano, Italy) with the target represented by: a case depth of  $250\text{-}350\mu\text{m}$  and the absence of compound layer around the subsurface pores and a surface microhardness of  $700\text{-}800\text{HV}0.05$ . The treatment parameters are listed in Table 7.1.

Table 7.1: PN treatments

Treatment	Temperature [°C]	Time [h]	
		Nitriding (80N <sub>2</sub> /20H <sub>2</sub> )	Diffusion (90N <sub>2</sub> /10H <sub>2</sub> )
PN 1	480	20	8
PN 2	480	48	24

### 7.1. Microstructures and microhardness profiles

#### 7.1.1. 20 hours nitriding and 8 hours diffusion at $480^\circ\text{C}$

Microstructures and microhardness profiles of  $7.0\text{g/cm}^3$  ACrL and AD4 sintered at  $1250^\circ\text{C}$  are reported in figures 7.1- 7.6.

## Chapter 7: Plasma Nitriding of Chromium Steels

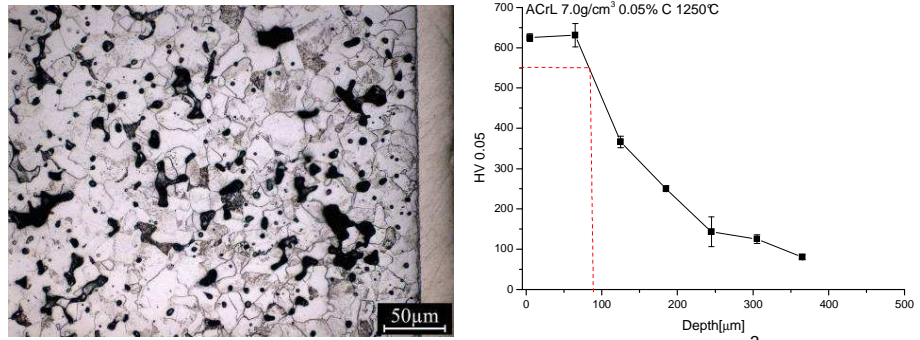


Figure 7.1: microstructure and microhardness profile of  $7.0\text{g}/\text{cm}^3$  0.05% C ACrL sintered at  $1250^\circ\text{C}$

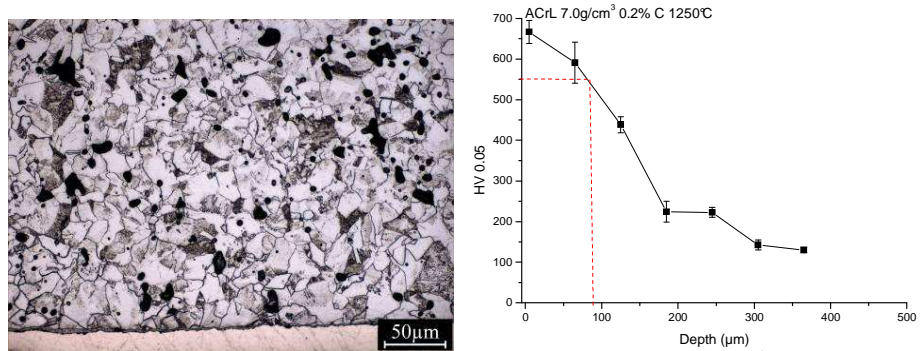


Figure 7.2: microstructure and microhardness profile of  $7.0\text{g}/\text{cm}^3$  0.2% C ACrL sintered at  $1250^\circ\text{C}$

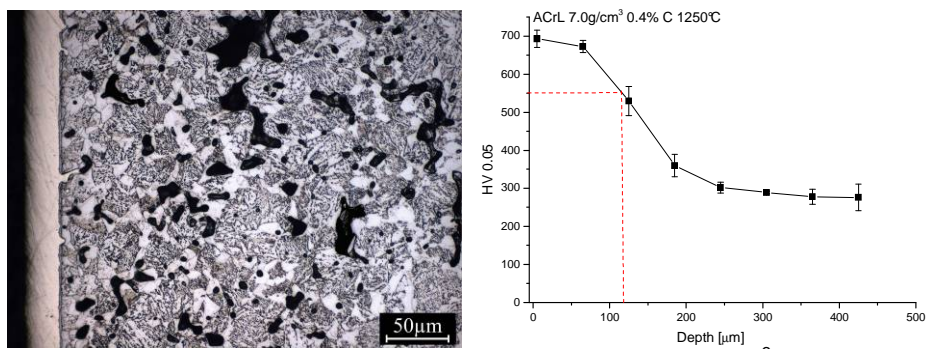


Figure 7.3: microstructure and microhardness profile of  $7.0\text{g}/\text{cm}^3$  0.4% C ACrL sintered at  $1250^\circ\text{C}$

## Chapter 7: Plasma Nitriding of Chromium Steels

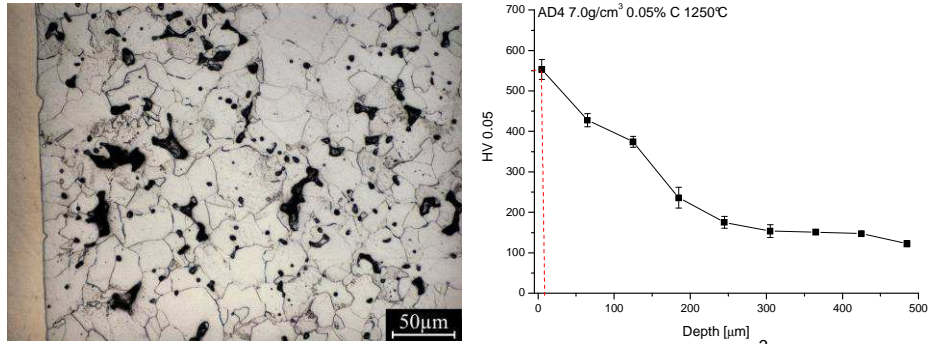


Figure 7.4: microstructure and microhardness profile of  $7.0\text{g}/\text{cm}^3$  0.05%C AD4 sintered at  $1250^\circ\text{C}$

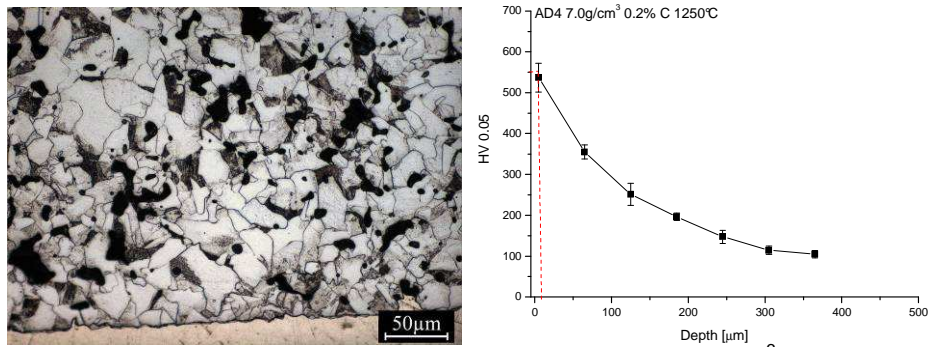


Figure 7.5: microstructure and microhardness profile of  $7.0\text{g}/\text{cm}^3$  0.2%C AD4 sintered at  $1250^\circ\text{C}$

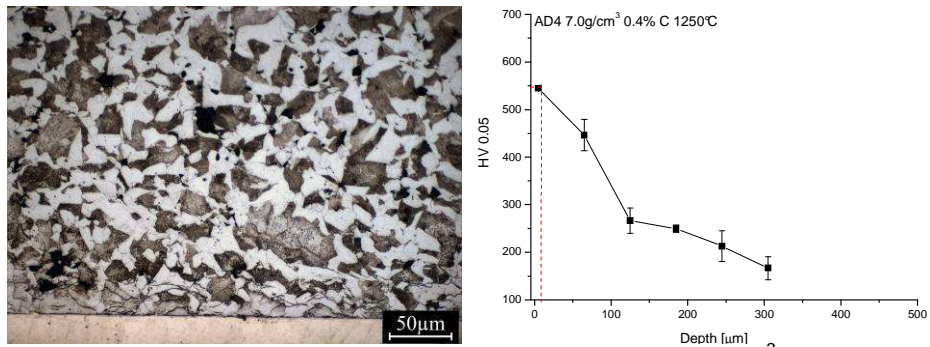


Figure 7.6: microstructure and microhardness profile of  $7.0\text{g}/\text{cm}^3$  0.4%C AD4 sintered at  $1250^\circ\text{C}$

## *Chapter 7: Plasma Nitriding of Chromium Steels*

---

PN 1 is poorly effective on the steels and even in the best case, 0.4%C ACrL, surface microhardness and case depth are too low with reference to the target (tab. 7.2)

Table 7.2: surface microhardness and case depths of PN 1 steels

<b>ACrL</b>	<b>0.05%C</b>	<b>0.2%C</b>	<b>0.4%C</b>	<b>Target</b>
HV0.05	630	670	700	700-800
$d_{550}$ [ $\mu\text{m}$ ]	90	90	120	250-350

<b>AD4</b>	<b>0.05%C</b>	<b>0.2%C</b>	<b>0.4%C</b>	<b>Target</b>
HV0.05	550	550	550	700-800
$d_{550}$ [ $\mu\text{m}$ ]	10	10	10	250-350

The ferritic (ferritic-perlitic) microstructure and the less content of chromium reduce the nitridability of AD4 respect to ACrL. Therefore AD4 and the ferritic 0.05% C ACrL, which do not show satisfactory results after nitriding, will be neglected in the next study.

### *7.1.2. 48 hours nitriding and 24 hours diffusion at 480°C*

Microstructures and microhardness profiles of 6.8g/cm<sup>3</sup> and 7.4g/cm<sup>3</sup> ACrL sintered at 1120°C are shown in figures 7.7- 7.10, whilst those of the steels sintered at 1250°C are reported in appendix. The microstructures and microhardness profiles of nitrided 7.0g/cm<sup>3</sup> ACrL sintered at 1120°C and 1250°C are also present in appendix.

Chapter 7: Plasma Nitriding of Chromium Steels

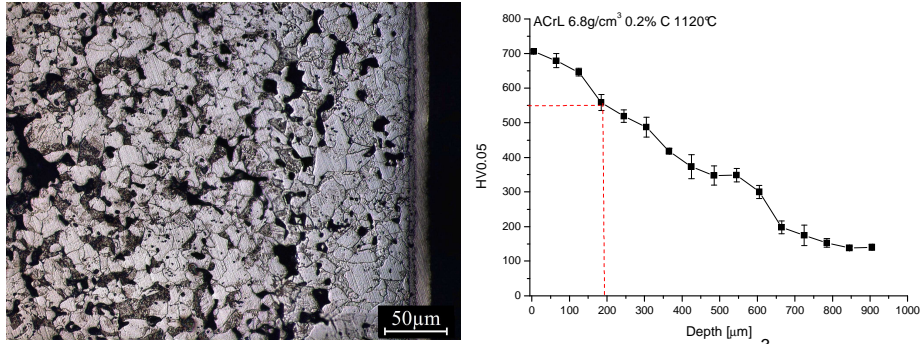


Figure 7.7: microstructure and microhardness profile of 6.8g/cm<sup>3</sup> 0.2%C ACrL sintered at 1120°C

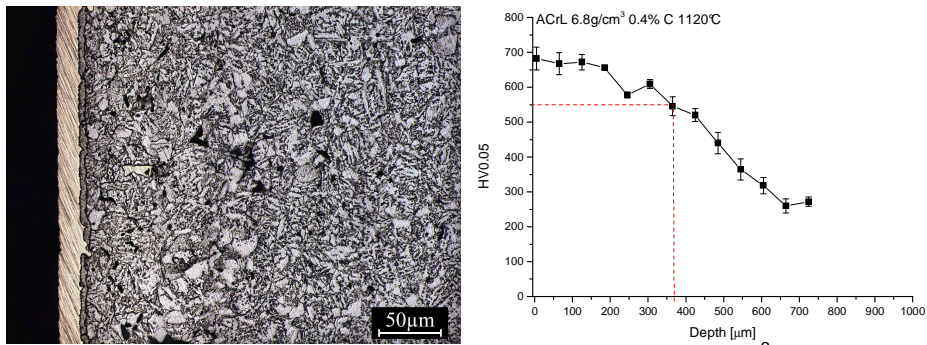


Figure 7.8: microstructure and microhardness profile of 6.8g/cm<sup>3</sup> 0.4%C ACrL sintered at 1120°C

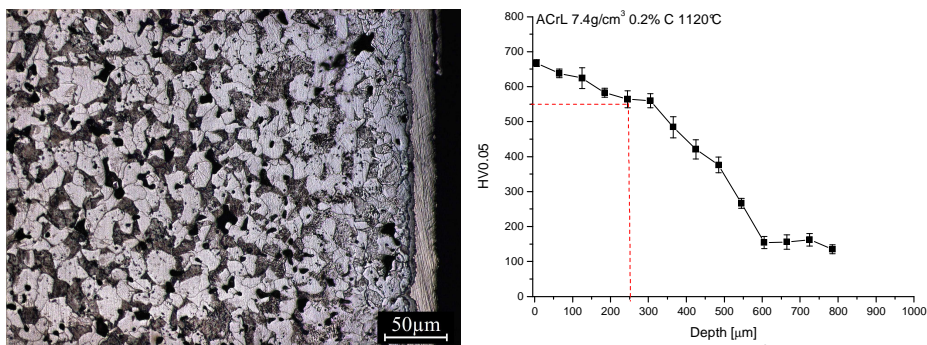


Figure 7.9: microstructure and microhardness profile of 7.4g/cm<sup>3</sup> 0.2%C ACrL sintered at 1120°C

## Chapter 7: Plasma Nitriding of Chromium Steels

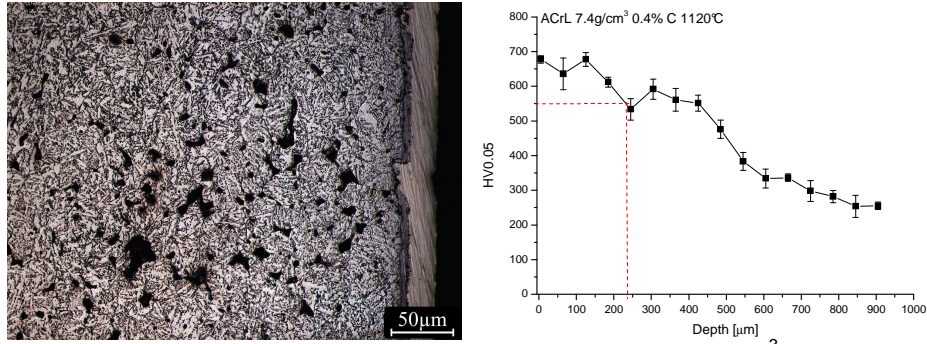


Figure 7.10: microstructure and microhardness profile of  $7.4\text{g/cm}^3$  0.4%C ACrL sintered at  $1120^\circ\text{C}$

A  $10\mu\text{m}$  thick compound layer is present in all the materials. The XRD pattern of the nitrided  $7.0\text{g/cm}^3$  0.2%C ACrL sintered at  $1250^\circ\text{C}$  is reported in figure 7.11 and gives the composition of the compound layer and of the diffusion one: ferrite ( $\alpha$ ),  $\text{Fe}_4\text{N}$  ( $\gamma'$ ) and  $\text{Fe}_{2-3}\text{N}$  ( $\epsilon$ ).

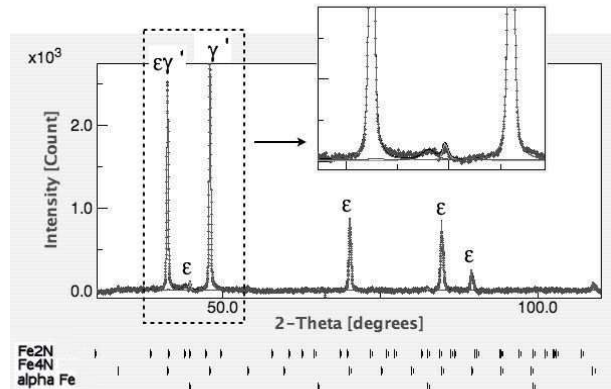


Figure 7.11: XRD pattern of nitrided  $7.0\text{g/cm}^3$  0.2%C ACrL sintered at  $1250^\circ$

The surface microhardness and the case depths ( $d_{550}$ ) are summarized in table 7.3. The surface microhardness is around  $700\text{HV}0.05$ ; it slightly increases on increasing the sintering temperature whilst it does not depend on density and the carbon content. Case depth increases with carbon content and sintering

## Chapter 7: Plasma Nitriding of Chromium Steels

temperature, mainly because of the base microhardness (around 70HV0.05 higher in the material sintered at 1250°C or containing 0.4%C) and it does not depend on density. Anyway, it ranges from 200 to 450µm. The results correspond quite well with the target.

Table 7.3: surface microhardness and case depths of PN 2 steels

		6.8g/cm <sup>3</sup>		7.0g/cm <sup>3</sup>		7.4g/cm <sup>3</sup>		Target
		0.2%C	0.4%C	0.2%C	0.4%C	0.2%C	0.4%C	
1120°C	HV0.05	700	690	700	730	690	690	700-800
	d <sub>550</sub> [µm]	200	360	250	450	250	250	250-350
1250°C	HV0.05	730	730	720	720	700	730	700-800
	d <sub>550</sub> [µm]	400	480	440	410	350	355	250-350

### 7.1.3. Effect of surface densification

PN 2 was carried out on 7.0g/cm<sup>3</sup> 0.2%C ACrL, previously surface densified, in order to study the effect of the surface densification. The microstructural characterization is shown in figure 7.12.

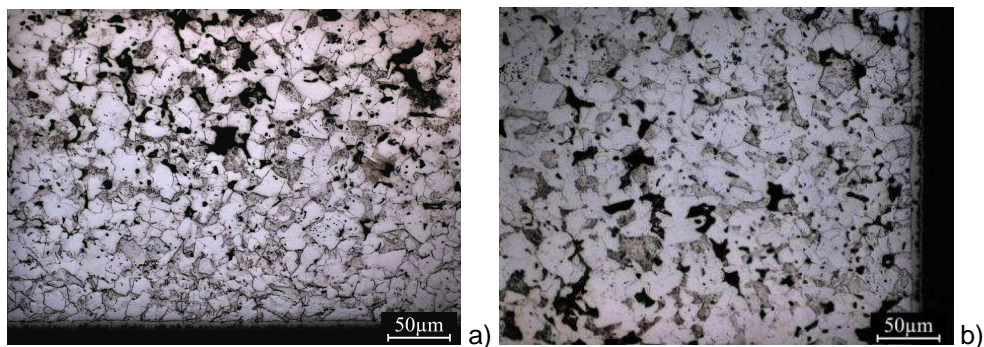


Figure 7.12: microstructures of nitrided 0.2%C ACrL, sintered at 1120°C: a) 7.0g/cm<sup>3</sup> surface densified and b) 7.0g/cm<sup>3</sup>



## Chapter 7: Plasma Nitriding of Chromium Steels

The microstructure of surface densified and nitrided materials (fig. 7.12a) is similar to that of nitrided steels (fig. 7.12b) and the densified surface layer is clearly evident.

The surface densification does not lead to a further improvement in the microhardness profile (fig. 7.13). The surface microhardness of the surface densified steel is around 650HV0.1, independently on density and sintering temperature, lower than that of nitrided material (700HV0.1). The case depth slightly increases in the surface densified specimens (180 $\mu\text{m}$ ) with reference to the nitrided ones (160 $\mu\text{m}$ ), without any systematic effect of density and sintering temperature.

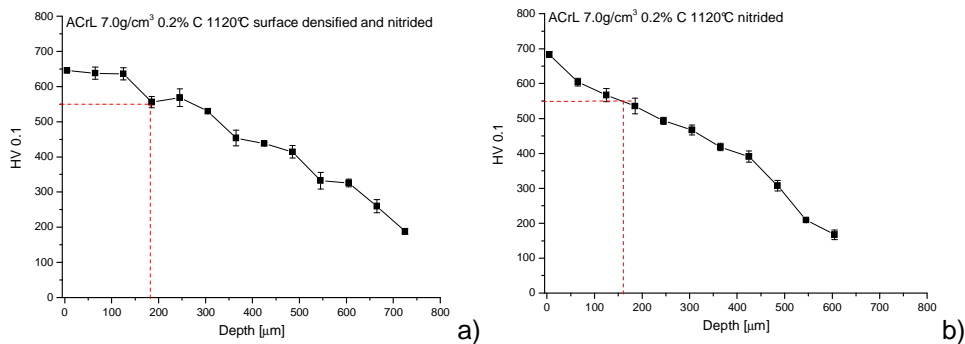


Figure 7.13: microhardness profiles of nitrided 0.2%C ACrL sintered at 1120°C: a) 7.0 g/cm<sup>3</sup> surface densified and b) 7.0 g/cm<sup>3</sup>

There is not a contribution on the final microhardness profile provided by shot peening. Nitriding prevails noticeably on shot peening, as shown by the comparison between the microhardness profiles of the nitrided (fig. 7.14a) and the surface densified (fig. 7.14b) material.

## Chapter 7: Plasma Nitriding of Chromium Steels

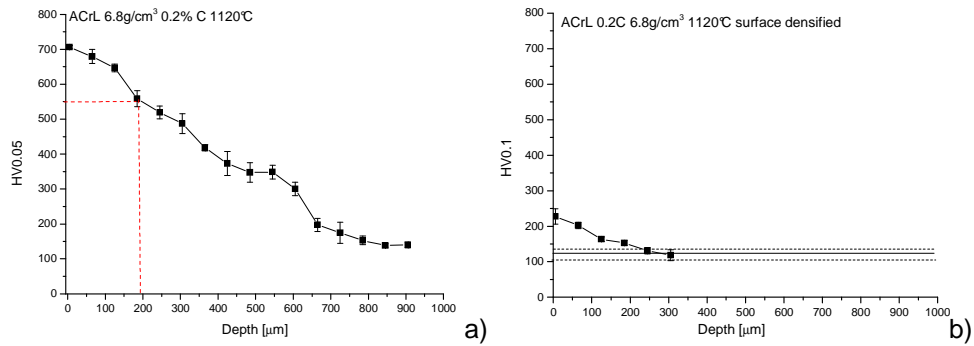


Figure 7.14: microhardness profiles of 6.8g/cm<sup>3</sup> ACrL 0.2%C sintered at 1120°C: a) nitrided and b) surface densified

### 7.2. Impact toughness

The results of the impact tests are listed in the table 7.4.

Table 7.4: impact tests results of PN2 steels

			Impact Energy [J]		P <sub>y</sub> [KN]		P <sub>max</sub> [KN]	
ACrL			As sint	Nitrided	As sint	Nitrided	As sint	Nitrided
%C	Density [g/cm <sup>3</sup> ]	T sint [°C]						
0.2	6.8	1120	21±1	4	9	-	12	9
0.2	6.8	1250	34±2	6	9	-	14	12
0.2	7.0	1120	29±2	5	11	-	14	10
0.2	7.0	1250	52±7	7	10	-	16	13
0.2	7.4	1120	72±5	6	13	-	24	14
0.2	7.4	1250	95±4	11	12	-	18	16
0.4	6.8	1120	13±2	4	12	-	17	11
0.4	6.8	1250	23±4	5.	13	-	20	12
0.4	7.0	1120	19±1	4	12	-	19	11
0.4	7.0	1250	33±4	5	11	-	21	12
0.4	7.4	1120	40	4	14	-	25	12
0.4	7.4	1250	72±1	5	15	-	26	13

## Chapter 7: Plasma Nitriding of Chromium Steels

Some of the load-deflection curves of PN2 ACrL are reported in figure 7.15 comparing the as sintered condition to the nitrided one.

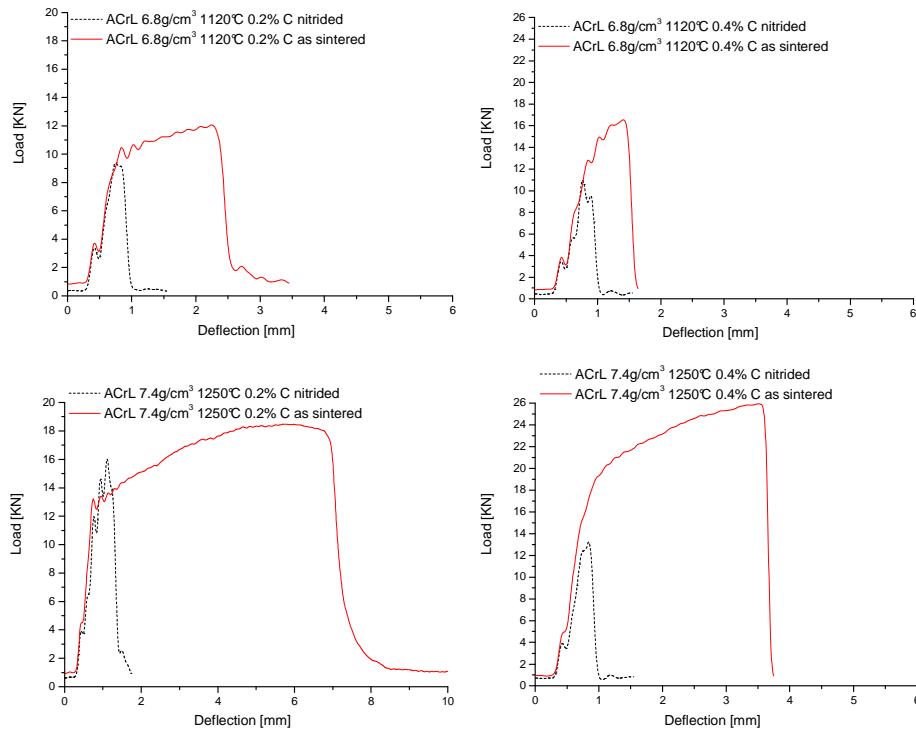


Figure 7.15: examples of load-deflection curves

In 0.2%C materials, plasma nitriding causes the reduction of the plastic field, but resilience (the energy adsorbed in the elastic field) either remains unchanged or slightly increases ( $P_{\max}$  of the nitrided material is comparable to  $P_y$  of the corresponding as sintered one).

In 0.4%C steels, the plastic field is completely eliminated and the resilience is strongly reduced ( $P_{\max}$  of the nitrided material is lower than  $P_y$  of the corresponding as sintered one). This trend was confirmed for all the density and sintering temperature conditions.

## *Chapter 7: Plasma Nitriding of Chromium Steels*

---

Impact energy decreases significantly because of the quite low intrinsic fracture toughness of the diffusion layer (around 10-15MPa m<sup>0.5</sup>) which, in combination with porosity, results in a brittle behaviour under impact loading. Anyway, the higher impact toughness is shown by the 0.2%C materials.

The results of impact tests carried out on surface densified and nitrided ACrL were reported in table 7.5.

Table 7.5: impact tests results of surface densified PN 2 steels

SURFACE DENSIFIED SPECIMENS			Impact Energy [J]	P <sub>max</sub> [KN]
ACrL				
%C	Density [g/cm <sup>3</sup> ]	T sint [°C]		
0.2	6.8	1120	3	10
0.2	6.8	1250	4	11
0.2	7.0	1120	4	11
0.2	7.0	1250	5	13
0.4	6.8	1120	2	10
0.4	6.8	1250	3	11
0.4	7.0	1120	3	12
0.4	7.0	1250	3	13

Some load-deflection curves are reported in figure 7.16 comparing the as sintered condition to the nitrided one.

## Chapter 7: Plasma Nitriding of Chromium Steels

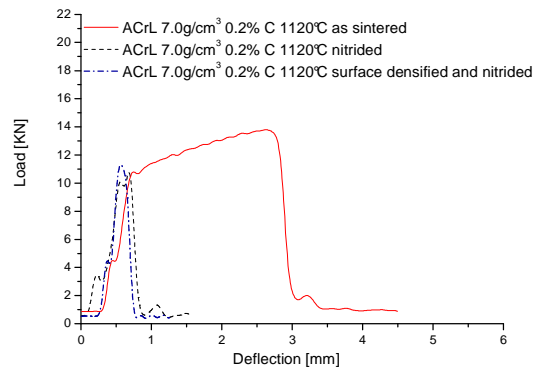


Figure 7.16: impact curves of 7.0g/cm<sup>3</sup> 0.2%C ACrL sintered at 1120°C: as sintered, nitrided and surface densified and nitrided

Surface densification does not have a positive effect on the impact resistance even in this case impact energy decreases significantly because of the embrittlement induced by the nitriding.

### 7.3. Fatigue resistance

The study of the fatigue resistance of nitrided (PN 2) steels was carried out on different steels, with the task of evaluating the influence of the as sintered microstructure (mainly porosity) on the resistance after nitriding. The 7.0g/cm<sup>3</sup> 1120°C sintered steel was taken as a reference and the following variants were considered:

- a higher sintering temperature (1250°C), which increases density slightly and improves pore morphology significantly;
- a surface densification, which eliminates the surface pores;
- a 7.4g/cm<sup>3</sup> steel, which has higher density and higher fraction of closed porosity;
- a 7.4g/cm<sup>3</sup> steel sintered at 1250°C, which has higher density and an almost closed porosity, i.e. the best microstructure.

The list of specimens is reported in table 7.6.

Table 7.6: materials considered in fatigue tests of nitrided steels

	<b>Description</b>
ACrL 7.0g/cm <sup>3</sup> 0.2%C 1120°C	Base
ACrL 7.0g/cm <sup>3</sup> 0.2%C 1250°C	Increase in density and improve pore morphology
ACrL 7.0g/cm <sup>3</sup> 0.2%C 1120°C	Densified surface
ACrL 7.4g/cm <sup>3</sup> 0.2%C 1120°C	Increase in density and closed porosity
ACrL 7.4g/cm <sup>3</sup> 0.2%C 1250°C	Increase in density and closed porosity

The results of the stair case method are reported in figure 7.17 and the fatigue resistances at 2x10<sup>6</sup> cycles are summarized in figure 7.18.

Chapter 7: Plasma Nitriding of Chromium Steels

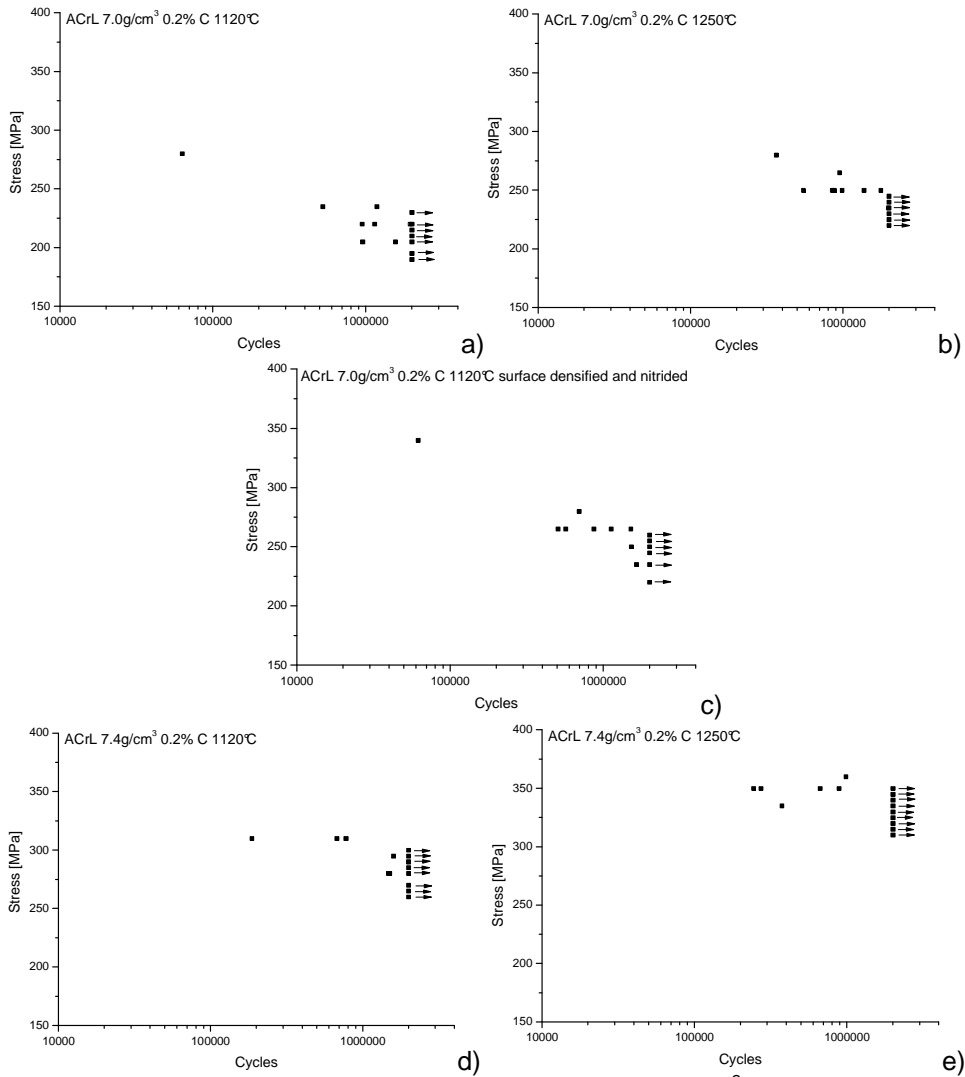


Figure 7.17: fatigue results of nitrided 0.2%C ACrL: a) 7.0g/cm<sup>3</sup> sintered at 1120°C, b) 7.0g/cm<sup>3</sup> sintered at 1250°C, c) surface densified, d) 7.4g/cm<sup>3</sup> sintered at 1120°C and e) 7.4g/cm<sup>3</sup> sintered at 1250°C

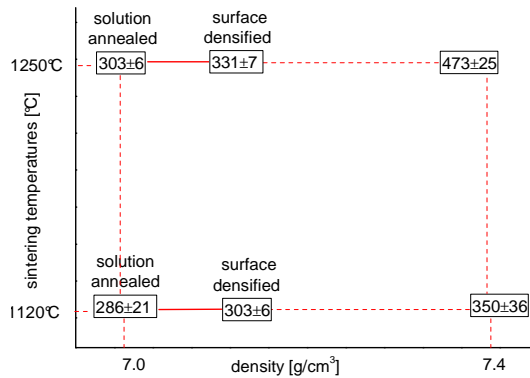


Figure 7.18: fatigue resistance of PN 2 steels

It is well evident that the positive effect of density and sintering temperature on the fatigue resistance is maintained after nitriding. The nitrided 7.4g/cm<sup>3</sup> 0.2%C ACrL sintered at 1250°C and 1120°C have the highest fatigue resistance. Surface densification leads to an improvement of the fatigue resistance comparable to that attained by increasing sintering temperature from 1120°C up to 1250°C, but lower than that attainable by increasing density from 7.0g/cm<sup>3</sup> up to 7.4g/cm<sup>3</sup>.

#### 7.4. Post nitriding shot peening

A post nitriding shot peening was carried out on 7.0g/cm<sup>3</sup> and 7.4g/cm<sup>3</sup> 0.2%C ACrL sintered at 1120°C and 1250°C in order to investigate the fatigue resistance.

##### 7.4.1. Microstructure

The microstructures of post nitriding shot peened 7.0g/cm<sup>3</sup> ACrL sintered at 1120°C and at 1250°C are reported in figure 7.19.



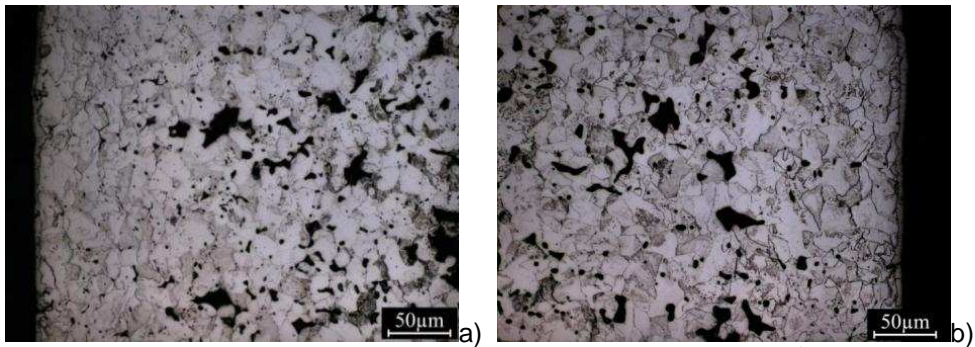


Figure 7.19: microstructures of post nitriding shot peened 7.0g/cm<sup>3</sup> 0.2%C ACrL sintered at: a) 1120°C and b) 1250°C

The compound layer (around 10µm) is still present after shot peening, confirming the good adhesion to the substrate. The SEM characterization of the post nitriding shot peened surfaces indicates that shot peening closes the surface porosity but the plastic deformation is not well controlled, and some residual defects are left on the surface (fig. 20), in particular in the steel with lower density (fig. 20a).

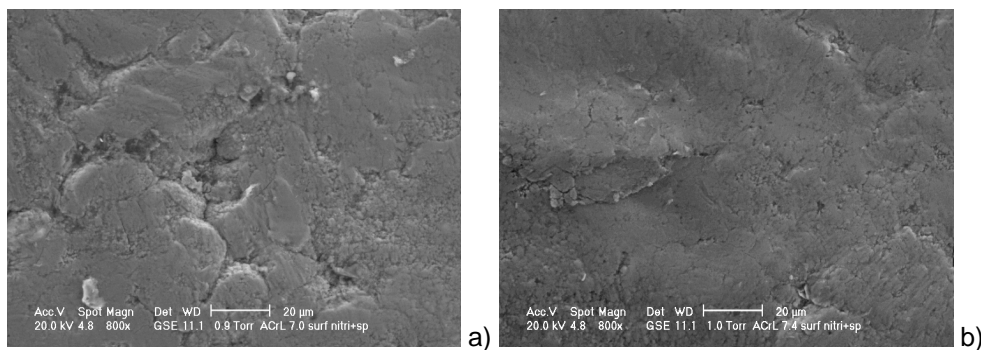


Figure 7.20: surface of post nitriding shot peened 0.2%C ACrL sintered at 1120°C: a) 7.0g/cm<sup>3</sup> and b) 7.4g/cm<sup>3</sup>

#### 7.4.2. Microhardness profile

The microhardness profiles of post nitriding shot peened steels are shown in figure 7.21.

## Chapter 7: Plasma Nitriding of Chromium Steels

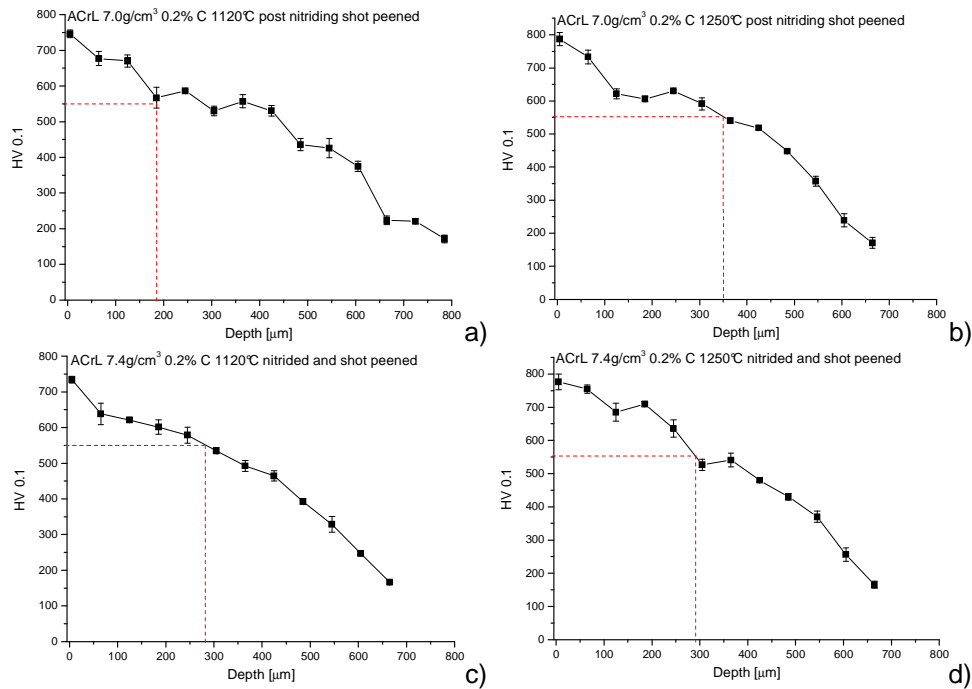


Figure 7.21: microhardness profiles of post nitriding shot peened 0.2%C ACrL: a) 7.0g/cm<sup>3</sup> sintered at 1120°C, b) 7.0g/cm<sup>3</sup> sintered at 1250°C, c) 7.4g/cm<sup>3</sup> sintered at 1120°C and d) 7.4g/cm<sup>3</sup> sintered at 1250°C

The post nitriding shot peening effectively increases the surface microhardness and case depth, respect to that of nitrided steels, up to 790HV0.1 and 350μm, respectively (tab. 7.7). This is due to the compressive residual stresses and work hardening induced by shot peening near the surface. The compressive residual stress in post nitriding shot peened specimens are reported in table 7.8. The values increase on increasing sintering temperature and density because the yield strength increases.

*Chapter 7: Plasma Nitriding of Chromium Steels*

Table 7.7: surface microhardness and case depth of PN 2 and post nitriding shot peened steels

		7.0g/cm <sup>3</sup> 0.2%C ACrL		7.4g/cm <sup>3</sup> 0.2%C ACrL	
		Nitrided	Post nitriding shot peened	Nitrided	Post nitriding shot peened
1120°C	HV0.1	680	750	650	730
	d <sub>550</sub> [µm]	160	190	160	280
1250°C	HV0.1	710	790	700	780
	d <sub>550</sub> [µm]	170	350	230	290

Table 7.8: compressive residual stresses of post nitriding shot peened materials

Residual stresses [MPa]					
		7.0g/cm <sup>3</sup> 0.2%C ACrL		7.4g/cm <sup>3</sup> 0.2%C ACrL	
		On surface	30µm depth	On surface	30µm depth
1120°C		-558 ± 17	-771 ± 14	-770 ± 17	-767 ± 14
1250°C		-769 ± 22	-839 ± 15	-863 ± 22	-911 ± 14

*7.4.3. Fatigue resistance*

The results of the fatigue tests carried out on post nitriding shot peened steels are shown in figure 7.22 and the fatigue resistances at 2x10<sup>6</sup> cycles are summarized in table 7.9.

## Chapter 7: Plasma Nitriding of Chromium Steels

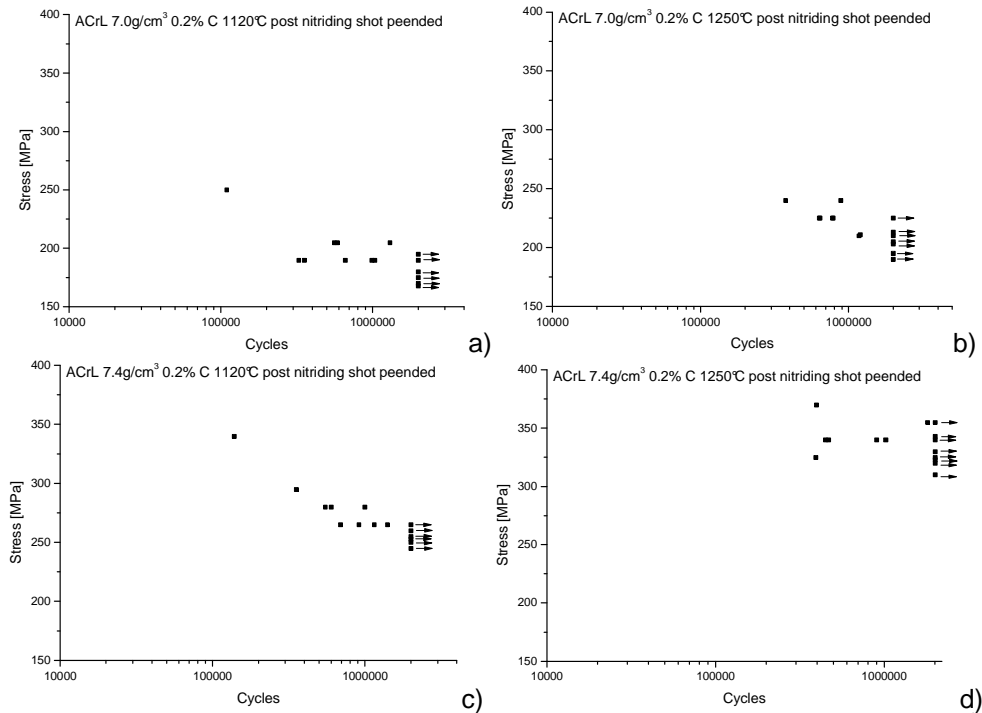


Figure 7.22: fatigue results of post nitriding shot peened 0.2% C ACrL: a)  $7.0\text{g/cm}^3$  sintered at  $1120^\circ\text{C}$ , b)  $7.0\text{g/cm}^3$  sintered at  $1250^\circ\text{C}$ , c)  $7.4\text{g/cm}^3$  sintered at  $1120^\circ\text{C}$  and d)  $7.4\text{g/cm}^3$  sintered at  $1250^\circ\text{C}$

Table 7.9: fatigue resistance at  $2 \times 10^6$  cycles of post nitriding shot peened steels

Fatigue resistance at $2 \times 10^6$ cycles [MPa]				
7.0g/cm <sup>3</sup> 0.2% C ACrL		7.4g/cm <sup>3</sup> 0.2% C ACrL		
	Nitrided	Post nitriding shot peened	Nitrided	Post nitriding shot peened
1120°C	$213 \pm 15$	$188 \pm 6$	$290 \pm 20$	$263 \pm 6$
1250°C	$240 \pm 4$	$215 \pm 11$	$343 \pm 9$	$337 \pm 20$

The fatigue values of post nitriding shot peened steels are similar to those of nitrided ones.

### 7.5. Fracture surface analysis

The fracture surfaces of nitrided specimens show two different morphologies in the diffusion layer (fig. 7.23a) and in the bulk (fig. 7.23b). The former is brittle (cleavages) whilst the latter is ductile (localized dimples).

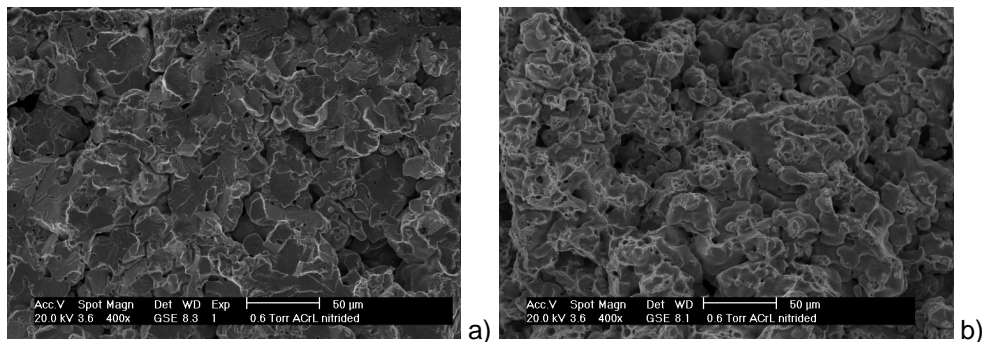


Figure 7.23: fracture surface of nitrided  $7.0\text{g/cm}^3$  0.2%C ACrL sintered at  $1120^\circ\text{C}$ :  
a) diffusion layer and b) bulk

Since in plasma nitrided steels the maximum tensile stress is below the surface according to the superimposition of residual stress and applied stress, crack nucleates in depth and stops growing inside the diffusion layer, improving the high cycle fatigue resistance [34]. The analysis of the fracture surface of the nitrided steels shows subsurface crack nucleation in all the nitrided materials. In nitrided  $7.0\text{g/cm}^3$  material (fig. 7.24) and in surface densified one (fig. 7.25), fatigue crack nucleates beneath the surface in correspondence of a cluster of pores and propagates along the network of interconnected pores, as usual in sintered steels. In post nitriding shot peened  $7.4\text{g/cm}^3$  steel (fig. 7.26) crack starts from a well-defined fish eye.

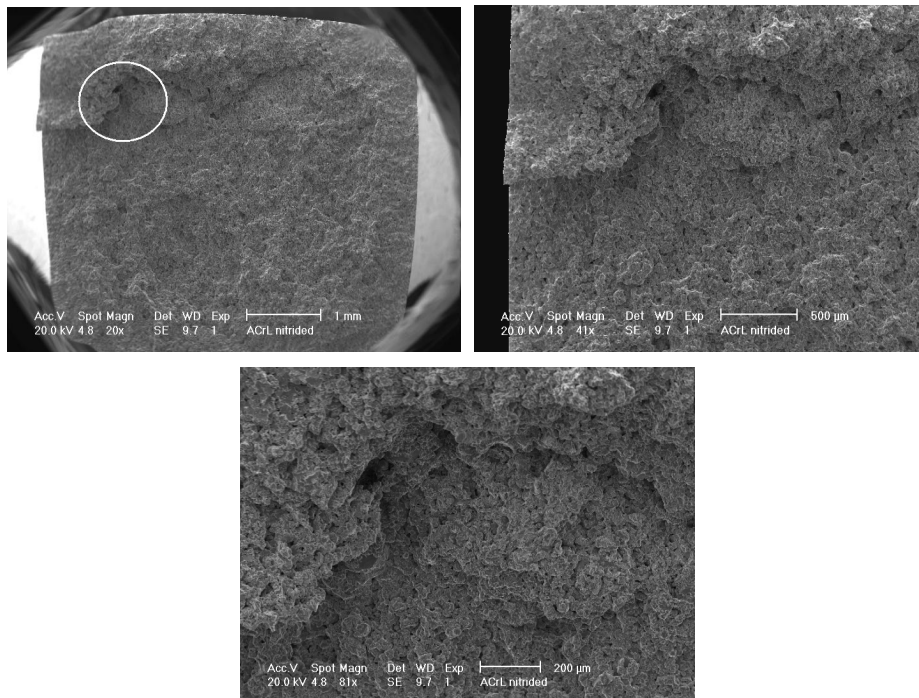


Figure 7.24: fracture surface of nitrided 7.0g/cm<sup>3</sup> 0.2%C ACrL sintered at 1120°C

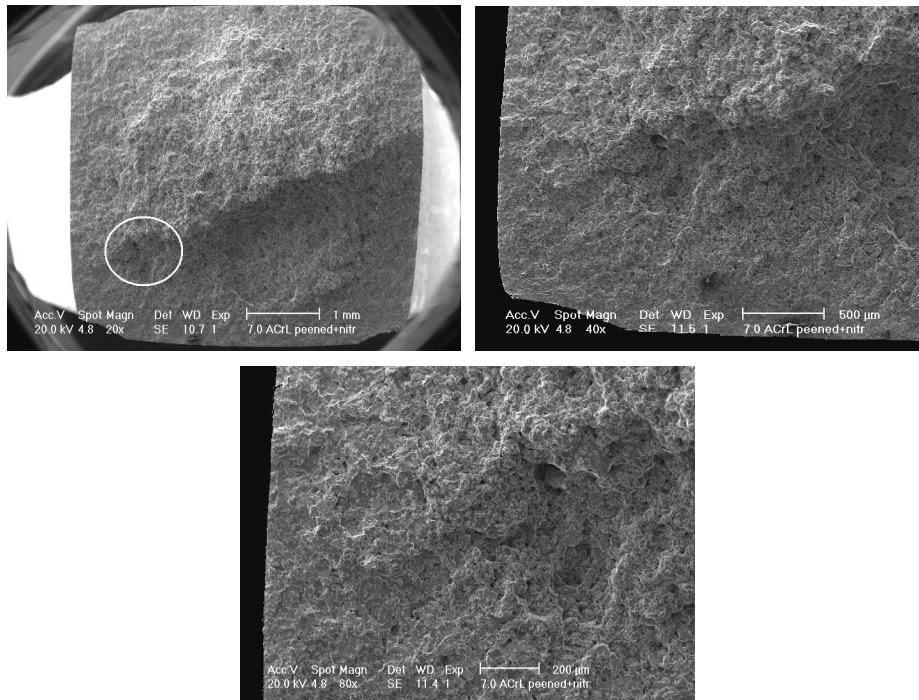


Figure 7.25: fracture surface of nitrided  $7.0\text{g}/\text{cm}^3$  surface densified 0.2%C ACrL sintered at  $1120^\circ\text{C}$

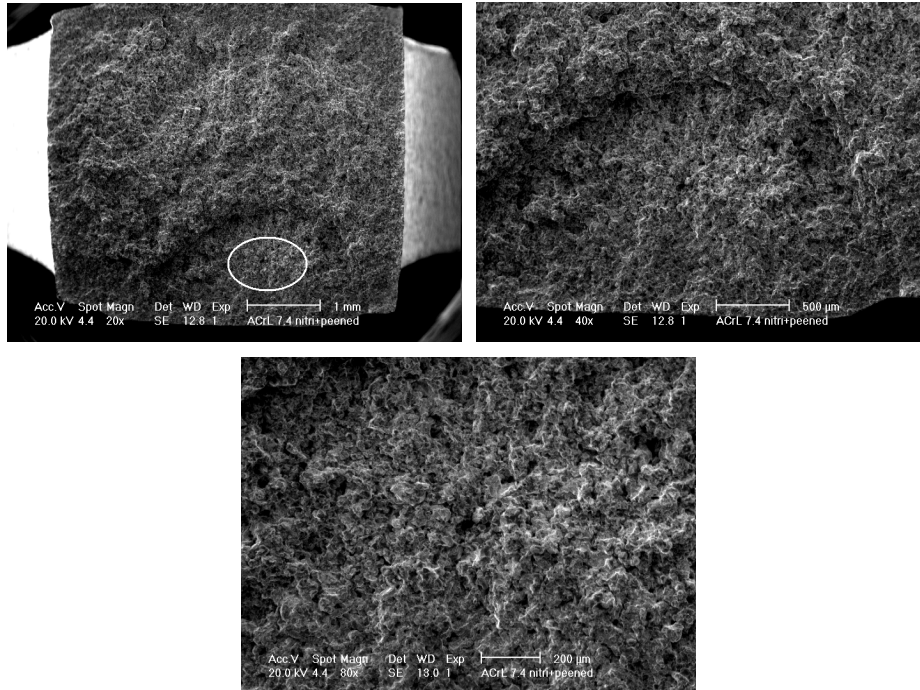


Figure 7.26: fracture surface of post nitriding shot peened  $7.4\text{g/cm}^3$  0.2%C ACrL sintered at  $1120^\circ\text{C}$

The effect of nitriding is that of moving the site for crack nucleation towards the interior (around 1mm), where the stress intensity is higher than at the surface. The surface densification and post nitriding shot peening do not modify this depth.

### 7.6. Evaluation of the plasma nitriding effect on the fatigue resistance

To evaluate the effect of plasma nitriding on the fatigue resistance of the ACrL steel, reference with data reported in literature is made considering materials with a carbon content higher than 0.2% [35, 55- 57]. There is no interest on using a 0.2%C as sintered steel in structural application. Data are compared in table 7.10.



**Chapter 7: Plasma Nitriding of Chromium Steels**

Table 7.10: fatigue resistances of ACrL steels

Density [g/cm <sup>3</sup> ]	T sintering	%C	Fatigue resistance at 2x10 <sup>6</sup> cycles [MPa]	
			As sintered	Plasma nitrided
7.0- 7.2	1120°C	0.2		213±15 250±15 (surface densified)
		0.6	204±16 [35]	
		0.55	236±9 [57]	
		0.8	261 [55, 56]	
	1250°C	0.2		240±15
		0.6	257±4 [35]	
		0.55	250 [57]	
		0.8	320 [56]	
7.3- 7.4	1120°C	0.2		290±20
		0.55	213±8 [57]	
		0.6	270 [35]	
	1250°C	0.2		343±9
		0.6	256±20 [35]	

The fatigue resistance of plasma nitrided 0.2%C steel is comparable to that of an as sintered 0.55-0.6%C material when density is 7.0- 7.2g/cm<sup>3</sup>. The effect is significantly higher when density is 7.3- 7.4g/cm<sup>3</sup>.

**7.7. Concluding remarks**

The main results of the effect of plasma nitriding on Cr steels can be summarized as follows.

- 0.05%C ACrL, 0.05% and 0.4%C AD4 are not suitable materials for nitriding because of ferritic- perlitic microstructure.
- Two steps treatment, made of 48 hours of nitriding and 24 hours of diffusion, results in a case depth of 250-400µm, which increases on

### *Chapter 7: Plasma Nitriding of Chromium Steels*

---

increasing carbon content and sintering temperature. Surface microhardness is 700HV0.05 independent on carbon content, density and sintering temperature.

- Surface densification does not improve microhardness profile, since nitriding effect prevails noticeably on shot peening.
- All the materials become brittle after nitriding and the impact behavior of all the carburized steels is purely elastic. 0.2%C ACrL has an higher impact toughness than 0.4%C one after nitriding.
- Surface densification leads to an improvement in fatigue resistance comparable to that attained by increasing sintering temperature up to 1250°C.
- Post shot peening increases case depth and surface microhardness, but it does not lead to a further improvement in fatigue resistance.
- Fatigue resistance of nitrided 0.2%C steel is comparable to that of as sintered 0.55- 0.6%C ones, when density is 7.0- 7.2g/cm<sup>3</sup>, and significantly higher with 7.3- 7.4g/cm<sup>3</sup>.
- Analysis of fracture surface shows subsurface crack nucleation in correspondence of mainly a cluster of pores.

## 8. Shot Peening of Chromium Steels

In order to evaluate the effect of shot peening treatment on the fatigue properties of sintered steels, six different shot peening conditions have been carried out on  $7.1\text{g/cm}^3$  and  $7.2\text{g/cm}^3$  0.5%C ACrM sintered at  $1250^\circ\text{C}$ .

The steel have tensile properties and microstructure shown in figure 8.1. Microstructure is mainly martensitic with some bainitic regions. Hardness and tensile properties of the as-sintered steel are reported in table 8.1.

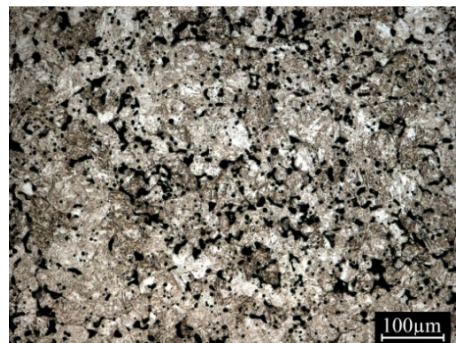


Figure 8.1: microstructure of  $7.2\text{g/cm}^3$  ACrM

Table 8.1: Hardness, microhardness and tensile properties of the investigated materials

Materials	HV30	HV0.1	$\sigma_y$ [Mpa]	UTS [MPa]	$\epsilon$ [%]
ACrM 0.5%C $7.1\text{g/cm}^3$ 1250°C	$367 \pm 24$	$545 \pm 42$	1070	1230	1.7
ACrM 0.5%C $7.2\text{g/cm}^3$ 1250°C	$396 \pm 14$	$550 \pm 56$	1170	1430	2.2

## *Chapter 8: Shot Peening of Chromium Steels*

---

Shot peening was carried out with an intensity of 12 Almen A (measured by a conventional A-type strip) by a pressurized air machine, with a nozzle diameter of 10mm and a nozzle-specimen distance of 100mm. Steel shots (1%C and 0.8%Mn) hardened to 55–62HRc with three different diameters were used, as reported in table 8.2. The incidence angle was between 75° and 80°. Coverage was 100% and 150%.

Table 8.2: Shot peening parameters

<b>Code</b>	<b>Shot type</b>	<b>Shot diameter [mm]</b>	<b>Coverage [%]</b>
A	ASH 170	0.4	100
B	ASH 170	0.4	150
C	ASH 230	0.6	100
D	ASH 230	0.6	150
E	ASH 330	0.8	100
F	ASH 330	0.8	150

The effect of shot peening on a porous sintered steel is the combination of three phenomena: surface densification by plastic deformation; strain hardening by the accumulation of structural defects (dislocations in a martensitic steel) and residual stresses.

### **8.1. Surface densification**

Densification is due to the extensive plastic deformation and the energy spent for plastic deformation in shot peening is proportional to the shot mass.

Figure 8.2 shows the formation of a densified surface layer, where porosity has been almost completely closed. Only a few micrometric pores are still present.

## Chapter 8: Shot Peening of Chromium Steels

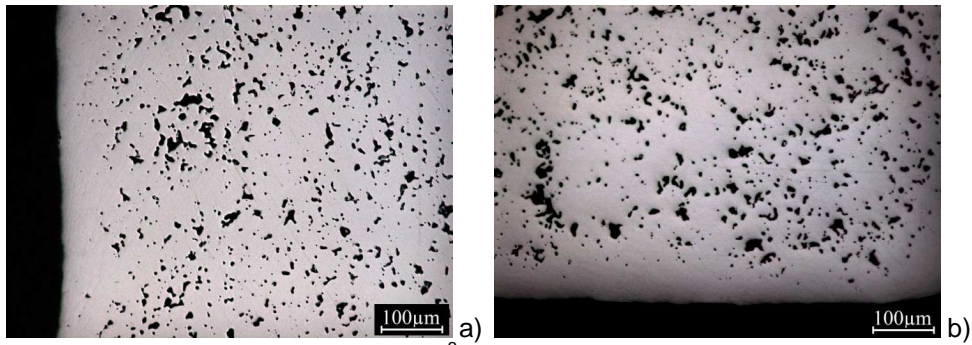


Figure 8.2: microstructure of  $7.1\text{g/cm}^3$  0.5%C ACrM differently shot peened: a) D condition and b) E condition

The thickness of this layer was measured by Image Analysis of five LOM micrographs at 100x. The profiles in figure 8.3 show a  $50\mu\text{m}$  fully dense surface layer depth and the transition to the bulk porosity takes place at  $70\text{--}80\mu\text{m}$ . The thickness of the densified layer is the highest in specimen A, whilst the transition to the bulk porosity occurs at the same depth in all specimens. Since the thickest densified layer has been obtained on specimen A there is a saturation of the shot diameter effect and, as well as, of coverage. This confirms that, once a certain thickness of densified material is formed, it prevents yielding in the remaining porous material.

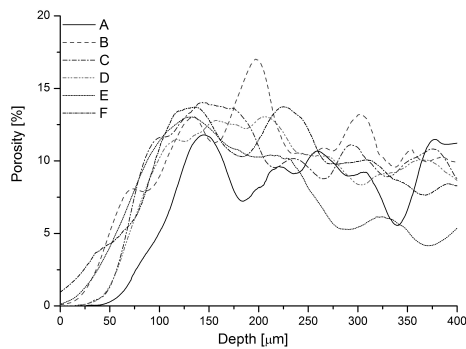


Figure 8.3: porosity profile due to shot peening.

## Chapter 8: Shot Peening of Chromium Steels

The plastic deformation dramatically changed the morphology of the external surface, as shown in figure 8.4, relevant to specimen D before and after shot peening. The surface porosity was effectively closed even if some narrow cavities still remain. However shot peening does not modify the dimensional and geometrical precision of the specimens.

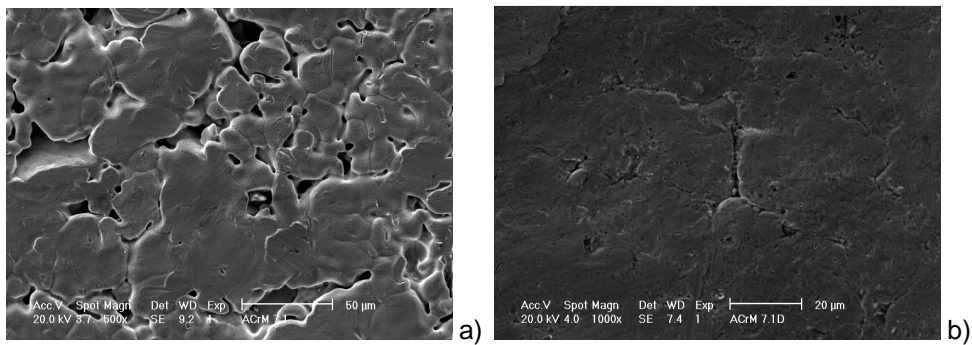


Figure 8.4: surface morphology of: a) as sintered specimen and b) after shot peening D

### 8.2. Strain hardening

Figure 8.5 shows the microhardness profile of the specimens  $7.1 \text{ g/cm}^3$  ACrM peened by A, B, C and E, to study the effect of the shot diameter (A, C and E) and the coverage (A and B, D). The thickness of the strain hardened layer (the distance from the surface to the point where the microhardness drops to the core hardness) is larger than that of the densified one in all the specimens, which confirms that plastic strain penetrates more than the densification. The microhardness profiles of specimens A, C and E show that the thickness of the strain hardened layer tends to decrease on increasing the shot diameter. This could be a confirmation of the saturation attained, the excess of mechanical energy activates microdeformation involving accumulated dislocation. The profiles A, B and D indicate that coverage does not have a significant effect on strain hardening.

## Chapter 8: Shot Peening of Chromium Steels

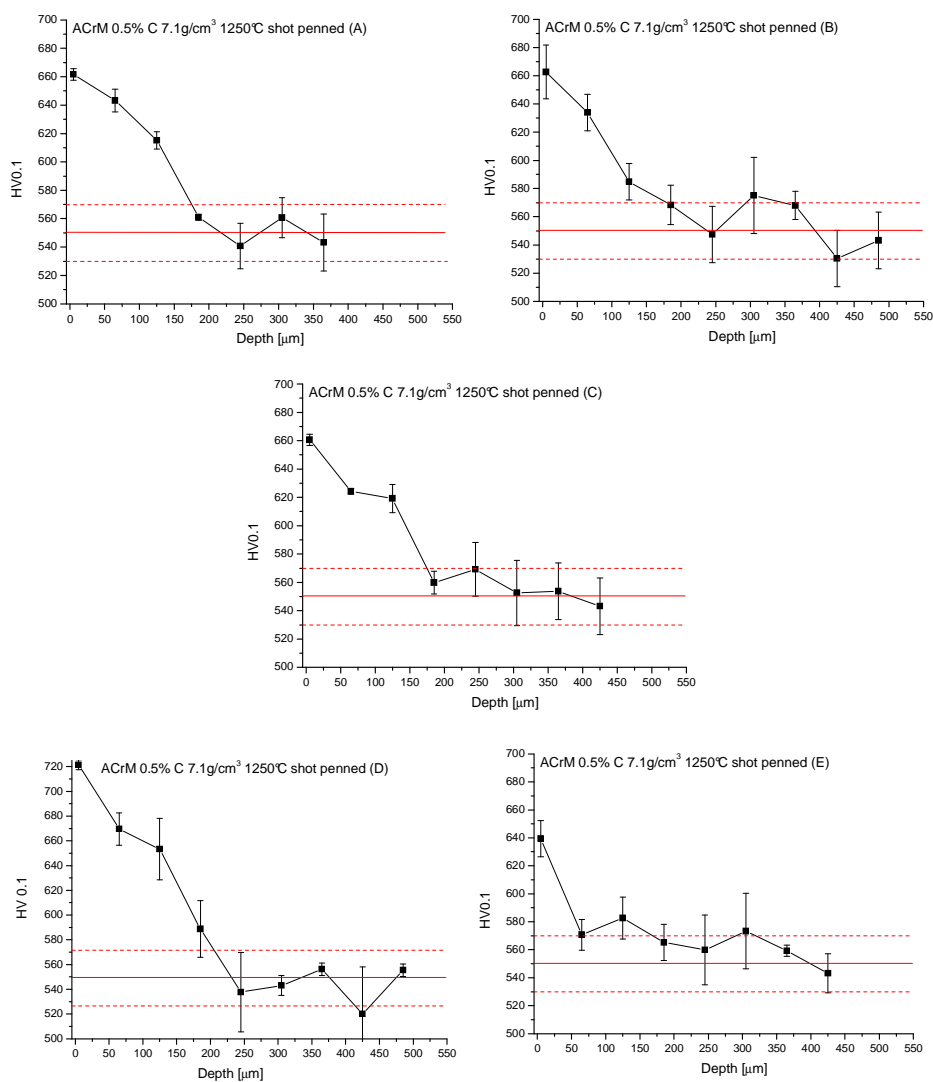


Figure 8.5: microhardness profiles of specimens A, C, E and B.

### 8.3. Residual stresses

Figure 8.6 shows the compressive residual stresses profile of specimen A. The surface residual stress is around  $-730\text{MPa}$ . On moving in depth, residual stresses

## Chapter 8: Shot Peening of Chromium Steels

first decrease, then increase up to around  $-750\text{MPa}$  in correspondence of the densified layer boundary. In the end they decrease again. The maximum residual stress accumulated is quite high; it is around 70% of yield strength of the material. The compressive residual stresses tends to zero at about  $100\text{-}150\mu\text{m}$ .

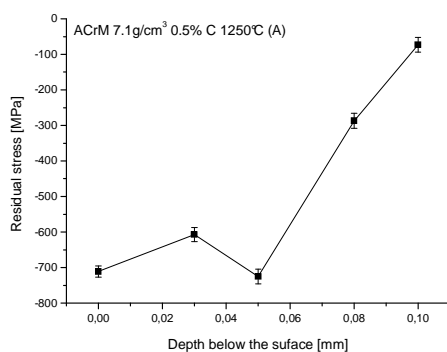


Figure 8.6: the residual stress profile of specimen A.

On increasing the shot diameter (A, C, E and B, D, F in figure 8.7), surface and maximum compressive residual stresses tend to decrease slightly, whilst the residual stresses distance tends to increase. The effect of coverage is still negligible.

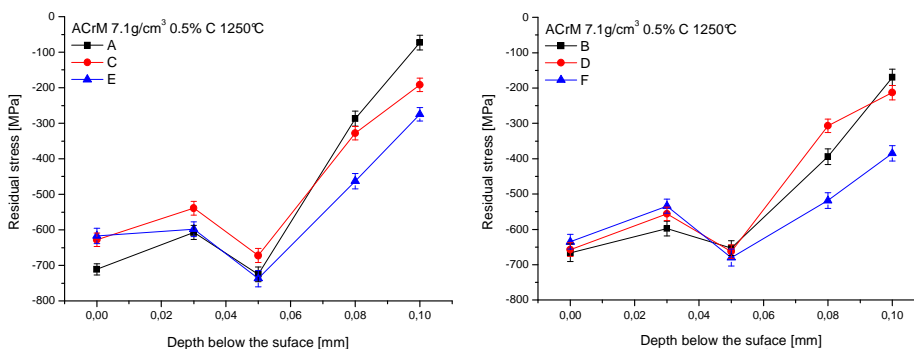


Figure 8.7: residual stress profiles in surface densified  $7.1\text{ g/cm}^3$  specimens.



## *Chapter 8: Shot Peening of Chromium Steels*

---

The results of the surface densified  $7.2 \text{ g/cm}^3$  steel are very similar to those above reported. On the base of these results it is possible to conclude that shot peening energy is at first spent for extensive plastic deformation and densification, then, residual stresses are accumulated.

### **8.4. Fatigue resistance**

Fatigue tests were carried out in a plane bending condition ( $R=-1$ ) up to  $2 \times 10^6$  cycles on unnotched specimens and surface densified ones. The results are reported in tables 8.3 and 8.4. Shot peening improves the fatigue strength in all the peening conditions. The maximum increment is of 25% for the lower density and 30% for the higher density with respect to the unpeened material. Results are slightly influenced by the shot peening conditions; however, condition D, in the case of  $7.1 \text{ g/cm}^3$ , and E, in case of  $7.2 \text{ g/cm}^3$ , result in the highest mean value and the smaller standard deviation.

Table 8.3: plane bending fatigue strength of  $7.1 \text{ g/cm}^3$  ACrM under different shot peening conditions

<b>Fatigue strength <math>2 \times 10^6</math> cycles</b>						
<b>[MPa]</b>						
<b>As sintered</b>	<b>A</b>	<b>B</b>	<b>C</b>	<b>D</b>	<b>E</b>	<b>F</b>
265±4	330±55	329±16	333±47	340±4	323±10	332±20

Table 8.4: plane bending fatigue strength of  $7.2 \text{ g/cm}^3$  ACrM under different shot peening conditions

<b>Fatigue strength <math>2 \times 10^6</math> cycles</b>						
<b>[MPa]</b>						
<b>As sintered</b>	<b>A</b>	<b>B</b>	<b>C</b>	<b>D</b>	<b>E</b>	<b>F</b>
285±49	358±14	359±7	338±30	344±45	373±6	370±20

In the fracture surface (fig. 8.8) the crack initiates in the subsurface layers, at a distance of 250–300 $\mu\text{m}$  from the surface, in correspondence of either a cluster of

## Chapter 8: Shot Peening of Chromium Steels

pores (as in this case) or a large and irregular pore and this is common to all the surface densified specimens.

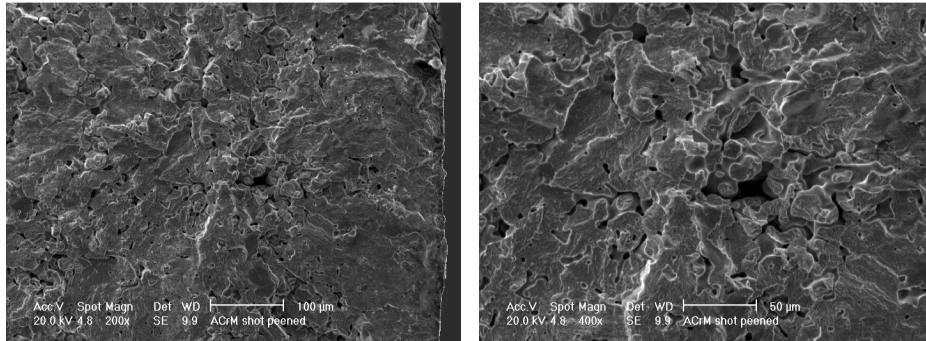


Figure 8.8: fracture surface of the D shot peened specimen

In porous sintered steels, pores and pore clusters near the surface act as sites for fatigue crack nucleation because of the high localized stress associated with these defects. After shot peening fatigue crack nucleates in the interior, in the tensile residual stresses zone, beneath the strain hardened layer, where microhardness has not been modified by shot peening. The increase in the plane bending fatigue strength is comparable to that attainable with an increased bulk densification up to  $7.4\text{--}7.5\text{g/cm}^3$  [58].

### 8.5. Concluding remarks

The results of the shot peening effect on the fatigue resistance of ACrM can be summarized as follows.

- Shot peening increases surface density forming a near fully dense layer of around  $50\mu\text{m}$ . On increasing shot diameter and coverage thickness decreases.

### *Chapter 8: Shot Peening of Chromium Steels*

---

- Strain hardened layer is deeper than densified one. Its thickness tends to decrease on increasing shot diameter, whilst coverage does not have a significant effect.
- Residual stress profile is deeper on increasing shot diameter, whilst the effect of coverage is still negligible.
- An increase of 25%, for the lower density, and 30%, for the higher density, in plane bending fatigue strength was measured irrespective to shot diameter.
- Fatigue crack nucleates in tensile residual stress zone, beneath the strain hardened layer, in correspondence to either cluster of pores or large irregular pores.

## 9. Chromium Free Steels: as sintered microstructure and mechanical properties

### 9.1. Effect of carbon content, density and sintering temperature on microstructure and microhardness

The materials studied in this part are ALH and DLH. Graphite was added to the base powder in order to obtain 0.05% ( $\pm 0.04$ ) and 0.2% ( $\pm 0.03$ ) carbon.

Impact bars were compacted to green density of  $6.8\text{g/cm}^3$ ,  $7.0\text{g/cm}^3$  and  $7.4\text{g/cm}^3$ . Sintering was carried out at  $1120^\circ\text{C}$  (L).

The carbon content in the as sintered materials is listed in table 9.1 with reference to the nominal one. The analysis was carried out only on  $6.8\text{g/cm}^3$  steels.

Table 9.1: results of carbon analysis

	Green/nominal %C	As sintered %C
ALH $6.8\text{g/cm}^3$ $1120^\circ\text{C}$	0.05	0.09
ALH $6.8\text{g/cm}^3$ $1120^\circ\text{C}$	0.2	0.24
DLH $6.8\text{g/cm}^3$ $1120^\circ\text{C}$	0.05	0.10
DLH $6.8\text{g/cm}^3$ $1120^\circ\text{C}$	0.2	0.17

The as sintered density is presented in figure 9.1 as a function of carbon content.

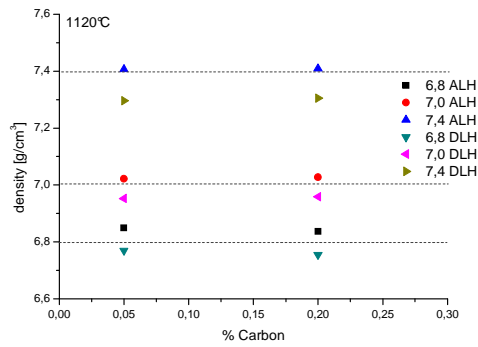


Figure 9.1: as sintered density of ALH and DLH

The DLH density is lower than that of ALH because of the copper addition. On increasing the carbon content the density does not change. Total porosity, presented in figure 9.2 as sum of closed and open porosity, decreases on increasing green density and the effect of carbon content is rather poor. The residual porosity is almost fully closed in 7.4g/cm<sup>3</sup> ALH.

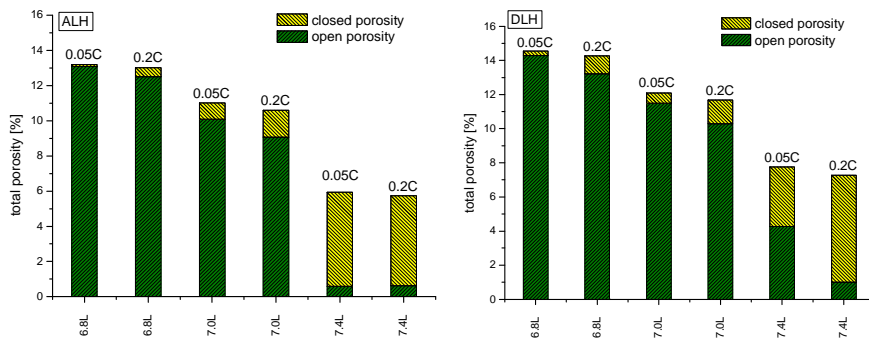


Figure 9.2: porosity of ALH and DLH

Figure 9.3 shows the typical microstructures of the two materials. As sintered ALH and DLH present heterogeneous microstructures formed by ferrite and bainite. The bainite amount increases on increasing the carbon content, whilst the increase in density does not influence the microstructure. All the other microstructures are reported in appendix.

Chapter 9: Chromium Free Steels

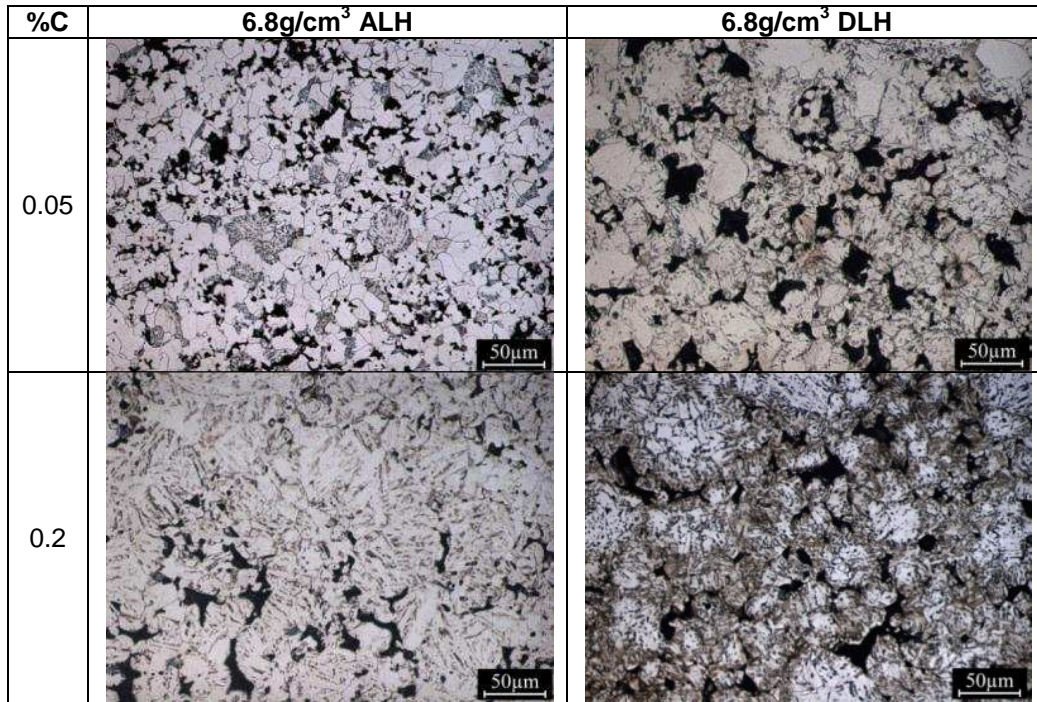


Figure 9.3: microstructures of 6.8g/cm<sup>3</sup> 0.05% and 0.2%C ALH and DLH sintered at 1120°C

Hardness and microhardness of the steels are listed in tables 9.2-9.3.

Table 9.2: hardness and microhardness of as sintered ALH

Material	%C	Density [g/cm <sup>3</sup> ]	HV10	HV0.05
ALH	0.05%C	6.8	64 ± 3	128 ± 36
		7.0	70 ± 3	132 ± 15
		7.4	135 ± 7	159 ± 31
	0.2%C	6.8	102 ± 2	206 ± 6
		7.0	118 ± 2	207 ± 13
		7.4	137 ± 2	213 ± 18

Table 9.3: hardness and microhardness of as sintered DLH

Material	%C	Density [g/cm <sup>3</sup> ]	HV10	HV0.05
DLH	0.05%C	6.8	102 ± 8	129 ± 6
		7.0	113 ± 6	144 ± 22
		7.4	134 ± 4	156 ± 20
	0.2%C	6.8	130 ± 3	218 ± 31
		7.0	138 ± 3	222 ± 22
		7.4	182 ± 1	233 ± 11

Hardness decreases from DLH to ALH because of greater amount of bainite in DLH.

To confirm the different microstructures described above, a dilatometry investigation of the austenite transformations on cooling was carried.

The variation of the relative change in length as a function of temperature achieved by 7.0g/cm<sup>3</sup> ALH is reported in figure 9.4. The dilatometric and the metallographic analysis show the formation of ferrite, in the case of the lowest carbon content, and ferrite plus bainite on increasing the carbon percentage. The transformation temperatures are shown in table 9.4 and the amounts of the different phases are reported in table 9.5.

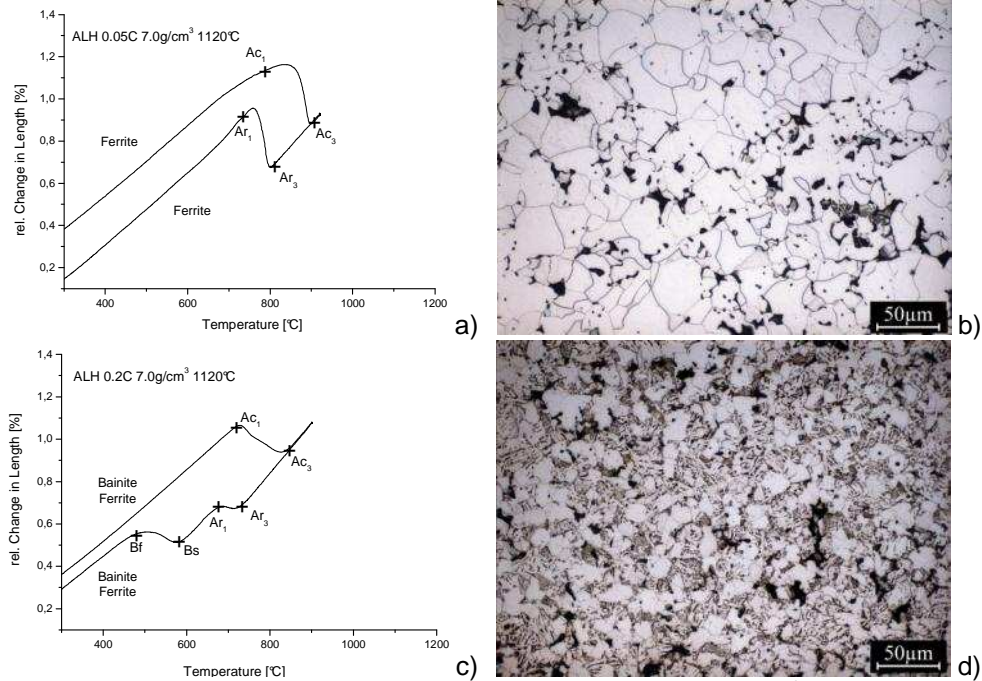


Figure 9.4: dilatometric curve (a) and microstructure (b) of  $7.0\text{g/cm}^3$  0.05% C ALH, dilatometric curve (c) and microstructure (d) of  $7.0\text{g/cm}^3$  0.2% C ALH

Table 9.4: transformation temperatures determined by dilatometry

T [°C]	ALH		DLH	
	0.05%C	0.2%C	0.05%C	0.2%C
$A_{c1}$	780	730	750	720
$A_{c3}$	905	845	890	850
$A_{r3}$	791	725	775	
$A_{r1}$	763	672	725	
$B_s$		578	580	587
$B_f$		502	501	492

Table 9.5: phase fractions

Microstructure	ALH		DLH	
	0.05%C	0.2%C	0.05%C	0.2%C
Ferrite	100%	80%	10%	7%
Perlite				
Bainite		20%	90%	93%



## Chapter 9: Chromium Free Steels

The dilatometric curves carried out on  $7.0\text{g/cm}^3$  DLH are reported in figure 9.5 for 0.05%C and 0.2%C.

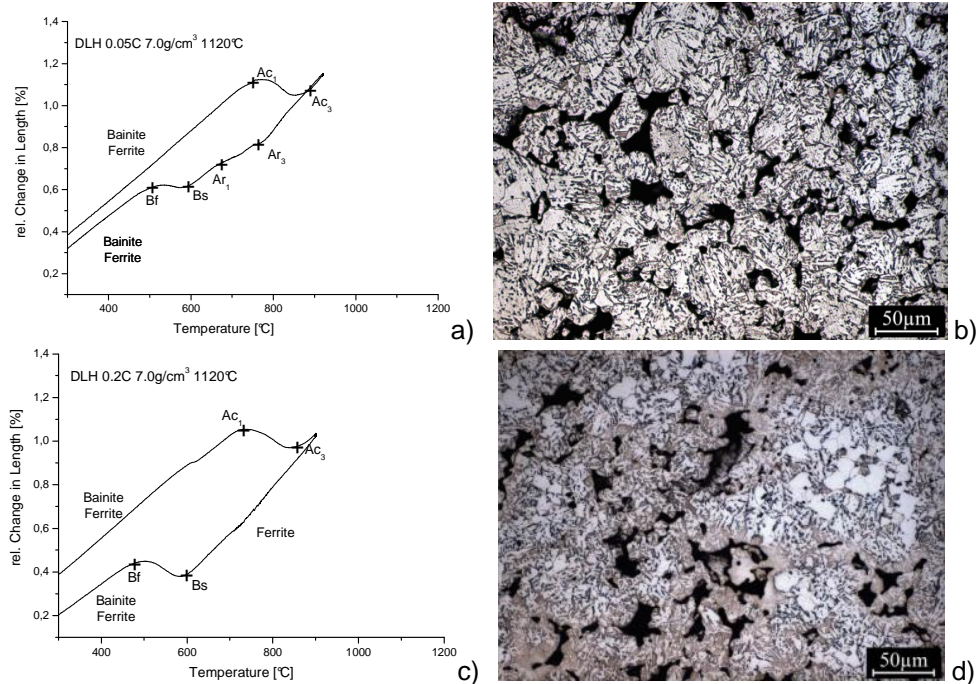
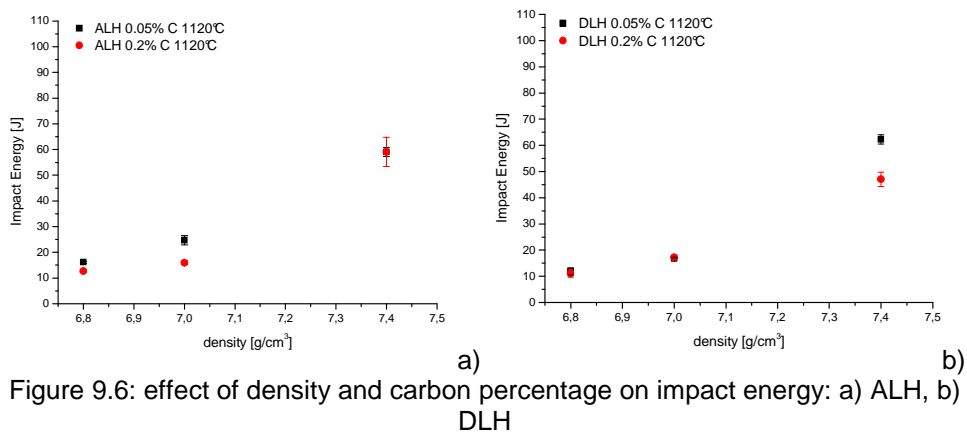


Figure 9.5: dilatometric curve (a) and microstructure (b) of  $7.0\text{g/cm}^3$  0.05% C DLH, dilatometric curve (c) and microstructure (d) of  $7.0\text{g/cm}^3$  0.2% C DLH

The expansions on cooling show that the microstructure contains bainite just at lower carbon content. The transformation temperatures are listed in table 9.4 and the amount of the bainite and ferrite are reported in table 9.5. The dilatometric investigation confirms that the presence of molybdenum and copper favors the formation of bainite, even with low carbon content.

## 9.2. Impact toughness

Figure 9.6 shows impact energy of the investigated materials as a function of density.



Impact energy increases with density and decreases with the carbon content, as expected.

On increasing density from  $6.8\text{g/cm}^3$  to  $7.4\text{g/cm}^3$ , yield load ( $P_y$ ), maximum load ( $P_{\max}$ ) and deflection increase, as indicated by the impact curves of 0.05% C ALH reported in figure 9.7a, because of the increase in the load bearing section.

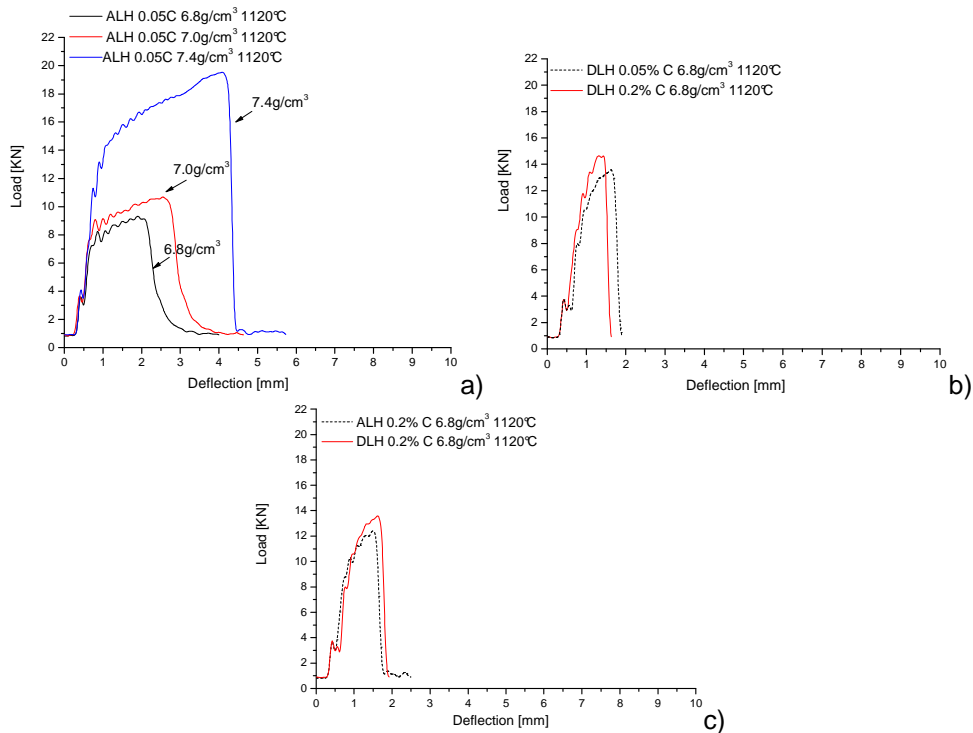


Figure 9.7: load- deflection curves as a function of: a) density, b) carbon percentage and c) chemical composition

Depending on the carbon content, materials have different impact behaviors, characterized by general yielding with extensive (ALH) and slight (DLH) strain hardening with 0.05%C and localized yielding with poor plastic deformation with 0.2%C. The load-deflection curves of 6.8g/cm<sup>3</sup> DLH in figure 9.7b, indicate that deflection decreases and  $P_y$  and  $P_{max}$  increase on increasing the carbon content, because of the increased amount of bainite. Anyway the overall effect is a decrease of impact energy. Figure 9.7c shows the curves of the materials, having the same carbon content (0.2%) and density (6.8g/cm<sup>3</sup>);  $P_y$  and  $P_{max}$  are higher in DLH with reference to ALH because of the different amount of bainite in the microstructure. The results of the impact test (impact energy,  $P_y$  and  $P_{max}$ ) are reported in appendix.

9.3. Surface densification by shot peening

Shot peening is study as a preliminary treatment before carburizing and nitriding. Shot peening was carried out on  $6.8\text{g}/\text{cm}^3$  materials sintered at  $1120^\circ\text{C}$ , with the following parameters: intensity 12A, shot ASH230, coverage 150%.

9.3.1. Effect on microstructure and microhardness

The microstructural analysis in figure 9.8 confirms the surface densification, due to extensive plastic deformation.

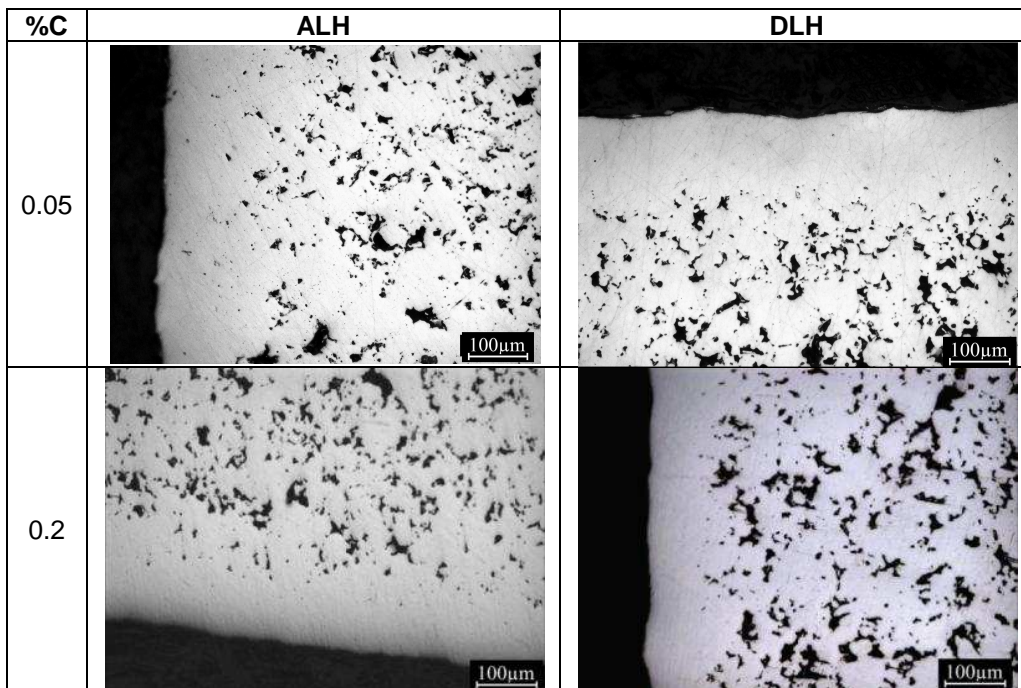


Figure 9.8: microstructures of  $6.8\text{g}/\text{cm}^3$  surface densified 0.05% and 0.2% C ALH and DLH

### Chapter 9: Chromium Free Steels

---

The thickness of the densified layers is reported in table 9.6. On increasing the carbon content the thickness tends to decrease because of the less ductility of the materials. The thickness ranges between 110 and 160 $\mu\text{m}$ . The strain hardening layer (the distance from the surface to the point where the microhardness drops to the core hardness) is larger than the surface densified one (fig. 9.9), confirming that the plastic strain penetrates in depth beneath the densified layer.

Table 9.6: densification depth of surface densified 6.8g/cm<sup>3</sup> 0.05% and 0.2%C ALH

<b>Materials</b>	<b>Thickness of densified layer [<math>\mu\text{m}</math>]</b>
ALH 0.05%C	161.5
ALH 0.2%C	115

<b>Materials</b>	<b>Thickness of densified layer [<math>\mu\text{m}</math>]</b>
DLH 0.05%C	129
DLH 0.2%C	112

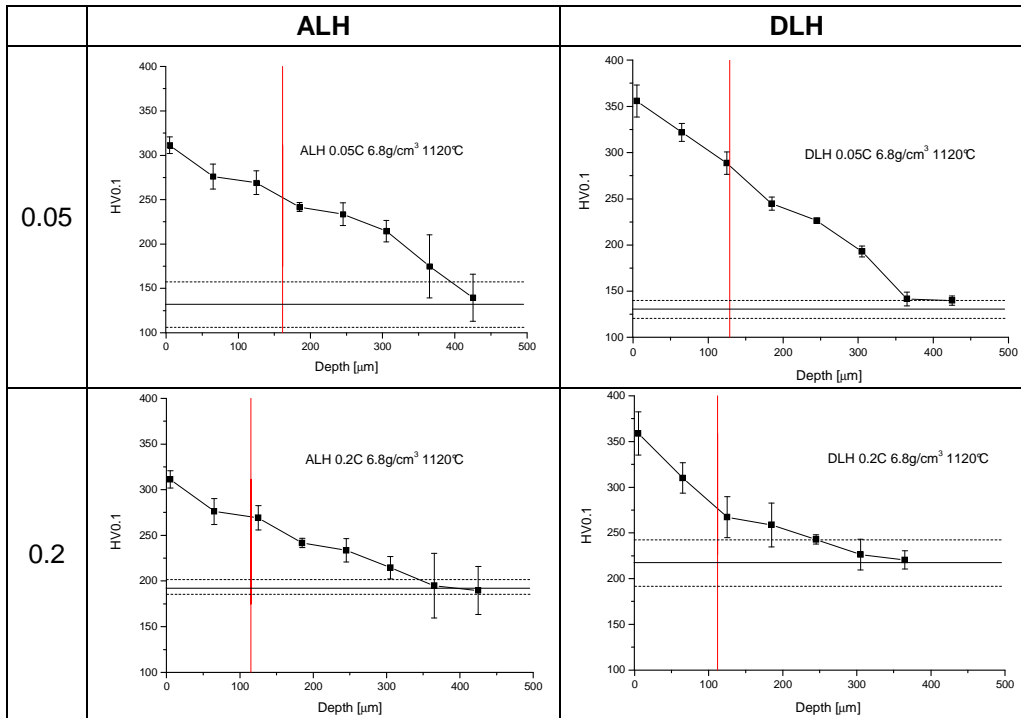


Figure 9.9: microhardness profiles and densified depths of 6.8g/cm<sup>3</sup> surface densified 0.05%C and 0.2%C ALH and DLH

### 9.3.2. Surface morphology

The surface morphology is shown in figure 9.10. The surface densification is clearly evident for both the steels, but several residual defects are left on the surface, which result quite irregular, significant of a poor surface quality.

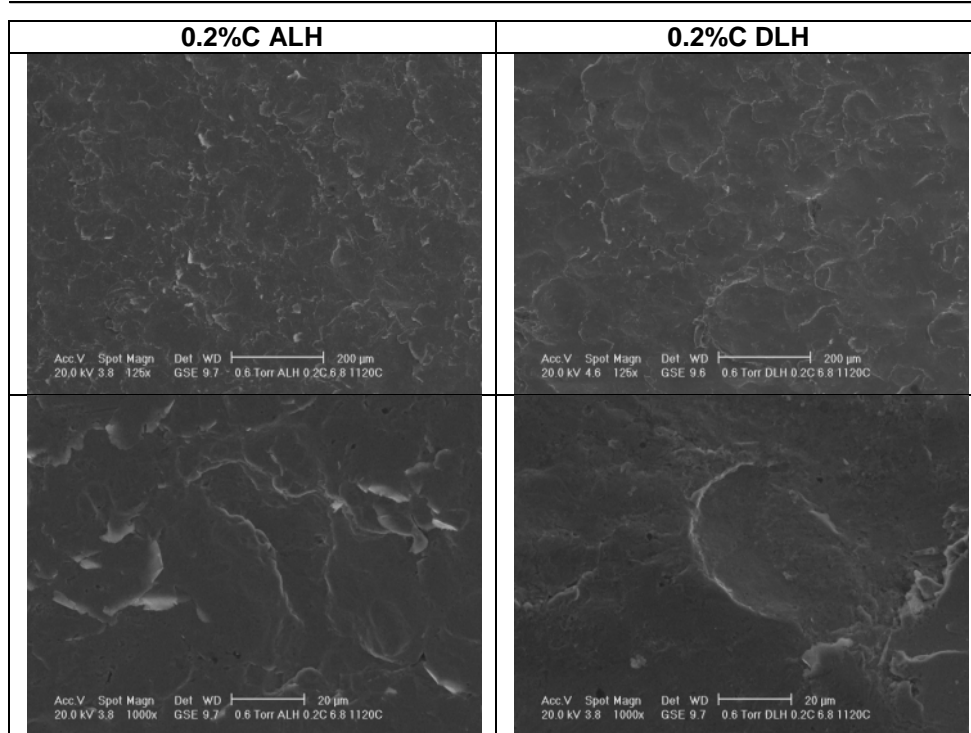


Figure 9.10:  $6.8\text{g/cm}^3$  surface densified 0.2%C ALH and DLH

#### 9.4. Concluding remarks

The influence of carbon content, density and sintering temperature on microstructure and impact properties can be summarized as follows.

- Materials have heterogeneous microstructures formed by ferrite and bainite. The dilatometric investigation confirms that molybdenum and copper favors the bainite formation, even at low carbon content.
- Impact tests show that on increasing density, yield load, maximum load and deflection increase because of the increase in load bearing section. On increasing carbon content, impact toughness decreases because of the increased amount of bainite.

### *Chapter 9: Chromium Free Steels*

---

- Shot peening forms a densified surface layer, whose thickness is around 110- 160 $\mu$ m and decreases on increasing carbon content. The surface morphology is quite irregular due to some defects leave on the surface.



## 10. Low Pressure Carburizing of Chromium Free Steels

ALH and DLH with density  $6.8\text{g/cm}^3$ ,  $7.0\text{g/cm}^3$  and  $7.4\text{g/cm}^3$ , sintered at  $1120^\circ\text{C}$  and with two carbon contents (0.05% and 0.2%C) were considered. Some samples have been previously shot peened to densify the surface layers. After shot peening specimens have been polished and grinded with SiC paper up to 1200 to remove the surface defects.

The low pressure carburizing treatment was carried out in an ALD plant in DANA Company (Arco di Trento, Italy) in order to obtain a surface microhardness of 800-900 HV0.1 and a case depth around 500-600 $\mu\text{m}$ . The treatment parameters are reported in table 10.1. The carburizing temperature was  $945^\circ\text{C}$  and gas was acetylene. Quenching was carried out with a nitrogen flux at 6 bar. Tempering at  $180^\circ\text{C}$  for 2 hours was carried out after LPC.

Table 10.1: LPC treatments

Treatment code	Boost + diffusion time (minutes)				
	I	II	III	IV	V
LPC 1	2 + 15	1 + 1	1 + 4		
LPC 2	2 + 10	1 + 15	1 + 19	1 + 27	1 + 4

## Chapter 10: Low Pressure Carburizing of Chromium Free Steels

### 10.1. Three steps LPC- LPC 1

#### 10.1.1. Effect of porosity

Microstructures and microhardness profiles of 0.2%C ALH and DLH are reported in figures 10.1- 10.4.

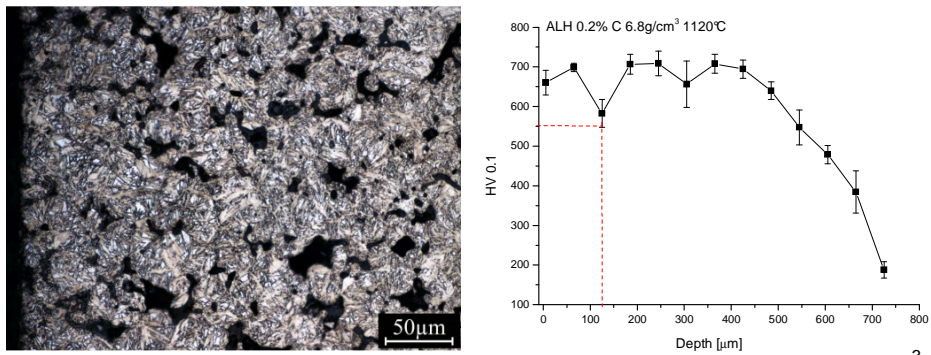


Figure 10.1: microstructure and microhardness profile of carburized 6.8g/cm<sup>3</sup> 0.2%C ALH

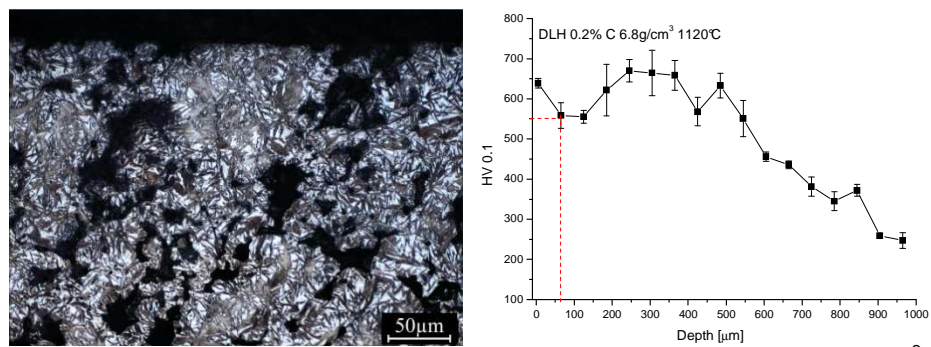


Figure 10.2: microstructure and microhardness profile of carburized 6.8g/cm<sup>3</sup> 0.2%C DLH

*Chapter 10: Low Pressure Carburizing of Chromium Free Steels*

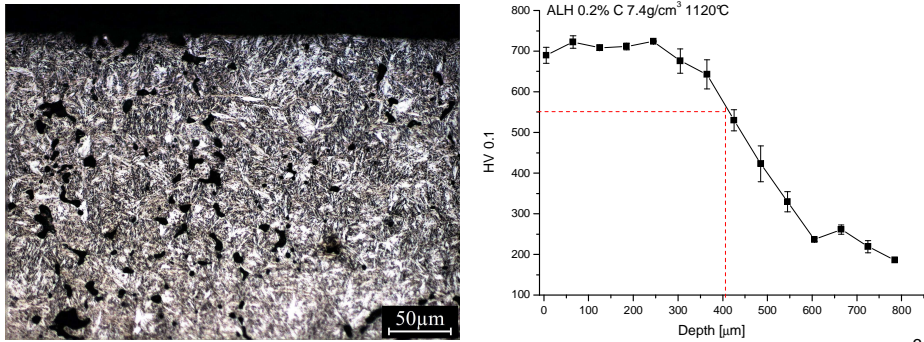


Figure 10.3: microstructure and microhardness profile of carburized  $7.4\text{g/cm}^3$  0.2%C ALH

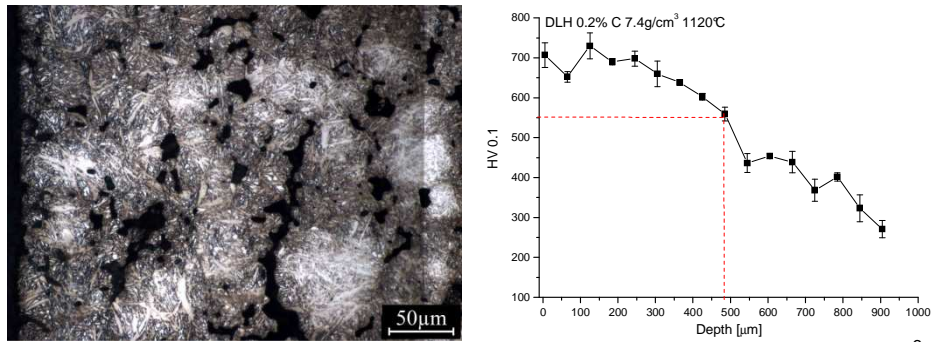


Figure 10.4: microstructure and microhardness profile of carburized  $7.4\text{g/cm}^3$  0.2%C DLH

The microstructure of  $6.8\text{g/cm}^3$  steels is not homogenous, overcarburizing occurs and it results in the formation of a large amount of retained austenite in the case. The presence of interconnected porosity enhances carbon pick up. The amount of austenite in the DLH specimen was measured by XRD and quantified in 25%. The XRD spectrum is reported in figure 10.5.

*Chapter 10: Low Pressure Carburizing of Chromium Free Steels*

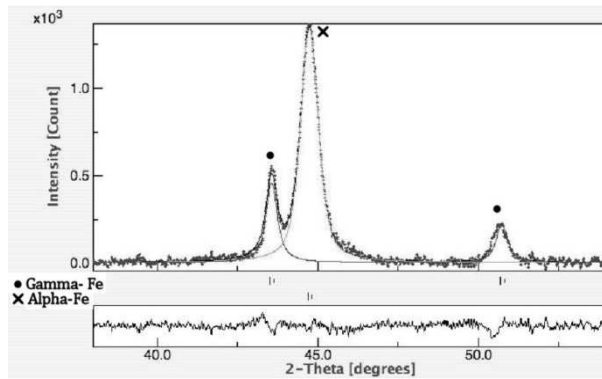


Figure 10.5: XRD pattern of LPC 1 DLH

Overcarburizing is fully avoided in  $7.4\text{g/cm}^3$  ALH, whilst in  $7.4\text{g/cm}^3$  DLH some retained austenite is still present. This is due to the amount of residual open porosity, which is higher in DLH than in ALH as shown in table 10.2. To confirm the different C-pick up between the two  $7.4\text{g/cm}^3$  steels the surface carbon content was analyzed and reported in table 10.3. The carbon content is 1% in DLH.

Table 10.2: density and porosity of  $7.4\text{g/cm}^3$  materials

Materials	Density [ $\text{g/cm}^3$ ]	Total porosity $\epsilon\%$	Open porosity $\epsilon_0\%$
ALH 0.05%C $7.4\text{g/cm}^3$	7.4	6.5	1.6
DLH 0.05%C $7.4\text{g/cm}^3$	7.3	7.8	4.3

Table 10.3: carbon analyses

0.05%C	$7.4\text{g/cm}^3$
ALH	0.69
DLH	1.00

The surface microhardness and case depth of overcarburized steels are low respect to the target (tab. 10.4), independently on the base carbon content. In  $7.4\text{g/cm}^3$  steels the surface microhardness and case depth effectively increase up to 700HV0.1 and 400- 480 $\mu\text{m}$ , respectively; anyway the target is not matched.

**Chapter 10: Low Pressure Carburizing of Chromium Free Steels**

Table 10.4: surface microhardness and case depths of LPC 1 steels

ALH	0.2%C 6.8/cm <sup>3</sup>	0.2%C 7.4g/cm <sup>3</sup>	Target
HV0.1	650	700	800-900
d <sub>550</sub> [μm]	130	400	500-600

DLH	0.2%C 6.8/cm <sup>3</sup>	0.2%C 7.4g/cm <sup>3</sup>	Target
HV0.1	650	700	800-900
d <sub>550</sub> [μm]	60	480	500-600

10.1.2. Comparison between closed porosity and surface densification

Microstructures and microhardness profiles of 7.4g/cm<sup>3</sup> and surface densified 0.05%C steels are reported in figures 10.6- 10.9. The microstructures and microhardness profiles of the 0.2%C steels are shown in appendix.

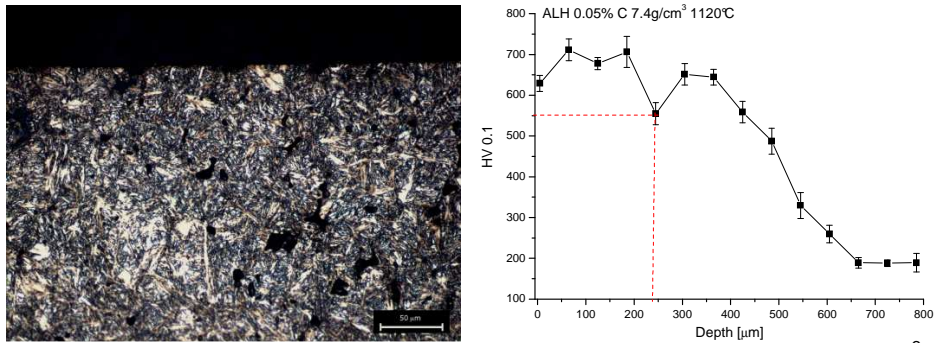


Figure 10.6: microstructure and microhardness profile of carburized 7.4g/cm<sup>3</sup> 0.05%C ALH

*Chapter 10: Low Pressure Carburizing of Chromium Free Steels*

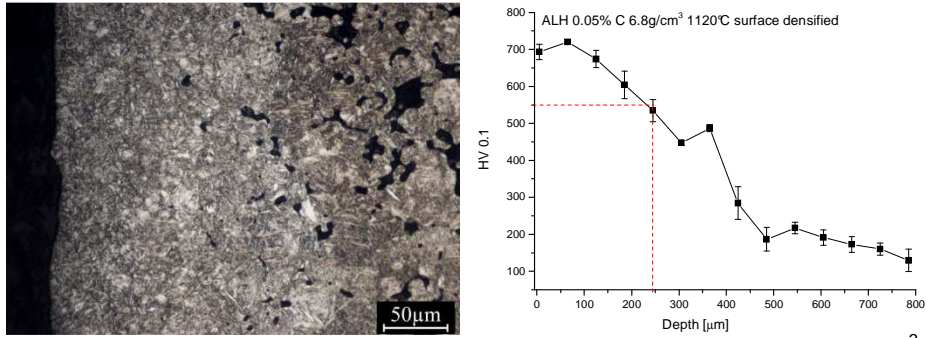


Figure 10.7: microstructure and microhardness profile of carburized  $6.8\text{g/cm}^3$  surface densified  $0.05\%C$  ALH

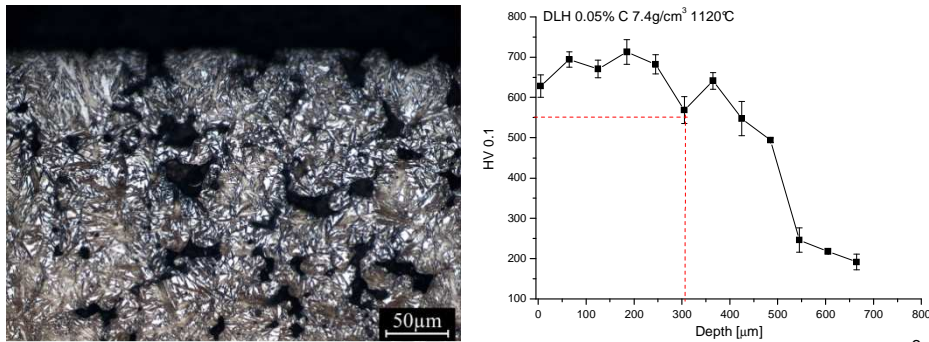


Figure 10.8: microstructure and microhardness profile of carburized  $7.4\text{g/cm}^3$   $0.05\%C$  DLH

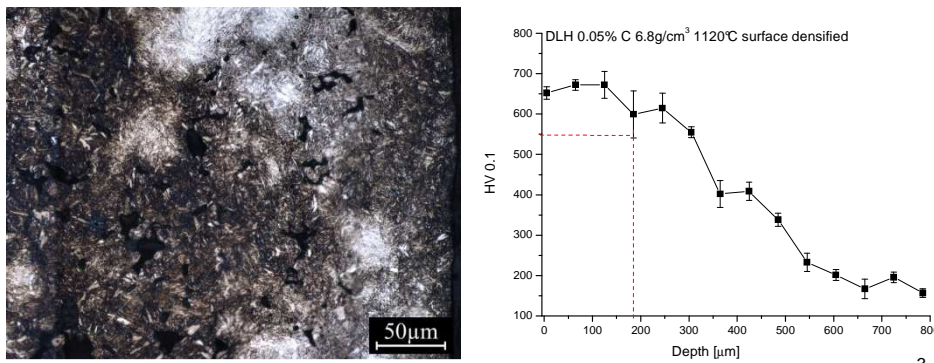


Figure 10.9: microstructure and microhardness profile of carburized  $6.8\text{g/cm}^3$  surface densified  $0.05\%C$  DLH

## *Chapter 10: Low Pressure Carburizing of Chromium Free Steels*

Overcarburizing is fully avoided in the surface densified steels because of the absence of residual open porosity. The comparison between warm compacted and surface densified materials shows a deeper microhardness profiles in 7.4g/cm<sup>3</sup> specimens than in surface densified ones (tab. 10.5) especially for DLH steel. This is due to the residual open porosity in 7.4g/cm<sup>3</sup> materials (tab. 10.2), which increases the carbon- pick up as shown in table 10.6.

Table 10.5: surface microhardness and case depths of LPC 1 steels

ALH	7.4g/cm <sup>3</sup>		6.8g/cm <sup>3</sup> surface densified		Target
	0.05%C	0.2%C	0.05%C	0.2%C	
HV0.1	630	700	700	700	800-900
d <sub>550</sub> [μm]	240	400	250	410	500-600

DLH	7.4g/cm <sup>3</sup>		6.8g/cm <sup>3</sup> surface densified		Target
	0.05%C	0.2%C	0.05%C	0.2%C	
HV0.1	630	700	650	600	800-900
d <sub>550</sub> [μm]	300	480	190	190	500-600

Table 10.6: carbon analyses

0.05%C	7.0g/cm <sup>3</sup> surface densified	7.4g/cm <sup>3</sup>
ALH	0.39	0.69
DLH	0.49	1.00

However, the surface microhardness and case depth are low with respect to the target.

### 10.2. Five steps LPC- LPC 2

A second low pressure carburizing treatment (LPC 2) was carried out in DANA Company, in order to increase the surface microhardness and the case depth up to

## Chapter 10: Low Pressure Carburizing of Chromium Free Steels

800-900HV0.1 and 500- 600 $\mu\text{m}$ , respectively. LPC 2 was carried out only on 7.4g/cm<sup>3</sup> and surface densified steels, since in 6.8g/cm<sup>3</sup> specimens low pressure carburizing causes overcarburizing.

### 10.2.1. Microstructures and microhardness profiles

Microstructures and microhardness profiles of 0.05%C ALH and DLH are shown in figures 10.10- 10.13, whilst those of 0.2%C steels are reported in appendix.

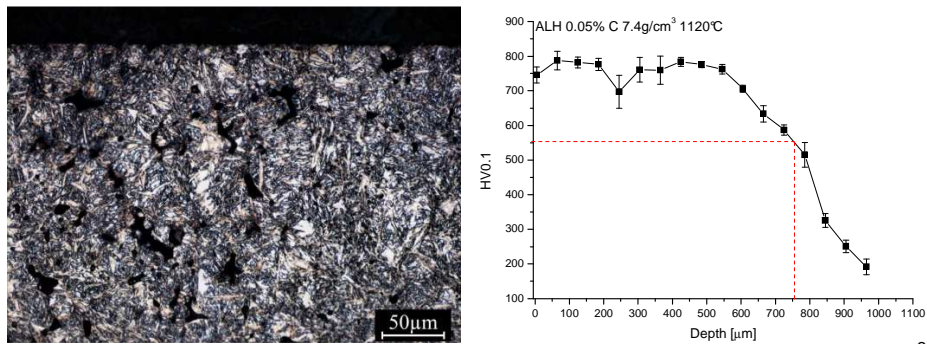


Figure 10.10: microstructure and microhardness profile of carburized 7.4g/cm<sup>3</sup> 0.05%C ALH

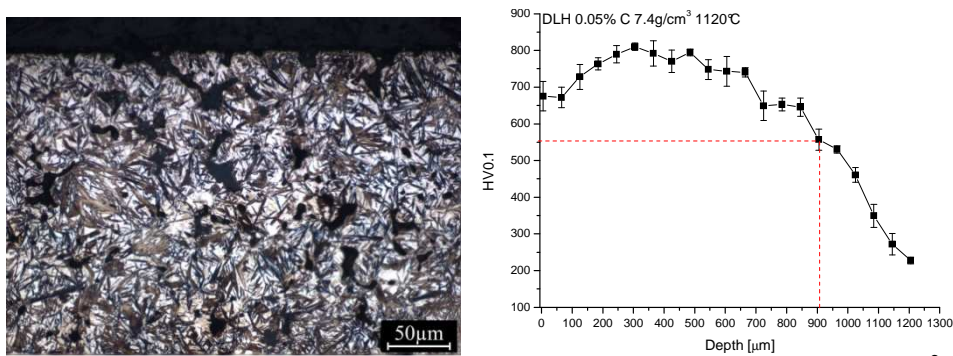


Figure 10.11: microstructure and microhardness profile of carburized 7.4g/cm<sup>3</sup> 0.05%C DLH



*Chapter 10: Low Pressure Carburizing of Chromium Free Steels*

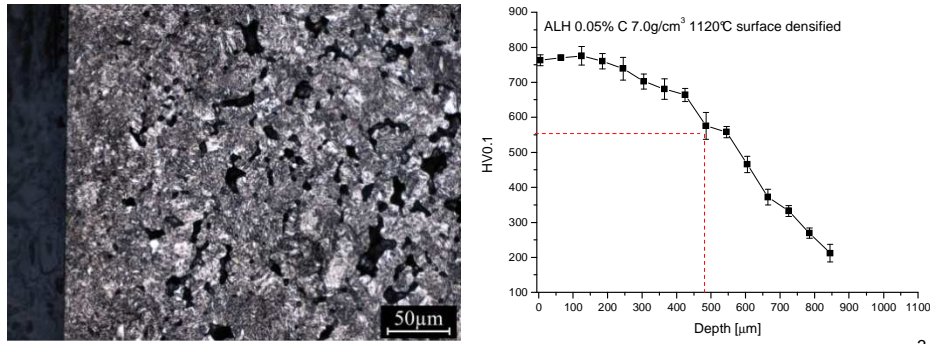


Figure 10.12: microstructure and microhardness profile of carburized 7.0g/cm<sup>3</sup> surface densified 0.05%C ALH

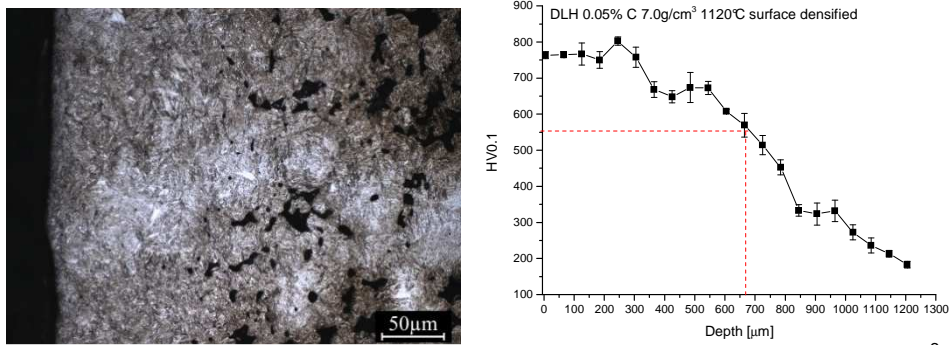


Figure 10.13: microstructure and microhardness profile of carburized 7.0g/cm<sup>3</sup> surface densified 0.05%C DLH

The presence of retained austenite in warm compacted (7.4 g/cm<sup>3</sup>) DLH and its absence in surface densified one, clearly indicates the role of open porosity, which causes a deeper case depth in the 7.4g/cm<sup>3</sup> specimens than in the surface densified ones.

Table 10.7 summarizes the representative data of the microhardness profiles: surface microhardness and case depth ( $d_{550}$ ).

**Chapter 10: Low Pressure Carburizing of Chromium Free Steels**

---

Table 10.7: surface microhardness and case depth of LPC 2 steels

ALH	7.4g/cm <sup>3</sup>		7.0g/cm <sup>3</sup> surface densified		Target
	0.05%C	0.2%C	0.05%C	0.2%C	
HV0.1	750	780	750	800	800-900
d <sub>550</sub> [μm]	750	1100	490	750	500-600

DLH	7.4g/cm <sup>3</sup>		7.0g/cm <sup>3</sup> surface densified		Target
	0.05%C	0.2%C	0.05%C	0.2%C	
HV0.1	680	740	750	750	800-900
d <sub>550</sub> [μm]	900	1100	660	660	500-600

LPC 2 effectively increases the microhardness and the case depth of the materials with respect to the results of the previous investigation (LPC 1) and it matches the target.

*10.2.2. Impact toughness*

The results of impact tests carried out on surface densified 6.8g/cm<sup>3</sup> and 7.0g/cm<sup>3</sup> specimens and 7.4g/cm<sup>3</sup> samples are compared with the as sintered ones and listed in Table 10.8.

**Chapter 10: Low Pressure Carburizing of Chromium Free Steels**

Table 10.8: impact test results of LPC 2 steels

SURFACE DENSIFIED SPECIMENS			Impact Energy [J]		P <sub>y</sub> [KN]		P <sub>max</sub> [KN]	
			As sint	Surface densified and carburized	As sint	Surface densified and carburized	As sint	Surface densified and carburized
ALH								
%C	Density [g/cm <sup>3</sup> ]	T sint [°C]						
0.05	6.8	1120	16	13	7	-	9	17
0.05	7.0	1120	25	15	8	-	11	19
0.2	6.8	1120	13	13	9	-	12	20
0.2	7.0	1120	16	16	11	-	14	21
DLH								
0.05	6.8	1120	12	12	8	-	14	17
0.05	7.0	1120	17	19	8	-	14	22
0.2	6.8	1120	11	16	9	-	15	21
0.2	7.0	1120	17	18	9	-	17	23

7.4g/cm <sup>3</sup> SPECIMENS			Impact Energy [J]		P <sub>y</sub> [KN]		P <sub>max</sub> [KN]	
			As sint	Carburized	As sint	Carburized	As sint	Carburized
ACrL								
%C	Density [g/cm <sup>3</sup> ]	T sint [°C]						
0.05	7.4	1120	59	10	11	-	19	21
0.2	7.4	1120	59	12	11	-	19	24
DLH								
0.05	7.4	1120	62	11	9	-	20	25
0.2	7.4	1120	47	14	10	-	23	28

Some the load-deflection curves are reported in figure 10.14.

## Chapter 10: Low Pressure Carburizing of Chromium Free Steels

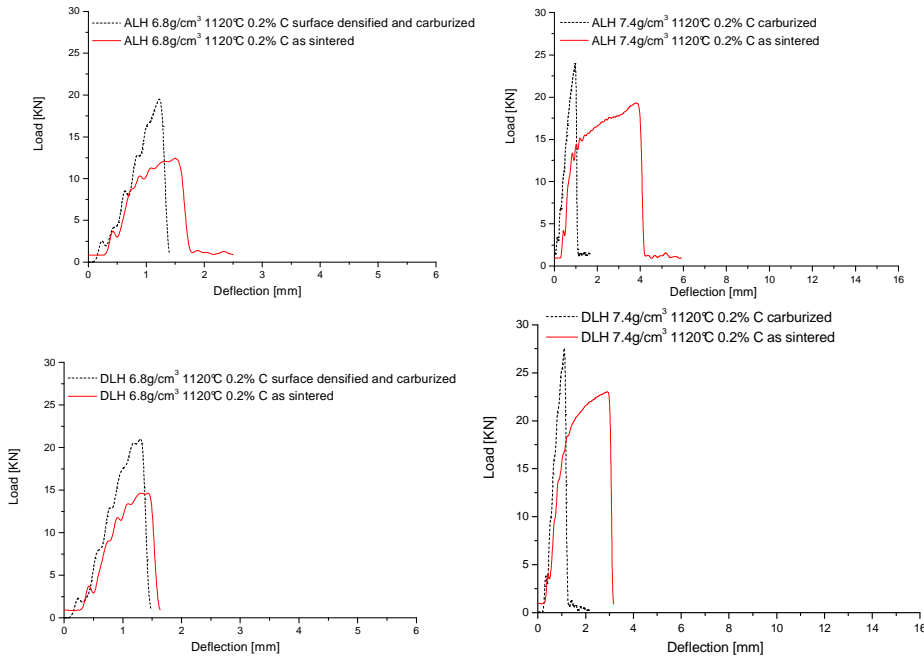


Figure 10.14: examples of load-deflection curves

All the carburized materials have an elastic behavior without any significant plastic deformation. Surface densification does not improve the impact energy of LPC 2 materials despite the increase of  $P_{max}$ . The impact energy of  $7.4\text{g/cm}^3$  steels strongly decreases independent on the carbon content.

### 10.3. Microstructural improvement of overcarburized materials

#### 10.3.1. Tempering treatment

In order to improve the overcarburized microstructures, retained austenite has to be transformed by tempering. Thanks to the presence of molybdenum, the tempering temperature can be increased up to  $500^\circ\text{C}$  to evaluate the effect of the secondary carbides precipitation on microhardness.

## *Chapter 10: Low Pressure Carburizing of Chromium Free Steels*

Three different tempering treatments, 300°C, 400°C and 500°C, are carried out on 6.8g/cm<sup>3</sup> 0.2%C ALH and DLH. The case microstructure, shown in figure 10.15, results homogeneous and retained austenite disappears completely.

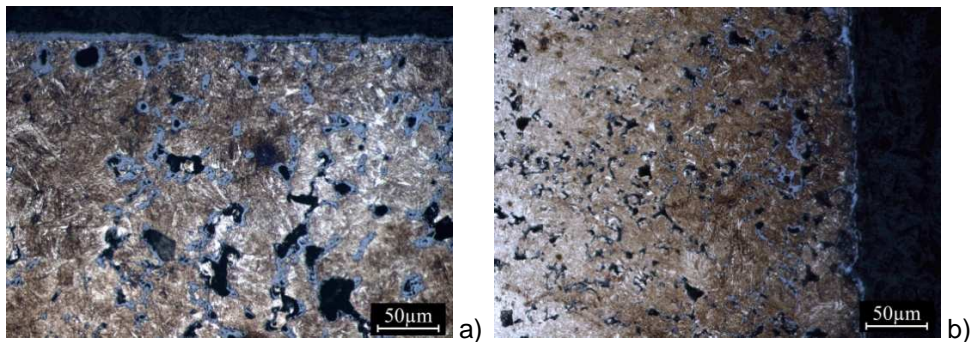


Figure 10.15: microstructures of: a) ALH and b)DLH

The microhardness profiles are quite good for all the tempering temperatures investigated (fig. 10.16). The microhardness decreases on tempering at 400°C, but it increases after tempering at 500°C, even more in DLH than in ALH, confirming the expected secondary precipitation of carbides. These carbides are submicrometric, therefore they are not observed at the optical microscope.

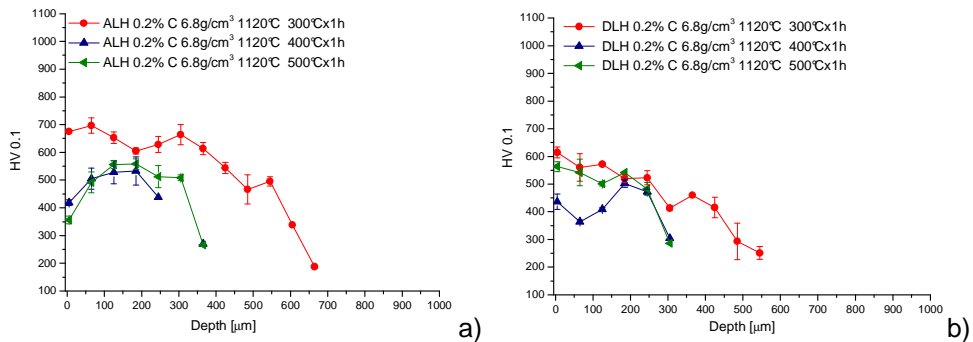


Figure 10.16: microhardness profiles: a) ALH and b) DLH

## Chapter 10: Low Pressure Carburizing of Chromium Free Steels

### 10.4. Fatigue resistance

A four steps low pressure carburizing (LPC 3) was carried out on  $7.0\text{g/cm}^3$  0.2%C DLH and surface densified one to evaluate the effect of residual austenite on the fatigue resistance of the steels.

#### 10.4.1. Microstructure and microhardness profile

Microstructures and microhardness profiles of the steels are shown in figures 10.17- 10.18.

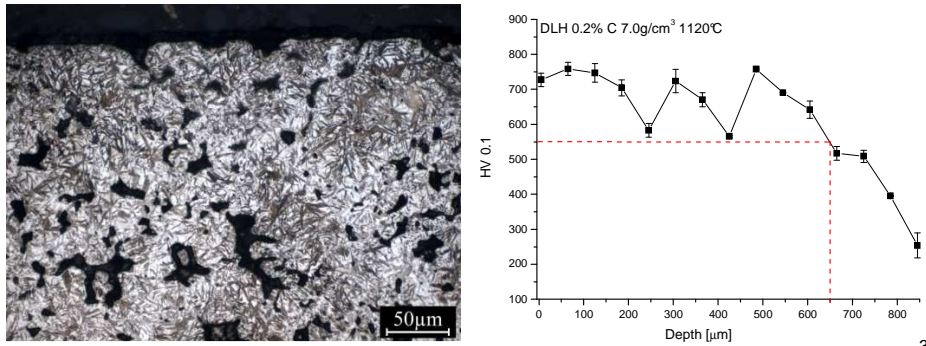


Figure 10.17: microstructure and microhardness profile of carburized  $7.0\text{g/cm}^3$  0.2%C DLH

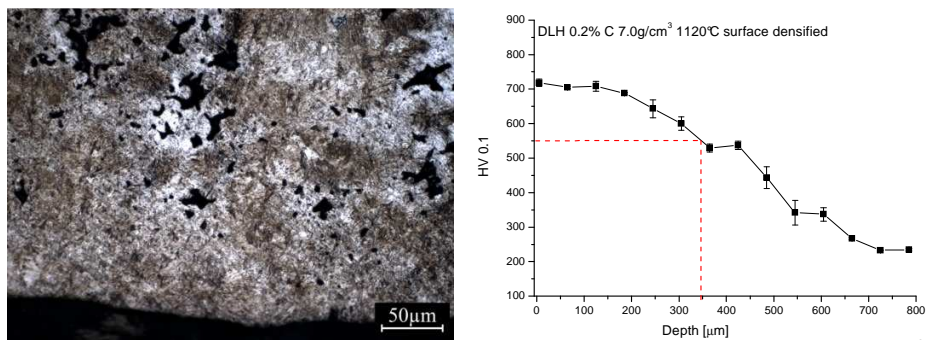


Figure 10.18: microstructure and microhardness profile of carburized  $7.0\text{g/cm}^3$  surface densified 0.2%C DLH

## *Chapter 10: Low Pressure Carburizing of Chromium Free Steels*

Figure 10.17 shows the formation of a large amount of retained austenite in the case of 7.0g/cm<sup>3</sup> steel, as expected. The absence of open porosity prevents overcarburizing (fig. 10.18).

The microhardness profile is strongly influenced by retained austenite, which is mainly localized in the outer part of the case, whereas it is regular in surface densified specimen. The case depth is deeper in 7.0g/cm<sup>3</sup> DLH respect to the surface densified one, because of the different amount of surface porosity. The surface microhardness are similar to the target (tab. 10.9).

Table 10.9: microhardness and case depths of carburized steels

<b>0.2%C DLH</b>	<b>7.0g/cm<sup>3</sup></b>	<b>7.0g/cm<sup>3</sup> surface densified</b>	<b>Target</b>
<b>HV0.1</b>	720	720	800-900
<b>d<sub>50</sub> [μm]</b>	650	350	500-600

### 10.4.2. Fatigue resistance

The results of the stair case method are reported in figure 10.19 and the fatigue resistance at 2x10<sup>6</sup> cycles are listed in table 10.10.

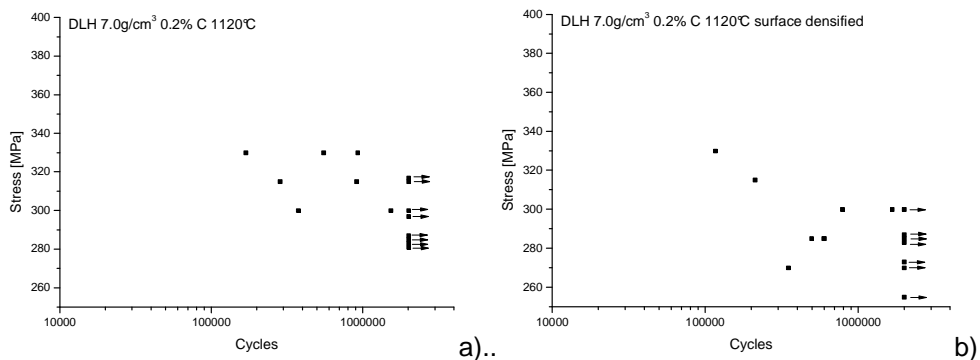


Figure 10.19: fatigue results of carburized 0.2%C DLH: a) 7.0g/cm<sup>3</sup> and b) surface densified 7.0g/cm<sup>3</sup>

**Chapter 10: Low Pressure Carburizing of Chromium Free Steels**

Table 10.10: fatigue resistance at  $2 \times 10^6$  cycles of low pressure carburized steels

	Fatigue resistance at $2 \times 10^6$ cycles [MPa]	
	7.0g/cm <sup>3</sup> 0.2%C DLH	7.0g/cm <sup>3</sup> 0.2%C DLH surface densified
1120°C	310±18	286±21

The fatigue resistance is higher in 7.0g/cm<sup>3</sup> 0.2%C DLH with respect to the surface densified steel because of the depth of the diffusion layer.

The fatigue resistance of 7.0g/cm<sup>3</sup> 0.2%C DLH is close to that of surface densified ACrL and to the solution annealed one (tab 10.11), in which overcarburizing is avoided. The fatigue strength is also quite similar to that of plasma carburized 7.1g/cm<sup>3</sup> ACrL sintered at 1120°C. Confirming that Cr free steels are attractive materials for low pressure carburizing.

Table 10.11: fatigue resistance of low pressure carburized and plasma carburized ACrL steels

ACrL	Fatigue resistance at $2 \times 10^6$ cycles [MPa]	
	Low pressure carburized	Plasma carburized [35]
7.0g/cm <sup>3</sup> 0.2%C surface densified	303±6	
7.0g/cm <sup>3</sup> 0.2%C solution annealed	286±21	
7.1g/cm <sup>3</sup> 0.2%C		305±8



## Chapter 10: Low Pressure Carburizing of Chromium Free Steels

### 10.4.3. Fracture surface analysis

The fracture surfaces of carburized are reported in figures 10.20- 10.21.

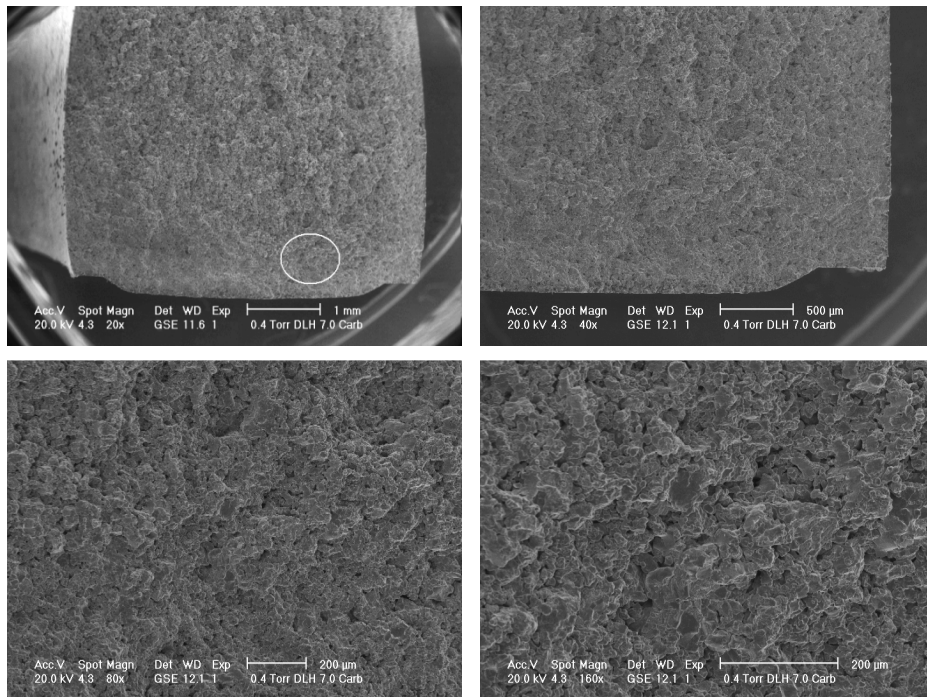


Figure 10.20: fracture surface of carburized 7.0g/cm<sup>3</sup> 0.2%C DLH

## Chapter 10: Low Pressure Carburizing of Chromium Free Steels

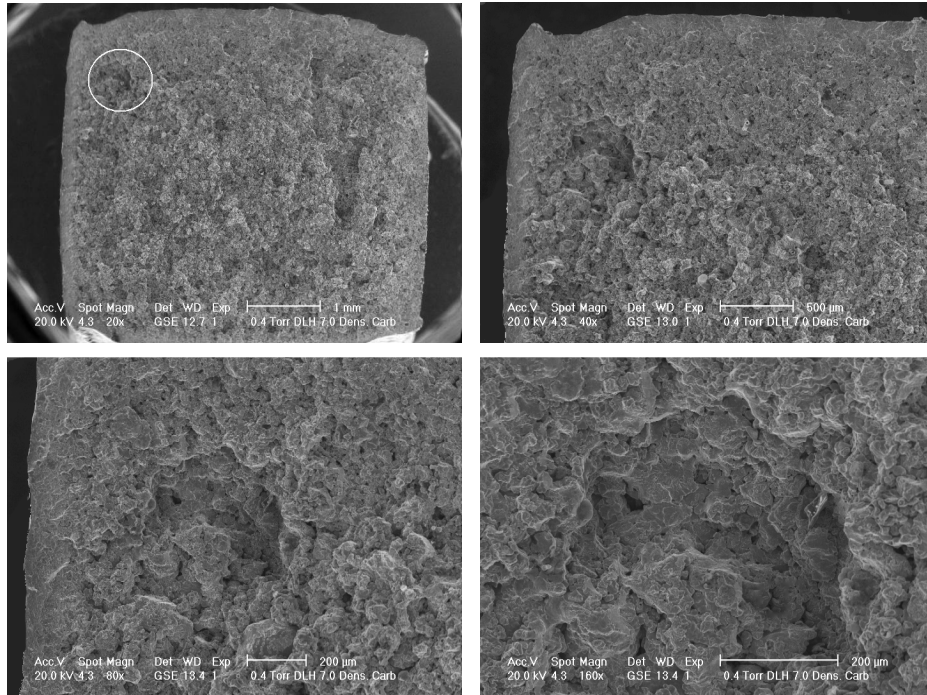


Figure 10.21: fracture surface of carburized  $7.0\text{g}/\text{cm}^3$  surface densified 0.2% C DLH

The analysis of the fracture surface of carburized steels shows the movement of the fatigue crack initiation below the case depth in correspondence of the maximum total tensile stress, resulting from residual stress distribution and outer load. The nucleation point is in correspondence of either a cluster of pores or a large pore, as usual in sintered steels.

### 10.5. Concluding remarks

The results of the work on low pressure carburized Cr free steels can be summarized as follows.

- In presence of open porosity materials are overcarburized, which causes the formation of retained austenite.

### *Chapter 10: Low Pressure Carburizing of Chromium Free Steels*

---

- Surface densification prevents overcarburizing.
- Case depth is deeper in warm compacted materials than in surface densified ones because of different surface porosity.
- Microhardness profiles correspond quite well to the target after five steps carburizing (6minutes of boosting and 115minutes of diffusion).
- Carburizing causes the embrittlement of the materials, independently on bulk density. Impact behavior is purely elastic, without any significant plastic deformation.
- Retained austenite can be destabilized by tempering treatment.
- The plane bending fatigue resistance increases on increasing the case depth. The analysis of the fracture surface of the carburized steels shows subsurface crack nucleation.

## **11. Conclusions**

The results of the study on the effect of surface treatments on the impact and fatigue resistance of some sintered steels can be summarized as follows.

### **11.1. Low pressure carburizing**

1. In presence of an open porosity, overcarburizing causes the precipitation of grain boundary carbides in the Cr steels and the formation of retained austenite in the Cr free ones.
2. No overcarburizing occurs in the surface densified and in  $7.4\text{g/cm}^3$  steels. Some retained austenite is still present in  $7.4\text{g/cm}^3$  DLH, due to residual open porosity.
3. The surface microhardness and the case depth of carburized materials are around  $800\text{HV}_{0.1}$  and  $600\mu\text{m}$ , respectively. Case depth is deeper in ACrL because of the greater hardenability.
4. The case depth is higher  $7.4\text{g/cm}^3$  materials than in surface densified ones because of different surface porosity.
5. Shot peening effectively closes the surface porosity (surface densification), but leaves some residual defects and an irregular morphology on the treated surface.
6. Impact tests show the expected embrittlement caused by LPC, which is lower in the case of the Cr free materials.
7. By means of a solution annealing treatment grain boundaries carbides can be effectively dissolved in austenite and by means of a fast cooling the precipitation is avoided.

Tempering at 200°C improves the microstructure of the case and surface layers are satisfactorily hardened even if the microhardness profile is slightly lower than that of the as carburized steel.

8. The retained austenite in the Ni-Mo-Cu overcarburized steels can be transformed by tempering treatment. The significant tempering resistance is provided by Mo.
9. Low pressure carburized  $7.4\text{g/cm}^3$  0.2%C ACrL sintered at 1250°C has a bending fatigue resistance of 470MPa. The fatigue resistance of solution annealed material (around 303- 333MPa) is similar to that of surface densified one (around 286- 303MPa), confirming that solution annealing is a real alternative to surface densification.
10. Fractography shows crack initiation below the surface, in the tensile residual stress field where the hardening promoted by carburizing is negligible. Here the stress amplitude is lower than on the surface. The fatigue cracks nucleates in correspondence of pores cluster and propagates in the pores network, as usual in porous sintered steels.

### **11.2. Plasma nitriding**

1. The study was carried out on the two Cr materials only, since in absence of this element plasma nitriding is poorly effective and the hardness of the diffusion layer is too low.
2. The surface microhardness and the case depth of the nitrided materials are around 700HV0.1 and 200- 350 $\mu\text{m}$ , respectively. The preliminary surface densification by shot peening does not improve microhardness profile, since nitriding effect prevails on that of shot peening.
3. Impact toughness is strongly reduced since the materials loose the plastic properties completely.

## *Chapter 11: Conclusions*

---

4. The fatigue resistance of the nitrided  $7.4\text{g/cm}^3$  0.2%C ACrL sintered at  $1250^\circ\text{C}$  is 343MPa.
5. Post nitriding shot peening increases case depth and surface microhardness, but it does not lead to further improvement in fatigue resistance.
6. The fatigue crack in nitrided steels nucleates in the subsurface layer, where the tensile stress is the highest and the hardness is comparable to the matrix. Here the stress amplitude is lower than that on the surface.

The comparison between the impact properties of the two treatments shows that plasma nitriding causes a greater embrittlement in the base material than carburizing: both processes cause a reduction of ductility but this is accomplished by an increase in strength in carburizing only. Considering the fatigue strength, it is higher in low pressure carburized steels than in plasma nitrided ones. This is likely due to the different microhardness profile; despite the surface microhardness is very similar, the case depth of LPC steels is deeper than that of plasma nitrided materials. The fatigue cracks nucleates below the compression-tension stress transition where the hardness is not affected by the treatment, in correspondence of subsurface pores, and it tends to propagate through the inter-pore ligaments. Therefore the higher the case depth the higher the fatigue strength of the steel.

### **11.3. Shot peening**

1. Shot peening forms a surface fully dense layer ( $50\mu\text{m}$ ). The thickness decreases on increasing shot diameter and coverage.
2. Strain hardened layer is deeper than the densified one and the thickness tends to decrease on increasing shot diameter, whilst the effect of coverage is negligible.

## *Chapter 11: Conclusions*

---

3. Residual stress profile is deeper on increasing shot diameter without any significant effect of the coverage.
4. An increase of 25- 30%, in plane bending fatigue strength was measured irrespective to shot diameter.
5. Fatigue crack nucleates in tensile residual stress zone, beneath the strain hardened layer.

Since the improvement in fatigue resistance is due to the shift of crack nucleation towards the interior, where the stress amplitude is lower than on the surface, all the surface treatments which are able to avoid surface crack nucleation increase the fatigue strength.

Considering the Cr steels, low pressure carburizing as well as plasma nitriding and shot peening can be used. However, LPC requires high density, surface densification or solution annealing treatment, which are not necessary in the cases of plasma nitriding or shot peening.

Considering the Cr free materials, low pressure carburizing is also effective, in particular in presence of surface densification.

Therefore, the best surface treatment is that which moves cracks in depth reducing processing costs and technical complexity.

## 12. Appendix

### 12.1. Impact properties of as sintered steels

ACrL			Impact Energy [J]	$P_y$ [KN]	$P_{max}$ [KN]	$E_{el}$ [J]	$E_{nucl}$ [J]	$E_{prop}$ [J]
%C	Density [g/cm <sup>3</sup> ]	T sintering						
0.05	6.8	1120°C	28 ± 2	8	10	2	21	5
0.05	6.8	1250°C	42 ± 1	8	11	2	30	10
0.05	7.0	1120°C	39 ± 1	9	12	2	30	7
0.05	7.0	1250°C	69 ± 3	10	13	2	46	21
0.05	7.4	1120°C	103 ± 5	11	16	3	74	25
0.05	7.4	1250°C	15 ± 4	11	16	4	119	33
0.2	6.8	1120°C	21 ± 1	9	12	2	15	4
0.2	6.8	1250°C	34 ± 2	9	14	2	25	6
0.2	7.0	1120°C	29 ± 2	11	14	3	21	5
0.2	7.0	1250°C	52 ± 7	10	16	2	41	8
0.2	7.4	1120°C	72 ± 5	13	24	3	61	8
0.2	7.4	1250°C	95 ± 4	12	18	3	68	24
0.4	6.8	1120°C	13 ± 2	12	17	4	7	2
0.4	6.8	1250°C	23 ± 4	13	20	4	16	3
0.4	7.0	1120°C	19 ± 1	12	19	3	13	3
0.4	7.0	1250°C	33 ± 4	11	21	2	28	3
0.4	7.4	1120°C	40 ± 1	14	25	3	32	5
0.4	7.4	1250°C	72 ± 1	15	26	4	42	26



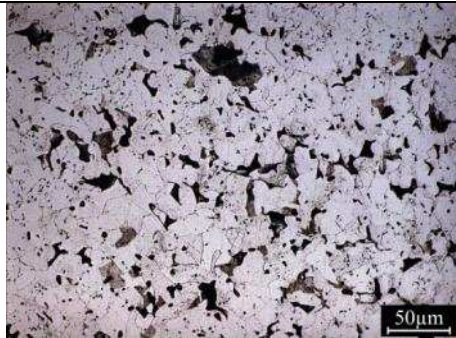

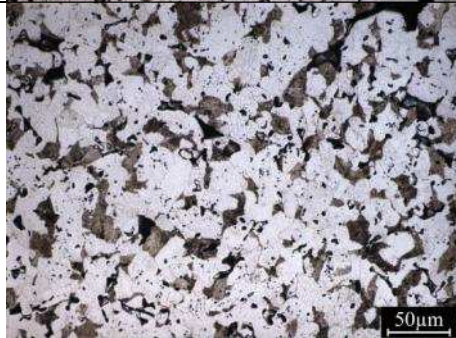

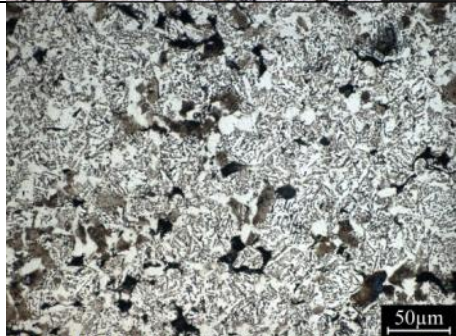
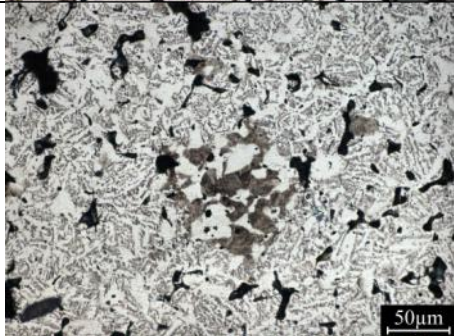
AD4			Impact Energy [J]	P <sub>y</sub> [KN]	P <sub>max</sub> [KN]	E <sub>el</sub> [J]	E <sub>nucl</sub> [J]	E <sub>prop</sub> [J]
%C	Density [g/cm <sup>3</sup> ]	T sintering						
0.05	6.8	1120°C	18 ± 1	9	10	3	10	5
0.05	6.8	1250°C	33 ± 2	8	11	2	24	8
0.05	7.0	1120°C	28 ± 1	9	11	2	19	7
0.05	7.0	1250°C	47 ± 1	9	12	2	38	8
0.05	7.4	1120°C	95 ± 7	11	14	2	76	17
0.05	7.4	1250°C	124 ± 10	11	14	3	98	23
0.2	6.8	1120°C	16 ± 1	8	13	2	9	4
0.2	6.8	1250°C	28 ± 1	8	11	2	18	7
0.2	7.0	1120°C	22 ± 1	9	14	2	16	4
0.2	7.0	1250°C	40 ± 3	11	14	3	32	5
0.2	7.4	1120°C	74 ± 5	12	17	3	60	11
0.2	7.4	1250°C	100 ± 2	12	17	3	75	22
0.4	6.8	1120°C	15 ± 1	10	13	3	10	2
0.4	6.8	1250°C	22 ± 2	11	14	3	16	3
0.4	7.0	1120°C	20 ± 2	10	15	2	14	4
0.4	7.0	1250°C	29 ± 2	12	16	3	21	5
0.4	7.4	1120°C	54 ± 8	13	21	3	46	5
0.4	7.4	1250°C	64 ± 5	13	20	3	52	9

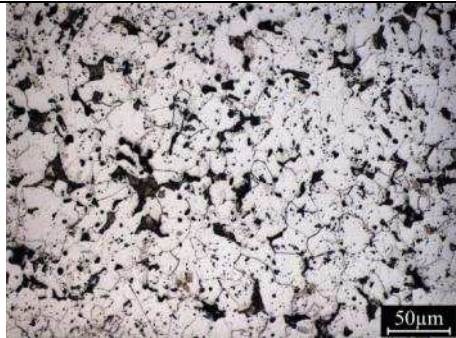
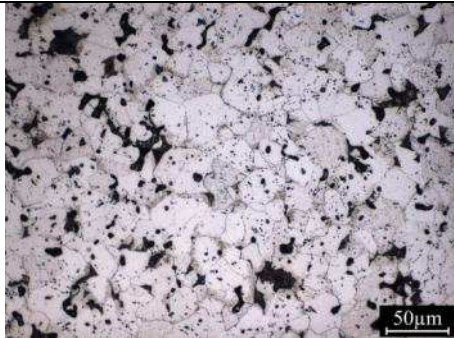
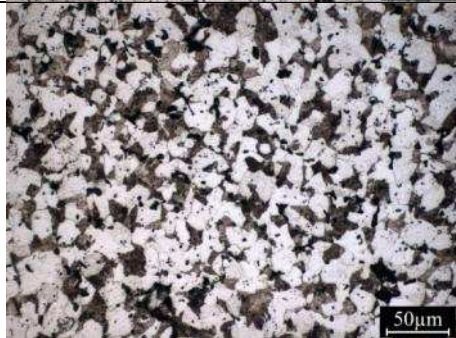
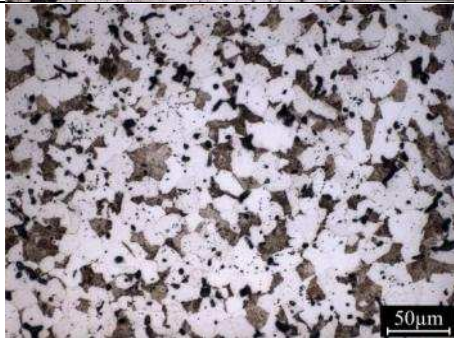
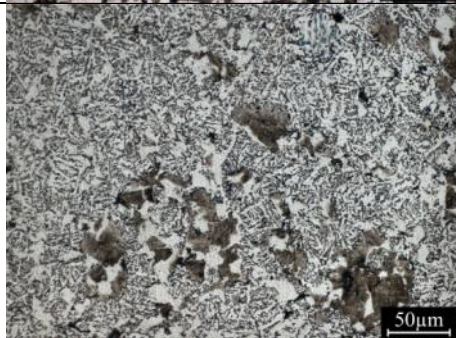
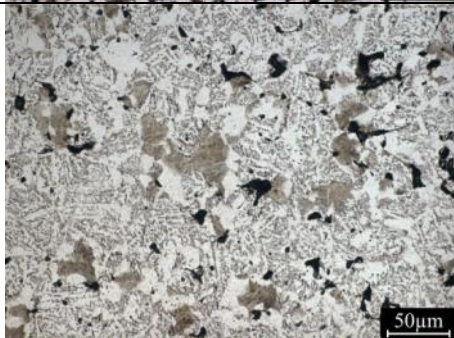
ALH			Impact Energy [J]	P <sub>y</sub> [KN]	P <sub>max</sub> [KN]	E <sub>el</sub> [J]	E <sub>nucl</sub> [J]	E <sub>prop</sub> [J]
%C	Density [g/cm <sup>3</sup> ]	T sintering						
0.05	6.8	1120°C	16 ± 1	7	9	2	9	6
0.05	7.0	1120°C	25 ± 2	8	11	2	17	6
0.05	7.4	1120°C	59 ± 2	11	19	2	50	7
0.2	6.8	1120°C	13 ± 1	9	12	2	8	3
0.2	7.0	1120°C	16 ± 1	11	14	3	10	3
0.2	7.4	1120°C	59 ± 6	11	19	2	51	6


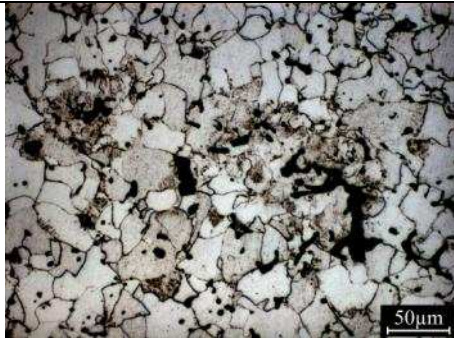


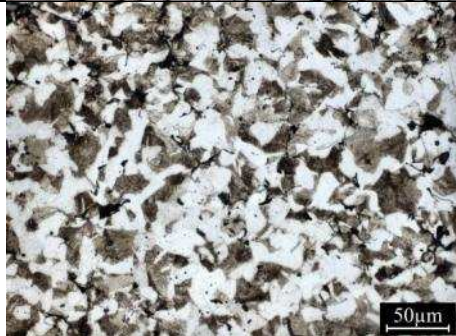

*Chapter 12: Appendix*

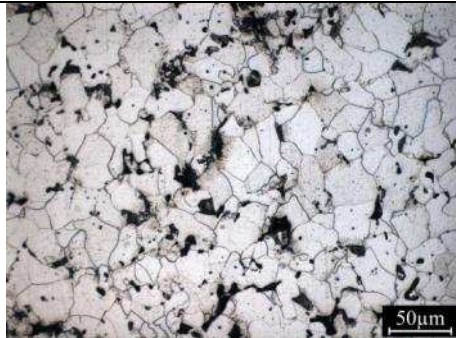
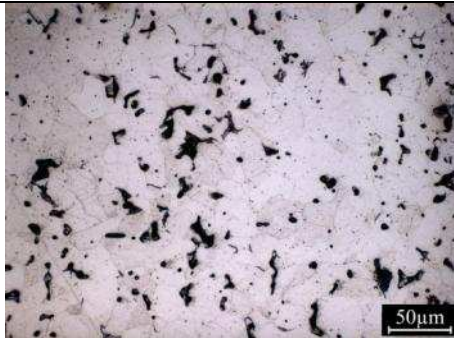
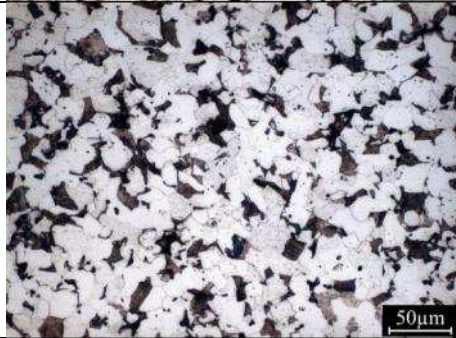

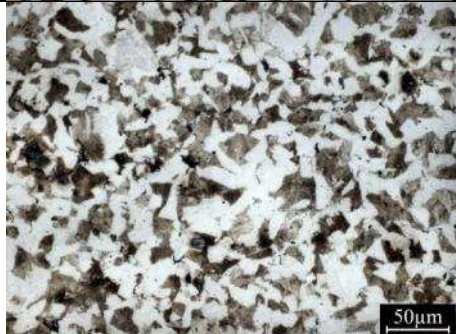
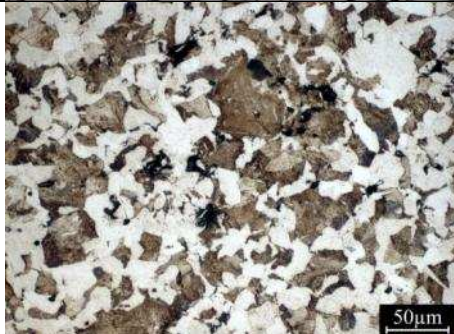
DLH			Impact Energy [J]	P <sub>y</sub> [KN]	P <sub>max</sub> [KN]	E <sub>el</sub> [J]	E <sub>nucl</sub> [J]	E <sub>prop</sub> [J]
%C	Density [g/cm <sup>3</sup> ]	T sintering						
0.05	6.8	1120°C	12 ± 1	8	14	2	8	2
0.05	7.0	1120°C	17 ± 1	8	14	2	12	3
0.05	7.4	1120°C	62 ± 2	9	20	2	56	4
0.2	6.8	1120°C	11 ± 1	9	15	2	8	1
0.2	7.0	1120°C	17 ± 1	9	17	2	13	2
0.2	7.4	1120°C	47 ± 3	10	23	2	41	4

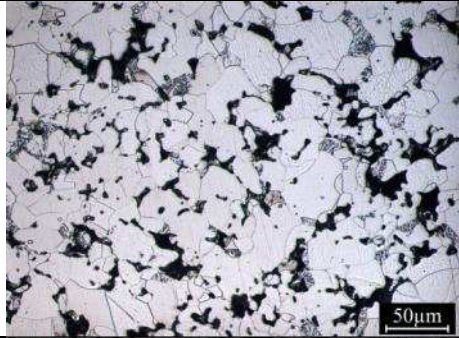
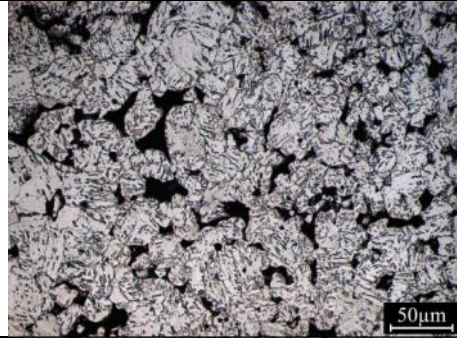
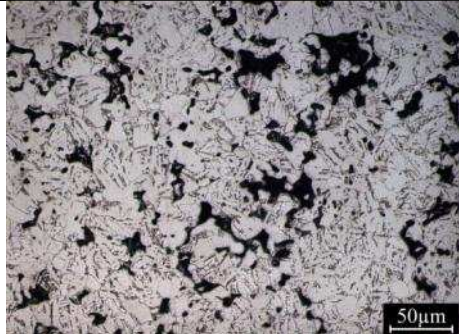
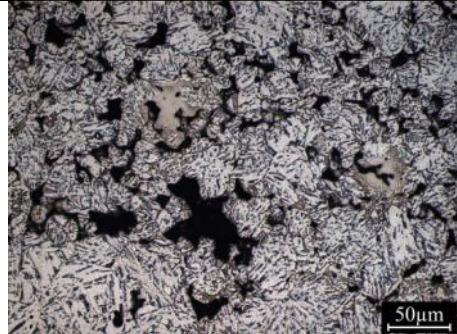
12.2 Microstructures of as sintered steels

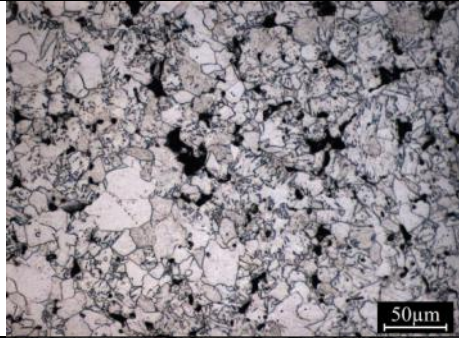
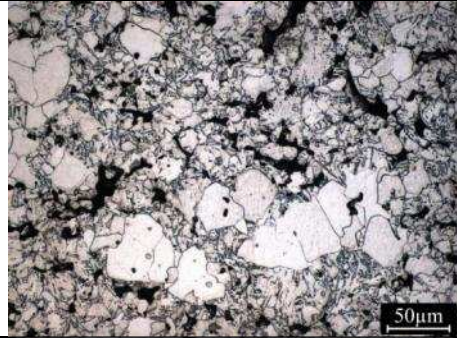
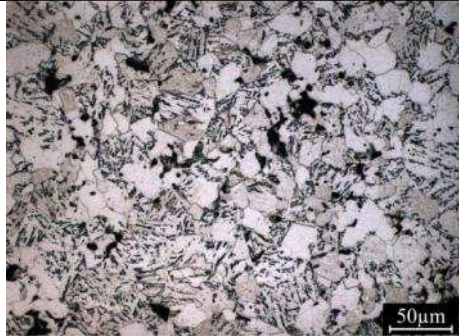
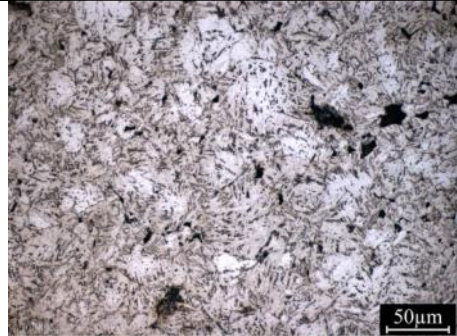
%C	7.0g/cm <sup>3</sup> ACrL sintered at 1120°C	7.0g/cm <sup>3</sup> ACrL sintered at 1250°C
0.05	 Micrograph showing the microstructure of 0.05% carbon steel sintered at 1120°C. The structure consists of a light-colored matrix with dark, irregularly shaped particles. A 50µm scale bar is located in the bottom right corner.	 Micrograph showing the microstructure of 0.05% carbon steel sintered at 1250°C. The structure is similar to the 1120°C sample but with slightly more refined features. A 50µm scale bar is located in the bottom right corner.
0.2	 Micrograph showing the microstructure of 0.2% carbon steel sintered at 1120°C. The structure shows a light matrix with dark particles and some larger, more complex shapes. A 50µm scale bar is located in the bottom right corner.	 Micrograph showing the microstructure of 0.2% carbon steel sintered at 1250°C. The structure is similar to the 1120°C sample but with slightly more refined features. A 50µm scale bar is located in the bottom right corner.
0.4	 Micrograph showing the microstructure of 0.4% carbon steel sintered at 1120°C. The structure shows a light matrix with dark particles and some larger, more complex shapes. A 50µm scale bar is located in the bottom right corner.	 Micrograph showing the microstructure of 0.4% carbon steel sintered at 1250°C. The structure is similar to the 1120°C sample but with slightly more refined features. A 50µm scale bar is located in the bottom right corner.

%C	7.4g/cm <sup>3</sup> ACrL sintered at 1120°C	7.4g/cm <sup>3</sup> ACrL sintered at 1250°C
0.05		
0.2		
0.4		

%C	7.0g/cm <sup>3</sup> AD4 sintered at 1120°C	7.0g/cm <sup>3</sup> AD4 sintered at 1250°C
0.05		
0.2		
0.4		

%C	7.4g/cm <sup>3</sup> AD4 sintered at 1120°C	7.4g/cm <sup>3</sup> AD4 sintered at 1250°C
0.05		
0.2		
0.4		

%C	7.0g/cm <sup>3</sup> ALH	7.0g/cm <sup>3</sup> DLH
0.05		
0.2		

%C	7.4g/cm <sup>3</sup> ALH	7.4g/cm <sup>3</sup> DLH
0.05		
0.2		

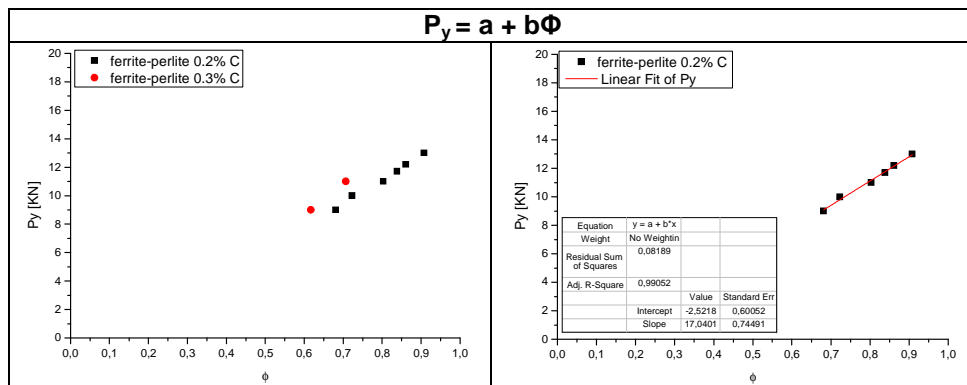


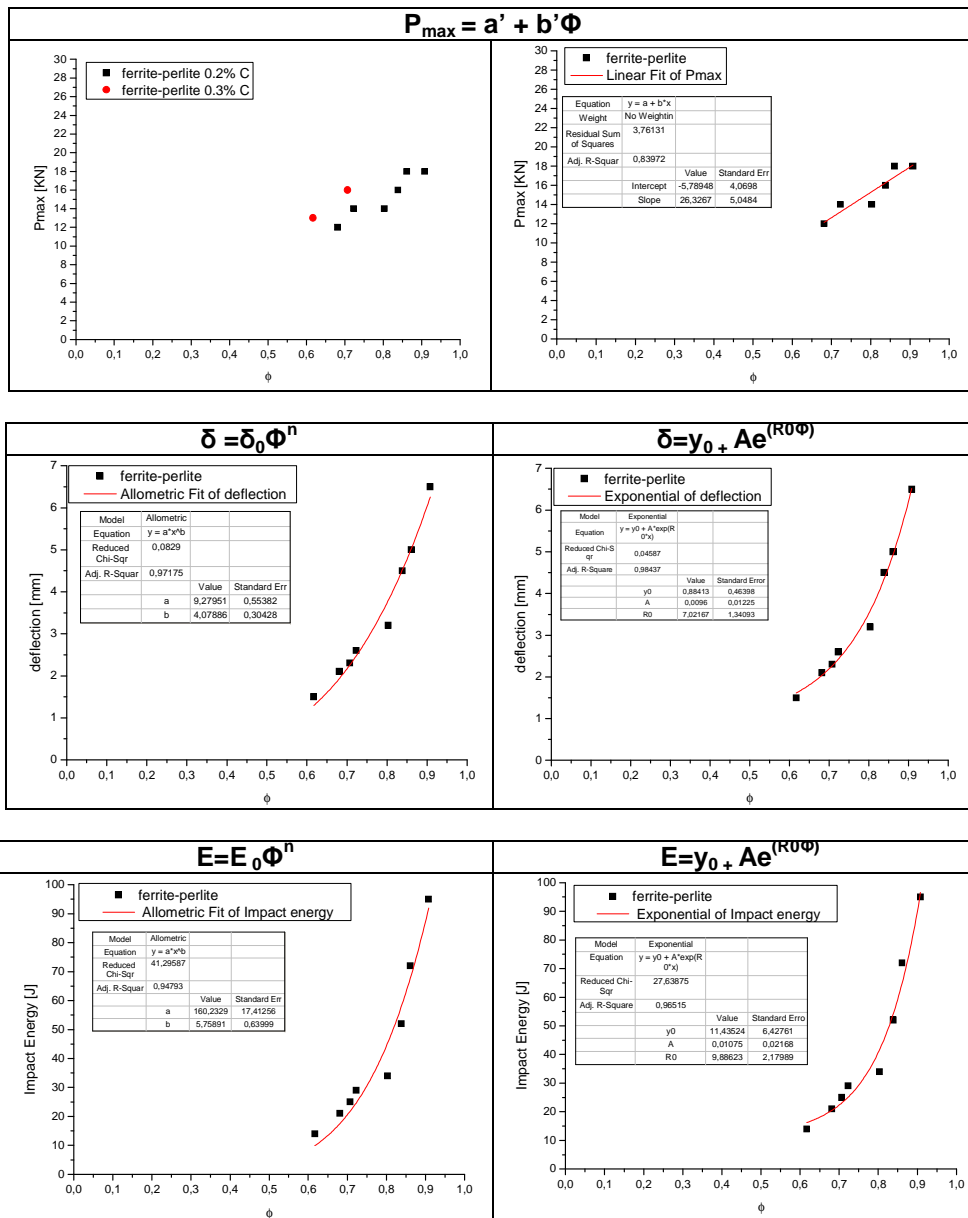
12.3. A simplified model for impact strength of sintered steels

12.3.1. Ferritic- Perlitic steels

0.2%C ACrL	6.8g/cm <sup>3</sup>		7.0g/cm <sup>3</sup>		7.4g/cm <sup>3</sup>	
	1120°C	1250°C	1120°C	1250°C	1120°C	1250°C
<b>F<sub>circle</sub></b>	0.71	0.81	0.70	0.81	0.74	0.81
<b>ε</b>	0.114	0.108	0.094	0.088	0.053	0.049
<b>K<sub>p</sub></b>	1.53	0.96	1.59	0.96	1.36	0.96
<b>Φ</b>	0.68	0.80	0.72	0.84	0.86	0.91

0.3%C ACrL	6.8g/cm <sup>3</sup>	7.0g/cm <sup>3</sup>
	1120°C	1120°C
<b>F<sub>circle</sub></b>	0.71	0.7
<b>ε</b>	0.14	0.1
<b>K<sub>p</sub></b>	1.53	1.59
<b>Φ</b>	0.62	0.71
<b>E [J]</b>	14	25
<b>Deflection [mm]</b>	1.5	2.2
<b>P<sub>y</sub> [KN]</b>	9	11
<b>P<sub>max</sub> [KN]</b>	13	16
<b>HV0.05</b>	259.1±42.0	209.8±28.6

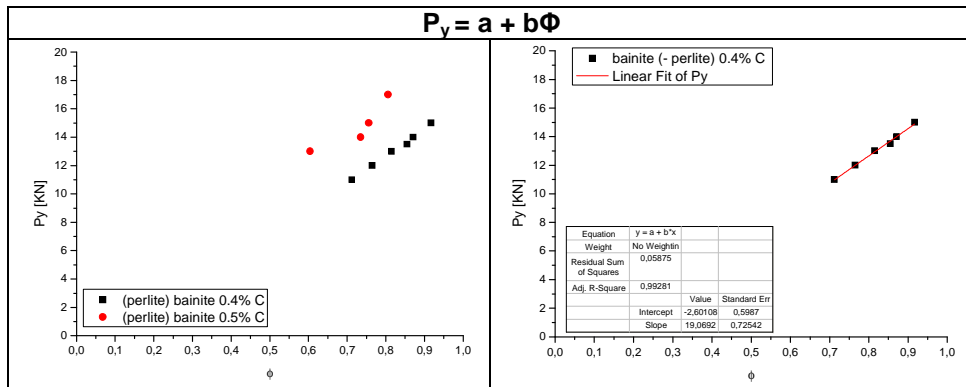


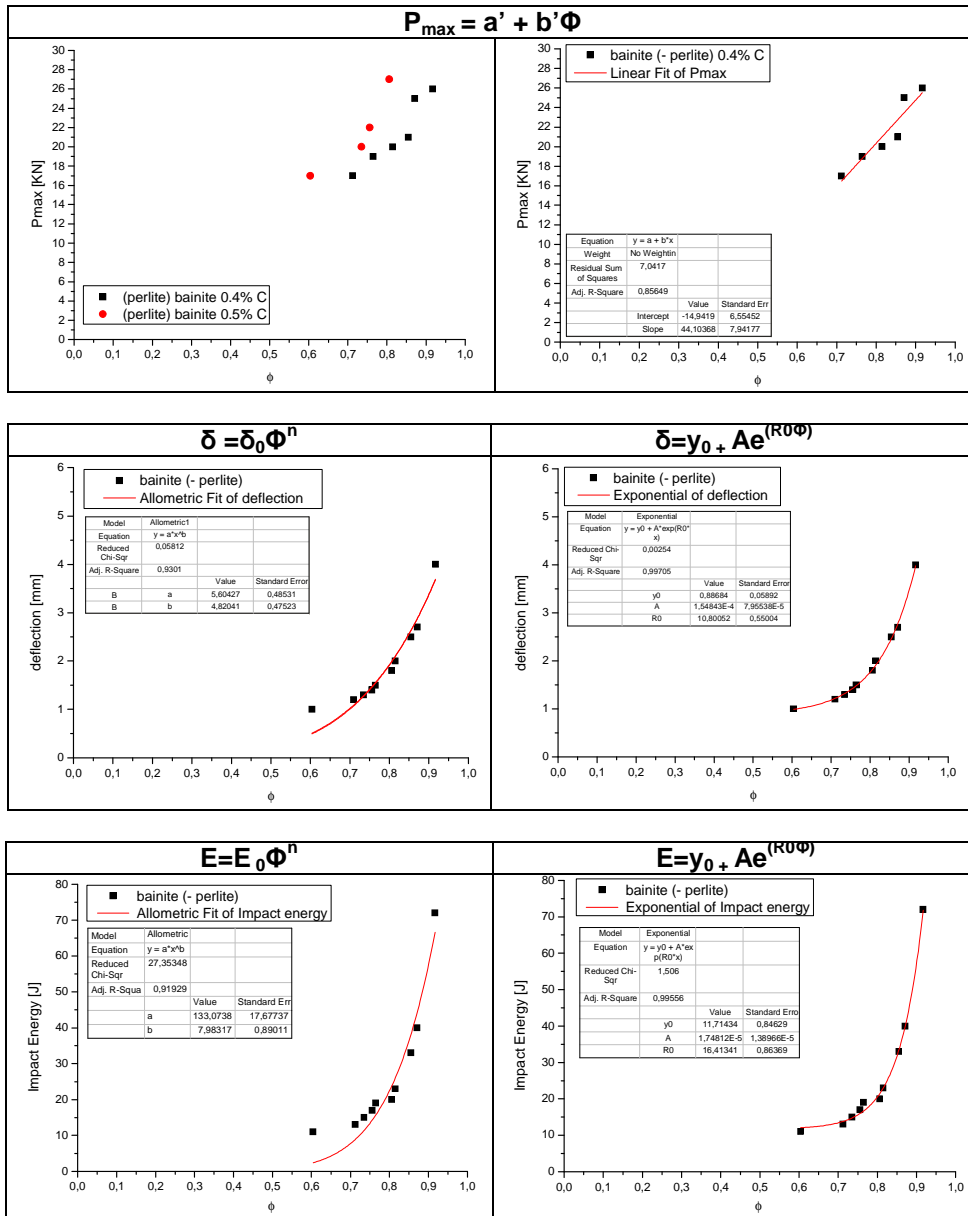


12.3.2. Bainitic (- Perlitic) steels

0.4%C ACrL	6.8g/cm <sup>3</sup>		7.0g/cm <sup>3</sup>		7.4g/cm <sup>3</sup>	
	1120°C	1250°C	1120°C	1250°C	1120°C	1250°C
<b>F<sub>circle</sub></b>	0.71	0.81	0.70	0.81	0.74	0.81
<b>ε</b>	0.102	0.101	0.079	0.078	0.049	0.044
<b>Kp</b>	1.53	0.96	1.59	0.96	1.36	0.96
<b>Φ</b>	0.71	0.82	0.77	0.86	0.87	0.92

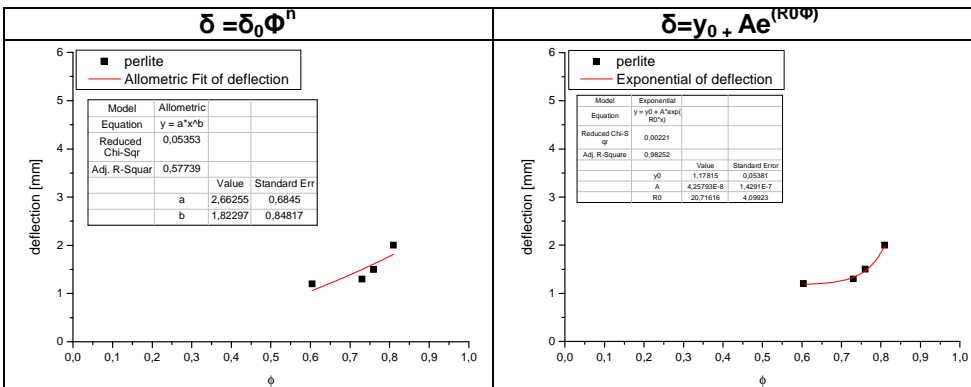
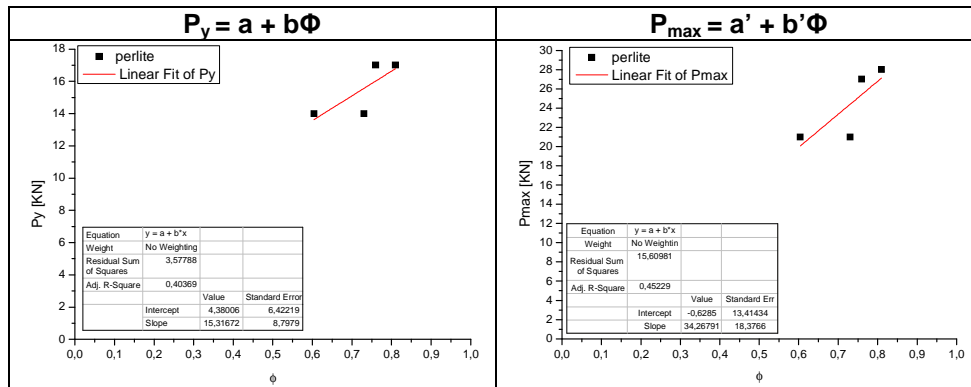
0.5%C ACrL	6.8g/cm <sup>3</sup>		7.0g/cm <sup>3</sup>	
	1120°C	1250°C	1120°C	1250°C
<b>F<sub>circle</sub></b>	0.70	0.80	0.75	0.80
<b>ε</b>	0.14	0.14	0.10	0.10
<b>Kp</b>	1.59	1.02	1.31	1.02
<b>Φ</b>	0.60	0.74	0.76	0.81
<b>E [J]</b>	11	15	17	20
<b>Deflection [mm]</b>	1.0	1.3	1.4	1.8
<b>P<sub>y</sub> [KN]</b>	13	14	15	17
<b>P<sub>max</sub> [KN]</b>	17	20	22	27
<b>HV0.05</b>	323.4±28.4	355.5±43.1	320.2±31.9	337.4±35.2

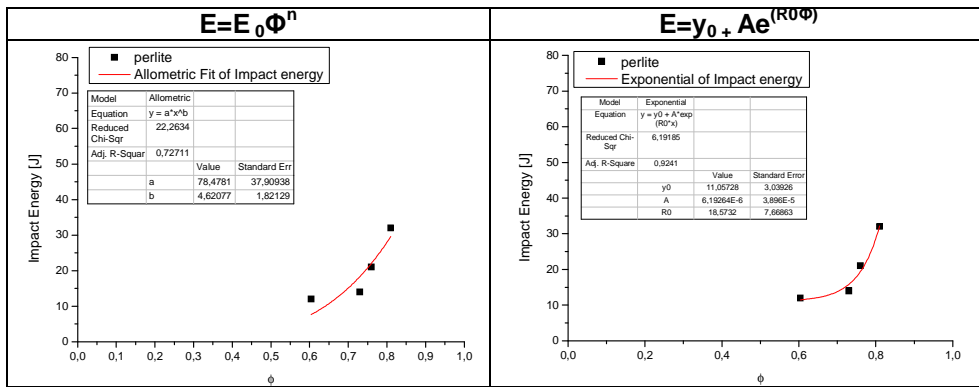




12.3.3. Perlitic steels

0.8%C ACrL	6.8g/cm <sup>3</sup>		7.0g/cm <sup>3</sup>	
	1120°C	1250°C	1120°C	1250°C
<b>F<sub>circle</sub></b>	0.70	0.80	0.75	0.80
<b>ε</b>	0.14	0.14	0.10	0.10
<b>Kp</b>	1.59	1.02	1.31	1.02
<b>Φ</b>	0.60	0.73	0.76	0.81
<b>E [J]</b>	12	14	21	32
<b>Deflection [mm]</b>	1.2	1.3	1.5	2
<b>P<sub>y</sub> [KN]</b>	14	14	17	17
<b>P<sub>max</sub> [KN]</b>	21	21	27	28
<b>HV0.05</b>	409.2±31.2	412.4±30.6	404.8±16.8	397.4±27.1





12.4. Microstructures and microhardness profiles of LPC steels

12.4.1. Three steps LPC- LPC 1

Treatment	Boost + Diffusion time [min]				
	I	II	III	IV	V
LPC1	2 + 15	1 + 1	1 + 4		

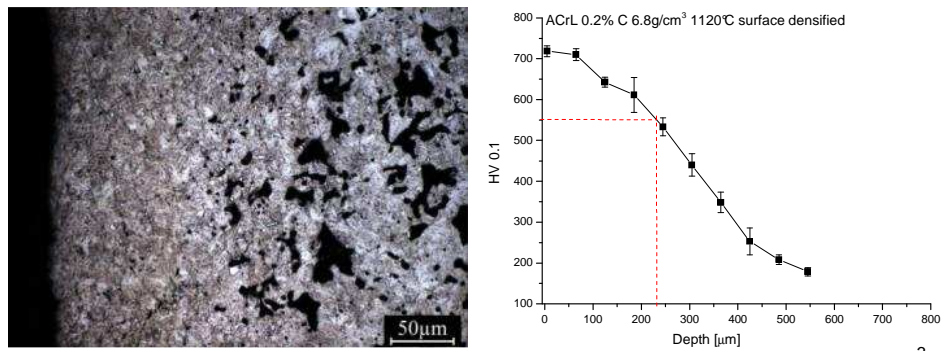


Figure 12.1: microstructure and microhardness profile of carburized 6.8g/cm<sup>3</sup> 0.2%C ACrL sintered at 1120°C

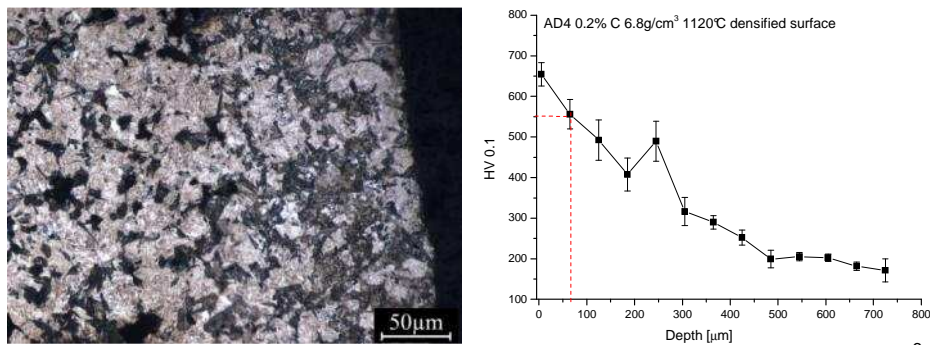


Figure 12.2: microstructure and microhardness profile of carburized 6.8g/cm<sup>3</sup> 0.2%C surface densified AD4 sintered at 1120°C

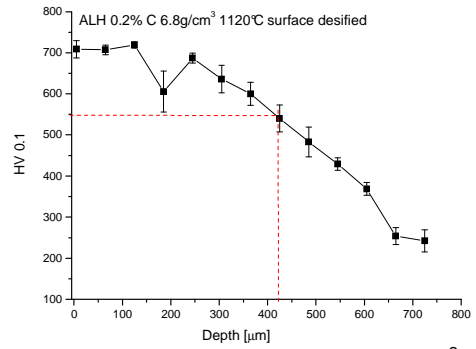
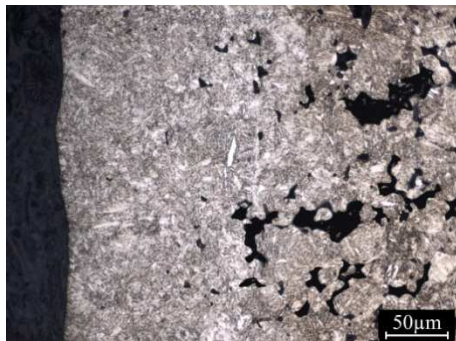


Figure 12.3: microstructure and microhardness profile of carburized 6.8g/cm<sup>3</sup> surface densified 0.2% C ALH

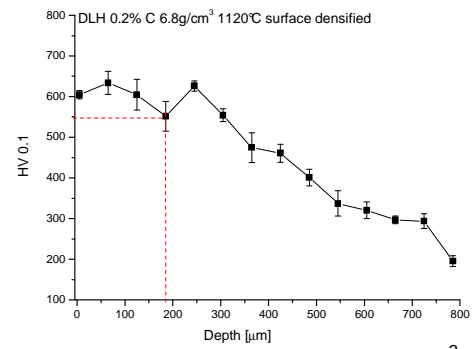
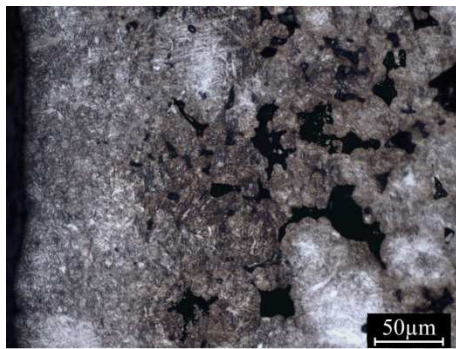


Figure 12.4: microstructure and microhardness profile of carburized 6.8g/cm<sup>3</sup> surface densified 0.2% C DLH



13.4.2. Five steps LPC- LPC 2

Treatment	Boost + Diffusion time [min]				
	I	II	III	IV	V
LPC2	2 + 10	1 + 15	1 + 19	1 + 27	1 + 4

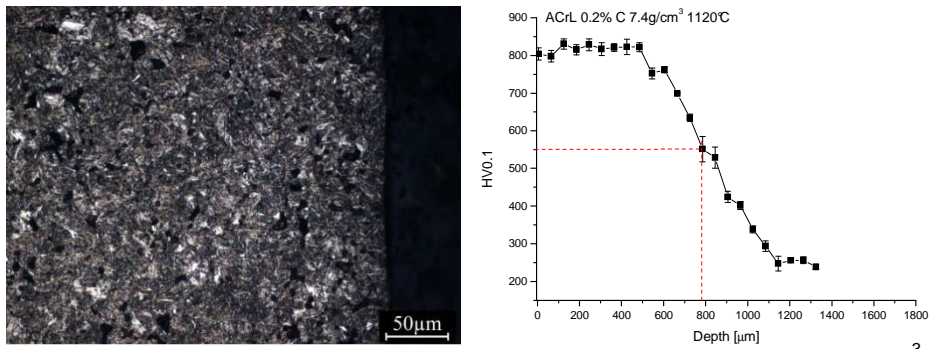


Figure 12.5: microstructure and microhardness profile of carburized 7.4g/cm<sup>3</sup> 0.2%C ACrL sintered at 1120°C

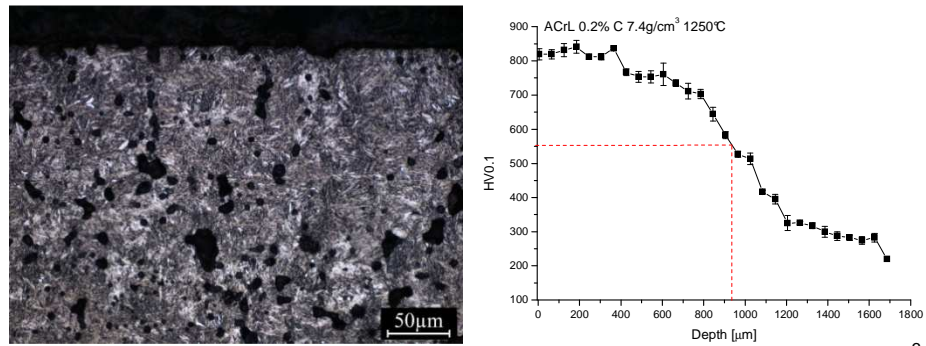


Figure 12.6: microstructure and microhardness profile of carburized 7.4g/cm<sup>3</sup> 0.2%C ACrL sintered at 1250°C

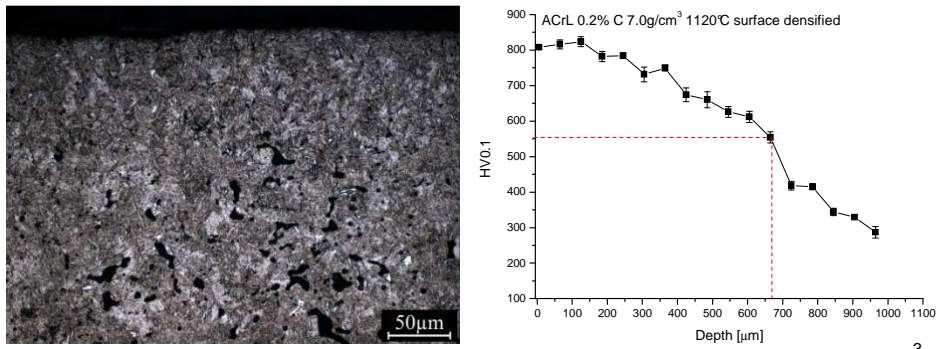


Figure 12.7: microstructure and microhardness profile of carburized 7.0g/cm<sup>3</sup> surface densified 0.2%C ACrL sintered at 1120°C

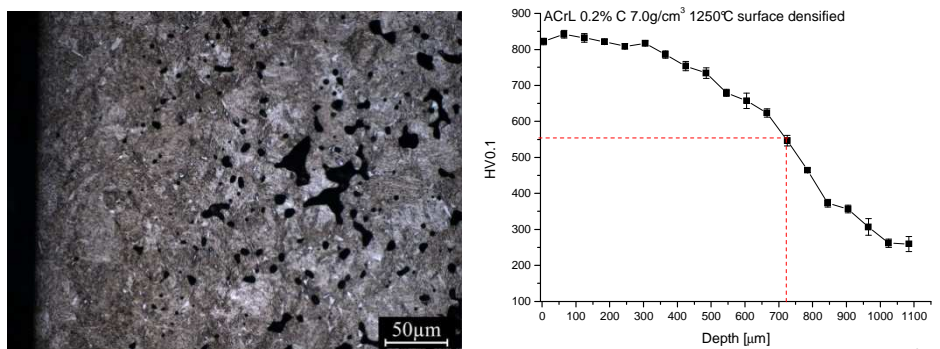


Figure 12.8: microstructure and microhardness profile of carburized 7.0g/cm<sup>3</sup> surface densified 0.2%C ACrL sintered at 1250°C

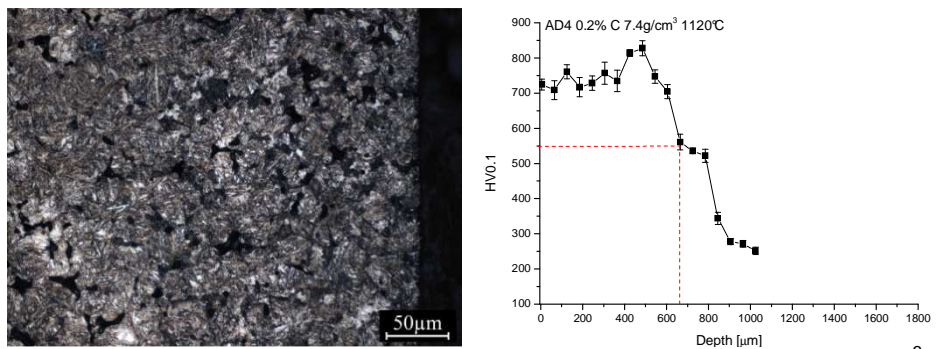


Figure 12.9: microstructure and microhardness profile of carburized 7.4g/cm<sup>3</sup> 0.2%C AD4 sintered at 1120°C

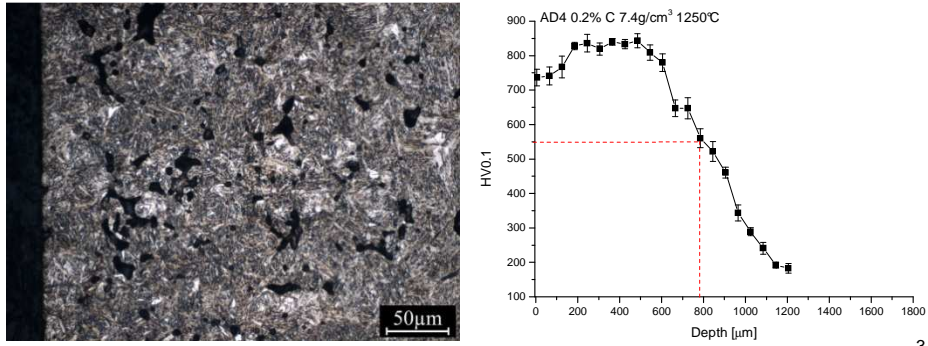


Figure 12.10: microstructure and microhardness profile of carburized 7.4g/cm<sup>3</sup> 0.2%C AD4 sintered at 1250°C

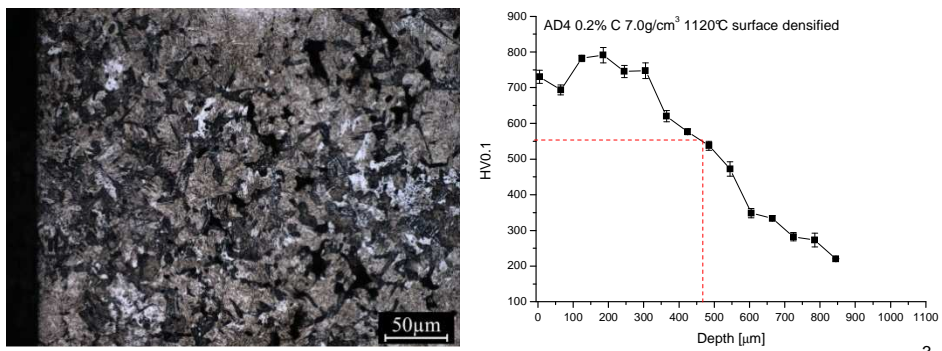


Figure 12.11: microstructure and microhardness profile of carburized 7.0g/cm<sup>3</sup> surface densified 0.2%C AD4 sintered at 1120°C

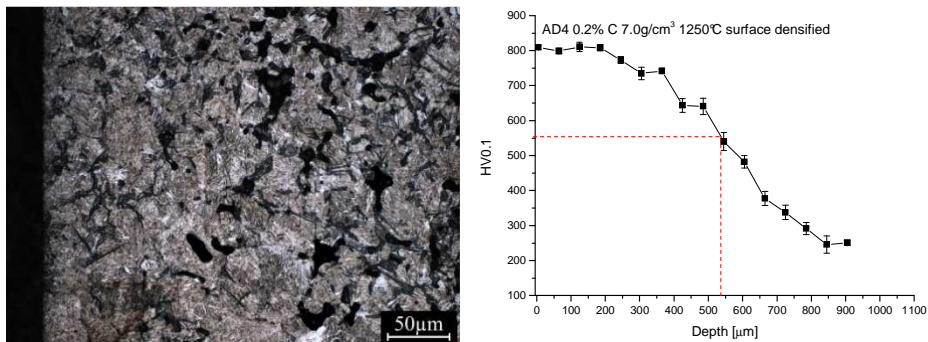


Figure 12.12: microstructure and microhardness profile of carburized 7.0g/cm<sup>3</sup> surface densified 0.2%C AD4 sintered at 1250°C

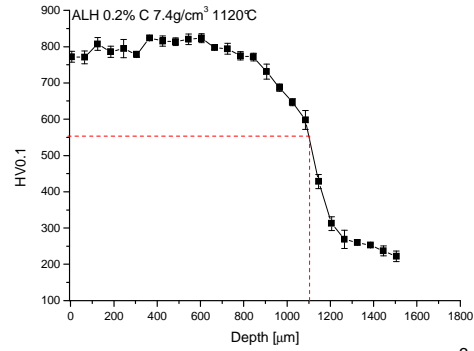
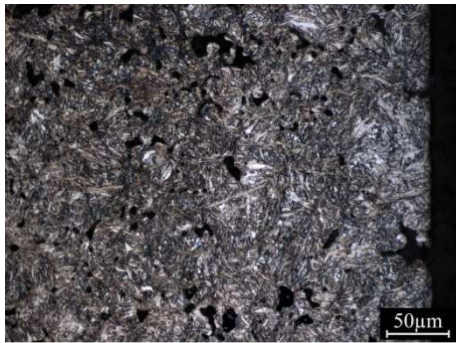


Figure 12.13: microstructure and microhardness profile of carburized 7.4g/cm<sup>3</sup> 0.2%C ALH

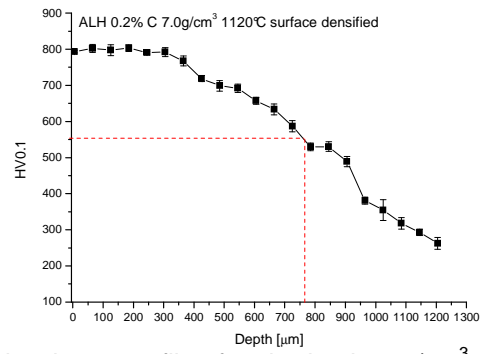
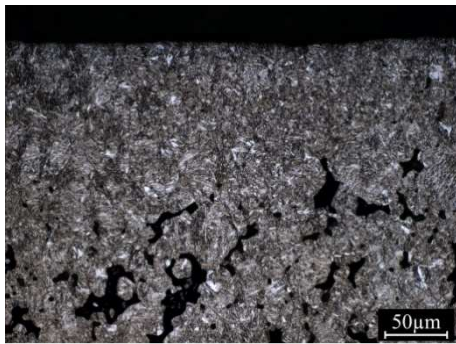


Figure 12.14: microstructure and microhardness profile of carburized 7.0g/cm<sup>3</sup> surface densified 0.2%C ALH

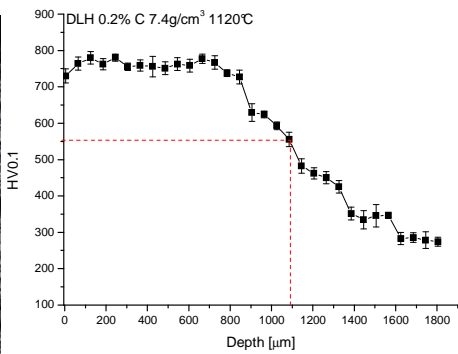


Figure 12.15: microstructure and microhardness profile of carburized 7.4g/cm<sup>3</sup> 0.2%C DLH

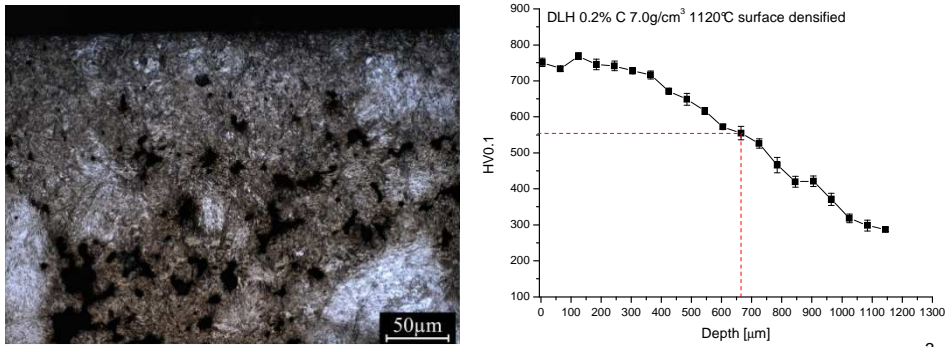


Figure 12.16: microstructure and microhardness profile of carburized 7.0g/cm<sup>3</sup> surface densified 0.2%C DLH

12.5. Microstructures and microhardness profiles of nitrided steels

Treatment	Temperature [°C]	Time [h]	
		Nitriding (80N <sub>2</sub> /20H <sub>2</sub> )	Diffusion (90N <sub>2</sub> /10H <sub>2</sub> )
PN 2	480	48	24

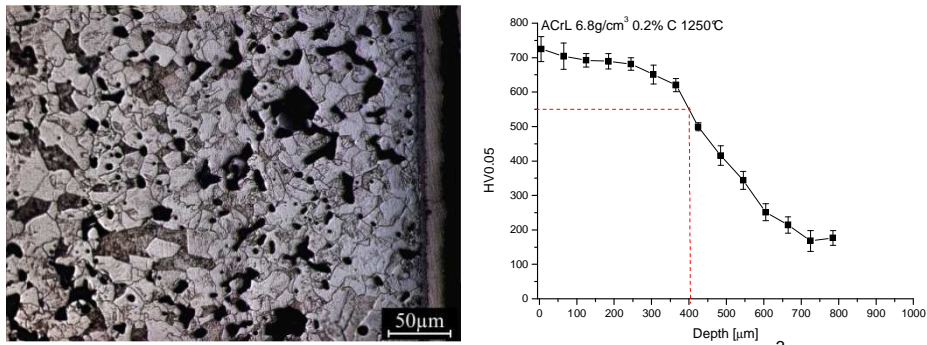


Figure 12.17: microstructure and microhardness profile of 6.8g/cm<sup>3</sup> 0.2%C ACrL sintered at 1250°C

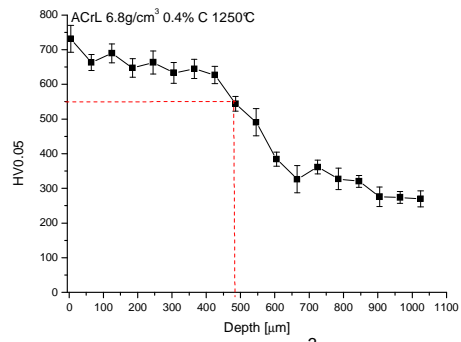
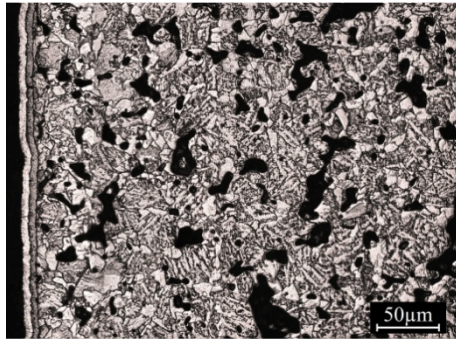


Figure 12.18: microstructure and microhardness profile of  $6.8\text{g/cm}^3$  0.4%C ACrL sintered at  $1250^\circ\text{C}$

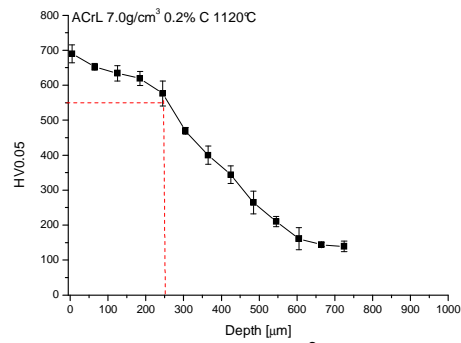
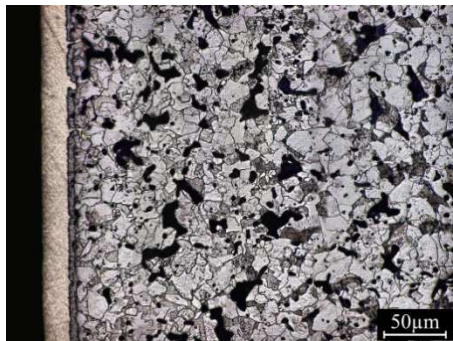


Figure 12.19: microstructure and microhardness profile of  $7.0\text{g/cm}^3$  0.2%C ACrL sintered at  $1120^\circ\text{C}$

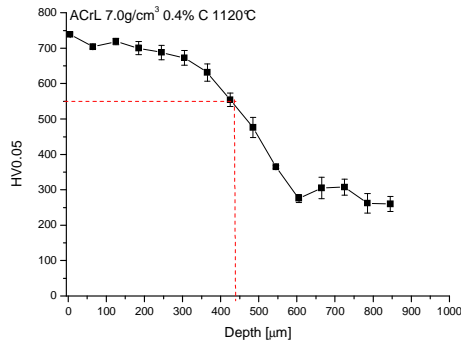
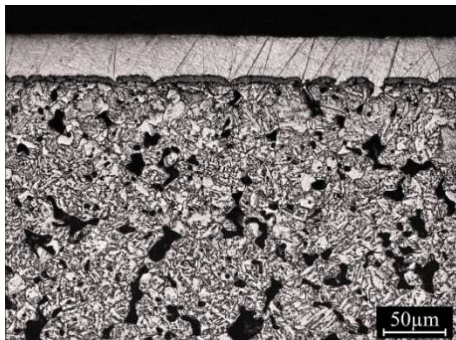


Figure 12.20: microstructure and microhardness profile of  $7.0\text{g/cm}^3$  0.4%C ACrL sintered at  $1120^\circ\text{C}$

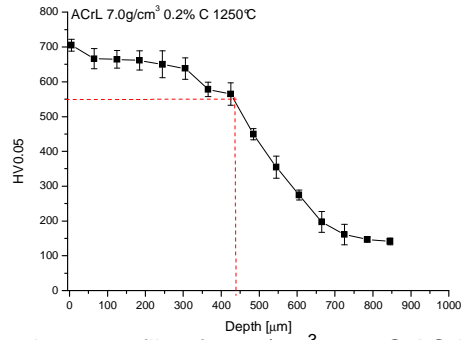
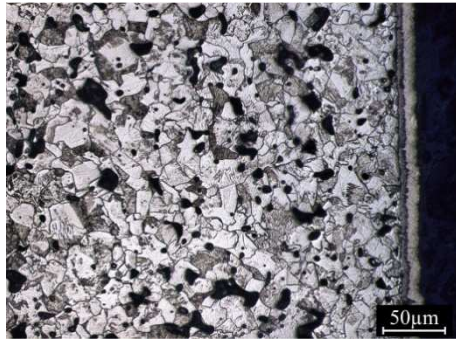


Figure 12.21: microstructure and microhardness profile of  $7.0\text{g}/\text{cm}^3$  0.2%C ACrL sintered at  $1250^\circ\text{C}$

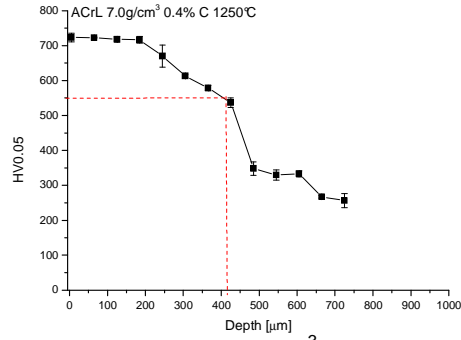
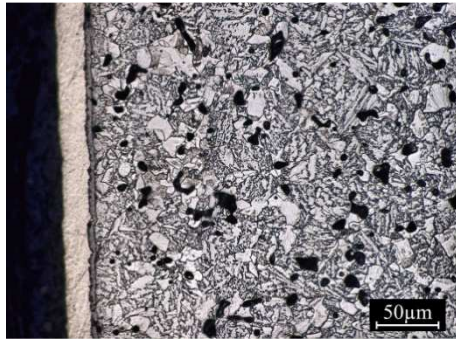


Figure 12.22: microstructure and microhardness profile of  $7.0\text{g}/\text{cm}^3$  0.4%C ACrL sintered at  $1250^\circ\text{C}$

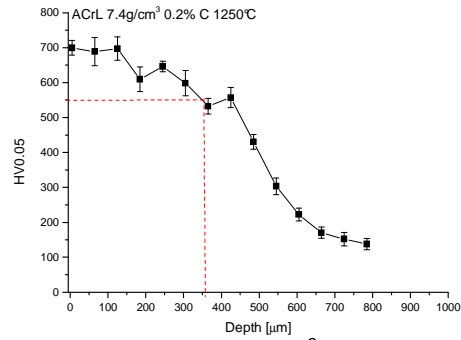
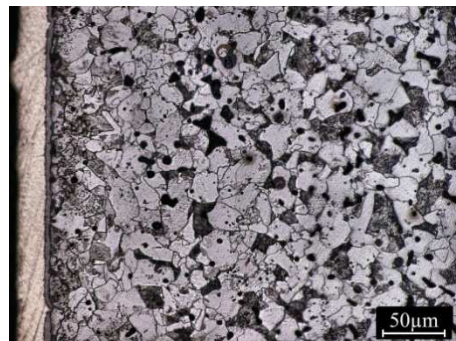


Figure 12.23: microstructure and microhardness profile of  $7.4\text{g}/\text{cm}^3$  0.2%C ACrL sintered at  $1250^\circ\text{C}$

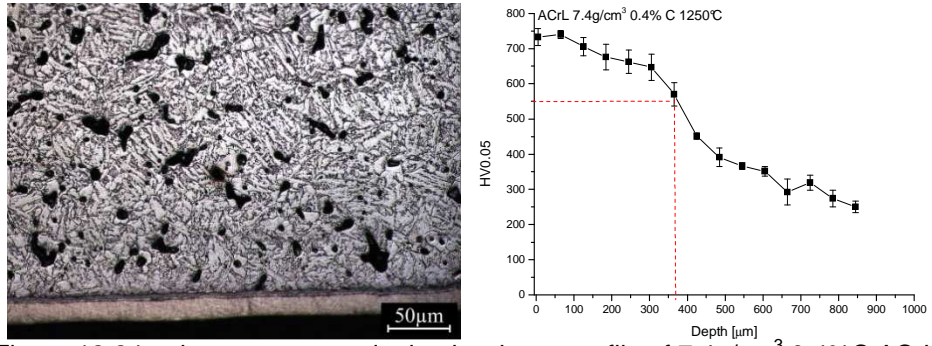


Figure 12.24: microstructure and microhardness profile of 7.4g/cm<sup>3</sup> 0.4%C ACrL sintered at 1250°C



## 13. References

- [1] N. Chawla, X. Deng, *Material Science and Engineering A*, 2005, vol. 390, pp. 98–112.
- [2] S. Polasik, J.J. Williams, N. Chawla, *Metall. Mater Trans. A*, 2002, vol. 33:1, pp. 73–81.
- [3] H. Danninger, D. Spoljaric, B. Weiss, *IJPM*, 1997, vol. 33, pp. 43-53.
- [4] S. Kremel, H. Danninger, H. Altea, Y. Yu, *Powder Metall. Prog*, 2004, Vol. 4, pp. 119-131.
- [5] S. Bengtsson, T. Marcu, *Adv. Powder Metall. Particulate Mater*, 2008, Vol. 6, pp. 152-166.
- [6] Molinari, B. Tesi, T. Bacci, G. Pradelli, *Journal de Phisique IV*, 1993, Vol. 3, pp. 949-954.
- [7] Molinari, B. Tesi., T. Bacci, T. Marcu, *Surf. and Coat. Techno.*, 2001, Vol. 140, pp. 251-255.
- [8] M. Sonsino, F. Müller, R. Mueller, *Int. J. Fatigue*, 1992, Vol. 14, pp. 3-13.
- [9] S. Saritas, C. Dogan, R. Varol, *Powder Metall.*, 1999, Vol. 42, pp. 126-130.
- [10] R.E. Reed-Hill: *Physical Metallurgy Principles*, Second edition, PWS-KENT Publishing Company–Boston, 1994.
- [11] *Metals Handbook*, vol. 4, 10<sup>th</sup> ed., ASM, Materials Park Ohio (USA), 1990.
- [12] M. M. A. Bepari, K. M. Shorowordi, *J. Mater. Process. Technol.*, 2004, Vol. 155-156, pp. 1972-1979.
- [13] V. Stayanova, L Girardini, A. Molinari, *La Metallurgia Italiana, Steels*, 2006, pp. 31-36.
- [14] G. Krauss, *Principles of heat treatment of steel*, ed. ASM, Metals Park Ohio (USA), 1980.

### *Chapter 13: References*

---

- [15] P. Beiss, case hardening, report presented at the Höganäs PM seminar, 2000  
Trento University
- [16] H. Altena, F. Schrank, *Gear Technology*, 2004, Vol. 2, pp. 27-32.
- [17] W. Grafen, B. Edenhofer, *Ipsen on Top*, 1999, Vol. 2, pp. 9-16.
- [18] W. Grafen, F. Bless, *Heat Treat. Met.*, 2003, Vol. 3, pp. 68-73.
- [19] M. Dlapka, C. Gierl, H. Danninger, H. Altea, G. Stetina, P. Orth, *Proc. of PM World Congress 2010*, Florence, Italy, 2010, ed. EPMA, Shrewsbury (UK), Vol. 2, pp. 459-466.
- [20] K. Kanno, Y. Takeda, A. Bergmark, L. Alzati, B. Lindqvist, Y. Ueda, K. Kanda and A. Zandonati, *Proc. of PM World Congress 2004*, Vienna, Austria, 2004, ed. EPMA, Shrewsbury (UK), Vol. 3, pp. 178-184.
- [21] K-E Thelning, *Steels and its heat treatment*, Second edition, Butterworths, London, 1984.
- [22] A. Molinari, T. Marcu, G. Straffelini, Y. Yu, *Adv. Powder Metall. Particulate Mater*, 2001, Vol. 6, pp. 88-101.
- [23] A. M. Maliska, A. N. Klein, A. R. de Souza, *Proc. of PM World Conference 1994*, Washington, USA, 1994, Secondary operation, p.2201-2004.
- [24] P. De la Cruz, M. Oden, T. Ericsson, *Mat. Sci. Eng. A*, 1998, Vol. 242, pp. 181-194.
- [25] S. Y. Sirin, K. Sirin, E. Kaluc, *Mater. Characterization*, 2008, Vol. 59, pp. 351-358.
- [26] W. Rembges, *Adv. Powder Metall. Particulate Mater.*, 1992, Vol. 4, pp. 41-46.
- [27] G. F. Bocchini, A. Molinari, B. Tesi, T. Bacci, *Metal Powder Rep.*, 1990, Vol. 45, pp. 772-779.
- [28] G. Prandelli, T. Bacci, B. Tesi, A. Molinari, G. F. Bocchini, *La Metallurgia Italiana*, 1992, Vol. 84, pp. 243-248.
- [29] M. R. Pinasco, G. Palombarini, M.G. Ienco, G. F. Bocchini, *Journal of alloy and compounds*, 1995, Vol. 220, pp. 217-224.

### *Chapter 13: References*

---

- [30] M. Campos, J. M. Torralba, Surf. and Coat. Techno., 2004, Vol. 182, pp. 351-362.
- [31] S. Mansoorzadeh, F. Ashrafizadeh, Surf. and Coat. Techno., 2005, Vol. 192, pp. 231-238.
- [32] C. Menapace, V. Stoyanova, L. Cislighi, A. Molinari, Powder Metall., 2008, Vol. 51, pp. 310-317.
- [33] G. Straffellini, T. Marcu Puscas, A. Molinari, Proc. of EURO PM2004, Wien, 2004, Vol. 3, pp. 159-164.
- [34] E. Santuliana, C. Menapace, S. Libardi, G. Lorenzi, A. Molinari, submitted to IJPM.
- [35] Vanya Stoyanova in "Mechanical Properties of High Density Low Alloyed PM steels: Effect of Sintering and Secondary Heat treatment" published by Trento University (2005).
- [36] R.S. Schneider, H. Hiebler, Journal of the material science, 1998, Vol. 33, pp. 1737-1744.
- [37] M. Guagliano, L. Vergani, Eng. Frac. Mech., 2004, Vol. 71, pp. 501-507.
- [38] S. Wang, Y. Li, M. Yao, R. Wang, J. of Mater. Proc. Techno., 1998, Vol. 73, pp. 57-73.
- [39] H. Guechichi, L. Castex, J of Mater. Proc. Techno., 2006, Vol. 172, pp. 381-387.
- [40] M. Frija, T. Hassine, R. Fathallah, C. Bouraoui, A. Dogui, Mat. Sci. Eng., 2006, Vol. 426, pp. 173-180.
- [41] M. Guagliano, M. Guidetti, E. Riva, Eng. Fail. Anal., 2002, Vol. 9, pp. 147-152.
- [42] M. Kobayashi, T. Matsui, Y. Murakami, Int. J. Fatigue, 1998, Vol. 20, pp. 351-357.
- [43] A. M. Eleiche, M. M Megahed, N. M. Abd-Allah, J. of Mater. Proc. Techno., 2001, Vol. 113, pp. 502-508.
- [44] Standard AMS-S-13165.
- [45] M. A. S. Torres, H. J. C. Voorwald, Int. J. Fatigue, 2002, Vol. 24, pp. 877-884.

### *Chapter 13: References*

---

- [46] D Croccolo, L. Cristofolini, M. Bandini, A. Freddi, *Fatigue Fract. Eng. Mater. Struct.*, 2002, Vol. 25, pp. 695- 707.
- [47] I. F. Pariente, M. Guagliano, *Surf. Coatings Technol.*, 2008, Vol. 202, pp. 3072-3080.
- [48] Höganäs Handbook for sintering components, 2002, vol. 1-5.
- [49] J. Tengzelius, *Adv. Powder Metall. Particulate Mater*, 1996, Vol. 4, pp. 152-166.
- [50] H. Danninger, C. Gierl, *Science of sintering*, 2008, Vol. 40, pp. 33-46.
- [51] H. Danninger, C. Gierl, S. Kremel, G. Leitner, K. Jaenicke-Rossler, Y. Yu, *Powder Metall. Prog.*, 2002, Vol. 2, pp. 125-140.
- [52] C. Garcia de Andrés, F. G. Caballero, C. Capdevila and L. F. Álvarez, *Mater. Characterization*, 2002, Vol. 48, pp. 101-111.
- [53] M. Gomez, S .F. Medina, G. Caruana, *ISIJ International*, 2003, Vol. 43, pp. 1228-1237.
- [54] G. Straffelini, A. Molinari, *La Metallurgia Italiana*, 2002, Vol. 2, pp. 31-35.
- [55] O. Bergman, A. Bergmark, *Adv. Powder Metall. Particulate Mater*, 2003, Vol. 7, pp. 270-278.
- [56] O. Bergman, *Proc. of Euro PM 2003, Valencia, Spain, 2003*, ed. EPMA, Shrewsbury (UK), Vol. 1, pp. 317-323
- [57] L. Alzati, A .Bergmark, J. Andersson, *PMAI 2005, Mumbai, India, 2005*.
- [58] H. Danninger, H.B. Weiss, *Powder Metall. Progress*, 2001, Vol. 1, pp. 19-40.

---

## List of publications

1. A. Molinari, E. Santuliana, I. Cristofolini, A. Rao, S. Libardi, P. Marconi, **Surface modifications induced by shot peening and their effect on the plane bending fatigue strength of a Cr-Mo steel produced by powder metallurgy**, Materials Science & Engineering A, 2011, vol. 528, pp. 2904-2911.
2. A. Molinari, E. Santuliana, S. Libardi, G. Lorenzi, **Influence of plasma nitriding on the plane bending fatigue resistance of a Cr-Mo steel produced by Powder Metallurgy**, IJPM, 2011, **submitted**.
3. E. Santuliana, C. Menapace, G. Meli, A. Molinari, **Low Pressure Carburizing of PM steels with different chemical composition and porosity**, La Metallurgia Italiana, 4, 2011.
4. E. Santuliana, C. Menapace, G. Ischia, A. Molinari, **Effect of the austenitization temperature on the austenite transformations in a 0.7%C Cr-Mo PM steel**, Powder Metall., 2011, DOI: 10.1179/003258909X12553422176844.
5. A. Molinari, E. Santuliana, I. Cristofolini, A. Rao, S. Libardi, P. Marconi, **Influence of shot peening on the fatigue resistance of Cr-Mo sintered steels**, Adv. Powder Metall. Particulate Mater, 2010, vol. 6, pp. 41- 48.
6. E. Santuliana, C. Menapace, A. Molinari, **Influence of porosity on low pressure carburizing of low alloy sintered steels**, Powder Metall. Prog., 2010, vol. 10, pp 32- 42.

- 
7. E. Santuliana, C. Menapace, A. Molinari, G. Lorenzi, S. Libardi, **Resistenza a fatica di acciaio al Cromo-Molibdeno sinterizzato e nitrurato in plasma**, in Atti 33° Convegno Nazionale AIM, Brescia, Italy, 2010.
  8. E. Santuliana, A. Molinari, **Microstructural improvement of low pressure carburized low alloy sintered steels**, in Proc. of PM World Congress 2010, Florence, Italy, 2010, ed. EPMA, Shrewsbury (UK), vol. 2, pp. 451- 458.
  9. E. Santuliana, C. Menapace, A. Molinari, **Studio delle trasformazioni al raffreddamento dell'austenite in un acciaio sinterizzato al Cr-Mo**, in Atti 22° Convegno Nazionale Trattamenti Termici, Salsomaggiore Terme, Italy, 2009.
  10. E. Santuliana, A. Molinari, **Microstructure and impact properties of low alloy sintered steels**, Proc of EuroPM2009, Copenhagen, Denmark, 2009, ed. EPMA, Shrewsbury (UK), vol. 1, pp. 169-176.
  11. M. Zendron, L. Girardini, E. Santuliana, A. Molinari, **Microstructure and fatigue strength of through hardened and sinterhardened Cr-Mo and Cr-Mn steels**, Proceedings CD of EuroPM2008, Mannheim, Germany, 2008, ed. EPMA, Shrewsbury (UK).

---

## Acknowledgements

I want to thank all the Höganäs Chair team for the great experience during this work. In particular to Björn Lindqvist and Sven Bengtsson without whom this work could not be performed.

Thanks to Prof. Molinari for the support given to me in this years.

Thanks to my family and my friends.

## Ringraziamenti

Ed eccoci qui di nuovo, è la terza volta che scrivo dei ringraziamenti, ufficiali ed ufficiosi, di conseguenza non ho più molto da aggiungere se non per le persone conosciute in questi ultimi anni.

Innanzitutto i miei mentori: Mario, Luca e Francesco (anche se un po' meno mentore e un po' più pirla). A voi posso solo dire Grazie!.

Un ringraziamento va anche al Prof. Molinari per avermi sopportata per tre anni.

Non posso dimenticare la mia amica di sempre e per sempre Ketner con cui ho condiviso tutte le ansie del dottorato. E rimanendo nel continente brasiliano, Nerio sei sempre il mio addominale scolpito preferito.

Grazie Anna per essermi stata vicina quando ne avevo bisogno e grazie Ivan per le lunghe chiacchierate sulla dissoluzione dei carburi. Giusina senza te la vita di laboratorio non ha più senso.

Poi ci sono le mamme: Cinzia (beh mamma sprint grazie per le chiacchiere e i commenti post partita), Marianna (mah ancora non ci credo sposata e mamma,

---

adesso devo dire: "sempre dopo la Giusy") e l' Ale (a cui dedico tutto il mio cuore anche se devi dividerlo con "Beatrice").

Lo so che ti stai già agitando, mi ricordo di te, mio Mirko (tegolino) anche se sei lontano so che mi pensi ogni tanto.

Infine la mia famiglia perché credo che quello che si legge per ultimo rimanga più impresso e quindi sia più importante. In ordine di età: il mio papi, il Max e la Roby (aspettando Samuele e un battito di occhi). Poi ci sei tu...TCA.